

The Effect of Soft and Hard Gauge Corrections on Thermal Leptogenesis

Master's Thesis

Paul Frederik Depta



Institut für Theoretische Physik
Goethe-Universität Frankfurt am Main
October 24, 2017

Supervisor and First Referee: Prof. Dr. Owe Philipsen
Second Referee: Prof. Dr. Carsten Greiner

Contents

Abstract	v
Zusammenfassung	vi
1. Introduction	1
2. Leptogenesis and Other Models for Baryogenesis	5
2.1. Baryon Asymmetry in the Universe	5
2.2. Sakharov Conditions	5
2.3. Models for Creating a Baryon Asymmetry	6
2.4. Leptogenesis	7
3. Nonequilibrium Quantum Field Theory	9
3.1. Correlation Functions	9
3.2. Kadanoff-Baym Equations for the Majorana Neutrino	11
3.3. Propagators	13
3.3.1. Connection Between the Majorana Neutrino Self-Energy and its Thermal Width	15
4. Boltzmann and Kadanoff-Baym Calculations for the Lepton Asymmetry	17
4.1. Physical Scenario	17
4.2. Boltzmann Calculation	18
4.3. Kadanoff-Baym Calculation	20
4.3.1. Lepton Number Matrix	20
4.3.2. Solution without Gauge Corrections	24
5. Resummation of the Majorana Neutrino Self-Energy	27
5.1. Momentum Scales	27
5.2. Hard Thermal Loops	28
5.3. Perturbation Theory Close to the Lightcone	28
5.3.1. Thermal Width and Asymptotic Mass	28
5.3.2. Lightcone Coordinates and Power Counting	29
5.3.3. Collinear Thermal Loops	30
5.4. Connection to the Landau-Pomeranchuk-Migdal Effect	32
5.5. Strategy of the Calculation	33
5.6. Calculation of the Resummed Majorana Neutrino Self-Energy	34
5.6.1. Left- and Right-Handed Majorana Neutrino Self-Energy	34
5.6.2. Calculation of the Two-Point Function without Soft Gauge Contri- butions	35
5.6.3. Derivation of the Recursion Relation	36
5.6.4. Integrating out the Soft Gauge Bosons and Result for the Right- Handed Majorana Neutrino Self-Energy	37
5.6.5. Symmetries of the Majorana Neutrino Self-Energy	40
5.6.6. Calculation of the Tree-Level Result	41

5.6.7. Thermal Width	43
6. Including Gauge Corrections to Thermal Leptogenesis	45
6.1. Including Gauge Corrections to the Lepton Number Matrix	45
6.1.1. Diagrammatic Viewpoint	45
6.1.2. Implementing the Resummed Majorana Neutrino Self-Energy in the Lepton Number Matrix	46
6.2. Approximating the Lepton Number Matrix	52
6.2.1. $t \rightarrow \infty$ Limit	53
6.2.2. Evaluation of the t_1, t_2 and t_3 Integrations: Dominating Regions for the Integrations over ω_{21} and ω_{23}	54
6.2.3. Approximating the Lepton Number Matrix for Finite Time	55
7. Numerical Results	59
7.1. Setup	59
7.1.1. Renormalization Group Equations	59
7.1.2. Numerical Methods	61
7.1.3. Overview over the Calculations	62
7.2. Results for the Differential Production Rate, the Thermal Width, and the Self-Energies	62
7.3. Results for the Lepton Number Matrix for $M = 10^{10}$ GeV	66
7.3.1. Cross-Check of Different Algorithms	66
7.3.2. Results for Infinite Time: Thermalized Results	70
7.3.3. Results for Finite Time	72
7.3.4. Thermalization Times	75
7.4. Results for the Lepton Number Matrix for $M = 10^7$ GeV	77
7.4.1. Results for Infinite Time: Thermalized Results	77
7.4.2. Results for Finite Time	79
7.4.3. Thermalization Times	82
7.5. Discussion	83
8. Conclusions and Research Perspectives	85
A. Conventions and Feynman Rules	87
A.1. Conventions	87
A.2. Feynman Rules	87
B. Details on the Resummation of the Majorana Neutrino Self-Energy and on the Lepton Number Matrix	89
B.1. Solving the Integral Equations	89
B.1.1. From Integral Equations to Ordinary Differential Equations	89
B.1.2. Boundary Conditions	91
B.1.3. Numerical Procedure	92
B.1.4. Modifying the ODEs for Numerical Evaluation	93
B.1.5. Numerical Details for Solving the ODEs	97
B.2. Proofs	98
B.2.1. Lepton Propagator	98
B.2.2. Perpendicular Momentum Integrations	99
B.2.3. Imaginary Part of the Retarded Self-Energy	100

B.3. Details for the Lepton Number Matrix	102
B.3.1. Evaluation of the t_1 , t_2 and t_3 Integrations	102
B.3.2. Details for the Numerical Evaluation	102
Bibliography	105
Danksagung	109
Selbstständigkeitserklärung	110

Abstract

The objective of this thesis is to study the effect of soft and hard gauge corrections, i.e. corrections due to interactions with gauge bosons of soft and hard momenta, to thermal leptogenesis. Thermal leptogenesis is one of the leading candidates for the explanation of the baryon asymmetry in the universe. It does so by introducing three heavy Majorana neutrinos. Their CP-violating out-of-equilibrium decay generates a lepton asymmetry that is converted into a baryon asymmetry via sphaleron processes in the standard model of particle physics. In the past, progress has been made to move from a description using Boltzmann equations to a calculation of the lepton asymmetry, the lepton number matrix, in the framework of Kadanoff-Baym equations [Ani+11]. Furthermore, gauge and other standard model corrections to the thermal production rate of Majorana neutrinos have been considered [ABB11]. This thesis follows [Hüt13] to combine the results of these calculations arriving at an expression for the lepton number matrix that systematically includes all leading order gauge and other standard model corrections. This expression is then approximated and numerically evaluated. With the approximations, one recovers the time-dependence of the solution of the Boltzmann equations. By numerically evaluating the expression, one finds that by omitting soft gauge corrections, a temperature region exists, where the generated lepton asymmetry is suppressed due to kinematic reasons. The inclusion of soft gauge corrections compensates for this suppression.

Zusammenfassung

Ziel dieser Masterarbeit ist die Untersuchung weicher und harter Eichkorrekturen, also Korrekturen aufgrund von Wechselwirkungen mit Eichbosonen, die weiche und harte Impulse haben, zur thermischen Leptogenese. Thermische Leptogenese ist einer der führenden Kandidaten zur Erklärung der Baryonenasymmetrie im Universum. Zur Erklärung dieser werden drei schwere Majorananeutrinos eingeführt. Ihr CP-verletzender Zerfall, der im Nichtgleichgewicht stattfindet, erzeugt eine Leptonenasymmetrie, die mittels Sphaleronprozesse im Standardmodell der Teilchenphysik in eine Baryonenasymmetrie umgewandelt wird. In der Vergangenheit wurden Fortschritte in der Beschreibung der Erzeugung der Leptonenasymmetrie gemacht, die von einer Berechnung mittels Boltzmann-Gleichungen zu einer Berechnung mithilfe von Kadanoff-Baym-Gleichungen in Form der Leptonenzahlmatrix übergehen [Ani+11]. Zudem wurde der Einfluss von Eich- und anderen Standardmodellkorrekturen auf die Produktionsrate von Majorananeutrinos untersucht [ABB11]. Diese Masterarbeit folgt der Betrachtung in [Hüt13], um die Resultate dieser Referenzen zu kombinieren und so einen Ausdruck für die Leptonenzahlmatrix zu berechnen, der systematisch alle Eich- und andere Standardmodellkorrekturen führender Ordnung enthält. Das Resultat wird dann genähert und numerisch ausgewertet. Durch die Näherung findet man die gleiche zeitliche Abhängigkeit wie in der Lösung der Boltzmann-Gleichungen. Die numerische Auswertung zeigt, dass wenn weiche Eichkorrekturen vernachlässigt werden, ein Temperaturbereich entsteht, in dem die erzeugte Leptonenasymmetrie aufgrund von kinematischen Gründen unterdrückt wird. Die Berücksichtigung weicher Eichkorrekturen kompensiert diese Unterdrückung.

1. Introduction

Why do we have matter in the universe?

This is one of the most intriguing and unanswered questions in physics up to date. To be more concrete, in most cases baryons are meant when talking about matter in this sense. Hence, one speaks of a baryon asymmetry in the universe.

The opening question mainly arises from two observations:

1. Matter (baryons) is observed in the universe, whereas there is barely any antimatter (antibaryons) observed.
2. All processes observed create the same amounts of matter (baryons) and antimatter (antibaryons)¹.

In the standard model of cosmology, cf. Fig. 1.1, the issue of this question arises in the following way. According to the model, the universe started out in a hot big bang. Shortly afterwards, it underwent a period of inflation, which led to an exponential expansion of the universe leaving it in a state far from equilibrium. Then, during the period of reheating, the particles thermalized into a hot and dense plasma. The problem now is that starting with no baryon asymmetry, i.e. the same amounts of baryons and antibaryons in the universe, would mean that no baryon number exists unless there was a process generating a baryon asymmetry. Similarly, starting with a baryon asymmetry at the big bang, the period of inflation would have thinned out this asymmetry, which makes this scenario very unlikely. Hence, a baryon asymmetry should be created after or during the period of inflation. The creation of the baryon asymmetry in the universe is called baryogenesis. In most scenarios, one assumes that baryogenesis took place in the hot and dense plasma of the early universe.

There are different models trying to explain the baryon asymmetry. In 1967, Sakharov found three conditions any theory or model, which tries to do so, has to fulfill [Sak67]. These conditions were later named after him. As it turns out, the standard model of particle physics, which will be called standard model from hereon, is not sufficient for generating a large enough baryon asymmetry consistent with observations, even though it is able to create a baryon asymmetry. Therefore, physics beyond the standard model is needed.

The model of choice for this thesis is thermal leptogenesis. This model introduces three heavy Majorana neutrinos. Their CP-violating out-of-equilibrium decay generates a lepton asymmetry, which is later converted into a baryon asymmetry using standard model sphaleron processes. Furthermore, it gives an explanation for the observed light neutrino masses.

Most standard leptogenesis calculations use Boltzmann equations, for an overview see e.g. [HPW09]. In the past years, efforts have been made to go beyond these and obtain a full quantum field theoretical description of the nonequilibrium processes needed for leptogenesis in the framework of Kadanoff-Baym equations. Most notably, this was done in [Ani+11]. In this work, a solution of the Kadanoff-Baym equations for the simplest case

¹Of course, this includes zero creation of matter and antimatter.

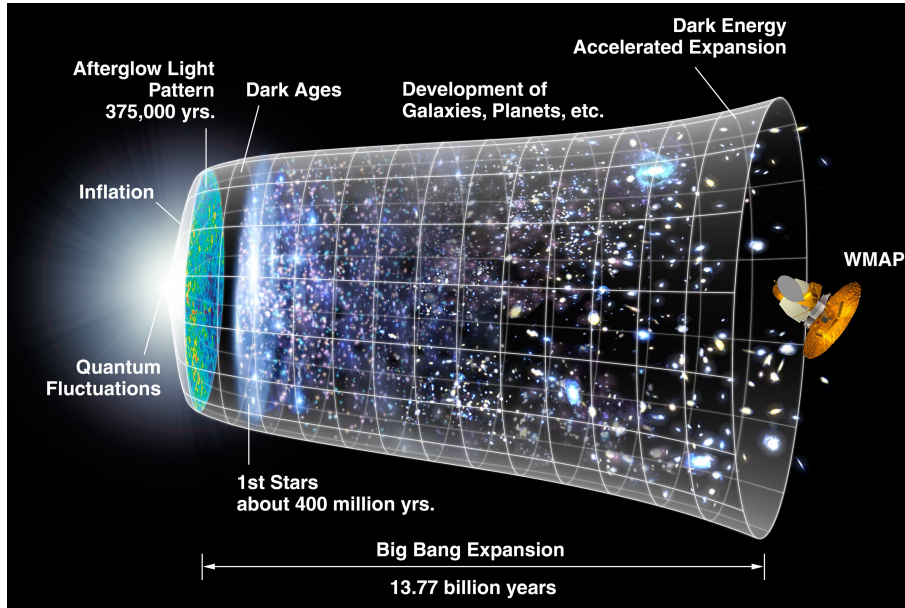


Figure 1.1.: History of the universe according to the standard model of cosmology. Starting with the big bang on the left hand side, an inflationary phase settled in with the expansion slowing again afterwards. The afterglow light pattern (cosmic microwave background) is depicted followed by the dark ages before the first stars form and the galaxies develop. The universe then entered an accelerated expansion due to dark energy. Of interest in this thesis is mainly the period after inflation and before the afterglow light pattern. Note that according to more recent data the age of the universe is 13.799(21) billion years [see Ade+16, p. 31]. From [NAS12] [as cited in Hüt13, p. 2].

of hierarchically ordered Majorana neutrino masses with two being much heavier than the other one was derived and presented. The hierarchical mass ordering enables one to integrate out the two heavier Majorana neutrinos, thus obtaining an effective theory. This approach considers a heavy Majorana neutrino out of equilibrium in a plasma of standard model particles. Using this solution, an expression for the resulting lepton asymmetry, the so-called lepton number matrix, was calculated.

One of the findings was that in order to make further progress towards a "theory of leptogenesis" [see Buc01, p. 10] [as cited in Ani+11, p. 42], gauge corrections, i.e. corrections due to interactions with gauge bosons, needed to be included and discussed [cf. Ani+11, p. 42]. This is due to the fact that thermal widths of standard model particles had to be introduced by hand. Gauge corrections were already found in [Giu+04; KPT10; ABB11] to be of importance for temperatures greater than or similar to the lightest Majorana neutrino mass by generating thermal masses for lepton and Higgs boson fields [cf. also Ani+11, p. 4].

Most importantly for this thesis, all leading order gauge corrections to the production rate of heavy Majorana neutrinos have been calculated in [ABB11]. These are soft and hard gauge corrections, i.e. corrections due to interactions with gauge bosons of soft and hard momenta. Furthermore, corrections coming from interactions with other standard model particles of hard momenta have been included. This was done using resummation techniques for the kinematic regime corresponding to the temperature being greater than the Majorana neutrino mass. Thereby, the Majorana neutrino self-energy, which can be

related to the Majorana neutrino production rate, was resummed. The corrections connect to the well-known Landau-Pomeranchuk-Migdal effect.

The objective of this thesis is to estimate the effect of soft and hard gauge corrections on thermal leptogenesis, hence including all leading order gauge corrections. To achieve this aim, the result of [Hüt13] is used, which combines the calculation for the lepton asymmetry from [Ani+11] with the resummed Majorana neutrino self-energy from [ABB11].

This thesis is structured as follows. Note that due to the fact that it uses the result of [Hüt13], the structure is very similar to this reference, since the same contents are needed. After giving a brief introduction on the observation of the baryon asymmetry in the universe, the Sakharov conditions, and different models fulfilling these conditions, thermal leptogenesis is presented shortly in Ch. 2. In Ch. 3, the basics of nonequilibrium quantum field theory are discussed and the propagators needed in this thesis, which were derived in [Ani+11], are given. These will be used in Ch. 4 to calculate an expression for the lepton asymmetry in the framework of Kadanoff-Baym equations as in [Ani+11] after first presenting the physical scenario considered in this thesis and the result from the Boltzmann equations for it. In Ch. 5, the resummation of the Majorana neutrino self-energy from [ABB11] is discussed. Having presented all needed expressions, the inclusion of gauge and other standard model corrections in the result for the lepton asymmetry is detailed following [Hüt13] in Ch. 6. The result is then approximated in the same chapter and numerically evaluated in Ch. 7. The thesis concludes with Ch. 8 giving an overview of what has been done and mentioning research perspectives.

Conventions, Feynman rules, and details on the resummation of the Majorana neutrino self-energy and the evaluation of the lepton number matrix including soft and hard gauge corrections are given in two appendices.

2. Leptogenesis and Other Models for Baryogenesis

In this chapter, the physical observation of a baryon asymmetry in the universe (BAU) is detailed together with the necessary conditions for a model to generate a BAU, the Sakharov conditions, as well as different models for doing so. Afterwards, the model used in this thesis, thermal leptogenesis, is introduced.

2.1. Baryon Asymmetry in the Universe

As visible in our everyday environment, barely any antimatter exists in the universe, whereas a lot of matter is observed. In fact, antimatter is only seen in extreme conditions, such as lab experiments, like particle colliders, or high-energy cosmic rays.

By measuring the primordial abundances of light elements in the universe, the BAU can be connected to big bang nucleosynthesis (BBN) [see CDS12, p. 6], which gives the value [see Ste10] [as cited in CDS12, p. 6]

$$\eta_B^{\text{BBN}} = \frac{n_b - n_{\bar{b}}}{n_\gamma} = 5.80(27) \cdot 10^{-10} \quad (2.1)$$

for the baryon asymmetry, where n_b , $n_{\bar{b}}$, and n_γ are the number densities of baryons, antibaryons, and photons, respectively. Measurements of acoustic peaks in the cosmic microwave background (CMB) from the WMAP seven year long observation gave a value of [see Kom+11] [as cited in CDS12, p. 7]

$$\eta_B^{\text{WMAP}} = \left(6.160_{-0.156}^{+0.153}\right) \cdot 10^{-10} \quad (2.2)$$

in good agreement with the value from BBN.

The explanation of the BAU is challenging, since in laboratory processes, only matter-antimatter creation or annihilation is observed in processes like $b + \bar{b} \rightleftharpoons 2\gamma$. If only these processes were allowed in general, then starting with symmetric initial conditions would mean that no BAU could exist. Furthermore, asymmetric initial conditions causing a BAU, i.e. starting with a BAU at the big bang, have problems with the standard model of cosmology due to the period of inflation that would have diluted a BAU from the time of the big bang. Hence, the creation of the BAU, which is called baryogenesis, should occur after the period of inflation and start with at least almost zero baryon asymmetry [cf. CDS12, p. 3]. The Sakharov conditions, which models aiming for an explanation of a BAU have to fulfill, are explained in the next section.

For more information and a review concerning matter and antimatter in the universe see [CDS12].

2.2. Sakharov Conditions

The three conditions necessary for the creation of a baryon asymmetry were first formulated by Sakharov in 1967. The conditions named after him are [see Sak67]

1. baryon number violation,
2. C- (charge conjugation) and CP- (charge parity) violation,
3. deviation from thermal equilibrium.

The first condition is clear. For the second condition, one has to consider that if C or CP were not violated, then for every process creating an asymmetry, a C or CP conjugate process would exist generating exactly the opposite asymmetry with the same probability [see CDS12, p. 3]. Hence, no baryon asymmetry would be generated. The third condition has to be fulfilled, since in thermal equilibrium, the expectation values of all operators, which includes the baryon number operator \mathcal{B} , are constant [see CDS12, p. 3]. Therefore, going from a state with no baryon asymmetry to a state with an asymmetry needs deviation from thermal equilibrium.

2.3. Models for Creating a Baryon Asymmetry

There are different models fulfilling the Sakharov conditions, which are candidates for a successful generation of the BAU.

The standard model of particle physics (SM) fulfills all three Sakharov conditions. Even though the baryon number is conserved perturbatively in the SM, non-perturbative effects can give baryon number violation [see CDS12, pp. 9-11]. This was first found by 't Hooft [t H76a; t H76b] based on the Adler-Bell-Jackiw anomaly [Adl69; BJ69]. A very important solution was found by Klinkhamer and Manton [KM84], the so-called sphaleron solution (from the greek word $\sigma\phi\alpha\lambda\epsilon\rho\acute{o}\zeta$: "ready to fall"). This solution is a saddle point in the potential of the electroweak theory [cf. KM84]. By moving from one minimum in this potential to a neighboring one through the sphaleron solution, the Chern-Simons number of the gauge field A_μ

$$N_{\text{CS}} = \frac{g^2}{32\pi^2} \int d^3x \epsilon^{ijk} \text{Tr} \left(A_i \partial_j A_k + \frac{2}{3} i A_i A_j A_k \right) \quad (2.3)$$

is changed by one, which connects to a change in baryon number N_B and lepton number N_L , the differences of the numbers of antibaryons/antileptons and baryons/leptons, via [cf. Rin88]

$$\Delta N_B = \Delta N_L = n_f \Delta N_{\text{CS}} , \quad (2.4)$$

where $n_f = 3$ is the number of families. This can be formulated using the baryon and lepton currents j_B^μ and j_L^μ violated by the Adler-Bell-Jackiw anomaly [cf. Adl69; BJ69] [as cited in Hüt13]

$$\partial_\mu j_B^\mu = \partial_\mu j_L^\mu = \frac{n_f}{32\pi^2} \left(g_W^2 \text{Tr} \left(W_{\mu\nu} \tilde{W}^{\mu\nu} \right) - g_Y^2 F_{\mu\nu} \tilde{F}^{\mu\nu} \right) , \quad (2.5)$$

where g_W and g_Y are the couplings of the gauge groups SU(2) and U(1) with corresponding field strength tensors $W_{\mu\nu}$ and $F_{\mu\nu}$ and their duals $\tilde{W}^{\mu\nu}$ and $\tilde{F}^{\mu\nu}$. Each sphaleron transition creates nine quarks (three for each generation due to color) and three leptons. In the vacuum, sphaleron transitions, which are then only possible via tunneling, are suppressed by a factor of around 10^{-160} [see t H76b]. For temperatures above the sphaleron energy $T \gtrsim 100$ GeV [see KRS85] [as cited in Hüt13, p. 6], where also electroweak symmetry becomes restored, these transitions are no longer suppressed, and therefore, the baryon

and lepton numbers are violated. Note that even though $N_B + N_L$ is violated, $N_B - N_L$ is conserved, cf. Eq. (2.4).

The second Sakharov condition is fulfilled due to the fact that the weak interaction violates P-invariance and the complex phase in the Cabibbo-Kobayashi-Maskawa matrix [cf. CDS12, p. 9]. This violation however misses at least eight orders of magnitude [see HS95] [as cited in Hüt13, p. 8].

Deviation from thermal equilibrium is achieved via the expansion of the universe bringing the SM plasma out of equilibrium [cf. CDS12, pp. 9, 11]. However, in order to achieve a large enough BAU, a first-order electroweak phase transition would be needed [cf. CDS12]. This is only possible for a small Higgs masses $m_H < 100$ GeV [BP95; Kaj+97] [as cited in Hüt13, p. 8]. Note that results from lattice SU(2)-Higgs calculations give a critical endpoint for the first order electroweak phase transition of $m_H = (72.4 \pm 1.7)$ GeV [CFH99]. Since the current value for the Higgs mass is $m_H = (125.09 \pm 0.24)$ GeV [Pat+16], successful SM baryogenesis is ruled out and one needs a theory beyond the SM.

Before continuing to the model of choice for creating a BAU for this thesis, which is called leptogenesis, one should note other models beyond the SM that are used for the explanation of a BAU. Prominent example for these are grand unified theories, electroweak baryogenesis, and Affleck-Dine baryogenesis. For some details on these see [Hüt13, pp. 8-9].

2.4. Leptogenesis

The model of choice for this thesis is thermal leptogenesis [FY86]. Using this model, one hopes to not only solve the question of the generation of a BAU, but also explain the observed light neutrino masses via the so-called seesaw mechanism. For leptogenesis, one introduces three right-handed heavy Majorana neutrinos in addition to the SM. Their CP-violating out-of-equilibrium decay at temperatures around their masses generates a lepton asymmetry that is later converted into a baryon asymmetry using SM sphaleron processes. Therefore, all three Sakharov conditions are fulfilled. Since the explanation of the observed light neutrino masses is not of interest in this thesis, it will not be discussed further. For overviews of thermal leptogenesis see e.g. [Di 12; BD12; FNR12].

Thermal leptogenesis is described via the Lagrangian [cf. FY86; Ani+11]

$$\mathcal{L} = \mathcal{L}_{\text{SM}} + \bar{\nu}_{Ri} i \not{\partial} \nu_{Ri} + \bar{l}_{Li} \tilde{\phi} \lambda_{ij}^* \nu_{Rj} + \bar{\nu}_{Rj} \lambda_{ij} l_{Li} \phi - \frac{1}{2} M_{ij} (\bar{\nu}_{Ri}^c \nu_{Rj} + \bar{\nu}_{Rj} \nu_{Ri}^c) , \quad (2.6)$$

where the right-handed Majorana neutrinos are described via electroweak singlet fermions ν_{Ri} , $i = 1, 2, 3$, with a Majorana mass term M_{ij} coupling via Yukawa couplings λ_{ij} to the left-handed SM leptons l_{Li} and the Higgs doublet ϕ . One has $\nu_{Ri}^c = C \bar{\nu}_{Ri}^T$ with C being the charge conjugation matrix and $\tilde{\phi} = i\sigma^2 \phi^*$. Summation over i and j is implied.

The masses of the Majorana neutrinos M_i , $i = 1, 2, 3$, are given by the eigenvalues of the Majorana mass matrix corresponding to M_{ij} [cf. Di 12, p. 10]. As this thesis follows [Hüt13], which is based on [Ani+11] and [ABB11], the simplest case, where the masses are hierarchically ordered according to $M_{i>1} \gg M_1 =: M$ and assuming small Yukawa couplings $\lambda_{i1} \ll 1$ of the lightest heavy neutrino $N_1 =: N$, is considered. This enables one to integrate out the heavier neutrinos arriving at an effective Lagrangian [see BF00; Ani+11]

$$\begin{aligned} \mathcal{L} = & \mathcal{L}_{\text{SM}} + \frac{1}{2} \bar{N} i \not{\partial} N + \bar{l}_{Li} \tilde{\phi} \lambda_{i1}^* N + N^T \lambda_{i1} l_{Li} \phi - \frac{1}{2} M N^T C N \\ & + \frac{1}{2} \eta_{ij} l_{Li}^T \phi C l_{Lj} \phi + \frac{1}{2} \eta_{ij}^* \bar{l}_{Li} \tilde{\phi} C \bar{l}_{Lj}^T \tilde{\phi} \end{aligned} \quad (2.7)$$

with $N = \nu_{R1} + \nu_{R1}^C$ and the effective coupling

$$\eta_{ij} = \sum_{k>1} \lambda_{ik} \frac{1}{M_k} \lambda_{kj}^T . \quad (2.8)$$

This case has the advantage that instead of the CP-asymmetry being obtained by the interference of tree-level and one-loop graphs, it is obtained from a single one [see BF00] [as cited in Ani+11, p. 4]. The CP-violating factor ϵ is related to the decay widths of the heavy Majorana neutrino into l, ϕ and $\bar{l}, \bar{\phi}$ via [see BF00, p. 2]

$$\Gamma(N \rightarrow l\phi) = \frac{1}{2}(1 + \epsilon)\Gamma , \quad (2.9)$$

$$\Gamma(N \rightarrow \bar{l}\bar{\phi}) = \frac{1}{2}(1 - \epsilon)\Gamma , \quad (2.10)$$

where Γ is the total decay width and $\epsilon \ll 1$ is given by [see BF00, p. 11]

$$\epsilon = \frac{3}{16\pi} \frac{\text{Im}(\lambda^\dagger \eta \lambda^*)_{11}}{(\lambda^\dagger \lambda)_{11}} M . \quad (2.11)$$

The Feynman rules for this effective model [see Ani+11, pp. 45-46] are given in the appendix, Sec. A.2. The choices of M , ϵ , and $(\lambda^\dagger \lambda)_{11}$ for the numerical evaluations will be detailed in Ch. 7.

In most practical calculations, one uses Boltzmann equations to describe the evolution of the distribution functions of the heavy Majorana neutrino and leptons. These are used to calculate the lepton asymmetry. An overview of the calculation for the physical scenario used in this thesis is given in Sec. 4.2. As already mentioned, the lepton asymmetry is converted to a baryon asymmetry using SM sphaleron processes. Note that a fraction of

$$a_{\text{sph}} = 28/79 \quad (2.12)$$

of $N_B - N_L$ is converted into a baryon asymmetry via these processes [see KS88; HT90] [as cited in BDP05, p. 4], i.e.

$$N_B = a_{\text{sph}}(N_B - N_L) . \quad (2.13)$$

3. Nonequilibrium Quantum Field Theory

In this chapter, the basic concepts of nonequilibrium quantum field theory (QFT) necessary for the calculations in the context of this thesis are presented following [Ani+11, pp. 7-16] and [Hüt13, pp. 17-25]. As in these references, this chapter works in the real-time formalism [cf. Le 96]. However, the resummation of the Majorana neutrino self-energy is performed in the imaginary-time formalism [cf. Le 96] and then analytically continued to real times in Ch. 5.

3.1. Correlation Functions

In statistical thermodynamics, one uses a statistical ensemble with density matrix ρ to describe a thermodynamic system, thus having [see Ani+11, p. 7]

$$\langle \mathcal{A} \rangle = \text{Tr}(\rho \mathcal{A}) \quad (3.1)$$

as the expectation value for an operator \mathcal{A} with $\text{Tr} \rho = 1$. In order to know this expectation value for all times using this equation, one has to know the density matrix ρ for all times and thus solve the von Neumann or quantum Liouville equation of motion as an initial value problem [cf. Ani+11, p. 7]. This turns out to be difficult and only doable perturbatively with additional assumptions in most cases [cf. Ani+11, pp. 7-8]. Instead, one can solve the equations of motions for the correlation functions mapping infinitely many degrees of freedom of the initial density matrix on infinitely many initial conditions [see Ani+11, p. 8]. For a full treatment, one would have to know all n -point functions, but in the case considered here, one- and two-point functions are sufficient [see Ani+11, p. 8].

Since leptogenesis occurs at temperatures well above the electroweak scale, the SM is in its symmetric phase, i.e. the Higgs doublet with its four real degrees of freedom can be described by four massless real scalar fields [see Ani+11, p. 8].

For a real scalar field, one defines the spectral function and the statistical propagator Δ^- and Δ^+ via [see Ani+11, p. 8]

$$\Delta^-(x_1, x_2) = i \langle [\phi(x_1), \phi(x_2)] \rangle, \quad (3.2)$$

$$\Delta^+(x_1, x_2) = \frac{1}{2} \langle \{\phi(x_1), \phi(x_2)\} \rangle \quad (3.3)$$

with the symmetry relations

$$\Delta^-(x_1, x_2) = -\Delta^-(x_2, x_1), \quad (3.4)$$

$$\Delta^+(x_1, x_2) = \Delta^+(x_2, x_1), \quad (3.5)$$

where only contributions from connected diagrams should be included in the computation of the dressed correlation functions. The Wightman functions are defined via [see Ani+11, p. 90]

$$\Delta^>(x_1, x_2) = \langle \phi(x_1) \phi(x_2) \rangle, \quad (3.6)$$

$$\Delta^<(x_1, x_2) = \langle \phi(x_2) \phi(x_1) \rangle, \quad (3.7)$$

which give the relations

$$\Delta^-(x_1, x_2) = i(\Delta^>(x_1, x_2) - \Delta^<(x_1, x_2)) , \quad (3.8)$$

$$\Delta^+(x_1, x_2) = \frac{1}{2}(\Delta^>(x_1, x_2) + \Delta^<(x_1, x_2)) . \quad (3.9)$$

With microcausality and the condition for canonical quantization, i.e.

$$[\phi(x_1), \phi(x_2)]|_{t_1=t_2} = 0 , \quad (3.10)$$

$$[\dot{\phi}(x_1), \dot{\phi}(x_2)]|_{t_1=t_2} = 0 , \quad (3.11)$$

$$[\phi(x_1), \dot{\phi}(x_2)]|_{t_1=t_2} = i\delta(\mathbf{x}_1 - \mathbf{x}_2) , \quad (3.12)$$

one obtains the boundary conditions in $y = t_1 - t_2$ [see Ani+11, p. 9]

$$\Delta^-(x_1, x_2)|_{t_1=t_2} = 0 , \quad (3.13)$$

$$\partial_{t_1} \Delta^-(x_1, x_2)|_{t_1=t_2} = -\partial_{t_2} \Delta^-(x_1, x_2)|_{t_1=t_2} = \delta(\mathbf{x}_1 - \mathbf{x}_2) , \quad (3.14)$$

$$\partial_{t_1} \partial_{t_2} \Delta^-(x_1, x_2)|_{t_1=t_2} = 0 \quad (3.15)$$

for Δ^- .

In the Lagrangian in Eq. (2.7), one also has massless left-handed leptons denoted by Weyl-fields l_{Li} . They can be considered to be massless because of the high temperatures. Their spectral function and statistical propagator are defined by

$$(S_{Lij}^-)_{\alpha\beta}(x_1, x_2) = i\langle \{l_{Li\alpha}(x_1), \bar{l}_{Lj\beta}(x_2)\} \rangle , \quad (3.16)$$

$$(S_{Lij}^+)_{\alpha\beta}(x_1, x_2) = \frac{1}{2}\langle [l_{Li\alpha}(x_1), \bar{l}_{Lj\beta}(x_2)] \rangle , \quad (3.17)$$

where α and β are spin indices, SU(2) indices have been suppressed, and the subscript L denotes the projection of the propagators for Dirac fermions S^\pm to left-handed fields via $S_L^\pm = P_L S^\pm$ [see Ani+11, p. 9]. The following properties also hold for the propagators of the Dirac fermions. One again has the Wightman functions with their relations to S_L^\pm [see Ani+11, pp. 9-10]

$$(S_{Lij}^>)_{\alpha\beta}(x_1, x_2) = \langle l_{Li\alpha}(x_1) \bar{l}_{Lj\beta}(x_2) \rangle , \quad (3.18)$$

$$(S_{Lij}^<)_{\alpha\beta}(x_1, x_2) = -\langle \bar{l}_{Lj\beta}(x_2) l_{Li\alpha}(x_1) \rangle , \quad (3.19)$$

$$S_{Lij}^-(x_1, x_2) = i(S_{Lij}^>(x_1, x_2) - S_{Lij}^<(x_1, x_2)) , \quad (3.20)$$

$$S_{Lij}^+(x_1, x_2) = \frac{1}{2}(S_{Lij}^>(x_1, x_2) + S_{Lij}^<(x_1, x_2)) . \quad (3.21)$$

The propagators have the symmetry properties [see Ani+11, p. 10]

$$\gamma^0 [S_{Lij}^-(x_1, x_2)]^\dagger \gamma^0 = -S_{Lji}^-(x_2, x_1) , \quad (3.22)$$

$$\gamma^0 [S_{Lij}^+(x_1, x_2)]^\dagger \gamma^0 = S_{Lji}^+(x_2, x_1) . \quad (3.23)$$

Using the canonical quantization condition

$$\{l_{Li\alpha}(x_1), l_{Lj\beta}^\dagger(x_2)\} = P_{L\alpha\beta} \delta_{ij} \delta(\mathbf{x}_1 - \mathbf{x}_2) \quad (3.24)$$

one obtains the boundary condition [see Ani+11, p. 10]

$$S_{Lij}^-(x_1, x_2)|_{t_1=t_2} = iP_L \delta_{ij} \delta(\mathbf{x}_1 - \mathbf{x}_2) . \quad (3.25)$$

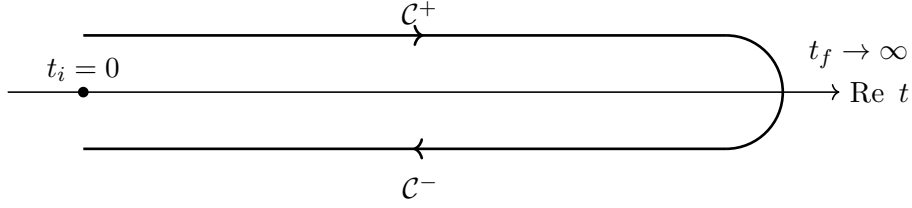


Figure 3.1.: Contour \mathcal{C} in the complex time plane for nonequilibrium Green's functions, i.e. propagators, from [Hüt13, p. 20]. It runs from $t_i + i\epsilon$ parallel to the real time axis to $t_f + i\epsilon$, goes to $t_f - i\epsilon$, and then back again to $t_i - i\epsilon$ parallel to the real time axis. For physical correlation functions for $t > t_i$, one has to take the limits $t_f \rightarrow \infty$ and $\epsilon \rightarrow 0$, whereas t_i is arbitrary and may be set to 0.

For the Majorana neutrino field N , one has the spectral function and statistical propagator [see Ani+11, p. 10]

$$G_{\alpha\beta}^-(x_1, x_2) = i\langle\{N_\alpha(x_1), N_\beta(x_2)\}\rangle, \quad (3.26)$$

$$G_{\alpha\beta}^+(x_1, x_2) = \frac{1}{2}\langle[N_\alpha(x_1), N_\beta(x_2)]\rangle. \quad (3.27)$$

The Wightman functions and the relations to the propagators are given by [see Ani+11, p. 10]

$$G_{\alpha\beta}^>(x_1, x_2) = \langle N_\alpha(x_1)N_\beta(x_2)\rangle, \quad (3.28)$$

$$G_{\alpha\beta}^<(x_1, x_2) = -\langle N_\beta(x_2)N_\alpha(x_1)\rangle, \quad (3.29)$$

$$G^-(x_1, x_2) = i(G^>(x_1, x_2) - G^<(x_1, x_2)), \quad (3.30)$$

$$G^+(x_1, x_2) = \frac{1}{2}(G^>(x_1, x_2) + G^<(x_1, x_2)). \quad (3.31)$$

The propagators have the symmetry properties [see Ani+11, p. 10]

$$G^-(x_1, x_2) = G^-(x_2, x_1)^T, \quad (3.32)$$

$$G^+(x_1, x_2) = -G^+(x_2, x_1)^T. \quad (3.33)$$

With the canonical quantization condition and the Majorana property $N = CN^T$, one obtains the boundary condition [see Ani+11, p. 10]

$$G^-(x_1, x_2)|_{t_1=t_2} = i\gamma^0\delta(\mathbf{x}_1 - \mathbf{x}_2)C^{-1}. \quad (3.34)$$

The Feynman rules are given in the appendix, Sec. A.2.

3.2. Kadanoff-Baym Equations for the Majorana Neutrino

In order to create a matter-antimatter asymmetry, deviation from thermal equilibrium is needed. In thermal leptogenesis, this is obtained via the out-of-equilibrium decay of heavy Majorana neutrinos [cf. FY86]. Therefore, the equations of motion for their correlation functions G^\pm are needed for a description from first principles. They can be found via the Keldysh-Schwinger formalism [cf. Kel64; Sch61] [as cited in Ani+11, p. 11]. This

formalism works with the Green's function with time arguments on the contour \mathcal{C} in the complex x^0 -plane, which is called the Keldysh contour, cf. Fig. 3.1, [see Ani+11, p. 11]

$$G_{\mathcal{C}}(x_1, x_2) = \theta_{\mathcal{C}}(x_1^0, x_2^0)G^>(x_1, x_2) + \theta_{\mathcal{C}}(x_2^0, x_1^0)G^<(x_1, x_2) , \quad (3.35)$$

where the $\theta_{\mathcal{C}}$ -functions (Heaviside step functions) follow the path ordering along the contour \mathcal{C} . One has to work with this contour due to the initial problem nature of nonequilibrium processes, i.e. the fact that only the initial and not later states of the system are known [see Ani+11, p. 11]. Therefore, the standard procedure for the definition of a S-matrix, which works with sending initial and final times to negative and positive infinity, cannot be used [see Ani+11, p. 11]. Instead, one starts and ends at the same time t_i ¹ and knowledge of the state of the system at $t = \pm\infty$ is not needed during the calculation of correlation functions [see Ani+11, p. 11].

The equation of motion for $G_{\mathcal{C}}$ is the Schwinger-Dyson equation [see Ani+11, p. 11]

$$C(i\cancel{\partial}_1 - M)G_{\mathcal{C}}(x_1, x_2) - i \int_{\mathcal{C}} d^4x' C\Sigma_{\mathcal{C}}(x_1, x')G_{\mathcal{C}}(x', x_2) = i\delta_{\mathcal{C}}(x_1 - x_2) , \quad (3.36)$$

where $C\Sigma_{\mathcal{C}}(x_1, x')$ is the self-energy, with the charge conjugation matrix C factored out for convenience in the calculations following [Ani+11, p. 11], and $\cancel{\partial}_1 = \gamma^\mu \partial / \partial x_1^\mu$. Analogously to the Green's function, one has for the self-energy

$$\Sigma_{\mathcal{C}}(x_1, x_2) = \theta_{\mathcal{C}}(x_1^0, x_2^0)\Sigma^>(x_1, x_2) + \theta_{\mathcal{C}}(x_2^0, x_1^0)\Sigma^<(x_1, x_2) . \quad (3.37)$$

Since the time coordinates of $G_{\mathcal{C}}$ and $\Sigma_{\mathcal{C}}$ can lie on the upper or lower branch of \mathcal{C} , i.e. \mathcal{C}^+ or \mathcal{C}^- , it is useful to rewrite the Green's function and the self-energy as (2×2) -matrices with entries G^{ij} and Σ^{ij} , where the first and second indices refer to the first and second time arguments, respectively, and an index equal to 1 and 2 refer to the time argument being on the upper and lower branch of \mathcal{C} , respectively. Therefore, the time-ordered Feynman propagator corresponds to G^{11} . In total, the components for the propagator are [see Ani+11, p. 12]

$$G^{12}(x_1, x_2) = G^<(x_1, x_2) , \quad (3.38)$$

$$G^{21}(x_1, x_2) = G^>(x_1, x_2) , \quad (3.39)$$

$$G^{11}(x_1, x_2) = G^+(x_1, x_2) - \frac{i}{2} \text{sign}(x_1^0 - x_2^0)G^-(x_1, x_2) , \quad (3.40)$$

$$G^{22}(x_1, x_2) = G^+(x_1, x_2) + \frac{i}{2} \text{sign}(x_1^0 - x_2^0)G^-(x_1, x_2) . \quad (3.41)$$

The self-energy components Σ^{ij} are analogous to these with Σ^{\lessgtr} being defined accordingly [see Ani+11, p. 12]. Analogously to Eqs. (3.30) and (3.31), the self-energies Σ^{\pm} fulfill the relations

$$\Sigma^-(x_1, x_2) = i(\Sigma^>(x_1, x_2) - \Sigma^<(x_1, x_2)) , \quad (3.42)$$

$$\Sigma^+(x_1, x_2) = \frac{1}{2}(\Sigma^>(x_1, x_2) + \Sigma^<(x_1, x_2)) . \quad (3.43)$$

When dealing with perturbative expansions of the Schwinger-Dyson equation (3.36) using Feynman diagrams, one has to respect that time arguments of internal vertices can lie on either branch of the Keldysh contour ("doubling of degrees of freedom"), where each time

¹This formalism is therefore sometimes called "in-in" formalism as opposed to the name "in-out" formalism for the S-matrix [see Ani+11, p. 11].

argument on the lower branch gives an additional factor -1 [see Ani+11, p. 12]. Vertices with time arguments on either branch are connected with the corresponding propagators G^{ij} [see Ani+11, p. 12].

With the relations for G^{ij} and Σ^{ij} , one may rewrite the Schwinger-Dyson equation (3.36) into two coupled integro-differential equations for G^\pm , which are called Kadanoff-Baym equations (KBEs) [KB62] [see Ani+11, p. 12]. In the context of this thesis, spatial homogeneity may be assumed. Therefore, the spatial dependence of the propagator and the self-energy is only on the difference $\mathbf{x}_1 - \mathbf{x}_2$. Using the definitions of the spatial Fourier transforms

$$G_{\mathbf{p}}^\pm(t_1, t_2) = \int d^3x e^{-i\mathbf{p}\mathbf{x}} G^\pm(t_1, \mathbf{x}_1, t_2, \mathbf{x}_1 - \mathbf{x}), \quad (3.44)$$

$$\Sigma_{\mathbf{p}}^\pm(t_1, t_2) = \int d^3x e^{-i\mathbf{p}\mathbf{x}} \Sigma^\pm(t_1, \mathbf{x}_1, t_2, \mathbf{x}_1 - \mathbf{x}), \quad (3.45)$$

one can consider each Fourier mode of the KBEs separately and obtains [see Ani+11, pp. 12-13]

$$C(i\gamma^0 \partial_{t_1} - \mathbf{p}\boldsymbol{\gamma} - M)G_{\mathbf{p}}^-(t_1, t_2) = - \int_{t_1}^{t_2} dt' C\Sigma_{\mathbf{p}}^-(t_1, t')G_{\mathbf{p}}^-(t', t_2), \quad (3.46)$$

$$C(i\gamma^0 \partial_{t_1} - \mathbf{p}\boldsymbol{\gamma} - M)G_{\mathbf{p}}^+(t_1, t_2) = - \int_{t_i}^{t_2} dt' C\Sigma_{\mathbf{p}}^+(t_1, t')G_{\mathbf{p}}^-(t', t_2) \\ - \int_{t_i}^{t_1} dt' C\Sigma_{\mathbf{p}}^-(t_1, t')G_{\mathbf{p}}^+(t', t_2). \quad (3.47)$$

One can also derive the KBEs for the lepton propagators $S_{L\mathbf{k}}^\pm$ and find that they fulfill analogous equations with the exchange of $C\Sigma_{\mathbf{p}}^\pm$ by the lepton self-energies $\Pi_{\mathbf{k}}^\pm$, no charge conjugation matrix C on the left hand sides in front of the kinetic term, and $M = 0$ [see Ani+11, pp. 13, 25-26].

Note that the KBEs are exact and contain all quantum and non-Markovian effects [cf. Ani+11, p. 13]. Also, it is worth remarking that in nonequilibrium QFT, the state of the system is characterized by correlation and not distribution functions, while interactions enter through the self-energies [cf. Ani+11, p. 13]. All processes that can occur can be recovered from the self-energies using generalized cutting rules [cf. Ani+11, p. 13].

3.3. Propagators

As detailed in [Ani+11, p. 13], one may assume for the solution of the KBEs (3.46) and (3.47) for the Majorana neutrino that there is one field (N) out of equilibrium in a thermal bath of SM fields (SM plasma). This is due to the smallness of the SM equilibration time $\tau_{\text{SM}} \sim 1/(g^2T)$, where g is any SM coupling, at temperatures $T \sim M$ compared to the Majorana neutrino equilibration time $\tau_N \sim 1/(\lambda^2T)$ giving the timescale of the generation of the lepton asymmetry [see Ani+11, p. 13]. Hence, backreactions from the plasma can be neglected. This enables one to solve the KBEs for the Majorana neutrino propagator using the equilibrium lepton and Higgs boson propagators to obtain a leading order solution [see Ani+11, p. 16]. Using the solutions G^\pm , one can then investigate lepton number changing processes in the thermal bath by solving the KBEs for the lepton propagator focusing on the CP violating interactions. However, for this one has to consider the finite equilibration time of the plasma and therefore possible contributions from the Higgs boson and lepton fields being out of equilibrium, cf. Ch. 4.3.

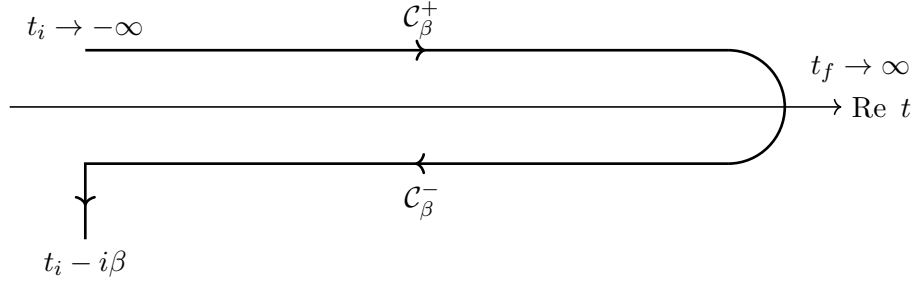


Figure 3.2.: Contour \mathcal{C}_β in the complex time plane for equilibrium Green's functions, i.e. propagators, from [Hüt13, p. 24].

Due to spatial homogeneity, equilibrium correlation functions only depend on space-time differences and it is useful to consider the Fourier transforms

$$\Delta_{\mathbf{q}}^\pm(\omega) = \int d^4x e^{i(\omega x^0 - \mathbf{q}\mathbf{x})} \Delta^\pm(x), \quad (3.48)$$

$$S_{\mathbf{k}}^\pm(\omega) = \int d^4x e^{i(\omega x^0 - \mathbf{k}\mathbf{x})} S^\pm(x). \quad (3.49)$$

The Higgs boson and lepton propagators fulfill the Kubo-Martin-Schwinger relations [cf. Le 96, p. 25], [see Ani+11, p. 15],

$$\Delta_{\mathbf{q}}^<(\omega) = e^{-\beta\omega} \Delta_{\mathbf{q}}^>(\omega), \quad (3.50)$$

$$S_{\mathbf{k}}^<(\omega) = -e^{-\beta\omega} S_{\mathbf{k}}^>(\omega), \quad (3.51)$$

which imply that [see Ani+11, p. 15]

$$\Delta_{\mathbf{q}}^+(\omega) = -i \left(\frac{1}{2} + f_B(\omega) \right) \Delta_{\mathbf{q}}^-(\omega) = -\frac{i}{2} \coth \left(\frac{\beta\omega}{2} \right) \Delta_{\mathbf{q}}^-(\omega), \quad (3.52)$$

$$S_{\mathbf{k}}^+(\omega) = -i \left(\frac{1}{2} - f_F(\omega) \right) S_{\mathbf{k}}^-(\omega) = -\frac{i}{2} \tanh \left(\frac{\beta\omega}{2} \right) S_{\mathbf{k}}^-(\omega), \quad (3.53)$$

where

$$f_B(\omega) = \frac{1}{e^{\beta\omega} - 1}, \quad (3.54)$$

$$f_F(\omega) = \frac{1}{e^{\beta\omega} + 1} \quad (3.55)$$

are the Bose-Einstein and Fermi-Dirac distribution functions, $\beta = 1/T$ is the inverse temperature of the SM plasma, and ω can be off-shell.

The equilibrium propagators can be calculated in the real-time formalism using the contour \mathcal{C}_β shown in Fig. 3.2. For the lepton (S) and Higgs boson (Δ) fields, this calculation gives [see Ani+11, pp. 15, 43-44] [as cited in Hüt13, p. 24]

$$\Delta_{\mathbf{q}}^-(y) = \frac{1}{q} \sin(qy), \quad (3.56)$$

$$\Delta_{\mathbf{q}}^+(y) = \frac{1}{2q} \coth \left(\frac{\beta q}{2} \right) \cos(qy), \quad (3.57)$$

$$S_{\mathbf{k}}^-(y) = i\gamma^0 \cos(ky) - \frac{\mathbf{k}\boldsymbol{\gamma}}{k} \sin(ky), \quad (3.58)$$

$$S_{\mathbf{k}}^+(y) = -\frac{1}{2} \tanh \left(\frac{\beta k}{2} \right) \left(i\gamma^0 \sin(ky) + \frac{\mathbf{k}\boldsymbol{\gamma}}{k} \cos(ky) \right), \quad (3.59)$$

where $q = |\mathbf{q}|$, $k = |\mathbf{k}|$, and the time-variable has not been Fourier-transformed. The relations from Sec. 3.1 give the other propagators. Note that without Fourier transformations and before implementing the fact that the propagators only depend on space-time differences, analogously to the Keldysh contour in Fig. 3.1 also in the contour \mathcal{C}_β , the time arguments can lie on either \mathcal{C}_β^+ or \mathcal{C}_β^- . Hence, one has components depending on the position of the time arguments on the contour analogously to the Majorana propagator (P represents Δ or S)

$$P^{12}(x_1, x_2) = P^<(x_1, x_2), \quad (3.60)$$

$$P^{21}(x_1, x_2) = P^>(x_1, x_2), \quad (3.61)$$

$$P^{11}(x_1, x_2) = P^+(x_1, x_2) - \frac{i}{2} \text{sign}(x_1^0 - x_2^0) P^-(x_1, x_2), \quad (3.62)$$

$$P^{22}(x_1, x_2) = P^+(x_1, x_2) + \frac{i}{2} \text{sign}(x_1^0 - x_2^0) P^-(x_1, x_2). \quad (3.63)$$

Using the time-translation invariance of the diagrams contributing to the Majorana neutrino self-energy, the spectral propagator of the Majorana neutrino only depends on the time difference, i.e. $G_{\mathbf{p}}^-(t_1, t_2) \rightarrow G_{\mathbf{p}}^-(y)$ with $y = t_1 - t_2$ [see Ani+09] [as cited in Ani+11, pp. 16-17]. This enables one to find the general solution of the KBEs (3.46) and (3.46) for small coupling $\lambda \ll 1$, which implies a small width $\Gamma_{\mathbf{p}} \ll M$, in the Breit-Wigner approximation [see Ani+11, pp. 17-24] [as cited in Hüt13, p. 24]

$$G_{\mathbf{p}}^-(y) = \left(i\gamma^0 \cos(\omega_{\mathbf{p}}y) + \frac{M - \mathbf{p}\gamma}{\omega_{\mathbf{p}}} \sin(\omega_{\mathbf{p}}y) \right) e^{-\Gamma_{\mathbf{p}}|y|/2} C^{-1}, \quad (3.64)$$

$$\begin{aligned} G_{\mathbf{p}}^+(t_1, t_2) = & - \left(i\gamma^0 \sin(\omega_{\mathbf{p}}y) - \frac{m - \mathbf{p}\gamma}{\omega_{\mathbf{p}}} \cos(\omega_{\mathbf{p}}y) \right) \\ & \times \left[\frac{1}{2} \tanh\left(\frac{\beta\omega_{\mathbf{p}}}{2}\right) e^{-\Gamma_{\mathbf{p}}|y|/2} + f_N^{\text{eq}}(\omega_{\mathbf{p}}) e^{-\Gamma_{\mathbf{p}}t} \right] C^{-1}, \end{aligned} \quad (3.65)$$

where the width $\Gamma_{\mathbf{p}} = \Gamma_{\mathbf{p}}(\omega_{\mathbf{p}})$ will be discussed later, $t = (t_1 + t_2)/2$, and $f_N^{\text{eq}}(\omega_{\mathbf{p}}) = f_F(\omega_{\mathbf{p}})$. The KMS relation as well as the choice $t_i = 0$ were used in order to obtain the second equation [see Hüt13, pp. 24-25]. Note that its time dependence is not only on y .

3.3.1. Connection Between the Majorana Neutrino Self-Energy and its Thermal Width

In the derivation of the nonequilibrium Majorana propagator in [Ani+11], the width $\Gamma_{\mathbf{p}}$ is connected to the Majorana self-energy. Explicitly, the retarded Majorana self-energy is given by [see Ani+11, pp. 17-18]

$$\Sigma^{\text{ret}}(p) = \tilde{\Sigma}^-(-ip^0 + 0^+, \mathbf{p}) = i \text{P.V.} \int_{-\infty}^{\infty} \frac{d\omega}{2\pi} \frac{\Sigma^-(\omega, \mathbf{p})}{p^0 - \omega} + \frac{1}{2} \Sigma^-(p), \quad (3.66)$$

where $\Sigma^-(p)$ is considered to be purely imaginary, since the real part is negligible due to the smallness of the Yukawa coupling of the Majorana neutrino [cf. Ani+11, pp. 18-19], and P.V. denotes the Cauchy principal value. Therefore, one finds

$$\text{Im} \Sigma^{\text{ret}}(p) = \frac{1}{2i} \Sigma^-(p), \quad (3.67)$$

where the real and imaginary part of a matrix $A \in \mathbb{C}^{n \times n}$ is defined via

$$\operatorname{Re} A = \frac{A + A^\dagger}{2}, \quad (3.68)$$

$$\operatorname{Im} A = \frac{A - A^\dagger}{2i}. \quad (3.69)$$

Due to the high temperatures in the thermal bath, the lepton and the Higgs boson are massless. This implies that the Majorana neutrino self-energy is a pure vector in Lorentz space [see MQF99] [as cited in Men10, p. 45], i.e.

$$\Sigma^-(p) = c_{\mathbf{p}}(p^0)\not{p} + d_{\mathbf{p}}(p^0)\not{u}, \quad (3.70)$$

where u is the four-velocity of the plasma. Note that thermal masses do not change this, since they give a term $\sim \gamma^0$ in the lepton propagator, whereas the thermal mass in the scalar propagator cannot change the Dirac structure. This will become more clear in Ch. 5. In the plasma rest-frame, one has $u = (1, \mathbf{0})$, which implies that one can rewrite this relation according to [cf. Ani+11, p. 19]

$$\Sigma^-(p) = ia_{\mathbf{p}}(p^0)\gamma^0 + ib_{\mathbf{p}}(p^0)\mathbf{p}\boldsymbol{\gamma}. \quad (3.71)$$

Therefore, this relation holds not only in the one-loop case considered in [Ani+11], but in general. In the imaginary time formalism, as it will be used in Ch. 5, the relation (3.71) directly follows from the rotational invariance of the self-energy [Wel82]. During the calculation of the spectral density $\rho_{\mathbf{p}}(\omega)$, which is done in [Ani+11, p. 19] and only uses Eq. (3.71) for the self-energy, one then finds [see Ani+11, p. 20]

$$p^0\Gamma_{\mathbf{p}}(p^0) = p^0a_{\mathbf{p}}(p^0) + \mathbf{p}^2b_{\mathbf{p}}(p^0). \quad (3.72)$$

This gives

$$\begin{aligned} \operatorname{Tr}[\not{p}\operatorname{Im}\Sigma^{\operatorname{ret}}(p)] &= \frac{1}{2i}\operatorname{Tr}[\not{p}\Sigma^-(p)] \\ &= 2[p^0a_{\mathbf{p}}(p^0) + \mathbf{p}^2b_{\mathbf{p}}(p^0)] = 2p^0\Gamma_{\mathbf{p}}(p^0) \end{aligned}$$

and therefore

$$\Gamma_{\mathbf{p}}(p^0) = \frac{1}{2p^0}\operatorname{Tr}[\not{p}\operatorname{Im}\Sigma^{\operatorname{ret}}(p)]. \quad (3.73)$$

During the calculation of the nonequilibrium Majorana neutrino propagator, the Breit-Wigner approximation then gives the constraint to on-shell $\omega = \omega_{\mathbf{p}}$. Therefore, whenever the argument p^0 is omitted, $\Gamma_{\mathbf{p}} = \Gamma_{\mathbf{p}}(\omega_{\mathbf{p}})$ is meant. In this thesis, a resummed width including gauge corrections is used². Still, one should cite the on-shell one-loop result for the width from [Ani+11, p. 20], which is given by

$$\Gamma_{\mathbf{p}}(\omega_{\mathbf{p}}) = (\lambda^\dagger\lambda)_{11}\frac{2}{\omega_{\mathbf{p}}}\int\frac{d^3q}{(2\pi)^32q}\int\frac{d^3k}{(2\pi)^32k}p \cdot k f_{l\phi}(k, q)(2\pi)^4\delta^{(4)}(p - k - q), \quad (3.74)$$

where

$$f_{l\phi}(k, q) := 1 - f_F(k) + f_B(q) \quad (3.75)$$

and the lepton and Higgs have been assumed to be massless. Note that q and k both mean the absolute value of the three-momentum as well as the four-momentum. However, it is clear from context, which one is meant ($p \cdot k := p_\mu k^\mu$).

The form of Eq. (3.73) is needed in order to implement the resummation scheme for the inclusion of gauge corrections in the same manner as in [ABB11] in Ch. 5.

²Note that this is not in conflict with the derivation of the non-equilibrium Majorana propagator, since this only assumes the form Eq. (3.73) and $\Gamma_{\mathbf{p}} \ll M$, which still holds.

4. Boltzmann and Kadanoff-Baym Calculations for the Lepton Asymmetry

In this chapter, the calculations for the lepton asymmetry are presented. First, the resulting asymmetry from the solution of the Boltzmann equations is discussed. Afterwards, as it is necessary for a complete "theory of leptogenesis" [see Buc01, p. 10] [as cited in Ani+11, p. 42] to know the result from a calculation from first principles [cf. Ani+11], a calculation of the lepton asymmetry using the KBEs (3.46) and (3.47) from [Ani+11] is presented.

4.1. Physical Scenario

A standard leptogenesis scenario solved using Boltzmann equations is depicted in Fig. 4.1, where the time evolution of the heavy Majorana neutrino abundance N_{N_1} and the lepton asymmetry N_{B-L} is depicted with $z = M/T$ as time variable for thermal and zero initial Majorana neutrino abundance. The choice of z as time variable is possible due to the fact that the Hubble expansion gives a cooling (and possibly also departure from thermal equilibrium) and therefore, with increasing time the temperature decreases. For thermal initial abundance, the Hubble expansion causes the Majorana neutrino abundance to be larger than the equilibrium abundance at $T \approx 0.3M$ and shortly afterwards, the lepton asymmetry is "frozen in" because washout processes are not in equilibrium anymore [see Ani+11, pp. 3-4]. For zero initial Majorana neutrino abundance, interactions with the SM particles bring the Majorana neutrino in equilibrium whilst generating an initial lepton asymmetry because of the departure from thermal equilibrium. The initial asymmetry is washed out and at $T \approx 0.3M$, the final asymmetry is generated, which has about the same size as the initial asymmetry [see Ani+11, p. 4].

Following [Ani+11], this thesis uses the second scenario with zero initial Majorana neutrino abundance and concentrates on the initial asymmetry. For the generation of this asymmetry, the change in temperature due to the Hubble expansion of the universe and washout terms can be neglected [see Ani+11, p. 4]. In the context of this thesis, the effect of soft and hard gauge corrections on the generated lepton asymmetry are studied using the calculation from [Hüt13] with some modifications. These corrections are expected to be important for $T \gtrsim M$ [cf. Giu+04; KPT10; ABB11] [as cited in Ani+11, p. 4], where also thermal masses of the lepton and Higgs boson are relevant. Hence, it is instructive to consider the generation of the initial asymmetry as in [Ani+11], but at higher (constant) temperatures to estimate the effect of gauge corrections. Therefore, the result from [Ani+11] can be used as a starting point.

Summarizing, the physical scenario studied in the context of this thesis starts with zero heavy Majorana neutrino abundance, i.e. vacuum initial conditions, in a thermal bath of SM particles in equilibrium with constant temperature T . The interactions with the thermal bath then bring the Majorana neutrino in equilibrium whilst generating a lepton asymmetry, the initial asymmetry in Fig. 4.1.

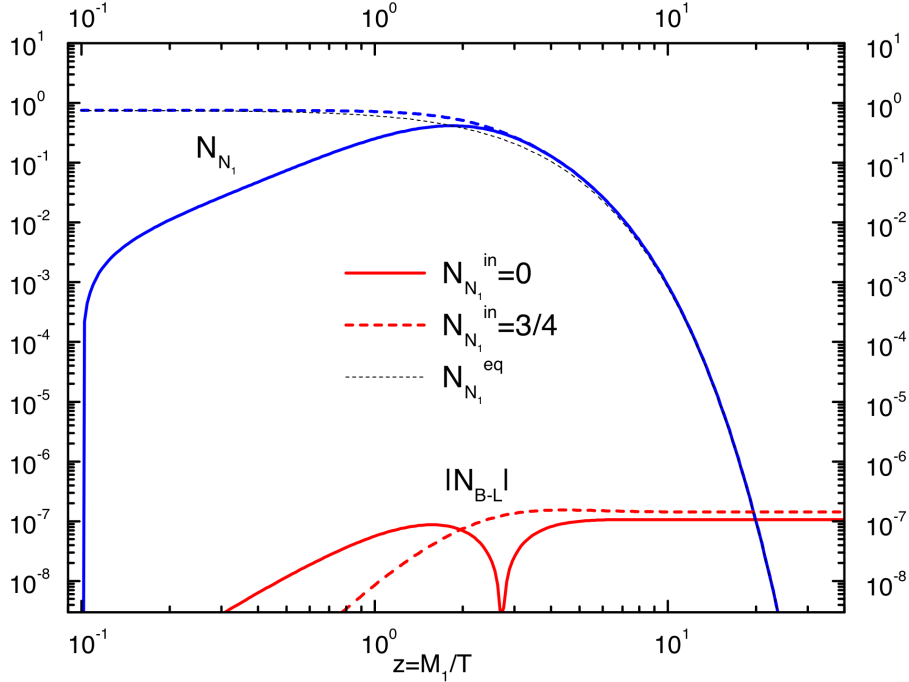


Figure 4.1.: Heavy Majorana neutrino abundance N_{N_1} and lepton asymmetry $N_{B-L} = N_B - N_L$, since N_L is changed by leptogenesis, evolution for typical leptogenesis parameters $M = M_1 = 10^{10}$ GeV, $\tilde{m}_1 = 8\pi\Gamma_1(v_{ew}/M_1)^2 = 10^{-3}$ eV, $\epsilon = 10^{-6}$. Dashed and full lines represent thermal and vacuum initial heavy Majorana neutrino abundance, respectively, whereas the dotted line is the equilibrium abundance at each z . From [BDP02, p. 22] [as cited in Ani+11, p. 3].

4.2. Boltzmann Calculation

For a discussion of the well-known Boltzmann equations for a heavy Majorana neutrino, a lepton, and a Higgs doublet see [HPW09]. Neglecting the Hubble expansion and washout terms and working at constant temperature of the SM plasma, one finds for the distribution function of heavy Majorana neutrinos in the physical scenario of interest [see Ani+11, p. 5]

$$\begin{aligned} \frac{\partial}{\partial t} f_N(t, \omega_{\mathbf{p}}) = & -\frac{2}{\omega_{\mathbf{p}}} \int \frac{d^3k}{(2\pi)^3 2k} \int \frac{d^3q}{(2\pi)^3 2q} (2\pi)^4 \delta^4(k+q-p) (\lambda^\dagger \lambda)_{11p} \cdot k \\ & \times [f_N(t, \omega_{\mathbf{p}})(1 - f_l(k))(1 + f_\phi(q)) - f_l(k)f_\phi(q)(1 - f_N(t, \omega_{\mathbf{p}}))], \end{aligned} \quad (4.1)$$

where $\omega_{\mathbf{p}} = \sqrt{M^2 + \mathbf{p}^2}$, k , and q are the energies of N , l , and ϕ^1 , respectively, $f_l(k) \equiv f_F(k)$ and $f_\phi(q) \equiv f_B(q)$ are the equilibrium distribution functions of the indexed fields, and the averaged decay matrix element is $|\mathcal{M}(N(p) \rightarrow l(k)\phi(q))|^2 = 2(\lambda^\dagger \lambda)_{11p} \cdot k$ [cf. BF00] [as cited in Ani+11, p. 5]. The number density of heavy Majorana neutrinos is then given by [see Ani+11, pp. 5-6]

$$n_N(t) = \int \frac{d^3p}{(2\pi)^3} f_N(t, \omega_{\mathbf{p}}) \quad (4.2)$$

with the assumption of kinetic equilibrium. This number density corresponds to the comoving number density N_{N_1} from Fig. 4.1 [see Ani+11, p. 7]. Using the vacuum initial

¹The lepton and Higgs boson are assumed to be massless.

condition $f_N(0, \omega_{\mathbf{p}}) \equiv 0$, one finds for the solution of the Boltzmann equation (4.1)

$$f_N(t, \omega_{\mathbf{p}}) = f_N^{\text{eq}}(\omega_{\mathbf{p}})(1 - e^{-\Gamma_{\mathbf{p}}t}), \quad (4.3)$$

where $f_N^{\text{eq}}(\omega_{\mathbf{p}}) \equiv f_F(\omega_{\mathbf{p}})$ is the Majorana neutrino equilibrium distribution function and $\Gamma_{\mathbf{p}}$ is the sum of decay and inverse decay widths [cf. Wel83] [as cited in Ani+11, p. 6] given by Eq. (3.74), i.e. the thermal width. Note that even though this solution is given only for neglecting the momentum dependence of $\Gamma_{\mathbf{p}}$ in [Ani+11], it also holds for the momentum-dependent $\Gamma_{\mathbf{p}}$ from Eq. (3.74).

In order to compute the lepton asymmetry, the Boltzmann equation for the lepton distribution function is needed, which is given by

$$\begin{aligned} \frac{\partial}{\partial t} f_l(t, k) = & -\frac{1}{2k} \int \frac{d^3q}{(2\pi)^3 2q} \int \frac{d^3p}{(2\pi)^3 2\omega_{\mathbf{p}}} (2\pi)^4 \delta^4(k + q - p) \\ & \times [|\mathcal{M}(l(k)\phi(q) \rightarrow N(p))|^2 f_l(k) f_\phi(q) (1 - f_N(t, \omega_{\mathbf{p}})) \\ & - |\mathcal{M}(N(p) \rightarrow l(k)\phi(q))|^2 f_N(t, \omega_{\mathbf{p}}) (1 - f_l(k)) (1 + f_\phi(q))] , \end{aligned} \quad (4.4)$$

where $\mathcal{O}(\lambda^4)$ corrections to the matrix elements have to be kept [cf. Ani+11, p. 6]. Note that l here can stand for either a lepton or anti-lepton of i -th family, i.e. l_i or \bar{l}_i . The distribution function for the lepton asymmetry is defined via

$$f_{Li}(t, k) = f_{l_i}(t, k) - f_{\bar{l}_i}(t, k). \quad (4.5)$$

With the initial condition $f_{Li}(0, k) = 0$ one finds using Eq. (4.3) [see Ani+11, pp. 6-7]

$$\begin{aligned} f_{Li}(t, k) = & -\epsilon_{ii} \frac{1}{2k} \int \frac{d^3q}{(2\pi)^3 2q} \int \frac{d^3p}{(2\pi)^3 2\omega_{\mathbf{p}}} (2\pi)^4 \delta^4(k + q - p) p \cdot k \\ & \times f_{l\phi}(k, q) f_N^{\text{eq}}(\omega_{\mathbf{p}}) \frac{1 - e^{-\Gamma_{\mathbf{p}}t}}{\Gamma_{\mathbf{p}}} \end{aligned} \quad (4.6)$$

with $f_{l\phi}$ according to Eq. (3.75) and the definition

$$\epsilon_{ij} = \frac{3}{16\pi} \text{Im}(\lambda_{i1}^* (\eta \lambda^*)_{j1}) M. \quad (4.7)$$

After summation over all lepton flavors, the generated lepton asymmetry is thus proportional to the CP-asymmetry [see BF00, p. 11] [as cited in Ani+11, p. 7]

$$\epsilon = \sum_i \frac{\epsilon_{ii}}{(\lambda^\dagger \lambda)_{11}} = \frac{3}{16\pi} \frac{\text{Im}(\lambda^\dagger \eta \lambda^*)_{11} M}{(\lambda^\dagger \lambda)_{11}}. \quad (4.8)$$

For easier comparison to the solutions of the Kadanoff-Baym equations, it is useful to rewrite Eq. (4.6) as

$$\begin{aligned} f_{Li}(t, k) = & -\epsilon_{ii} \frac{32\pi}{k} \int \frac{d^3q}{(2\pi)^3 2q} \int \frac{d^3p}{(2\pi)^3 2\omega_{\mathbf{p}}} \int \frac{d^3q'}{(2\pi)^3 2q'} \int \frac{d^3k'}{(2\pi)^3 2k'} \\ & \times k \cdot k' (2\pi)^4 \delta^4(k + q - p) (2\pi)^4 \delta^4(k' + q' - p) \\ & \times f_{l\phi}(k, q) f_N^{\text{eq}}(\omega_{\mathbf{p}}) \frac{1 - e^{-\Gamma_{\mathbf{p}}t}}{\Gamma_{\mathbf{p}}} \end{aligned} \quad (4.9)$$

so that the integrand is proportional to the averaged matrix element $|\mathcal{M}(l(k)\phi(q) \rightarrow \bar{l}(k')\bar{\phi}(q'))|^2 = 2k \cdot k' (\lambda^\dagger \lambda)_{11} / M^2$ [see BF00, p. 11] [as cited in Ani+11, p. 7]. For $T \ll M$

the integrand is strongly suppressed due to a falloff according to $e^{-\beta\omega_{\mathbf{p}}} < e^{-\beta M}$ [cf. Ani+11, p. 7]. Eq. (4.9) can be rewritten to [see Ani+11, pp. 47-49]

$$f_{Li}(t, k) = -\frac{\epsilon_{ii}}{2\pi k} \int_{p_{\min}(k)} dp \int_{k'_{\min}(p)}^{k'_{\max}(p)} dk' k' \frac{1}{\omega_{\mathbf{p}}} \left(1 - \frac{2\omega_{\mathbf{p}}k - M^2}{2pk} \frac{2\omega_{\mathbf{p}}k' - M^2}{2pk'} \right) \times f_{l\phi}(k, \omega_{\mathbf{p}} - k) f_F(\omega_{\mathbf{p}}) \frac{1 - e^{-\Gamma_{\mathbf{p}}t}}{\Gamma_{\mathbf{p}}}, \quad (4.10)$$

where

$$p_{\min}(k) = \frac{|M^2 - 4k^2|}{4k}, \quad (4.11)$$

$$k'_{\min}(p) = \frac{\omega_{\mathbf{p}} - p}{2}, \quad (4.12)$$

$$k'_{\max}(p) = \frac{\omega_{\mathbf{p}} + p}{2}. \quad (4.13)$$

Integration over the three-momentum \mathbf{k} and summation over the lepton families gives the integrated lepton asymmetry, i.e. the number density

$$n_L(t) = \sum_i \int \frac{d^3k}{(2\pi)^3} f_{Li}(t, k) \quad (4.14)$$

corresponding to the comoving number density $|N_{B-L}|$ in Fig. 4.1 [see Ani+11, p. 7].

4.3. Kadanoff-Baym Calculation

4.3.1. Lepton Number Matrix

The starting point of the calculation of the lepton asymmetry using KBEs is the flavor non-diagonal lepton current, which is related to the statistical propagator via [see Ani+11, p. 24]

$$j_{ij}^{\mu}(x) = -\text{Tr} \left[\gamma^{\mu} S_{Lij}^{+}(x, x') \right]_{x \rightarrow x'}, \quad (4.15)$$

where i and j are flavor indices. Due to spatial homogeneity, the spatial dependence of S_{ij}^{+} is only on the difference $\mathbf{x} - \mathbf{x}'$. The zeroth component of the Fourier transform then gives the lepton number matrix [see Ani+11, p. 24]

$$L_{\mathbf{k},ij}(t, t') = -\text{Tr} \left[\gamma^0 S_{L\mathbf{k}ij}^{+}(t, t') \right]. \quad (4.16)$$

For free fields in equilibrium, the lepton number matrix is related to the lepton and anti-lepton distribution functions by [see Ani+11, pp. 24-25]

$$L_{\mathbf{k},ii}(t, t) = f_{li}(k) - \bar{f}_{\bar{l}i}(k). \quad (4.17)$$

As discussed in Sec. 3.3, lepton number changing processes are studied using the KBEs for the lepton propagator. This means that the propagator in Eq. (4.16) fulfills the

KBEs [see Ani+11, pp. 25-26]

$$(i\gamma^0\partial_t - \mathbf{k}\boldsymbol{\gamma})S_{L\mathbf{k}}^+(t, t') = + \int_0^t dt_1 \Pi_{\mathbf{k}}^-(t, t_1) S_{L\mathbf{k}}^+(t_1, t') - \int_0^{t'} dt_1 \Pi_{\mathbf{k}}^+(t, t_1) S_{L\mathbf{k}}^-(t_1, t'), \quad (4.18)$$

$$S_{L\mathbf{k}}^+(t, t')(-i\gamma^0\overleftarrow{\partial}_{t'} - \mathbf{k}\boldsymbol{\gamma}) = - \int_0^t dt_1 S_{L\mathbf{k}}^+(t, t_1) \Pi_{\mathbf{k}}^-(t_1, t') + \int_0^{t'} dt_1 S_{L\mathbf{k}}^-(t, t_1) \Pi_{\mathbf{k}}^+(t_1, t'), \quad (4.19)$$

where $\Pi_{\mathbf{k}}$ is the lepton self-energy and flavor indices are suppressed. Note that in principle, the lepton and Higgs boson fields have to be considered to be out of equilibrium now. Using these equations, one finds [see Ani+11, p. 26]

$$\begin{aligned} \partial_t L_{\mathbf{k}}(t, t) &= i \text{Tr} \left[(i\gamma^0\partial_t + i\gamma^0\partial_{t'}) S_{L\mathbf{k}}^+(t, t') \right]_{t=t'} \\ &= i \text{Tr} \left[(i\gamma^0\partial_t - \mathbf{k}\boldsymbol{\gamma}) S_{L\mathbf{k}}^+(t, t') + S_{L\mathbf{k}}^+(t, t') (i\gamma^0\overleftarrow{\partial}_{t'} + \mathbf{k}\boldsymbol{\gamma}) \right]_{t=t'} \\ &= i \text{Tr} \left[(i\gamma^0\partial_t - \mathbf{k}\boldsymbol{\gamma}) S_{L\mathbf{k}}^+(t, t') + S_{L\mathbf{k}}^+(t, t') (i\gamma^0\overleftarrow{\partial}_{t'} + \mathbf{k}\boldsymbol{\gamma}) \right]_{t=t'} \\ &= i \text{Tr} \left[\int_0^t dt_1 \Pi_{\mathbf{k}}^-(t, t_1) S_{L\mathbf{k}}^+(t_1, t') - \int_0^{t'} dt_1 \Pi_{\mathbf{k}}^+(t, t_1) S_{L\mathbf{k}}^-(t_1, t') \right. \\ &\quad \left. + \int_0^t dt_1 S_{L\mathbf{k}}^+(t, t_1) \Pi_{\mathbf{k}}^-(t_1, t') - \int_0^{t'} dt_1 S_{L\mathbf{k}}^-(t, t_1) \Pi_{\mathbf{k}}^+(t_1, t') \right]. \quad (4.20) \end{aligned}$$

After integration over the time, this gives [see Ani+11, p. 26]

$$\begin{aligned} L_{\mathbf{k}}(t, t) &= i \int_0^t dt_1 \int_0^t dt_2 \text{Tr} \left[\Pi_{\mathbf{k}}^-(t_1, t_2) S_{L\mathbf{k}}^+(t_2, t_1) - \Pi_{\mathbf{k}}^+(t_1, t_2) S_{L\mathbf{k}}^-(t_2, t_1) \right] \\ &= - \int_0^t dt_1 \int_0^t dt_2 \text{Tr} \left[\Pi_{\mathbf{k}}^>(t_1, t_2) S_{L\mathbf{k}}^<(t_2, t_1) - \Pi_{\mathbf{k}}^<(t_1, t_2) S_{L\mathbf{k}}^>(t_2, t_1) \right], \quad (4.21) \end{aligned}$$

where the relations between the Wightman functions, the spectral function, and the statistical propagator from Eqs. (3.20) and (3.21), which also hold for the solutions of the KBEs as well as the components of the self-energy, have been used. This expression is to be evaluated at leading order in the small Yukawa coupling λ .

At this step of the calculation, one should specify which diagrams should be included in the lepton self-energy. Up to two-loop level all diagrams are depicted in Fig. 4.2. Since this calculation neglects washout terms and only CP-violating terms contribute to a lepton asymmetry, one has to investigate, which diagrams correspond to the latter. It turns out that only the diagrams e) and f) in Fig. 4.2 have vertex factors, i.e. combinations of Yukawa couplings, proportional to the known CP-asymmetry ϵ from Eq. (4.8) [see Ani+11, pp. 13-14]². Therefore, only these diagrams, which are depicted in Fig. 4.3 with the conventions for this calculation, are considered in [Ani+11] and this thesis as contributions to the lepton self-energy.

The Majorana neutrino and lepton propagators as well as the lepton self-energy may be

²Note that for finite chemical potential, which is neglected here, also washout terms violate CP [see Men10, pp. 75-76].

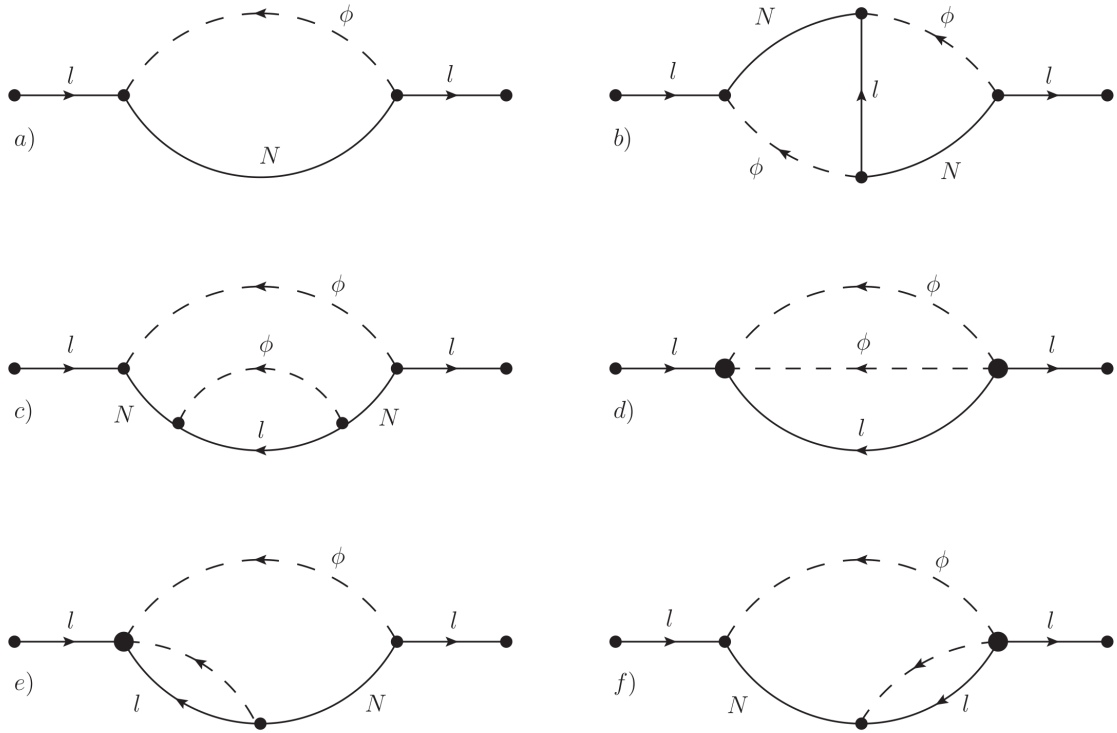


Figure 4.2.: One- and two-loop contributions to the lepton self-energy with correspondences to washout terms a) - d) and CP-violating terms e) + f) generating a lepton asymmetry [from Ani+11, p. 14].

decomposed into an equilibrium and a nonequilibrium part following

$$G_{\mathbf{p}}(t_1, t_2) = G_{\mathbf{p}}^{\text{eq}}(t_1, t_2) + \tilde{G}_{\mathbf{p}}(t_1, t_2), \quad (4.22)$$

$$S_{L\mathbf{k}}(t_1, t_2) = S_{L\mathbf{k}}^{\text{eq}}(t_1, t_2) + \delta S_{L\mathbf{k}}(t_1, t_2), \quad (4.23)$$

$$\Pi_{\mathbf{k}}(t_1, t_2) = \Pi_{\mathbf{k}}^{\text{eq}}(t_1, t_2) + \delta \Pi_{\mathbf{k}}(t_1, t_2). \quad (4.24)$$

It can be shown [see Ani+11, pp. 26, 52-53] that the equilibrium part of the Majorana neutrino propagator does not contribute to a lepton asymmetry. Inserting $S_{\mathbf{k}}^{\text{eq}}$ and $\Pi_{\mathbf{k}}^{\text{eq}}$ into the lepton number matrix obviously gives $L_{\mathbf{k},ii} \equiv 0$ because of the lack of a lepton asymmetry in thermal equilibrium [see Ani+11, p. 27]. At leading order in λ , one finds for the lepton number matrix [see Ani+11, p. 27]

$$L_{\mathbf{k}}(t, t) = i \int_0^t dt_1 \int_0^t dt_2 \text{Tr} \left[\delta \Pi_{\mathbf{k}}^-(t_1, t_2) S_{L\mathbf{k}}^{\text{eq}+}(t_2, t_1) - \delta \Pi_{\mathbf{k}}^+(t_1, t_2) S_{L\mathbf{k}}^{\text{eq}-}(t_2, t_1) \right], \quad (4.25)$$

where

$$\delta \Pi_{\mathbf{k}}(t_1, t_2) = \Pi_{\mathbf{k}}^{(1)}(t_1, t_2) + \Pi_{\mathbf{k}}^{(2)}(t_1, t_2) \quad (4.26)$$

is calculated using equilibrium Higgs boson and lepton propagators as well as the nonequilibrium part of the Majorana neutrino propagator, and $\Pi_{\mathbf{k}}^{(1)}$ and $\Pi_{\mathbf{k}}^{(2)}$ are the diagrams in Fig. 4.3. Since the nonequilibrium part of the lepton and Higgs boson propagators are not needed from now on, $S_{\mathbf{k}}$ and $\Delta_{\mathbf{q}}$ again denote the equilibrium parts. The diagrams in Fig. 4.3 can be evaluated using the Feynman rules given in the appendix, Sec. A.2. Factoring out the Yukawa couplings containing the flavor dependence, one finds [cf. Ani+11,

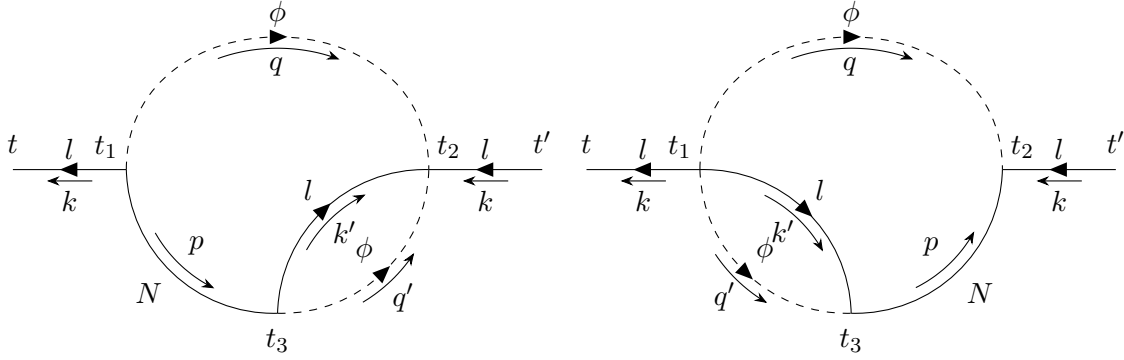


Figure 4.3.: Two-loop contributions to lepton self-energies $\Pi_{\mathbf{k}}^{\pm}$, $\Pi_{\mathbf{k}}^{(1)\pm}$ (left-hand side) and $\Pi_{\mathbf{k}}^{(2)\pm}$ (right-hand side), contributing to a non-zero lepton asymmetry, from [Ani+11, p. 24].

pp. 27-28]

$$\Pi_{\mathbf{k}ij}^{(1)}(t_1, t_2) = -3i\lambda_{i1}^*(\eta\lambda^*)_{j1}\Pi_{\mathbf{k}}^{(1)}(t_1, t_2), \quad (4.27)$$

$$\Pi_{\mathbf{k}ij}^{(2)}(t_1, t_2) = 3i(\eta^*\lambda)_{i1}\lambda_{j1}\Pi_{\mathbf{k}}^{(1)}(t_1, t_2). \quad (4.28)$$

Chiral projections at the vertices cause only the scalar parts of the nonequilibrium Majorana neutrino propagator to contribute, and thus, one has

$$\begin{aligned} \tilde{G}_{\mathbf{p}}(t_1, t_2) &= \tilde{G}_{\mathbf{p}}^{>}(t_1, t_2) = \tilde{G}_{\mathbf{p}}^{<}(t_1, t_2) = \tilde{G}_{\mathbf{p}}^{11}(t_1, t_2) = \tilde{G}_{\mathbf{p}}^{22}(t_1, t_2) \\ &= \frac{M}{\omega_{\mathbf{p}}} \cos(\omega_{\mathbf{p}}(t_1 - t_2)) f_F(\omega_{\mathbf{p}}) e^{-\Gamma_{\mathbf{p}}(t_1+t_2)/2} \end{aligned} \quad (4.29)$$

inside the expressions for the diagrams [cf. Ani+11, p. 28]. Using symmetry properties for the propagators as well as relations between the contributions of the diagrams, one finds [cf. Ani+11, p. 29]

$$L_{\mathbf{k},ii}(t, t) = \frac{64\pi\epsilon_{ii}}{M} \int_0^t dt_1 \int_0^t dt_2 \operatorname{Re} \left(\operatorname{Tr} \left[\Pi_{\mathbf{k}}^{(1)>}(t_1, t_2) S_{\mathbf{k}}^{<}(y_{21}) \right] \right) \quad (4.30)$$

with

$$\begin{aligned} \Pi_{\mathbf{k}}^{(1)>}(t_1, t_2) &= \int_0^\infty dt_3 \int_{\mathbf{q}, \mathbf{q}', \mathbf{k}', \mathbf{p}} (2\pi)^3 \delta^3(\mathbf{p} - \mathbf{k}' - \mathbf{q}') (2\pi)^3 \delta^3(\mathbf{p} + \mathbf{k} + \mathbf{q}) \\ &\times \left[\tilde{G}_{\mathbf{p}}(t_1, t_3) \left(S_{\mathbf{k}'}^{11}(y_{23}) \Delta_{\mathbf{q}'}^{11}(y_{23}) - S_{\mathbf{k}'}^{<}(y_{23}) \Delta_{\mathbf{q}'}^{<}(y_{23}) \right) \Delta_{\mathbf{q}}^{<}(y_{21}) \right] P_L, \end{aligned} \quad (4.31)$$

where $\int_{\mathbf{q}} := \int d^3q/(2\pi)^3$ and $y_{ij} := t_i - t_j$. For a detailed calculation see [Ani+11, pp. 24-29]. Note that the momentum structure is corrected compared to the result in [Hüt13, p. 31] so that it agrees with the corresponding diagram.

4.3.2. Solution without Gauge Corrections

The solution of the lepton number matrix without gauge corrections is obtained by inserting the propagators from Sec. 3.3 in Eq. (6.1). This gives [see Ani+11, p. 30]

$$\begin{aligned}
L_{\mathbf{k},ii}(t,t) = & -\epsilon_{ii} \int_0^t dt_1 \int_0^t dt_2 \int_0^{t_2} dt_3 \int_{\mathbf{q},\mathbf{q}',\mathbf{k}',\mathbf{p}} \\
& \times \frac{8\pi}{qq'\omega_{\mathbf{p}}} (2\pi)^3 \delta^3(\mathbf{p} - \mathbf{k}' - \mathbf{q}') (2\pi)^3 \delta^3(\mathbf{p} + \mathbf{k} + \mathbf{q}) f_F(\omega_{\mathbf{p}}) e^{-\Gamma_{\mathbf{p}}(t_1+t_3)/2} \cos(\omega_{\mathbf{p}} y_{31}) \\
& \times \left[\left(f_{l\phi}(k,q) \cos((k+q)y_{21}) + \bar{f}_{l\phi}(k,q) \cos((k-q)y_{21}) \right) \right. \\
& \times \left(f_{l\phi}(k',q') \cos((k'+q')y_{23}) + \bar{f}_{l\phi}(k',q') \cos((k'-q')y_{23}) \right) \\
& + \frac{\mathbf{k} \cdot \mathbf{k}'}{kk'} \left(\left(f_{l\phi}(k,q) \sin((k+q)y_{21}) + \bar{f}_{l\phi}(k,q) \sin((k-q)y_{21}) \right) \right. \\
& \left. \left. \times \left(f_{l\phi}(k',q') \sin((k'+q')y_{23}) + \bar{f}_{l\phi}(k',q') \sin((k'-q')y_{23}) \right) \right) \right] , \tag{4.32}
\end{aligned}$$

where, cf. Eq. (3.75),

$$f_{l\phi}(k,q) = 1 - f_F(k) + f_B(q) , \tag{4.33}$$

$$\bar{f}_{l\phi}(k,q) = f_l(k) + f_\phi(q) . \tag{4.34}$$

Note that in [Ani+11], three-momentum conservation is implied only and not written explicitly. In order to compare this to the solution of the Boltzmann equations, one has to restrict the integrations to intervals with points satisfying the conditions $\omega_{\mathbf{p}} = k + q$ and $\omega_{\mathbf{p}} = k' + q'$. Furthermore, the limit $\Gamma_{\mathbf{p}}/M \rightarrow 0$ while $\Gamma_{\mathbf{p}}t = \text{const}$ has to be considered so that one finds for the dominating part of the lepton number matrix [see Ani+11, Erratum]

$$\begin{aligned}
L_{\mathbf{k},ii} = & -\frac{\epsilon_{ii}}{2\pi k} \int_{p_{\min}(k)} dp \int_{k'_{\min}(p)}^{k'_{\max}(p)} dk' k' \frac{1}{\omega_{\mathbf{p}}} \left(1 - \frac{2\omega_{\mathbf{p}}k - M^2}{2pk} \frac{2\omega_{\mathbf{p}}k' - M^2}{2pk'} \right) \\
& \times f_{l\phi}(k, \omega_{\mathbf{p}} - k) f_{l\phi}(k', \omega_{\mathbf{p}} - k') f_F(\omega_{\mathbf{p}}) \frac{1 - e^{-\Gamma_{\mathbf{p}}t}}{\Gamma_{\mathbf{p}}} , \tag{4.35}
\end{aligned}$$

where [see Ani+11, p. 49]

$$p_{\min}(k) = \frac{|M^2 - 4k^2|}{4k} , \tag{4.36}$$

$$k'_{\min}(p) = \frac{\omega_{\mathbf{p}} - p}{2} , \tag{4.37}$$

$$k'_{\max}(p) = \frac{\omega_{\mathbf{p}} + p}{2} . \tag{4.38}$$

This is the same as Eq. (4.10) apart from a statistical factor [see Ani+11, Erratum]. Most importantly, it has the same time-dependence as the solution of the Boltzmann equation.

Up to now, thermal damping widths of the Higgs boson and lepton fields due to gauge interactions have been neglected. This can be implemented by replacing the propagators according to [see Ani+11, p. 32]

$$\Delta_{\mathbf{q}}(y) \rightarrow e^{-\gamma_\phi|y|} \Delta_{\mathbf{q}}(y) , \tag{4.39}$$

$$S_{\mathbf{k}}(y) \rightarrow e^{-\gamma_l|y|} S_{\mathbf{k}}(y) , \tag{4.40}$$

where γ_ϕ and γ_l are the thermal damping widths. It is known that these widths are much greater than the thermal width of the heavy Majorana neutrino, i.e. $\gamma_\phi \sim \gamma_l \sim g^2 T \gg$

$\lambda^2 M \sim \Gamma_{\mathbf{p}}$ for $M \lesssim T$ [see Ani+11, p. 32]. For the dominating part of the lepton number matrix, one then obtains [see Ani+11, pp. 32-33]

$$\begin{aligned}
L_{\mathbf{k},ii}(t) = & -32\pi\epsilon_{ii} \int_{\mathbf{q},\mathbf{q}',\mathbf{k}',\mathbf{p}} (2\pi)^3 \delta^3(\mathbf{p} - \mathbf{k}' - \mathbf{q}') (2\pi)^3 \delta^3(\mathbf{p} + \mathbf{k} + \mathbf{q}) \frac{k \cdot k'}{4qq'kk'\omega_{\mathbf{p}}} \\
& \times \frac{\gamma\gamma'}{((\omega_{\mathbf{p}} - k - q)^2 + \gamma^2)((\omega_{\mathbf{p}} - k' - q')^2 + \gamma'^2)} \\
& \times f_{l\phi}(k, \omega_{\mathbf{p}} - k) f_{l\phi}(k', \omega_{\mathbf{p}} - k') f_F(\omega_{\mathbf{p}}) \frac{1 - e^{-\Gamma_{\mathbf{p}}t}}{\Gamma_{\mathbf{p}}}, \tag{4.41}
\end{aligned}$$

where $\gamma = \gamma_l(k) + \gamma_\phi(q)$ and $\gamma' = \gamma_l(k') + \gamma_\phi(q')$. Again, one finds the same time-dependence as the solution of the Boltzmann equation. However, it is also obvious that the inclusion of gauge interactions, which are emulated here with the replacement of the propagators, influence the resulting lepton number matrix. Hence, a systematic approach is needed, which is presented in Ch. 6.

5. Resummation of the Majorana Neutrino Self-Energy

In this chapter, the details on the resummation of the Majorana neutrino self-energy, which is needed for the systematic inclusion of all leading order gauge corrections, are presented. Note that the imaginary time formalism [cf. Le 96] is used here because of the usage of the result from [Ani+11], which is discussed in greater detail in [Bes10]. This chapter closely follows Ch. 5 from [Hüt13] being a summary of the corresponding chapters in [Ani+11; Bes10].

5.1. Momentum Scales

There are different momentum scales to consider in order to correctly describe particles in a hot thermal bath, e.g. heavy Majorana neutrinos in a SM plasma. In the context of this thesis, due to high temperatures $T \gtrsim M$, the relevant momentum scale is the lightcone scale. Therefore, the others will only be presented shortly. In the following, p stands for a four-momentum and $g \ll 1$ is the relevant coupling constant. Note that order estimates like $p \sim T$ concern the absolute value of the three-momentum. The different scales are [see Bes10, pp. 14-15]:

- Hard scale, $p \sim T$, $p^2 \sim T^2$: This is the only momentum scale for particles inside a plasma, where ordinary perturbation theory is valid. For $T \lesssim M$ the Majorana neutrino is in this momentum scale. Therefore, no resummation is needed there.
- Soft scale, $p \sim gT$: This momentum scale is the typical one for collective excitations in a plasma causing naive perturbation theory to break down. The interactions with the plasma change the propagation of particles giving corrections of $\mathcal{O}(1)$. This results in a thermal mass of the particle. One can treat this region using the hard thermal loop (HTL) resummation scheme [Pis89]. Since this is very similar to a step in the calculation of the resummed self-energy, this approach will be presented shortly in Sec. 5.2.
- Ultrasoft scale, $p \sim g^2T$: This momentum scale is the one of magnetic screening, i.e. transverse polarization of gauge fields become important. Since perturbation theory breaks down, one needs effective theories or lattice simulations for this regime.
- Lightcone scale, $p \sim T$, $p^2 \sim g^2T^2$: This momentum scale is of interest in the context of this thesis, since $T \gtrsim M$ and therefore, the absolute value of the three-momentum is of the same order as the energy of the Majorana neutrino. Here, collinear divergences occur and asymptotic masses, another sort of thermal masses, need to be considered. Only for scalars the asymptotic mass is equal to the thermal mass.

Note that these different kinematical regimes arise due to infrared and collinear divergences in finite temperature calculations not present in zero temperature calculations. There are no new ultraviolet divergences [see Bes10, p. 14].



Figure 5.1.: HTL resummed scalar propagator with self-interaction, from [Bes10, p. 15].

5.2. Hard Thermal Loops

As discussed in the previous section, in the soft momentum scale naive perturbation theory breaks down. This can already be seen in the simple example of the propagator with one-loop self-energy insertions of a scalar particle undergoing self-interactions (with an interaction corresponding to $g^2\phi^4/4!$), see Fig. 5.1.

With Δ being the bare propagator and Π the self-energy one finds in the imaginary time formalism as order estimates $\Delta(q) = -1/(q^2 - m^2) \sim 1/(gT)^2$, since $q^2, m^2 \sim g^2T^2$ in this momentum scale with the thermal mass m , and $-\Pi(q) \sim g^2 \sum_{q_0} \int d^3k \Delta(q) \sim g^2T^2$, where the loop momentum is assumed to be hard [see Bes10, pp. 10, 15]. Note that q is used for the momentum in the scalar propagator due to convention. One therefore finds for an arbitrary number of one-loop self-energy insertions to the bare propagator [see Bes10, p. 15]

$$\Delta(q)\Pi(q)\Delta(q)\cdots \sim \frac{1}{(gT)^2}(gT)^2\frac{1}{(gT)^2}\cdots \sim \frac{1}{(gT)^2} \quad (5.1)$$

This means that the bare propagator with an arbitrary number of one-loop self-energy insertions is of the same order as the bare one without any insertions. Hence, all of these contributions have to be summed up, cf. Fig. 5.1. This is called a resummation, which is done in the HTL resummation scheme in this case.

5.3. Perturbation Theory Close to the Lightcone

5.3.1. Thermal Width and Asymptotic Mass

A similar situation to the soft momentum scale and the HTL resummation scheme can arise in the lightcone scale. As it turns out, the condition for a scenario as in Sec. 5.2, where the bare propagator has to be replaced by its resummed counterpart due to the fact that self-energy insertions do not change the order, is strictly speaking not that all components of p are of $\mathcal{O}(gT)$, but $p^2 \sim g^2T^2$ is needed [see Bes10, pp. 18-19]. Therefore, a similar resummation is necessary at the lightcone scale $p \sim T$, $p^2 \sim g^2T^2$. This leads to asymptotic masses. In contrast to ordinary thermal masses, that change the dispersion relation differently for scalars, fermions, and gauge bosons, asymptotic masses change the dispersion relation according to $(p^0)^2 = \mathbf{p}^2 + m_\infty^2$ for all of these, where p^0 is the zero-component of the four-momentum, \mathbf{p} is the corresponding three-momentum, and m_∞ is the asymptotic mass [see Bes10, p. 14].

Considering a scalar particle with the resummed propagator Δ and the self-energy Π , one can parametrize the propagator using the thermal width Γ and the asymptotic mass $m_{\phi,\infty}$ [see Bes10, pp. 18-19]

$$\Delta(q) = \frac{-1}{q^2 - \Pi(q)} = \frac{-1}{(q^0 + i\Gamma(q))^2 - \mathbf{q}^2 - m_{\phi,\infty}^2}. \quad (5.2)$$

Comparing this to the HTL resummed propagator, one obtains with the assumption $\Gamma^2 \ll m_{\phi,\infty}^2$, which is necessary for the quasiparticle description of the degrees of freedom [see Bes10, p. 19],

$$\text{Re } \Pi(q) = m_{\phi,\infty}^2, \quad \text{Im } \Pi(q) = -2q^0\Gamma(q). \quad (5.3)$$

Because of Π being of order $\mathcal{O}(g^2T^2)$, also $m_{\phi,\infty}^2, q^0\Gamma$ are of order $\mathcal{O}(g^2T^2)$, which implies that Γ is of order $\mathcal{O}(g^2T)$. Therefore, the width and the asymptotic mass are a priori equally important. Since however, only hard loop momenta need to be considered here, the self-energy becomes purely real and the width can be neglected [see Bes10, p. 19].

The calculation of the resummed scalar and lepton propagators for light-like momenta in imaginary time can be found in [Bes10, pp. 76-81]. One finds for the scalar propagator

$$\Delta(q) = \frac{-1}{q^2 - m_{\phi,\infty}^2} \quad (5.4)$$

with the asymptotic mass (here only for the ϕ^4 case, see below for all relevant interactions)

$$m_{\phi,\infty}^2 = \frac{g^2T^2}{4} . \quad (5.5)$$

For the fermion propagator, the calculation gives

$$S(k) = -\frac{\not{k} - \frac{m_{l,\infty}^2}{2k_0}\gamma^0}{k^2 - m_{l,\infty}^2} \quad (5.6)$$

with the asymptotic mass (here only for one gauge coupling, see below for all relevant interactions)

$$m_{l,\infty}^2 = \frac{g^2C_2(r)T^2}{4} , \quad (5.7)$$

where $C_2(r)$ is the Casimir operator of the corresponding gauge group. Using all relevant interactions between the scalar/lepton and other SM particles, one finds for the asymptotic masses [see Bes10, pp. 76-81] [as cited in Hüt13, p. 36]

$$m_{\phi,\infty}^2 = \frac{1}{16}(3g_W^2 + g_Y^2 + 4\lambda_t^2 + 8\Lambda)T^2 , \quad (5.8)$$

$$m_{l,\infty}^2 = \frac{1}{16}(3g_W^2 + g_Y^2)T^2 , \quad (5.9)$$

where g_W and g_Y are the couplings corresponding to the gauge groups SU(2) and U(1), respectively, λ_t is the top quark Yukawa coupling, and Λ is the Higgs self-coupling. Note that the Yukawa couplings to all other quarks can be neglected due to smallness because of their masses [see Bes10, p. 78].

5.3.2. Lightcone Coordinates and Power Counting

When dealing with the lightcone scale, it is useful to introduce lightcone coordinates. This introduction is oriented on [Hüt13, p. 36]. For lightcone coordinates, one defines a light-like four-vector $v := (1, \mathbf{v})$ with $v^2 = 0$, i.e. $\mathbf{v}^2 = 1$, and correspondingly $p_{\parallel} := \mathbf{p} \cdot \mathbf{v}$ for a four-momentum p . \mathbf{p}_{\perp} is then defined as the three-momentum perpendicular to \mathbf{v} , which can be expressed with two components. This enables one to rewrite a four-momentum according to

$$p = (p^{\mu}) = (p_+, p_-, \mathbf{p}_{\perp}) , \quad (5.10)$$

where

$$p_+ = p_0 + p_{\parallel} , p_- = p_0 - p_{\parallel} . \quad (5.11)$$

With

$$p^2 = p_0^2 - p_{\parallel}^2 - \mathbf{p}_{\perp}^2 = (p_0 + p_{\parallel})(p_0 - p_{\parallel}) - \mathbf{p}_{\perp}^2 = p_+p_- - \mathbf{p}_{\perp}^2 \sim g^2T^2 \quad (5.12)$$

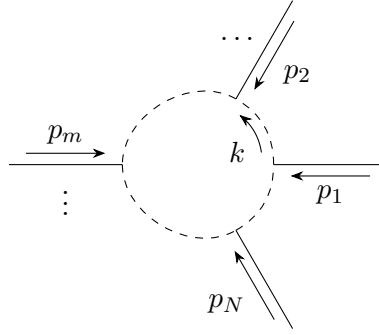


Figure 5.2.: One-loop contribution to CTL n -point function [cf. Bes10, p. 20]

the lightcone scale from Sec. 5.1 translates to

$$p_+ \sim T, \quad p_- \sim g^2 T, \quad |\mathbf{p}_\perp| \sim gT. \quad (5.13)$$

The measure becomes

$$d^4 p = \frac{1}{2} dp_+ dp_- d^2 p_\perp. \quad (5.14)$$

Now, a spin-1/2 fermion or a spin-1 gauge boson with light-like momentum as an external particle is studied in terms of Feynman diagrams. It is assumed that the interaction is via a gauge coupling g . In terms of the gauge coupling, one finds the following power counting [see Bes10, p. 21]:

- Loop integral: factor g^4
- Propagator: factor $1/(g^2 T^2)$
- Vertex involving gauge boson: factor g
- Trilinear vertex¹: another factor g

5.3.3. Collinear Thermal Loops

Consider one-loop diagrams like in Fig. 5.2 with light-like momenta p_i , $p_i \sim T$, $p_i^2 \sim g^2 T^2$, $i = 1, \dots, N$. These are called collinear thermal loops (CTL) [see Bes10, pp. 20-25]. The loop momentum k^2 is assumed to be also light-like $k \sim T$, $k^2 \sim g^2 T^2$, and collinear to the external momenta $k \cdot p_i \sim g^2 T^2$. This means that $p_{i,\parallel}, k_\parallel \sim T$, whereas $|\mathbf{k}_\parallel|, |\mathbf{p}_{i,\parallel}| \sim gT$. The angle between the vectors is then of order $\mathcal{O}(g)$ [see Bes10, p. 20]. Note that if collinearity is violated, the loop integrals and the vertices will give additional powers of g suppressing the contribution compared to the CTL result [see Bes10, p. 21].

The power counting rules from Sec. 5.3.2 then give for a CTL N -point function Π_{CTL}^N with n vertices involving gauge bosons and $m = N - n$ additional vertices [see Bes10, p. 22]

$$\Pi_{\text{CTL}}^N \sim g^4 \left(\frac{1}{g^2} \right)^N g^n g^m \sim g^{4-m}. \quad (5.15)$$

For $m = 2$, which is the case for two Majorana neutrinos, this means that all CTL N -point functions are of order $\mathcal{O}(g^2)$.

¹This corresponds e.g. to a Yukawa vertex in the context of this thesis. Note that the factor is additional to a possible factor for a vertex involving a gauge boson.

²Here, the momentum for each propagator in the loop is meant.

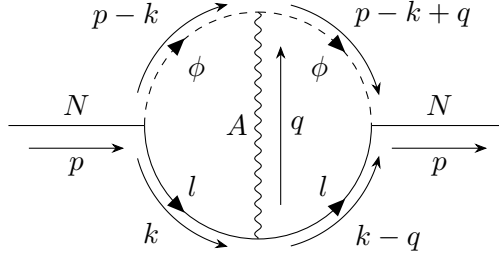


Figure 5.3.: Two-point function with one gauge boson rung [cf. Bes10, p. 23].

If one now explicitly considers two-point functions $\Pi_{1 \text{ rung}}$ as in Fig. 5.3, where however already the propagators for the Majorana neutrino self-energy are depicted, with an additional virtual soft gauge boson rung with momentum q , one finds for this diagram in the imaginary time formalism [see Bes10, p. 23]

$$\Pi_{1 \text{ rung}} \sim g^2 T \sum_{k^0} \int \frac{d^3 k}{(2\pi)^3} T \sum_{q^0} \int \frac{d^3 q}{(2\pi)^3} V(k, p, q) \Delta(k) \Delta(k-q) \Delta(p-k+q) \Delta(p-k) \Delta(q), \quad (5.16)$$

where $V(p, q, k)$ contains the structure from the vertices (possible Lorentz and/or Dirac indices suppressed) and a scalar loop is considered for simplicity, since apart from complexity nothing changes. One finds the following power counting for this diagram [see Bes10, pp. 23-24]:

- New gauge boson vertex: factor g^2
- Each new propagator: factor $1/g^2$ provided q is chosen such that $q \cdot p \sim g^2 T^2$
- Sum-integral: factor $1/g^4$ due to phase space suppression

The last rule is due to the soft momentum of the gauge boson. Specifically, one has

$$T \sum_{q^0} \int \frac{d^3 q}{(2\pi)^3} \sim \int \int dq_+ \int dq_- \left(\frac{1}{2} + f_B(q^0) \right) \int d^2 q_\perp, \quad (5.17)$$

where $q_+, |\mathbf{q}_\perp| \sim gT$, $q_- \sim g^2 T$, $q^0 \sim gT$ and $f_B(q^0) \sim 1/g$, which gives the above rule [see Bes10, pp. 23-24].

Applying these rules as well as the ones from Sec. 5.3.2, one finds

$$\Pi_{1 \text{ rung}} \sim g^2 g^2 \left(\frac{1}{g^2} \right)^5 (g^4)^2 \sim g^2. \quad (5.18)$$

This means that adding one soft gauge boson to a CTL two-point function does not change the order $\mathcal{O}(g^2)$ of the diagram. Since this procedure can be repeated, the same is true for an arbitrary number of soft gauge bosons as in Fig. 5.4. Therefore, all of these so-called ladder diagrams have to be summed up for a consistent leading-order treatment, whereas crossed ladder rungs turn out to give higher-order corrections due to the larger time scale between interactions [see Bes10, pp. 23-25, 34-35]. Note that if the gauge boson's momentum is not soft such that $q \sim gT$, the contribution to the self-energy is suppressed compared to the soft contribution [cf. Bes10, p. 25]. It is worth mentioning that because of the fact that the Higgs boson and the lepton propagators are resummed quantities themselves, since the asymptotic mass has to be included, one arrives at a "multifold resummation" [see Bes10, pp. 24-25]. This means that in fact, diagrams like in Fig. 5.6 need to be considered, which will be further discussed in Sec. 5.5.

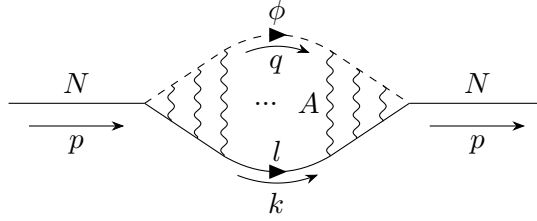


Figure 5.4.: Two-point function with arbitrary number of gauge bosons, so-called ladder diagram, [cf. Bes10, p. 24].



Figure 5.5.: Example for two interfering processes obtained by cutting Fig. 5.4, from [ABB11, p. 6].

5.4. Connection to the Landau-Pomeranchuk-Migdal Effect

The Landau-Pomeranchuk-Migdal (LPM) effect was first discovered in the electromagnetic showering of high-energy cosmic rays and named after the people who first described it in [LP53; Mig56]. It can arise when a particle travels through a medium and thus, its behavior is changed compared to the travel in vacuum. The LPM effect is of particular importance in the quark-gluon plasma. For a general overview see [Kle99]. The general phenomenon is that the formation time of an emitted particle is of the same order as the mean free time between collisions in the plasma. Therefore, the two processes interfere and a simple Boltzmann ansatz is not justified [cf. Bes10, pp. 32-33]. An example for two interfering processes, which are important for the context of this thesis, can be seen in Fig. 5.5.

As evident from Fig. 5.5, the LPM effect is closely related to particle production. In the present case, the produced particles are Majorana neutrinos. In fact, the production rate $\tilde{\Gamma}$ of Majorana neutrinos per unit time and unit volume is defined by [see ABB11, p. 3]

$$\frac{d\tilde{\Gamma}}{d^3p} = \frac{1}{(2\pi)^3 p^0} f_F(p^0) \text{Tr}[\not{p} \text{Im} \Sigma^{\text{ret}}(p)] , \quad (5.19)$$

where $\Sigma^{\text{ret}}(p)$ is the retarded self-energy of the Majorana neutrino and the convention from [ABB11] that the self-energy corresponds to (-1) times the Feynman diagrams is chosen. However, in the case of interest not the production rate per unit time and unit volume, but the thermal width $\Gamma_{\mathbf{p}}$ is needed. The two are related via, cf. Eq. (3.73),

$$\frac{d\tilde{\Gamma}}{d^3p} = \frac{2}{(2\pi)^3} f_F(p^0) \Gamma_{\mathbf{p}} , \quad (5.20)$$

which means that the difference is a phase space factor $2f_F(p^0)/(2\pi)^3$ (note the 2 because of the 2 spin degrees of freedom of the Majorana neutrino) that can be interpreted as the result from the fact that for the production rate, one considers an ensemble of Majorana neutrinos, whereas for the thermal width, one considers a single particle.

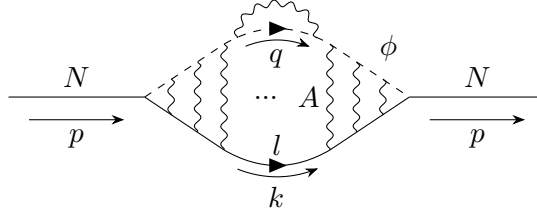


Figure 5.6.: Ladder diagram with gauge boson contributions to leading order treatment of Majorana neutrino self-energy [cf. ABB11, p. 7].

5.5. Strategy of the Calculation

This section details the strategy of the calculation needed to obtain the resummed Majorana neutrino self-energy, which includes all leading order gauge as well as other SM corrections. Due to the fact that gauge corrections turn out to be of particular importance, whereas other SM corrections, which are only hard ones, enter only as contributions to the asymptotic masses, sometimes only gauge corrections are named explicitly in the following. Nevertheless, all resummed results in the following contain the corrections from the hard interactions with other SM particles. The types of diagrams that need to be summed up are depicted in Fig. 5.6. In the following, q always denotes the momentum of the Higgs boson field, k the lepton momentum, and p the Majorana neutrino momentum. The strategy can be summarized in three steps described in [see ABB11, pp. 7-8]:

1. Integrate out the hard field modes. Here, the propagator of the Higgs boson and the lepton fields are resummed using the HTL resummation scheme at the lightcone scale discussed in Sec. 5.3.1 generating the asymptotic masses for the scale $q, k \sim T$ and $q^2, k^2 \sim g^2 T^2$. As discussed before, no thermal width is needed here, since it is a higher order correction. In this step, loop insertions with SM particles of hard momenta need to be considered for the scalar and lepton propagators³, cf. loop on top for scalar particle in Fig. 5.6. Note that this step is achieved by using the propagators from Eqs. (5.4) and (5.6) with the asymptotic masses from Eqs. (5.8) and (5.9), respectively.
2. Using the resummed Higgs boson and lepton propagators, compute a recursion relation for Majorana neutrino self-energy diagrams with an arbitrary number of soft gauge boson lines assuming that the Majorana neutrino, the Higgs boson, and the lepton momentum are light-like, i.e. have momenta on the lightcone scale, and collinear. For this, start with a one-loop diagram with two external Majorana neutrinos, but no soft gauge boson lines, i.e. like in Fig. 5.4 with no soft gauge bosons. There, only leading order terms are kept and the two-point function is computed explicitly. Then, a recursion relation that relates n -point functions with two external Majorana neutrinos and $n - 2$ external soft gauge bosons, see Fig. 5.7, with $(n - 1)$ -point functions, where one gauge boson has been removed, is derived. As it turns out, the most easy formulation of the relation is a current induced by background Majorana neutrino and gauge fields being defined as an integral over all external momenta contracted with the external fields [see Bes10, p. 35]. With the recursion relation, only the two-point function without any soft gauge boson is needed explicitly.

³Loops with soft gauge boson momentum are considered in the later steps.

3. Integrate out the soft gauge boson background. The gauge bosons appear only in self-energy insertions generating thermal widths for the lepton and the Higgs boson and as rungs in the ladder diagrams, cf. Fig. 5.6. This gives a new current satisfying an integral equation that is obtained from the result of the second step. The functional derivative with respect to the external fields results in an integral equation for the CTL self-energy that includes all diagrams like in Fig. 5.6. The numerical evaluation of this is discussed in the appendix, Sec. B.1.

5.6. Calculation of the Resummed Majorana Neutrino Self-Energy

5.6.1. Left- and Right-Handed Majorana Neutrino Self-Energy

In Weyl representation of the Dirac matrices, one can write $\text{Im } \Sigma^{\text{ret}}(p)$ as, cf. Eq. (3.71),

$$\begin{aligned} \text{Im } \Sigma^{\text{ret}}(p) &= \frac{1}{2}(a_{\mathbf{p}}(p^0)\gamma^0 + b_{\mathbf{p}}(p^0)\mathbf{p}\boldsymbol{\gamma}) = \frac{1}{2} \begin{pmatrix} 0 & a_{\mathbf{p}}(p^0)\mathbb{1}_2 + b_{\mathbf{p}}(p^0)\mathbf{p}\boldsymbol{\sigma} \\ a_{\mathbf{p}}(p^0)\mathbb{1}_2 - b_{\mathbf{p}}(p^0)\mathbf{p}\boldsymbol{\sigma} & 0 \end{pmatrix} \\ &=: \begin{pmatrix} 0 & \text{Im } \Sigma^{\text{R, ret}}(p) \\ \text{Im } \Sigma^{\text{L, ret}}(p) & 0 \end{pmatrix}, \end{aligned} \quad (5.21)$$

where

$$\text{Im } \Sigma^{\text{ret}}(p)P_R = \text{Im } \Sigma^{\text{ret}}(p) \begin{pmatrix} 0 & 0 \\ 0 & \mathbb{1}_2 \end{pmatrix} = \begin{pmatrix} 0 & \text{Im } \Sigma^{\text{R, ret}}(p) \\ 0 & 0 \end{pmatrix}, \quad (5.22)$$

$$\text{Im } \Sigma^{\text{ret}}(p)P_L = \text{Im } \Sigma^{\text{ret}}(p) \begin{pmatrix} \mathbb{1}_2 & 0 \\ 0 & 0 \end{pmatrix} = \begin{pmatrix} 0 & 0 \\ \text{Im } \Sigma^{\text{L, ret}}(p) & 0 \end{pmatrix}. \quad (5.23)$$

These conventions are chosen in order to comply with the conventions from [ABB11]. R and L denote the right- and the left-handed Majorana neutrino self-energy.

For the thermal width, this implies

$$\begin{aligned} \Gamma_{\mathbf{p}}(p^0) &= \frac{1}{2p^0} \text{Tr}[\not{p} \text{Im } \Sigma^{\text{ret}}(p)] \\ &= \frac{1}{4p^0} \text{Tr} \begin{pmatrix} (p^0\mathbb{1}_2 - \mathbf{p}\boldsymbol{\sigma})(a_{\mathbf{p}}\mathbb{1}_2 + b_{\mathbf{p}}\mathbf{p}\boldsymbol{\sigma}) & 0 \\ 0 & (p^0\mathbb{1}_2 + \mathbf{p}\boldsymbol{\sigma})(a_{\mathbf{p}}\mathbb{1}_2 - b_{\mathbf{p}}\mathbf{p}\boldsymbol{\sigma}) \end{pmatrix} \\ &= \frac{1}{p^0} \text{Tr}[(p^0\mathbb{1}_2 + \mathbf{p}\boldsymbol{\sigma}) \text{Im } \Sigma^{\text{R, ret}}(p)] \\ &= \frac{1}{p^0} \text{Tr}[\bar{\boldsymbol{\sigma}} \cdot p \text{Im } \Sigma^{\text{R, ret}}(p)], \end{aligned} \quad (5.24)$$

where $\bar{\boldsymbol{\sigma}}^0 = \mathbb{1}_2$, $\bar{\boldsymbol{\sigma}} = -\boldsymbol{\sigma}$, and $\text{Tr}(\sigma^j\sigma^k) = 2\delta_{jk}$ has been used. This is equivalent to the statement that both orientations of the internal lines, i.e. the Higgs boson and lepton lines, in Fig. 5.6 give the same contribution due to the neglect of SM CP-violation. Therefore, one can rewrite the self-energy in a 2×2 matrix [cf. ABB11, p. 4].

In the following, first the resummation of $\text{Im } \Sigma^{\text{R, ret}}(p)$ is discussed as a summary of the calculation presented in [ABB11]. Then, the connection between the left- and the right-handed Majorana neutrino self-energy as well as further details are presented.

5.6.2. Calculation of the Two-Point Function without Soft Gauge Contributions

As discussed in Sec. 5.5, the first step in the calculation is integrating out the hard field modes. The results are the resummed Higgs boson and lepton propagators. Hence, this step is done by using these propagators. From now on, the subscript ∞ is dropped at the asymptotic masses.

Keeping only the leading order $g^2 T^2$ terms in the denominator, i.e. approximating $q_+ \simeq 2q_{\parallel}$, one has for the Higgs boson [see BB10, p. 5] [as cited in ABB11, p. 8]

$$\begin{aligned} \Delta(q) &= \frac{-1}{q^2 - m_\phi^2} \\ &= \frac{-1}{q_+ q_- - \mathbf{q}_\perp^2 - m_\phi^2} \simeq \frac{D_\phi(q)}{2q_{\parallel}}, \end{aligned} \quad (5.25)$$

where

$$D_a(q) := \frac{-1}{v \cdot q - (\mathbf{q}_\perp^2 + m_a^2)/(2q_{\parallel})} \quad (5.26)$$

with a standing for ϕ or l , v being the light-like four-vector for lightcone coordinates as discussed in Sec. 5.3.2, and $q_- = q_0 - q_{\parallel} = v \cdot q$.

For the lepton propagator, one has to consider the projector P_R , which results in the fact that due to the multiplication from the right-hand side, one only has to consider a left-handed fermion in the loop for the right-handed Majorana neutrino self-energy, i.e.

$$\begin{aligned} S(k)P_R &= -\frac{\not{k} - \frac{m_l^2}{2k_0}\gamma^0}{k^2 - m_l^2} P_R = -P_L \frac{\not{k} - \frac{m_l^2}{2k_0}\gamma^0}{k^2 - m_l^2} \\ &= -\begin{pmatrix} \mathbb{1}_2 & 0 \\ 0 & 0 \end{pmatrix} \frac{1}{k^2 - m_l^2} \begin{pmatrix} 0 & (k_0 - \frac{m_l^2}{2k_0})\mathbb{1}_2 - k_k \sigma^k \\ (k_0 - \frac{m_l^2}{2k_0})\mathbb{1}_2 + k_k \sigma^k & 0 \end{pmatrix} \\ &=: \begin{pmatrix} \mathbb{1}_2 & 0 \\ 0 & 0 \end{pmatrix} \begin{pmatrix} 0 & S_L(k) \\ S_R(k) & 0 \end{pmatrix} \\ &= -\frac{1}{k^2 - m_l^2} \begin{pmatrix} 0 & (k_0 - \frac{m_l^2}{2k_0})\mathbb{1}_2 - k_k \sigma^k \\ 0 & 0 \end{pmatrix}. \end{aligned} \quad (5.27)$$

One finds with the same approximation for the lepton as for the Higgs boson momentum [see ABB11, pp. 8-9]

$$S_L(k) \simeq \frac{D_l(k)}{2k_{\parallel}} \sigma \cdot \tilde{k}, \quad (5.28)$$

where

$$\tilde{k}^\mu = k^\mu - \frac{m_l^2}{2k_{\parallel}} u^\mu, \quad (5.29)$$

$(\sigma^\mu) = (\mathbb{1}_2, \boldsymbol{\sigma})$, and $(u^\mu) = (1, \mathbf{0})$ is the four-velocity of the plasma. The loop integral is evaluated in the imaginary-time formalism and the imaginary part is taken. Then, the lepton propagator is on-shell and \mathbf{k} can be treated as a light-like four-vector allowing for the manipulation [see ABB11, p. 9]

$$\sigma \cdot \tilde{k} = 2k_{\parallel} \eta(\tilde{k}) \eta^\dagger(\tilde{k}), \quad (5.30)$$

where $\eta(\tilde{k})$ is the eigenvector of $\sigma \cdot \tilde{k}$ with eigenvalue $\tilde{k}^0 + |\tilde{\mathbf{k}}|$ [see Bes10, p. 80]. Choosing \mathbf{v} along the 3-axis, i.e. $k^3 = k_{\parallel}$, one can expand $\eta(\tilde{k})$ [see ABB11, p. 9]

$$\eta(\tilde{k}) = \begin{pmatrix} 0 \\ 1 \end{pmatrix} - \frac{\boldsymbol{\sigma} \tilde{\mathbf{k}}_{\perp}}{2\tilde{k}_{\parallel}} \begin{pmatrix} 0 \\ 1 \end{pmatrix} + \begin{pmatrix} \mathcal{O}(g^2) \\ 0 \end{pmatrix} = \begin{pmatrix} -\frac{\tilde{k}_{\perp}^2 - i\tilde{k}_{\perp}^2}{2\tilde{k}_{\parallel}} + \mathcal{O}(g^2) \\ 1 \end{pmatrix}, \quad (5.31)$$

where $\boldsymbol{\sigma} \tilde{\mathbf{k}}_{\perp}$ only concerns the one- and two-components. Due to normalization, only the upper component of η has an error of order $\mathcal{O}(g^2)$. The proof of Eq. (5.30) can be found in the appendix, Sec. B.2.1. Since the difference of \tilde{k} and k is of order $\mathcal{O}(g^2 T)$ and only the leading order of each component of η is needed, which is at most of order $\mathcal{O}(g)$, one can write $\eta(k)$ instead of $\eta(\tilde{k})$.

A partial fractioning gives [see ABB11, p. 9]

$$D_l(k)D_{\phi}(k-p) = \frac{1}{\epsilon(p, \mathbf{k})} [D_l(k) - D_{\phi}(k-p)] \quad (5.32)$$

with the difference of the energy poles of the Higgs boson and lepton propagators

$$\epsilon(p, \mathbf{k}) := v \cdot p + \frac{(\mathbf{k}_{\perp} - \mathbf{p}_{\perp})^2 + m_{\phi}^2}{2(k_{\parallel} - p_{\parallel})} - \frac{\mathbf{k}_{\perp}^2 + m_l^2}{2k_{\parallel}}, \quad (5.33)$$

which can be easily proven by converting the fractions to a common denominator. Note that in order to apply this to the momentum conventions in the diagrams here, that are chosen for later purposes, one has to use the fact that $\Delta(q) = \Delta(-q)$, since $q = p - k$ for the diagram in Fig. 5.6. Besides, p and k are exchanged here with respect to their meanings in [ABB11]. For the one-loop two-point function without any soft gauge boson lines, i.e. the self-energy without soft gauge contributions, one therefore finds in the imaginary-time formalism [see ABB11, pp. 9-10]

$$\Sigma^{\text{R, ret}}(p) = |\lambda|^2 \int \frac{d^3 k}{(2\pi)^3} \eta(k) \hat{\Sigma}(p, \mathbf{k}) \quad (5.34)$$

with the Yukawa coupling $|\lambda|^2 = \sum_i |\lambda_{1i}|^2 = (\lambda^{\dagger} \lambda)_{11}$ and the reduced self-energy

$$\hat{\Sigma}(p, \mathbf{k}) = -\frac{d(r)\mathcal{F}(p_{\parallel}, k_{\parallel})}{2\epsilon(p, \mathbf{k})} \frac{\eta^{\dagger}(k)}{k_{\parallel} - p_{\parallel}}, \quad (5.35)$$

where $d(r) = 2$ is the dimension of the gauge group representation for the lepton and the Higgs boson, and

$$\mathcal{F}(p_{\parallel}, k_{\parallel}) := f_F(k_{\parallel}) + f_B(k_{\parallel} - p_{\parallel}) = -\frac{f_F(k_{\parallel})f_B(p_{\parallel} - k_{\parallel})}{f_F(k_{\parallel})}. \quad (5.36)$$

5.6.3. Derivation of the Recursion Relation

Now, the recursion relation for the n -point function discussed in Sec. 5.5, see Fig. 5.7, is derived. One starts with the current J_{μ}^a defined as the background of external Majorana neutrino N and of gauge fields A_{μ}^a [see ABB11, p. 11] and given by [see BB10, p. 8]

$$J_{\mu}^a(p) = \int \frac{d^3 k}{(2\pi)^3} V_{\mu}(k, k-p) \text{Tr} \left[t^a \hat{J}(p, \mathbf{k}) \right] \quad (5.37)$$

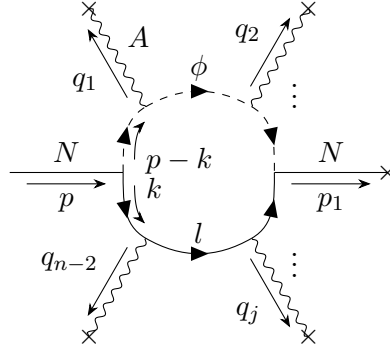


Figure 5.7.: One-loop diagram (n-point function) with soft external gauge boson lines, $2 \leq j \leq n-2$, from [ABB11, p. 10]. \times denotes external field.

with the vertex factor $V_\mu(k, k-p) := \frac{1}{2k_\parallel}(2k-p)_\mu$, the generators of the gauge group t^a , and the trace over the gauge group indices. The unintegrated current is defined via [cf. BB10, p. 8]

$$\begin{aligned} \hat{J}(p, \mathbf{k}) &= \sum_{n=2}^{\infty} \prod_{i=2}^{n-1} \left(\int_{q_i} A_{a_i}^{\mu_i}(q_i) \right) \int_{p_1} \tilde{\delta} \left(p - p_1 - \sum_{j=2}^{n-1} q_j \right) \\ &\times \hat{\Sigma}_{\mu_2 \dots \mu_{n-1}}^{(n) a_2 \dots a_{n-1}}(p_1, q_2, \dots, q_{n-2}, \mathbf{k}) N(p_1), \end{aligned} \quad (5.38)$$

where $\int_q = T \sum_{q^0=i\omega} \int d^3q / (2\pi)^3$ (already in the imaginary-time formalism with the Matsubara frequencies ω), $\tilde{\delta}(q) = T^{-1} \delta_{q^0,0} (2\pi)^3 \delta^3(\mathbf{q})$, and q_k are soft momenta for gauge bosons. $\hat{\Sigma}$ is again the reduced self-energy. Without gauge fields, one finds

$$\text{tr} \hat{J}(p, \mathbf{k}) = \hat{\Sigma}(p, \mathbf{k}) N(p), \quad (5.39)$$

where the trace tr refers to SU(2) indices. With the partial fraction decomposition Eq. (5.32) and the reduced self-energy Eq. (5.35), one obtains a recursion relation by leaving out one soft gauge boson propagator with momentum \mathbf{q} and the corresponding vertex, thus obtaining a $(n-1)$ -point function, and replacing $\mathbf{k} \rightarrow \mathbf{k} - \mathbf{q}$ and $k^0 \rightarrow k^0 + q^0$. Details on this can be found in [ABB11, pp. 10-12]. The recursion relation is given by

$$\begin{aligned} \epsilon(p, \mathbf{k}) \hat{J}(p, \mathbf{k}) &= -\frac{1}{2} \mathcal{F}(p_\parallel, k_\parallel) \frac{\eta^\dagger(k)}{k_\parallel - p_\parallel} N(p) \\ &+ \int_q \left[\hat{J}(p-q, \mathbf{k}) V \cdot A(q) - V \cdot A(q) \hat{J}(p-q, \mathbf{k} - \mathbf{q}) \right], \end{aligned} \quad (5.40)$$

where $A^\mu = A_a^{\mu t^a}$ contains SU(2) and U(1) gauge fields [see ABB11, p. 12].

5.6.4. Integrating out the Soft Gauge Bosons and Result for the Right-Handed Majorana Neutrino Self-Energy

Turning to the task of integrating out the soft gauge bosons, it is useful to rewrite Eq. (5.40) schematically as $\hat{J} = N + A\hat{J}$. One iteration of this expression gives $\hat{J} = N + A(N + A\hat{J})$. After integration over the gauge fields, terms linear in A vanish and $\langle AA\hat{J} \rangle = \langle AA \rangle \langle \hat{J} \rangle$ [see BB10, pp. 10, 14-16], where $\langle \dots \rangle$ denotes a path integral over the gauge field with soft

momentum. Explicitly, one has [see ABB11, p. 12]

$$\begin{aligned} \epsilon(p, \mathbf{k}) \text{tr} \langle \hat{J}(p, \mathbf{k}) \rangle &= -\frac{d(r)}{2} \mathcal{F}(p_{\parallel}, k_{\parallel}) \frac{\eta^{\dagger}(k)}{k_{\parallel} - p_{\parallel}} N(p) \\ &+ 2 \int_q \int_{q'} \frac{1}{V \cdot (p - q)} \text{tr} \left[\langle V \cdot A(q) V \cdot A(q') \rangle \langle \hat{J}(k, \mathbf{p}) - \hat{J}(k, p_{\parallel}, \mathbf{p}_{\perp} - \mathbf{q}_{\perp}) \rangle \right] \end{aligned} \quad (5.41)$$

with the trace tr over $\text{SU}(2)$ indices. At leading order, one has for the $\text{SU}(2) \times \text{U}(1)$ gauge fields [see ABB11, p. 13]

$$\langle A_{\mu}(q) A_{\nu}(q') \rangle = \tilde{\delta}(q + q') [C_2(r) g_W^2 \Delta_{\mu\nu}(q) + y_l^2 g_Y^2 \Delta'_{\mu\nu}(q')] \quad (5.42)$$

with the HTL resummed gauge boson propagators $\Delta_{\mu\nu}$ and $\Delta'_{\mu\nu}$ of $\text{SU}(2)$ and $\text{U}(1)$ gauge fields from [BP90] [as cited in Ani+11, p. 13], the Casimir operator $C_2(r) = 3/4$ for $\text{SU}(2)$, and the lepton hypercharge $y_l = -1/2$. In the expression

$$I(p, \mathbf{q}_{\perp}) := T \sum_{q^0=i\omega} \int \frac{dq_{\parallel}}{2\pi} \frac{V^{\mu} V^{\nu} \Delta_{\mu\nu}(q)}{V \cdot (p - q)} \quad (5.43)$$

encountered then (analogously for $\Delta'_{\mu\nu}$), one can perform the Matsubara summation and an analytical continuation to $p^0 + i0^+$ with p^0 being real, since the goal is to find the retarded self-energy. The result using HTL resummed propagators is [see ABB11, p. 13]

$$I(p^0 + i0^+, \mathbf{k}, \mathbf{q}_{\perp}) \simeq -\frac{i}{2} T \left(\frac{1}{\mathbf{q}_{\perp}^2} - \frac{1}{\mathbf{q}_{\perp}^2 + m_D^2} \right) \quad (5.44)$$

with the appropriate Debye mass m_D . Stripping off the background N -field, one finds [see ABB11, p. 14]

$$\begin{aligned} i\epsilon(p, \mathbf{k}) \hat{\Sigma}(p, \mathbf{k}) &= -\frac{i}{2} d(r) \mathcal{F}(p_{\parallel}, k_{\parallel}) \frac{\eta^{\dagger}(k)}{k_{\parallel} - p_{\parallel}} \\ &+ \int \frac{d^2 q_{\perp}}{(2\pi)^2} \mathcal{C}(\mathbf{q}_{\perp}) \left[\hat{\Sigma}(p, \mathbf{k}) - \hat{\Sigma}(p, k_{\parallel}, \mathbf{k}_{\perp}) \right] \end{aligned} \quad (5.45)$$

with the kernel

$$\mathcal{C}(\mathbf{q}_{\perp}) := T \left[C_2(r) g_W^2 \left(\frac{1}{\mathbf{q}_{\perp}^2} - \frac{1}{\mathbf{q}_{\perp}^2 + m_D^2} \right) + y_l^2 g_Y^2 \left(\frac{1}{\mathbf{q}_{\perp}^2} - \frac{1}{\mathbf{q}_{\perp}^2 + (m'_D)^2} \right) \right], \quad (5.46)$$

where m_D and m'_D are the Debye masses of $\text{SU}(2)$ and $\text{U}(1)$, respectively, given by [Car92]

$$m_D^2 = \frac{11}{6} g_W^2 T^2, \quad (5.47)$$

$$(m'_D)^2 = \frac{11}{6} g_Y^2 T^2. \quad (5.48)$$

The first step in solving Eq. (5.45) is to define the functions $\mathbf{f} = (f_1, f_2)$ and ψ as solutions to the integral equations

$$i\epsilon(p, \mathbf{k}) \mathbf{f}(\mathbf{k}_{\perp}) - \int \frac{d^2 q_{\perp}}{(2\pi)^2} \mathcal{C}(\mathbf{q}_{\perp}) [\mathbf{f}(\mathbf{k}_{\perp}) - \mathbf{f}(\mathbf{k}_{\perp} - \mathbf{q}_{\perp})] = 2\mathbf{k}_{\perp}, \quad (5.49)$$

$$i\epsilon(p, \mathbf{k}) \psi(\mathbf{k}_{\perp}) - \int \frac{d^2 q_{\perp}}{(2\pi)^2} \mathcal{C}(\mathbf{q}_{\perp}) [\psi(\mathbf{k}_{\perp}) - \psi(\mathbf{k}_{\perp} - \mathbf{q}_{\perp})] = 1, \quad (5.50)$$

where the dependences on p and k_{\parallel} has been suppressed. The solution of Eq. (5.45) is then given by [see ABB11, p. 15]⁴

$$\hat{\Sigma}(p, \mathbf{k}) = -\frac{i}{2} \frac{d(r)\mathcal{F}(p_{\parallel}, k_{\parallel})}{k_{\parallel} - p_{\parallel}} \begin{pmatrix} -\frac{f_1 + if_2}{4k_{\parallel}} & \psi \end{pmatrix}. \quad (5.51)$$

In the calculation, one has already chosen the 3-axis to be in the direction of \mathbf{v} . Due to the fact that p and k should be collinear for the leading order contribution, it makes sense to choose \mathbf{p} to also point in this direction, thus giving $\mathbf{p}_{\perp} = \mathbf{0}$ and $p_{\parallel} = |\mathbf{p}|$. Note that this is supported by the fact that all quantities calculated from the Majorana neutrino self-energy in the context of this thesis, i.e. the thermal width and the lepton number matrix, are invariant under rotation. For the retarded right-handed Majorana neutrino self-energy this gives

$$\begin{aligned} \Sigma^{\text{R, ret}}(p^0, p_{\parallel}) &= -|\lambda|^2 \frac{id(r)}{2} \int_{\mathbf{k}} \frac{\mathcal{F}(p_{\parallel}, k_{\parallel})}{k_{\parallel} - p_{\parallel}} \begin{pmatrix} -\frac{k^1 - ik^2}{2k_{\parallel}} \\ 1 \end{pmatrix} \begin{pmatrix} -\frac{f_1 + if_2}{4k_{\parallel}} & \psi \end{pmatrix} \\ &= -|\lambda|^2 \frac{id(r)}{2} \int_{\mathbf{k}} \frac{\mathcal{F}(p_{\parallel}, k_{\parallel})}{k_{\parallel} - p_{\parallel}} \begin{pmatrix} \frac{(k^1 - ik^2)(f_1 + if_2)}{8k_{\parallel}^2} & -\frac{k^1 - ik^2}{2k_{\parallel}} \psi \\ -\frac{f_1 + if_2}{4k_{\parallel}} & \psi \end{pmatrix}, \end{aligned} \quad (5.52)$$

where again $\int_{\mathbf{k}} = \int d^3k / (2\pi)^3$, so that one finds for the imaginary part using the definition (3.69)

$$\text{Im } \Sigma^{\text{R, ret}}(p^0, p_{\parallel}) = -|\lambda|^2 \frac{d(r)}{2} \int_{\mathbf{k}} \frac{\mathcal{F}(p_{\parallel}, k_{\parallel})}{k_{\parallel} - p_{\parallel}} \begin{pmatrix} \frac{\text{Re } \mathbf{k}_{\perp} \mathbf{f}}{8k_{\parallel}} & 0 \\ 0 & \text{Re } \psi \end{pmatrix}, \quad (5.53)$$

where all other terms vanish as shown in the appendix, Sec. B.2.3. Note that in contrast to [ABB11] and [Hüt13], the light-like approximation for the Majorana neutrino $p^0 \simeq p_{\parallel}$, i.e. $p_+ \simeq 2p_{\parallel}$ and $p_- \simeq M^2 / (2p_{\parallel})$, is not inserted explicitly because of the fact that for the lepton number matrix, an integration over p^0 has to be performed. Nevertheless, the resummation of the Majorana neutrino self-energy uses collinearity of its momentum with the Higgs boson and lepton momenta, for which the light-like approximation is needed during the calculation for the resummation. A comparison between explicitly entering the light-like approximation for the Majorana neutrino $p^0 \simeq p_{\parallel}$ and the on-shell $p^0 = \omega_{\mathbf{p}}$, i.e. without explicitly entering the approximation, is made in Ch. 7. For convenience, define

$$\sigma_h(p^0, p_{\parallel}) = \frac{d(r)}{2} \int \frac{dk_{\parallel}}{2\pi} \frac{\mathcal{F}(p_{\parallel}, k_{\parallel})}{k_{\parallel} - p_{\parallel}} \frac{1}{8k_{\parallel}^2} \int \frac{d^2k_{\perp}}{(2\pi)^2} \text{Re}(\mathbf{k}_{\perp} \mathbf{f}(\mathbf{k}_{\perp})), \quad (5.54)$$

$$\sigma_{\psi}(p^0, p_{\parallel}) = \frac{d(r)}{2} \int \frac{dk_{\parallel}}{2\pi} \frac{\mathcal{F}(p_{\parallel}, k_{\parallel})}{k_{\parallel} - p_{\parallel}} \int \frac{d^2k_{\perp}}{(2\pi)^2} \text{Re } \psi(\mathbf{k}_{\perp}), \quad (5.55)$$

where the subscript h is due to the procedure of the numerical evaluation for \mathbf{f} . With this, one has

$$\text{Im } \Sigma^{\text{R, ret}}(p^0, p_{\parallel}) = |\lambda|^2 \begin{pmatrix} \sigma_h(p^0, p_{\parallel}) & 0 \\ 0 & \sigma_{\psi}(p^0, p_{\parallel}) \end{pmatrix}. \quad (5.56)$$

Note that \mathbf{f} vanishes for $\mathbf{k}_{\perp} = \mathbf{0}$, whereas ψ vanishes for $M \rightarrow 0$. Due to the fact that fermions of different chirality are coupled via the Yukawa coupling, this means that \mathbf{f} and therefore σ_h can be related to a helicity changing process, whereas ψ and σ_{ψ} can be related to the helicity conserving process [see ABB11, p. 15].

⁴A factor of 1/4 is missing in [ABB11], [see Hüt13, p. 42].

5.6.5. Symmetries of the Majorana Neutrino Self-Energy

In this section, symmetry relations of the Majorana neutrino self-energy are discussed.

First, a relation between the left- and the right-handed Majorana neutrino self-energy is derived. For this, note that one has to use the right-handed lepton propagator S_R for the left-handed Majorana neutrino self-energy instead of the left-handed one S_L . It is obvious from Eqs. (5.27) that

$$S_R(k^0, \mathbf{k}) = S_L(k^0, -\mathbf{k}) . \quad (5.57)$$

Since an integration over the three-momentum \mathbf{k} of the loop is performed during the calculation of the right-handed self-energy, and $\Delta(q^0, \mathbf{q}) = \Delta(q^0, -\mathbf{q})$ holds for the Higgs boson propagator, one can change the integration variable from $\mathbf{k} \rightarrow -\mathbf{k}$ and therefore go from the left- to the right-handed lepton propagator. Due to momentum conservation this however gives $\mathbf{p} + \mathbf{k}$ as the three-momentum of the Higgs boson in the momentum directions as in Fig. 5.6. Therefore, after using the fact that the scalar propagator is an even function of the three-momentum, one arrives at the conclusion that going from the left- to the right-handed lepton propagator, which obviously corresponds to going from the right-handed to the left-handed Majorana neutrino self-energy, means also changing \mathbf{p} to $-\mathbf{p}$, i.e.

$$\begin{aligned} \text{Im } \Sigma^{\text{R, ret}}(p^0, \mathbf{p}) &\sim \int_{\mathbf{k}} S_L(k^0, \mathbf{k}) \Delta(p^0 - k^0, \mathbf{p} - \mathbf{k}) \\ &= \int_{-\mathbf{k}} S_L(k^0, -\mathbf{k}) \Delta(p^0 - k^0, \mathbf{p} + \mathbf{k}) \\ &= \int_{\mathbf{k}} S_R(k^0, \mathbf{k}) \Delta(p^0 - k^0, -\mathbf{p} - \mathbf{k}) \\ &\sim \text{Im } \Sigma^{\text{L, ret}}(p^0, -\mathbf{p}) . \end{aligned} \quad (5.58)$$

The soft gauge boson lines do not change this, since also for the additional lepton propagators and loop integrals, a substitution from the three-momentum to its negative can be made. In total, one arrives at the conclusion

$$\text{Im } \Sigma^{\text{R, ret}}(p^0, \mathbf{p}) = \text{Im } \Sigma^{\text{L, ret}}(p^0, -\mathbf{p}) \quad (5.59)$$

also for the resummed Majorana neutrino self-energy. The structure of the left- and the right-handed Majorana neutrino self-energy from Eq. (5.21) implies that for $\mathbf{p}_\perp = \mathbf{0}$, one has

$$\text{Im } \Sigma^{\text{L, ret}}(p^0, \mathbf{p}) = \begin{pmatrix} \left(\text{Im } \Sigma^{\text{R, ret}}(p^0, \mathbf{p}) \right)_{22} & 0 \\ 0 & \left(\text{Im } \Sigma^{\text{R, ret}}(p^0, \mathbf{p}) \right)_{11} \end{pmatrix} . \quad (5.60)$$

This gives

$$\text{Im } \Sigma^{\text{R, ret}}(p^0, p_\parallel) = |\lambda|^2 \begin{pmatrix} \sigma_\psi(p^0, p_\parallel) & 0 \\ 0 & \sigma_h(p^0, p_\parallel) \end{pmatrix} \quad (5.61)$$

with $\sigma_\psi(p^0, p_\parallel)$ and $\sigma_h(p^0, p_\parallel)$ as given in Eqs. (5.55) and (5.54), respectively. Together with (5.59), this implies that

$$\sigma_h(p^0, -p_\parallel) = \sigma_\psi(p^0, p_\parallel) , \quad (5.62)$$

$$\sigma_\psi(p^0, -p_\parallel) = \sigma_h(p^0, p_\parallel) . \quad (5.63)$$

Using the result for the not resummed one-loop Majorana neutrino self-energy from [Ani+11, p. 19] [cf. Wel83], which does not contain any gauge or other SM corrections to the one-loop result, and Eq. (3.67), one has

$$\text{Im } \Sigma^{\text{ret}, 1\text{-loop}}(p) = \frac{1}{2i} \Sigma^{-, 1\text{-loop}}(p) = (\lambda^\dagger \lambda)_{11} \int \frac{d^3 k}{(2\pi)^3 2k} \int \frac{d^3 q}{(2\pi)^3 2q} k \sigma(p; k, q) \quad (5.64)$$

with

$$\begin{aligned} \sigma(p; k, q) = & (1 - f_F(k) + f_B(q))(2\pi)^4 (\delta^4(p - k - q) + \delta^4(p + k + q)) \\ & + (f_F(k) + f_B(q))(2\pi)^4 (\delta^4(p + k - q) + \delta^4(p - k + q)), \end{aligned} \quad (5.65)$$

where p is off-shell and $k = (k, \mathbf{k})$ and $q = (q, \mathbf{q})$ are on-shell with $k = |\mathbf{k}|$ and $q = |\mathbf{q}|$ as zero components. Note that again, k is used to denote the absolute value of the three-momentum as well as the four-momentum. As can be easily seen using the symmetry of the δ -distribution $\delta^4(-p) = \delta^4(p)$, this gives

$$\text{Im } \Sigma^{\text{ret}, 1\text{-loop}}(-p) = \text{Im } \Sigma^{\text{ret}, 1\text{-loop}}(p). \quad (5.66)$$

Due to symmetry under time reflection, the same relation also holds after resummation [see Bes10, p. 47], i.e.

$$\text{Im } \Sigma^{\text{ret}}(-p) = \text{Im } \Sigma^{\text{ret}}(p), \quad (5.67)$$

which implies that

$$\text{Im } \Sigma^{\text{R}, \text{ret}}(-p) = \text{Im } \Sigma^{\text{R}, \text{ret}}(p), \quad (5.68)$$

where Eq. (5.21) has been used. Using Eq. (5.59), one also has

$$\text{Im } \Sigma^{\text{R}, \text{ret}}(-p^0, \mathbf{p}) = \text{Im } \Sigma^{\text{L}, \text{ret}}(p^0, \mathbf{p}) \quad (5.69)$$

and therefore

$$\sigma_h(-p^0, p_{\parallel}) = \sigma_\psi(p^0, p_{\parallel}), \quad (5.70)$$

$$\sigma_\psi(-p^0, p_{\parallel}) = \sigma_h(p^0, p_{\parallel}). \quad (5.71)$$

Note that the method for calculating the resummed and the tree-level $\sigma_h(p^0, p_{\parallel})$ and $\sigma_\psi(p^0, p_{\parallel})$ only works in the vicinity of $p^0 = p_{\parallel}$. Explicitly, for $p^0 \simeq -p_{\parallel}$ one does not take the correct pole of the propagators in the loop calculations into account [cf. BB10, p. 5]. Therefore, the relations presented in this chapter should be applied before attempting to integrate over p^0 by numerically evaluating the resummed Majorana neutrino self-energy.

5.6.6. Calculation of the Tree-Level Result

In this section, the tree-level result for the right-handed Majorana neutrino self-energy, i.e. the result without any soft gauge contributions from Eq. (5.35), is calculated. It is called tree-level result because of the fact that the contributions to the production rate from this are the contributions from the tree-level decay of the Higgs boson into a Majorana neutrino and a lepton and the inverse decay of the Majorana neutrino into a Higgs boson and a lepton [cf. ABB11, p. 16]. Note that hard gauge corrections as well as other corrections due to interactions with hard SM particles are included due to the usage of the resummed Higgs boson and lepton propagators. The tree-level result can be obtained from the integral

equations (5.45), (5.49), and (5.50) by neglecting the contribution from the integral and thus setting $\mathcal{C}(\mathbf{q}_\perp) \equiv 0$. Thus, one arrives at the same expression as in Eq. (5.34) with Eq. (5.35). As before, $\mathbf{p}_\perp = \mathbf{0}$ is chosen. For easier comparison to the fully resummed result, define

$$i\epsilon(p^0 + i0^+, \mathbf{p}, \mathbf{k}) \mathbf{f}^{\text{tree}}(\mathbf{k}_\perp) = 2\mathbf{k}_\perp, \quad (5.72)$$

$$i\epsilon(p^0 + i0^+, \mathbf{p}, \mathbf{k}) \psi^{\text{tree}}(\mathbf{k}_\perp) = 1, \quad (5.73)$$

and

$$\sigma_h^{\text{tree}}(p^0, p_\parallel) = \frac{d(r)}{2} \int \frac{dk_\parallel}{2\pi} \frac{\mathcal{F}(p_\parallel, k_\parallel)}{k_\parallel - p_\parallel} \frac{1}{8k_\parallel^2} \int \frac{d^2k_\perp}{(2\pi)^2} \text{Re}(\mathbf{k}_\perp \mathbf{f}^{\text{tree}}(\mathbf{k}_\perp)), \quad (5.74)$$

$$\sigma_\psi^{\text{tree}}(p^0, p_\parallel) = \frac{d(r)}{2} \int \frac{dk_\parallel}{2\pi} \frac{\mathcal{F}(p_\parallel, k_\parallel)}{k_\parallel - p_\parallel} \int \frac{d^2k_\perp}{(2\pi)^2} \text{Re} \psi^{\text{tree}}(\mathbf{k}_\perp). \quad (5.75)$$

In the above equations, a small positive imaginary part in $\epsilon(p, \mathbf{k})$ coming from the fact that one has $p^0 + i0^+$ to obtain the retarded self-energy has to be kept, i.e. $\epsilon(p^0 + i0^+, \mathbf{p}, \mathbf{k}) = \epsilon(p^0, \mathbf{p}, \mathbf{k}) + i0^+$. Using the relation [see Bes10, p. 11]

$$\frac{1}{x \pm i0^+} = \text{P.V.} \left(\frac{1}{x} \right) \mp i\pi\delta(x), \quad (5.76)$$

where $x \in \mathbb{R}$ and P.V. again denotes the Cauchy principal value, one therefore finds

$$\text{Re}(\mathbf{k}_\perp \mathbf{f}(\mathbf{k}_\perp)) = 2\mathbf{k}_\perp^2 \text{Im} \frac{1}{\epsilon(p^0, \mathbf{p}, \mathbf{k}) + i0^+} = -2\mathbf{k}_\perp^2 \pi\delta(\epsilon(p, \mathbf{k})), \quad (5.77)$$

$$\text{Re} \psi(\mathbf{k}_\perp) = \text{Im} \frac{1}{\epsilon(p^0, \mathbf{p}, \mathbf{k}) + i0^+} = -\pi\delta(\epsilon(p, \mathbf{k})). \quad (5.78)$$

It is useful to rewrite $\epsilon(p, \mathbf{k})$ to

$$\epsilon(p, \mathbf{k}) = \alpha(p^0, p_\parallel, k_\parallel) + \beta(p_\parallel, k_\parallel) \mathbf{k}_\perp^2, \quad (5.79)$$

where

$$\alpha(p^0, p_\parallel, k_\parallel) := p^0 - p_\parallel + \frac{m_\phi}{2(k_\parallel - p_\parallel)} - \frac{m_l^2}{2k_\parallel}, \quad (5.80)$$

$$\beta(p_\parallel, k_\parallel) := \frac{p_\parallel}{2k_\parallel(k_\parallel - p_\parallel)}. \quad (5.81)$$

As before, the light-like approximation $p^0 \simeq p_\parallel$ is not explicitly inserted here. A manipulation of the δ -distribution gives

$$\delta(\epsilon(p, \mathbf{k})) = \delta(\alpha(p^0, p_\parallel, k_\parallel) + \beta(p_\parallel, k_\parallel) \mathbf{k}_\perp^2) = \frac{1}{|\beta(p_\parallel, k_\parallel)|} \delta\left(\frac{\alpha(p^0, p_\parallel, k_\parallel)}{\beta(p_\parallel, k_\parallel)} + \mathbf{k}_\perp^2\right) \quad (5.82)$$

Since the dependence on \mathbf{k}_\perp of the integrands for σ_h^{tree} and $\sigma_\psi^{\text{tree}}$ is only on the absolute value, one can go to two-dimensional polar coordinates, integrate over the angular part, and then make a variable substitution to \mathbf{k}_\perp^2 so that one finds

$$\sigma_h^{\text{tree}}(p^0, p_\parallel) = -\frac{d(r)}{2} \int \frac{dk_\parallel}{2\pi} \frac{\mathcal{F}(p_\parallel, k_\parallel)}{k_\parallel - p_\parallel} \frac{1}{16k_\parallel^2} \int_0^\infty d(\mathbf{k}_\perp^2) \frac{\mathbf{k}_\perp^2}{|\beta(p_\parallel, k_\parallel)|} \delta\left(\frac{\alpha(p^0, p_\parallel, k_\parallel)}{\beta(p_\parallel, k_\parallel)} + \mathbf{k}_\perp^2\right), \quad (5.83)$$

$$\sigma_\psi^{\text{tree}}(p^0, p_\parallel) = -\frac{d(r)}{2} \int \frac{dk_\parallel}{2\pi} \frac{\mathcal{F}(p_\parallel, k_\parallel)}{k_\parallel - p_\parallel} \frac{1}{4} \int_0^\infty d(\mathbf{k}_\perp^2) \frac{1}{|\beta(p_\parallel, k_\parallel)|} \delta\left(\frac{\alpha(p^0, p_\parallel, k_\parallel)}{\beta(p_\parallel, k_\parallel)} + \mathbf{k}_\perp^2\right). \quad (5.84)$$

Carrying out the integral over \mathbf{k}_\perp^2 using the δ -distribution, one needs to consider that the contributing $\mathbf{k}_\perp^2 = -\alpha(p^0, p_\parallel, k_\parallel)/\beta(p_\parallel, k_\parallel) \geq 0$. For $p^0 > p_\parallel > 0$, which is the only case needed in the context of this thesis, this gives

$$\mathbf{k}_\perp^2 = -\frac{\alpha(p^0, p_\parallel, k_\parallel)}{\beta(p_\parallel, k_\parallel)} \geq 0 \quad (5.85)$$

$$\Leftrightarrow -2(p^0 - p_\parallel)k_\parallel^2 + Xk_\parallel - m_l^2 p_\parallel \geq 0 \quad (5.86)$$

$$\Rightarrow \text{if } Y \geq 0: k_{\text{low}} := \frac{X - \sqrt{Y}}{4(p^0 - p_\parallel)} \leq k_\parallel \leq \frac{X + \sqrt{Y}}{4(p^0 - p_\parallel)} =: k_{\text{high}}, \quad (5.87)$$

where

$$X := m_l^2 - m_\phi^2 + 2(p^0 - p_\parallel)p_\parallel, \quad (5.88)$$

$$Y := X^2 - 8m_l^2(p^0 - p_\parallel)p_\parallel. \quad (5.89)$$

If $Y \leq 0$, one has $\sigma_h^{\text{tree}}(p^0, p_\parallel) = \sigma_\psi^{\text{tree}}(p^0, p_\parallel) = 0$ (for $Y = 0$ only $k_\parallel = X/(4(p^0 - p_\parallel))$ contributes to the integral over k_\parallel , which has zero measure). This means that one finds the expressions

$$\sigma_h^{\text{tree}}(p^0, p_\parallel) = \frac{d(r)}{2} \int_{k_{\text{low}}}^{k_{\text{high}}} \frac{dk_\parallel}{2\pi} \frac{\mathcal{F}(p_\parallel, k_\parallel)}{k_\parallel - p_\parallel} \frac{\alpha(p^0, p_\parallel, k_\parallel)}{16k_\parallel^2 \beta(p_\parallel, k_\parallel) |\beta(p_\parallel, k_\parallel)|}, \quad (5.90)$$

$$\sigma_\psi^{\text{tree}}(p^0, p_\parallel) = -\frac{d(r)}{2} \int_{k_{\text{low}}}^{k_{\text{high}}} \frac{dk_\parallel}{2\pi} \frac{\mathcal{F}(p_\parallel, k_\parallel)}{k_\parallel - p_\parallel} \frac{1}{4|\beta(p_\parallel, k_\parallel)|} \quad (5.91)$$

that can now be solved numerically.

Note that if one applies the light-like approximation $p_+ \simeq 2p_\parallel$ and $p_- \simeq M^2/(2p_\parallel)$, one has

$$X = m_l^2 - m_\phi^2 + M^2, \quad (5.92)$$

$$Y = (m_\phi + m_l + M)(m_\phi - m_l + M)(m_\phi + m_l - M)(m_\phi - m_l - M), \quad (5.93)$$

so that the condition $Y \geq 0$ gives $m_\phi \geq M + m_l$, which has the decay of the Higgs boson as a corresponding process, or $M \geq m_\phi + m_l$, which corresponds to the inverse decay of the Majorana neutrino, [cf. ABB11, p. 16]. Otherwise, the tree-level Majorana neutrino self-energy is zero. The correspondences to the processes are obvious from cutting the one-loop tree-level Majorana neutrino self-energy diagram, which gives these.

These observations illustrate that the tree-level σ_h^{tree} and $\sigma_\psi^{\text{tree}}$ can be suppressed to a value of zero due to kinematic reasons. This suppression occurs for certain temperatures, as the asymptotic masses m_ϕ and m_l depend on the temperature, and, without the light-like approximation, for certain p^0 and p_\parallel . Explicitly, for a temperature, where the suppression occurs, and for fixed $p^0 = \omega_{\mathbf{p}}$, all $\sigma_h(\omega_{\mathbf{p}}, p_\parallel) = \sigma_\psi(\omega_{\mathbf{p}}, p_\parallel) \equiv 0$ above a certain p_\parallel , since for large $p_\parallel \gg M$, the light-like approximation is fulfilled and hence, the suppression does not depend on p_\parallel anymore. This means that σ_h and σ_ψ can only be non-zero for small p_\parallel at these temperatures.

5.6.7. Thermal Width

Note that with $\mathbf{p}_\perp = \mathbf{0}$, one has

$$\bar{\sigma} \cdot p = \begin{pmatrix} p^0 + p_\parallel & 0 \\ 0 & p^0 - p_\parallel \end{pmatrix}. \quad (5.94)$$

Therefore, Eq. (5.24) gives for the thermal width in terms of σ_h and σ_ψ

$$\Gamma_{p_{\parallel}}(p^0) = -\frac{|\lambda|^2}{p^0} [(p^0 + p_{\parallel})\sigma_h(p^0, p_{\parallel}) + (p^0 - p_{\parallel})\sigma_\psi(p^0, p_{\parallel})]. \quad (5.95)$$

For the tree-level expression one simply uses the tree-level σ_h^{tree} and $\sigma_\psi^{\text{tree}}$. In all further calculations only the on-shell $\Gamma_{\mathbf{p}} = \Gamma_{\mathbf{p}}(\omega_{\mathbf{p}})$ is needed.

6. Including Gauge Corrections to Thermal Leptogenesis

In this chapter, the systematic procedure for the inclusion of gauge and other SM corrections to thermal leptogenesis is presented following [Hüt13, pp. 51-57]. Afterwards, the necessary approximations for the numerical evaluation of this expression are discussed in detail.

6.1. Including Gauge Corrections to the Lepton Number Matrix

6.1.1. Diagrammatic Viewpoint

As discussed in [Hüt13, p. 51], a starting point for the inclusion of gauge corrections in the lepton number matrix is to consider three-loop contributions to the lepton self-energy of the form of the diagrams in Fig. 4.3, but with one loop involving a gauge boson¹. All of these diagrams can be found in Figs. 6.1, where contributions to Higgs boson and lepton propagator corrections are depicted, and 6.2, where contributions to vertex corrections are depicted. These diagrams have been checked for completeness in [Hüt13] using QGRAF².

As seen in Ch. 5, only including three-loop diagrams is not sufficient for the systematic inclusion of gauge corrections and thus, resummation is needed. In order to have a form, where gauge corrections can be implemented by a resummation of the Majorana neutrino self-energy, one can modify the two-loop diagrams according to the procedure depicted in Fig. 6.3 [see Hüt13, pp. 51-52]. First, one countermands the integration of the heavier Majorana neutrinos N_2 and N_3 (1). Then, the outer lepton line is closed (2) so that one arrives at a cylindrical diagram (3). In this diagram, the Majorana self-energy without any gauge corrections, cf. Fig. 5.4, appears twice. It becomes evident that in order to arrive at a lepton number matrix that consistently includes all leading order gauge corrections, one has to replace the Majorana neutrino self-energy by the resummed one. This results in the cylindrical diagram depicted in Fig. 6.4. Integrating out the heavier Majorana neutrinos N_2 and N_3 again gives an effective vertex on the right-hand side of the diagram with $t_2 \equiv t_4$.

In fact, the cylindrical diagram with the resummed Majorana neutrino self-energy from Ch. 5 includes all three-loop gauge corrections [see Hüt13, pp. 52-53]. The corrections to the Higgs boson and lepton propagator from Fig. 6.1 are included using the HTL resummation at the lightcone scale giving asymptotic masses m_l and m_ϕ . The vertex corrections from Fig. 6.2 (a), (f), and (g) are obviously included in the ladder diagram due to the closing of the outer lepton line. The remaining vertex corrections from Fig. 6.2 correspond to soft external gauge bosons that are integrated out in the last step of the calculation of the resummed Majorana neutrino self-energy.

¹Note that three-loop diagrams are necessary to have CP-violation and at least one gauge boson involved.

²<http://cfif.ist.utl.pt/~paulo/qgraf.html>

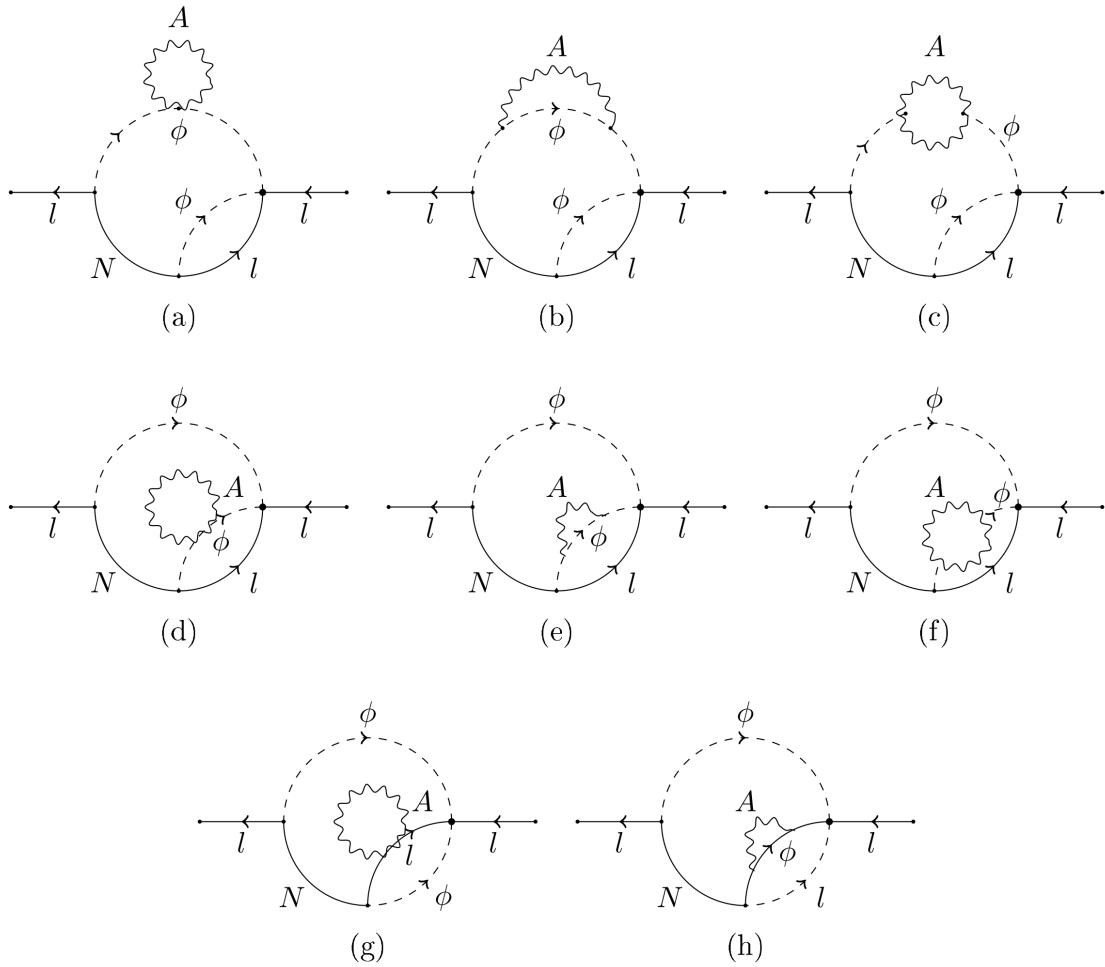


Figure 6.1.: Three-loop contributions to gauge corrections of Higgs boson (a) - (f) and lepton (g)-(h) propagators, from [Hüt13, p. 52].

Note that the resummed Majorana neutrino self-energy also includes corrections due to interactions with other hard SM particles as discussed before. It thus contains all leading order SM corrections.

6.1.2. Implementing the Resummed Majorana Neutrino Self-Energy in the Lepton Number Matrix

In order to implement the resummed Majorana neutrino self-energy in the lepton number matrix, the matrix has to be brought in a form that corresponds to the cylindrical diagram in Fig. 6.4 with $t_2 \equiv t_4$. This calculation was first done in [Hüt13]. This presentation therefore follows this reference with some errors being corrected. To do so, recall the result for the lepton number matrix from Eq. (6.1)

$$L_{\mathbf{k},ii}(t,t) = \frac{64\pi\epsilon_{ii}}{M} \int_0^t dt_1 \int_0^t dt_2 \operatorname{Re} \left(\operatorname{Tr} \left[\Pi_{\mathbf{k}}^{(1)>}(t_1, t_2) S_{\mathbf{k}}^{<}(y_{21}) \right] \right) \quad (6.1)$$

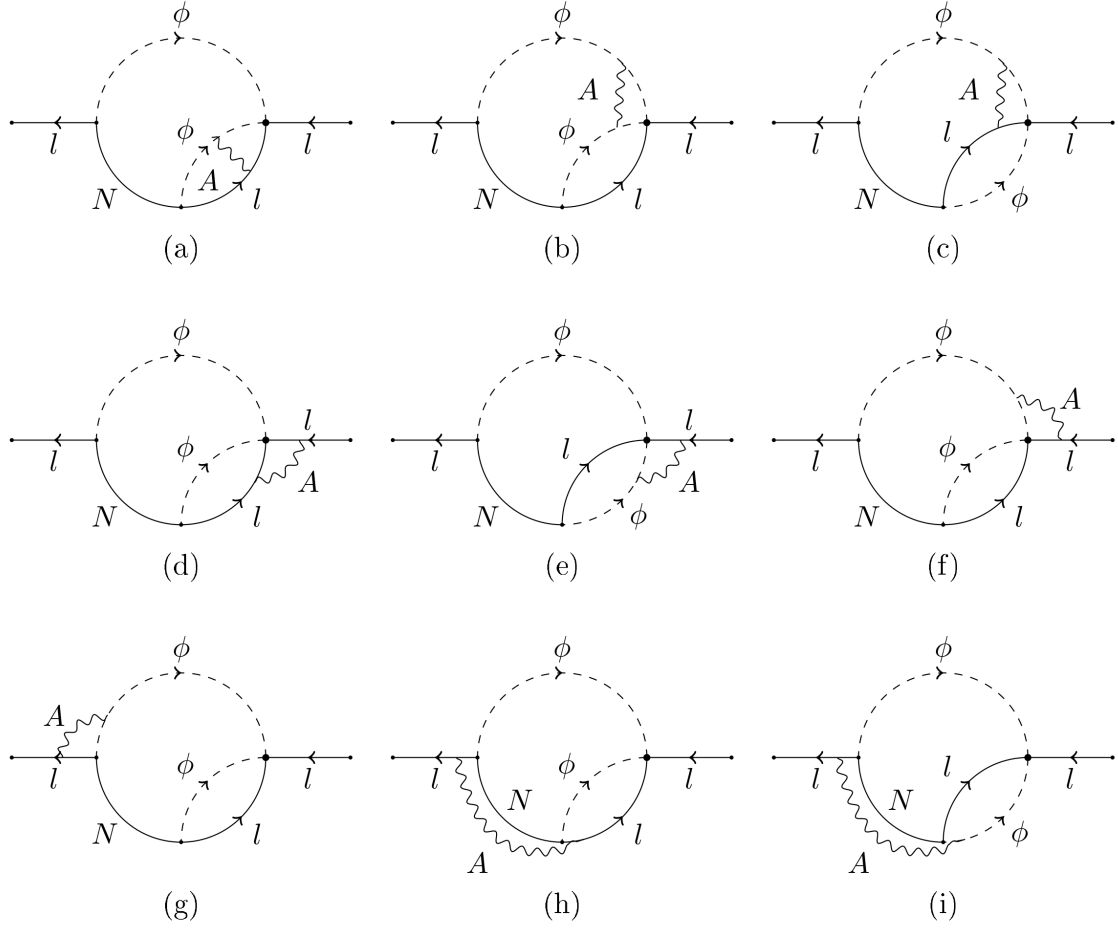


Figure 6.2.: Three-loop contributions to vertex corrections, from [Hüt13, p. 53].

with

$$\begin{aligned} \Pi_{\mathbf{k}}^{(1)>}(t_1, t_2) &= \int_0^\infty dt_3 \int_{\mathbf{q}, \mathbf{q}', \mathbf{k}', \mathbf{p}} (2\pi)^3 \delta^3(\mathbf{p} - \mathbf{k}' - \mathbf{q}') (2\pi)^3 \delta^3(\mathbf{p} + \mathbf{k} + \mathbf{q}) \\ &\quad \times \left[\tilde{G}_{\mathbf{p}}(t_1, t_3) \left(S_{\mathbf{k}'}^{11}(y_{23}) \Delta_{\mathbf{q}'}^{11}(y_{23}) - S_{\mathbf{k}'}^{\leq}(y_{23}) \Delta_{\mathbf{q}'}^{\leq}(y_{23}) \right) \Delta_{\mathbf{q}}^{\leq}(y_{21}) \right] P_L, \end{aligned} \quad (6.2)$$

where $\int_{\mathbf{q}} = \int d^3q / (2\pi)^3$ and $y_{ij} = t_i - t_j$. Note that the three-momentum dependence is corrected compared to [Hüt13]. Using Eqs. (3.8), (3.9), (3.20), (3.21), and (3.62), which also hold for the spatial Fourier transforms of the Higgs boson and lepton propagators due to linearity, one finds

$$\begin{aligned} S_{\mathbf{k}}^{11}(y) &= S_{\mathbf{k}}^+(y) - \frac{i}{2} \text{sign}(y) S_{\mathbf{k}}^-(y) \\ &= \frac{1}{2} (1 + \text{sign}(y)) S_{\mathbf{k}}^>(y) + \frac{1}{2} (1 - \text{sign}(y)) S_{\mathbf{k}}^<(y) \\ &= \theta(y) S_{\mathbf{k}}^>(y) + (1 - \theta(y)) S_{\mathbf{k}}^<(y), \\ \Delta_{\mathbf{q}}^{11}(y) &= \theta(y) \Delta_{\mathbf{q}}^>(y) + (1 - \theta(y)) \Delta_{\mathbf{q}}^<(y). \end{aligned} \quad (6.3)$$

Using the convention $\theta(0) = 1$, this gives [cf. Hüt13, p. 54]

$$S_{\mathbf{k}'}^{11}(y_{23}) \Delta_{\mathbf{q}'}^{11}(y_{23}) - S_{\mathbf{k}'}^{\leq}(y_{23}) \Delta_{\mathbf{q}'}^{\leq}(y_{23}) = \theta(y_{23}) \left(S_{\mathbf{k}'}^>(y_{23}) \Delta_{\mathbf{q}'}^>(y_{23}) - S_{\mathbf{k}'}^<(y_{23}) \Delta_{\mathbf{q}'}^<(y_{23}) \right). \quad (6.4)$$

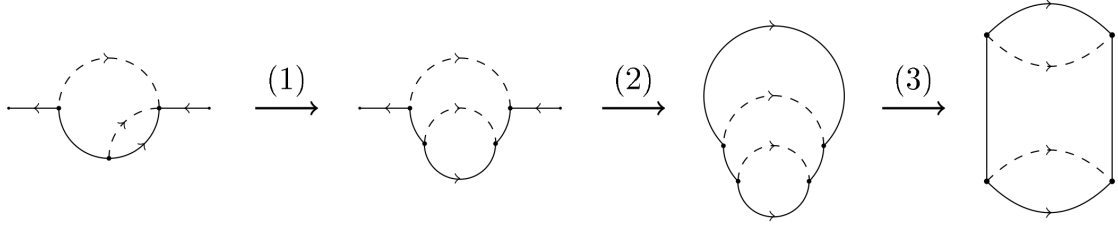


Figure 6.3.: Transformation of the two-loop diagram to a cylindrical diagram, from [Hüt13, p. 51].

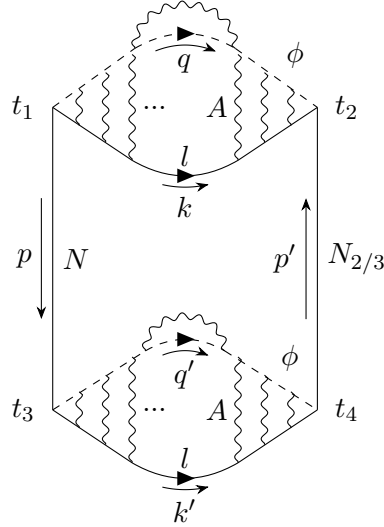


Figure 6.4.: Cylindrical diagram depicting gauge corrections for systematic inclusion, from [Hüt13, p. 54] with corrected momenta.

With the notation

$$\tilde{\Sigma}_{\mathbf{k},\mathbf{q}}^{\leq}(y) := S_{\mathbf{k}}^{\leq}(y)\Delta_{\mathbf{q}}^{\leq}(y) \quad (6.5)$$

the lepton number matrix can be rewritten into [cf. Hüt13, p. 54]

$$L_{\mathbf{k},ii}(t, t) = \frac{64\pi\epsilon_{ii}}{M} \int_0^t dt_1 \int_0^t dt_2 \int_0^{t_2} dt_3 \int_{\mathbf{k}',\mathbf{p}} \tilde{G}_{\mathbf{p}}(t_1, t_3) \\ \times \text{Re} \left(\text{Tr} \left[\tilde{\Sigma}_{\mathbf{k},-(\mathbf{p}+\mathbf{k})}^{\leq}(y_{21}) \left(\tilde{\Sigma}_{\mathbf{k}',\mathbf{p}-\mathbf{k}'}^{\geq}(y_{23}) - \tilde{\Sigma}_{\mathbf{k}',\mathbf{p}-\mathbf{k}'}^{\leq}(y_{23}) \right) P_L \right] \right), \quad (6.6)$$

where the θ -function, the δ -distributions, and the fact that $\tilde{G}_{\mathbf{p}}$ does not have any Dirac structure, i.e. only contains a scalar part, have been used. Considering the Fourier transform

$$\tilde{\Sigma}_{\mathbf{k},\mathbf{q}}^{\leq}(\omega) = \int dy e^{i\omega y} \tilde{\Sigma}_{\mathbf{k},\mathbf{q}}^{\leq}(y) = \int dy e^{i\omega y} S_{\mathbf{k}}^{\leq}(y)\Delta_{\mathbf{q}}^{\leq}(y) \\ = \int dy e^{i\omega y} \int \frac{d\omega'}{2\pi} e^{-i\omega' y} S_{\mathbf{k}}^{\leq}(\omega') \int \frac{d\omega_1}{2\pi} e^{-i\omega_1 y} \Delta_{\mathbf{q}}^{\leq}(\omega_1) \\ = \int \frac{d\omega'}{2\pi} \int \frac{d\omega_1}{2\pi} 2\pi \delta(\omega - \omega' - \omega_1) S_{\mathbf{k}}^{\leq}(\omega') \Delta_{\mathbf{q}}^{\leq}(\omega_1) \\ = \int \frac{d\omega'}{2\pi} S_{\mathbf{k}}^{\leq}(\omega') \Delta_{\mathbf{q}}^{\leq}(\omega - \omega'), \quad (6.7)$$

one finds with the KMS identities Eqs. (3.50) and (3.51)

$$\begin{aligned}\tilde{\Sigma}_{\mathbf{k},\mathbf{q}}^{\geq}(\omega) &= \int \frac{d\omega'}{2\pi} S_{\mathbf{k}}^{\geq}(\omega') \Delta_{\mathbf{q}}^{\geq}(\omega - \omega') \\ &= - \int \frac{d\omega'}{2\pi} e^{\beta\omega'} S_{\mathbf{k}}^{\leq}(\omega') e^{\beta(\omega - \omega')} \Delta_{\mathbf{q}}^{\leq}(\omega - \omega') = -e^{\beta\omega} \tilde{\Sigma}_{\mathbf{k},\mathbf{q}}^{\leq}(\omega).\end{aligned}\quad (6.8)$$

It is obvious from Eq. (6.7) that $\tilde{\Sigma}_{\mathbf{k},\mathbf{q}}^{\leq}(\omega)$ corresponds to the Majorana neutrino self-energy without integration over the loop three-momentum and vertex factors. Using Eq. (6.8), one can further evaluate

$$\begin{aligned}& \text{Re} \left(\text{Tr} \left[\tilde{\Sigma}_{\mathbf{k},-(\mathbf{p}+\mathbf{k})}^{\leq}(y_{21}) \left(\tilde{\Sigma}_{\mathbf{k}',\mathbf{p}-\mathbf{k}'}^{\geq}(y_{23}) - \tilde{\Sigma}_{\mathbf{k}',\mathbf{p}-\mathbf{k}'}^{\leq}(y_{23}) \right) P_L \right] \right) = \\ &= \int \frac{d\omega_{21}}{2\pi} \int \frac{d\omega_{23}}{2\pi} \text{Re} \left(e^{-i(\omega_{21}y_{21} + \omega_{23}y_{23})} \right. \\ &\quad \left. \times \text{Tr} \left[\tilde{\Sigma}_{\mathbf{k},-(\mathbf{p}+\mathbf{k})}^{\leq}(\omega_{21}) \left(\tilde{\Sigma}_{\mathbf{k}',\mathbf{p}-\mathbf{k}'}^{\geq}(\omega_{23}) - \tilde{\Sigma}_{\mathbf{k}',\mathbf{p}-\mathbf{k}'}^{\leq}(\omega_{23}) \right) P_L \right] \right) \\ &= - \int \frac{d\omega_{21}}{2\pi} \int \frac{d\omega_{23}}{2\pi} \text{Re} \left(e^{-i(\omega_{21}y_{21} + \omega_{23}y_{23})} \left(1 + e^{\beta\omega_{23}} \right) \right. \\ &\quad \left. \times \text{Tr} \left[\tilde{\Sigma}_{\mathbf{k},-(\mathbf{p}+\mathbf{k})}^{\leq}(\omega_{21}) \tilde{\Sigma}_{\mathbf{k}',\mathbf{p}-\mathbf{k}'}^{\leq}(\omega_{23}) P_L \right] \right) \\ &= - \int \frac{d\omega_{21}}{2\pi} \int \frac{d\omega_{23}}{2\pi} \left(1 + e^{\beta\omega_{23}} \right) \\ &\quad \times \left(\text{Re} \left(e^{-i(\omega_{21}y_{21} + \omega_{23}y_{23})} \right) \text{Re} \left(\text{Tr} \left[\tilde{\Sigma}_{\mathbf{k},-(\mathbf{p}+\mathbf{k})}^{\leq}(\omega_{21}) \tilde{\Sigma}_{\mathbf{k}',\mathbf{p}-\mathbf{k}'}^{\leq}(\omega_{23}) P_L \right] \right) \right. \\ &\quad \left. - \text{Im} \left(e^{-i(\omega_{21}y_{21} + \omega_{23}y_{23})} \right) \text{Im} \left(\text{Tr} \left[\tilde{\Sigma}_{\mathbf{k},-(\mathbf{p}+\mathbf{k})}^{\leq}(\omega_{21}) \tilde{\Sigma}_{\mathbf{k}',\mathbf{p}-\mathbf{k}'}^{\leq}(\omega_{23}) P_L \right] \right) \right) \\ &= - \int \frac{d\omega_{21}}{2\pi} \int \frac{d\omega_{23}}{2\pi} \left(1 + e^{\beta\omega_{23}} \right) \\ &\quad \times \text{Tr} \left[\left(\text{Re} \left(e^{-i(\omega_{21}y_{21} + \omega_{23}y_{23})} \right) \text{Re} \left(\tilde{\Sigma}_{\mathbf{k},-(\mathbf{p}+\mathbf{k})}^{\leq}(\omega_{21}) \tilde{\Sigma}_{\mathbf{k}',\mathbf{p}-\mathbf{k}'}^{\leq}(\omega_{23}) P_L \right) \right. \right. \\ &\quad \left. \left. - \text{Im} \left(e^{-i(\omega_{21}y_{21} + \omega_{23}y_{23})} \right) \text{Im} \left(\tilde{\Sigma}_{\mathbf{k},-(\mathbf{p}+\mathbf{k})}^{\leq}(\omega_{21}) \tilde{\Sigma}_{\mathbf{k}',\mathbf{p}-\mathbf{k}'}^{\leq}(\omega_{23}) P_L \right) \right) \right],\end{aligned}\quad (6.9)$$

where

$$\text{Re}(\text{Tr}(A)) = \frac{\text{Tr}(A) + (\text{Tr}(A))^*}{2} = \frac{\text{Tr}(A) + \text{Tr}(A^\dagger)}{2} = \text{Tr}(\text{Re}(A)), \quad (6.10)$$

$$\text{Im}(\text{Tr}(A)) = \frac{\text{Tr}(A) - (\text{Tr}(A))^*}{2i} = \frac{\text{Tr}(A) - \text{Tr}(A^\dagger)}{2i} = \text{Tr}(\text{Im}(A)), \quad (6.11)$$

for any $A \in \mathbb{C}^{n \times n}$ has been used. Plugging this expression into the lepton number matrix leads to

$$\begin{aligned}L_{\mathbf{k},ii}(t, t) &= - \frac{64\pi\epsilon_{ii}}{M} \int_0^t dt_1 \int_0^{t_1} dt_2 \int_0^{t_2} dt_3 \int \frac{d\omega_{21}}{2\pi} \int \frac{d\omega_{23}}{2\pi} \int_{\mathbf{k}',\mathbf{p}} \tilde{G}_{\mathbf{p}}(t_1, t_3) \left(1 + e^{\beta\omega_{23}} \right) \\ &\quad \times \text{Tr} \left[\left(\text{Re} \left(e^{-i(\omega_{21}y_{21} + \omega_{23}y_{23})} \right) \text{Re} \left(\tilde{\Sigma}_{\mathbf{k},-(\mathbf{p}+\mathbf{k})}^{\leq}(\omega_{21}) \tilde{\Sigma}_{\mathbf{k}',\mathbf{p}-\mathbf{k}'}^{\leq}(\omega_{23}) P_L \right) \right. \right. \\ &\quad \left. \left. - \text{Im} \left(e^{-i(\omega_{21}y_{21} + \omega_{23}y_{23})} \right) \text{Im} \left(\tilde{\Sigma}_{\mathbf{k},-(\mathbf{p}+\mathbf{k})}^{\leq}(\omega_{21}) \tilde{\Sigma}_{\mathbf{k}',\mathbf{p}-\mathbf{k}'}^{\leq}(\omega_{23}) P_L \right) \right) \right].\end{aligned}\quad (6.12)$$

Note that this result differs from the corresponding result in [Hüt13, p. 55], where additional factors of $1 \pm \exp(2\beta\omega_{23})$ are found and no $1 + \exp(\beta\omega_{23})$ appears. However, the result presented here has been checked in two independent calculations for this thesis and [Hal17]. Therefore, its correctness is assumed and the calculation continues with it.

Since $\tilde{\Sigma}_{\mathbf{k},\mathbf{q}}^{\leq}(\omega)$ corresponds to the Majorana neutrino self-energy without integration over the loop three-momentum and vertex factors, Eqs. (3.42), (3.67), and (6.8) give³

$$\tilde{\Sigma}_{\mathbf{k},\mathbf{q}}^{-}(\omega) = i \left(\tilde{\Sigma}_{\mathbf{k},\mathbf{q}}^{>}(\omega) - \tilde{\Sigma}_{\mathbf{k},\mathbf{q}}^{<}(\omega) \right) = -i \left(1 + e^{\beta\omega} \right) \tilde{\Sigma}_{\mathbf{k},\mathbf{q}}^{>}(\omega) = 2i \operatorname{Im} \tilde{\Sigma}_{\mathbf{k},\mathbf{q}}^{\text{ret}}(\omega) \quad (6.13)$$

$$\Rightarrow \tilde{\Sigma}_{\mathbf{k},\mathbf{q}}^{>}(\omega) = -2f_F(\omega) \operatorname{Im} \tilde{\Sigma}_{\mathbf{k},\mathbf{q}}^{\text{ret}}(\omega) . \quad (6.14)$$

Hence,

$$\left(\operatorname{Im} \tilde{\Sigma}_{\mathbf{k},\mathbf{q}}^{\text{ret}}(\omega) \right)^\dagger = \left(\frac{\tilde{\Sigma}_{\mathbf{k},\mathbf{q}}^{\text{ret}}(\omega) - \left(\tilde{\Sigma}_{\mathbf{k},\mathbf{q}}^{\text{ret}}(\omega) \right)^\dagger}{2i} \right)^\dagger = \operatorname{Im} \tilde{\Sigma}_{\mathbf{k},\mathbf{q}}^{\text{ret}}(\omega) \quad (6.15)$$

$$\Rightarrow \left(\tilde{\Sigma}_{\mathbf{k},\mathbf{q}}^{>}(\omega) \right)^\dagger = \tilde{\Sigma}_{\mathbf{k},\mathbf{q}}^{>}(\omega) . \quad (6.16)$$

Because of the fact that the Majorana self-energy is a vector in Lorentz-space, cf. Eq. (3.71), one can write

$$\begin{aligned} \operatorname{Im} \tilde{\Sigma}_{\mathbf{k},\mathbf{q}}^{\text{ret}}(\omega) &= s_{\mu,\mathbf{k},\mathbf{q}}(\omega) \gamma^\mu \\ &= \begin{pmatrix} 0 & s_{0,\mathbf{k},\mathbf{q}}(\omega) \mathbb{1}_2 + s_{j,\mathbf{k},\mathbf{q}}(\omega) \sigma^j \\ s_{0,\mathbf{k},\mathbf{q}}(\omega) \mathbb{1}_2 - s_{j,\mathbf{k},\mathbf{q}}(\omega) \sigma^j & 0 \end{pmatrix} \end{aligned} \quad (6.17)$$

$$=: \begin{pmatrix} 0 & \operatorname{Im} \tilde{\Sigma}_{\mathbf{k},\mathbf{q}}^{\text{R,ret}}(\omega) \\ \operatorname{Im} \tilde{\Sigma}_{\mathbf{k},\mathbf{q}}^{\text{L,ret}}(\omega) & 0 \end{pmatrix} \quad (6.18)$$

and find

$$\begin{aligned} &\operatorname{Tr} \left[\operatorname{Im} \tilde{\Sigma}_{\mathbf{k},-(\mathbf{p}+\mathbf{k})}^{\text{ret}}(\omega_{21}) \operatorname{Im} \tilde{\Sigma}_{\mathbf{k}',\mathbf{p}-\mathbf{k}'}^{\text{ret}}(\omega_{23}) P_L \right] = \\ &= \operatorname{Tr} \left[(s_{0,\mathbf{k},-(\mathbf{p}+\mathbf{k})}(\omega_{21}) \mathbb{1}_2 + s_{i,\mathbf{k},-(\mathbf{p}+\mathbf{k})}(\omega_{21}) \sigma^i) (s_{0,\mathbf{k}',\mathbf{p}-\mathbf{k}'}(\omega_{23}) \mathbb{1}_2 - s_{j,\mathbf{k}',\mathbf{p}-\mathbf{k}'}(\omega_{23}) \sigma^j) \right] \\ &= \operatorname{Tr} \left[\operatorname{Im} \tilde{\Sigma}_{\mathbf{k},-(\mathbf{p}+\mathbf{k})}^{\text{R,ret}}(\omega_{21}) \operatorname{Im} \tilde{\Sigma}_{\mathbf{k}',\mathbf{p}-\mathbf{k}'}^{\text{L,ret}}(\omega_{23}) \right] \end{aligned} \quad (6.19)$$

$$\begin{aligned} &= \operatorname{Tr} \left[s_{0,\mathbf{k},-(\mathbf{p}+\mathbf{k})}(\omega_{21}) s_{0,\mathbf{k}',\mathbf{p}-\mathbf{k}'}(\omega_{23}) \mathbb{1}_2 - s_{i,\mathbf{k},-(\mathbf{p}+\mathbf{k})}(\omega_{21}) s_{j,\mathbf{k}',\mathbf{p}-\mathbf{k}'}(\omega_{23}) \sigma^i \sigma^j \right] \\ &= \operatorname{Tr} \left[(s_{0,\mathbf{k},-(\mathbf{p}+\mathbf{k})}(\omega_{21}) \mathbb{1}_2 - s_{i,\mathbf{k},-(\mathbf{p}+\mathbf{k})}(\omega_{21}) \sigma^i) (s_{0,\mathbf{k}',\mathbf{p}-\mathbf{k}'}(\omega_{23}) \mathbb{1}_2 + s_{j,\mathbf{k}',\mathbf{p}-\mathbf{k}'}(\omega_{23}) \sigma^j) \right] \\ &= \operatorname{Tr} \left[\operatorname{Im} \tilde{\Sigma}_{\mathbf{k},-(\mathbf{p}+\mathbf{k})}^{\text{L,ret}}(\omega_{21}) \operatorname{Im} \tilde{\Sigma}_{\mathbf{k}',\mathbf{p}-\mathbf{k}'}^{\text{R,ret}}(\omega_{23}) \right] \end{aligned} \quad (6.20)$$

$$\begin{aligned} &= \operatorname{Tr} \left[(s_{0,\mathbf{k}',\mathbf{p}-\mathbf{k}'}(\omega_{23}) \mathbb{1}_2 + s_{j,\mathbf{k}',\mathbf{p}-\mathbf{k}'}(\omega_{23}) \sigma^j) (s_{0,\mathbf{k},-(\mathbf{p}+\mathbf{k})}(\omega_{21}) \mathbb{1}_2 - s_{i,\mathbf{k},-(\mathbf{p}+\mathbf{k})}(\omega_{21}) \sigma^i) \right] \\ &= \operatorname{Tr} \left[\operatorname{Im} \tilde{\Sigma}_{\mathbf{k}',\mathbf{p}-\mathbf{k}'}^{\text{ret}}(\omega_{23}) \operatorname{Im} \tilde{\Sigma}_{\mathbf{k},-(\mathbf{p}+\mathbf{k})}^{\text{ret}}(\omega_{21}) P_L \right] , \end{aligned} \quad (6.21)$$

where $\operatorname{Tr}[\sigma^i \sigma^j] = 2\delta_{ij}$, $\operatorname{Tr}[\sigma^i] = 0$, and the cyclicity of the trace have been used. The definitions of the left- and right-handed parts are made in accordance with the Majorana neutrino self-energy after integration over loop three-momentum and with vertex factors,

³Note that strictly speaking, these relations have only been proven after integration over the loop three-momentum. Since this will be performed anyhow, this is not a problem and therefore not considered any further.

cf. Eq. (5.21). With $P_L = P_L^\dagger$, this gives

$$\begin{aligned} & \text{Tr} \left[\text{Re} \left(\tilde{\Sigma}_{\mathbf{k}, -(\mathbf{p}+\mathbf{k})}^<(\omega_{21}) \tilde{\Sigma}_{\mathbf{k}', \mathbf{p}-\mathbf{k}'}^<(\omega_{23}) P_L \right) \right] = \\ & = \text{Tr} \left[\frac{\tilde{\Sigma}_{\mathbf{k}, -(\mathbf{p}+\mathbf{k})}^<(\omega_{21}) \tilde{\Sigma}_{\mathbf{k}', \mathbf{p}-\mathbf{k}'}^<(\omega_{23}) P_L + \left(\tilde{\Sigma}_{\mathbf{k}, -(\mathbf{p}+\mathbf{k})}^<(\omega_{21}) \tilde{\Sigma}_{\mathbf{k}', \mathbf{p}-\mathbf{k}'}^<(\omega_{23}) P_L \right)^\dagger}{2} \right] \\ & = 2f_F(\omega_{21})f_F(\omega_{23}) \text{Tr} \left[\text{Im} \tilde{\Sigma}_{\mathbf{k}, -(\mathbf{p}+\mathbf{k})}^{\text{ret}}(\omega_{21}) \text{Im} \tilde{\Sigma}_{\mathbf{k}', \mathbf{p}-\mathbf{k}'}^{\text{ret}}(\omega_{23}) P_L \right. \\ & \quad \left. + \text{Im} \tilde{\Sigma}_{\mathbf{k}', \mathbf{p}-\mathbf{k}'}^{\text{ret}}(\omega_{23}) \text{Im} \tilde{\Sigma}_{\mathbf{k}, -(\mathbf{p}+\mathbf{k})}^{\text{ret}}(\omega_{21}) P_L \right] \\ & = 4f_F(\omega_{21})f_F(\omega_{23}) \text{Tr} \left[\text{Im} \tilde{\Sigma}_{\mathbf{k}, -(\mathbf{p}+\mathbf{k})}^{\text{ret}}(\omega_{21}) \text{Im} \tilde{\Sigma}_{\mathbf{k}', \mathbf{p}-\mathbf{k}'}^{\text{ret}}(\omega_{23}) P_L \right], \end{aligned} \quad (6.22)$$

$$\text{Tr} \left[\text{Im} \left(\tilde{\Sigma}_{\mathbf{k}, -(\mathbf{p}+\mathbf{k})}^<(\omega_{21}) \tilde{\Sigma}_{\mathbf{k}', \mathbf{p}-\mathbf{k}'}^<(\omega_{23}) \right) P_L \right] = 0. \quad (6.23)$$

Inserting Eqs. (6.20), (6.22), and (6.23) into the lepton number matrix leads to the expression

$$\begin{aligned} L_{\mathbf{k}, ii}(t, t) &= -\frac{256\pi\epsilon_{ii}}{M} \int_0^t dt_1 \int_0^t dt_2 \int_0^{t_2} dt_3 \int_{\mathbf{k}', \mathbf{p}} \int \frac{d\omega_{21}}{2\pi} \int \frac{d\omega_{23}}{2\pi} \tilde{G}_{\mathbf{p}}(t_1, t_3) f_F(\omega_{21}) \\ & \quad \times \text{Re} \left(e^{-i(\omega_{21}y_{21} + \omega_{23}y_{23})} \right) \text{Tr} \left[\text{Im} \tilde{\Sigma}_{\mathbf{k}, -(\mathbf{p}+\mathbf{k})}^{L, \text{ret}}(\omega_{21}) \text{Im} \tilde{\Sigma}_{\mathbf{k}', \mathbf{p}-\mathbf{k}'}^{\text{R}, \text{ret}}(\omega_{23}) \right]. \end{aligned} \quad (6.24)$$

With this expression, one can now make the connection to the resummed Majorana neutrino self-energy. As discussed before, the integration over the loop three-momentum and the vertex factors have to be included. Therefore, one has [cf. Hüt13, p. 55]

$$\text{Im} \Sigma^{\text{R}, \text{ret}}(\omega, \mathbf{p}) = |\lambda|^2 \int \frac{d^3k}{(2\pi)^3} \text{Im} \tilde{\Sigma}_{\mathbf{k}, \mathbf{p}-\mathbf{k}}^{\text{R}, \text{ret}}(\omega), \quad (6.25)$$

$$\text{Im} \Sigma^{\text{L}, \text{ret}}(\omega, -\mathbf{p}) = |\lambda|^2 \int \frac{d^3k}{(2\pi)^3} \text{Im} \tilde{\Sigma}_{\mathbf{k}, -(\mathbf{p}+\mathbf{k})}^{\text{L}, \text{ret}}(\omega) = \text{Im} \Sigma^{\text{R}, \text{ret}}(\omega, \mathbf{p}), \quad (6.26)$$

$$(6.27)$$

where Eq. (5.59) has been used. These are the right- and left-handed retarded Majorana neutrino self-energy that have been resummed in Ch. 6. Note that a possible $--$ sign due to different conventions for the connection of the Feynman diagrams with the self-energy [see Hüt13, p. 39] can be ignored, since the self-energy appears quadratically in the lepton number matrix. Integrating the lepton number matrix over \mathbf{k} , one finds

$$\begin{aligned} L_{ii}(t, t) &= \int \frac{d^3k}{(2\pi)^3} L_{\mathbf{k}, ii} \\ &= -\frac{256\pi\epsilon_{ii}}{M(|\lambda|^2)^2} \int_0^t dt_1 \int_0^t dt_2 \int_0^{t_2} dt_3 \int \frac{d\omega_{21}}{2\pi} \int \frac{d\omega_{23}}{2\pi} \int_{\mathbf{p}} \tilde{G}_{\mathbf{p}}(t_1, t_3) f_F(\omega_{21}) \\ & \quad \times \text{Re} \left(e^{-i(\omega_{21}y_{21} + \omega_{23}y_{23})} \right) \text{Tr} \left[\text{Im} \Sigma^{\text{R}, \text{ret}}(\omega_{21}, \mathbf{p}) \text{Im} \Sigma^{\text{R}, \text{ret}}(\omega_{23}, \mathbf{p}) \right]. \end{aligned} \quad (6.28)$$

This is also called the integrated lepton number matrix [cf. Hüt13, p. 57]. Due to rotational symmetry of the integrand, which connects to the coefficients in front of the Dirac- and Pauli-matrices in Eq. (5.21), one can integrate over the angular part of \mathbf{p} , thus finding

$$\begin{aligned} L_{ii}(t, t) &= -\frac{128\epsilon_{ii}}{\pi} \int_0^t dt_1 \int_0^t dt_2 \int_0^{t_2} dt_3 \int_0^\infty dp \int \frac{d\omega_{21}}{2\pi} \int \frac{d\omega_{23}}{2\pi} \\ & \quad \times \frac{p^2}{\omega_p} f_F(\omega_p) e^{-\Gamma_p \frac{t_1+t_3}{2}} f_F(\omega_{21}) \cos(\omega_p y_{13}) \\ & \quad \times \text{Re} \left(e^{-i(\omega_{21}y_{21} + \omega_{23}y_{23})} \right) (\sigma_h(\omega_{21}, p) \sigma_h(\omega_{23}, p) + \sigma_\psi(\omega_{21}, p) \sigma_\psi(\omega_{23}, p)), \end{aligned} \quad (6.29)$$

where the nonequilibrium part of the Majorana neutrino propagator from Eq. (4.29)

$$\tilde{G}_{\mathbf{p}}(t_1, t_2) = \frac{M}{\omega_{\mathbf{p}}} \cos(\omega_{\mathbf{p}}(t_1 - t_2)) f_F(\omega_{\mathbf{p}}) e^{-\Gamma_{\mathbf{p}}(t_1+t_2)/2} \quad (6.30)$$

and the Majorana neutrino self-energy written using σ_h and σ_ψ from Eq. (5.56)

$$\text{Im } \Sigma^{\text{R, ret}}(p^0, p) = |\lambda|^2 \begin{pmatrix} \sigma_h(p^0, p) & 0 \\ 0 & \sigma_\psi(p^0, p) \end{pmatrix} \quad (6.31)$$

have been inserted. Note that due to rotational invariance, all \mathbf{p} have been replaced by p and one has $p_{\parallel} = p$. One should also remark that in contrast to [Hüt13], ω_{21} and ω_{23} have not been connected with the absolute value of the loop momenta $|\mathbf{k}|$ and $|\mathbf{k}'|$. The reason for this is firstly that they are the zeroth components of the arguments (four-momenta) of the self-energies and secondly that the integrations over ω_{21} and ω_{23} are done approximately in the next section. Because of this difference and the difference discussed before, the result here is not equal to the result in [Hüt13, p. 57].

A connection between the integrated lepton number matrix L_{ii} and the solution of the Boltzmann equation can be made using $L_{\mathbf{k}, ii} = (t, t) = f_{li}(k) - f_{\bar{l}i}(k) = f_{Li}(k)$ for free fields in equilibrium and $n_L(t) = \sum_i \int \frac{d^3k}{(2\pi)^3} f_{Li}(t, k)$, which give

$$\sum_i L_{ii}(t, t) = n_L(t) \quad (6.32)$$

for free fields in equilibrium. Therefore, the integrated lepton number matrix connects to the difference in number densities of leptons and anti-leptons. For simplicity, the integrated lepton number matrix is just called lepton number matrix from here on.

Even though it is possible to carry out the integrations over t_1 , t_2 and t_3 analytically⁴, cf. Sec. 6.2.2 and appendix, Sec. B.3.1, it is not possible to evaluate Eq. (6.29) directly using the procedure for calculating σ_h and σ_ψ by solving the integral equations. The main problem here are the integrations over ω_{21} and ω_{23} . The integrand is strongly and very narrowly peaked around $\omega_{21} = -\omega_{23} = \pm\omega_p$. Furthermore, it oscillates fast because it involves sines and cosines of $\omega_{21}t$ and $\omega_{23}t$ with $\omega_{21}, \omega_{23} \sim \pm\omega_p$, $t \sim 1/\Gamma_p$ and $p \sim T$ for the dominating region. Since typical values in the simulations later involve T between 10^6 GeV and 10^{12} GeV, which gives Γ_p between 10^{-3} GeV and 10^2 GeV, one finds these fast oscillations. Besides, the symmetries discussed in Sec. 5.6.5 have to be considered first. It is therefore necessary to approximate the lepton number matrix by approximating the integrations over ω_{21} and ω_{23} and integrating over t_1 , t_2 , and t_3 analytically.

6.2. Approximating the Lepton Number Matrix

In this section, the approximations of the lepton number matrix from Eq. (6.29) that are needed for a numerical evaluation are presented. As discussed, these approximations rely on the symmetries of the Majorana neutrino self-energy, cf. Sec. 5.6.5, and the peaks of the integrand of L_{ii} .

⁴Note that this is possible in contrast to the claim made in [Hüt13, p. 57], since the thermal width Γ_p does not depend on t_1 , t_2 , or t_3 .

6.2.1. $t \rightarrow \infty$ Limit

In this section, the lepton number matrix is calculated in the limit $t \rightarrow \infty$, i.e. the completely thermalized lepton number matrix is regarded. For this, consider the time-dependent part of Eq. (6.29)

$$\int_0^t dt_1 \int_0^t dt_2 \int_0^{t_2} dt_3 e^{-\Gamma_p \frac{t_1+t_3}{2}} \cos(\omega_p y_{13}) \operatorname{Re} \left(e^{-i(\omega_{21} y_{21} + \omega_{23} y_{23})} \right) \quad (6.33)$$

and take the desired limit

$$\begin{aligned} & \lim_{t \rightarrow \infty} \int_0^t dt_1 \int_0^t dt_2 \int_0^{t_2} dt_3 e^{-\Gamma_p \frac{t_1+t_3}{2}} \cos(\omega_p y_{13}) \operatorname{Re} \left(e^{-i(\omega_{21} y_{21} + \omega_{23} y_{23})} \right) = \\ & = \operatorname{Re} \left(\int_{-\infty}^{\infty} dt_1 \int_{-\infty}^{\infty} dt_2 \int_{-\infty}^{\infty} dt_3 e^{-\Gamma_p \frac{t_1+t_3}{2}} \cos(\omega_p (t_1 - t_3)) \theta(t_1) \theta(t_2) \theta(t_2 - t_3) \theta(t_3) \right. \\ & \quad \left. \times e^{-i(t_2(\omega_{21} + \omega_{23}) - t_1 \omega_{21} - t_3 \omega_{23})} \right) \\ & = \frac{4\pi(\Gamma_p^2 + 4(\omega_{21}^2 + \omega_p^2))}{\Gamma_p^4 + 16(\omega_{21}^2 - \omega_p^2)^2 + 8\Gamma_p^2(\omega_{21}^2 + \omega_p^2)} \delta(\omega_{21} + \omega_{23}) . \end{aligned} \quad (6.34)$$

Therefore, one finds

$$\begin{aligned} \lim_{t \rightarrow \infty} L_{ii}(t, t) &= -\frac{128\epsilon_{ii}}{\pi} \int_0^\infty dp \int_{-\infty}^\infty \frac{d\omega_{21}}{2\pi} \int_{-\infty}^\infty \frac{d\omega_{23}}{2\pi} \frac{p^2}{\omega_p} f_F(\omega_p) f_F(\omega_{21}) \\ & \quad \times \frac{4\pi(\Gamma_p^2 + 4(\omega_{21}^2 + \omega_p^2))}{\Gamma_p^4 + 16(\omega_{21}^2 - \omega_p^2)^2 + 8\Gamma_p^2(\omega_{21}^2 + \omega_p^2)} \delta(\omega_{21} + \omega_{23}) \\ & \quad \times [\sigma_h(\omega_{21}, p) \sigma_h(\omega_{23}, p) + \sigma_\psi(\omega_{21}, p) \sigma_\psi(\omega_{23}, p)] \\ & = -\frac{64\epsilon_{ii}}{\pi^2} \int_0^\infty dp \int_0^\infty \frac{d\omega_{21}}{2\pi} \frac{p^2}{\omega_p} f_F(\omega_p) \\ & \quad \times \frac{4\pi(\Gamma_p^2 + 4(\omega_{21}^2 + \omega_p^2))}{\Gamma_p^4 + 16(\omega_{21}^2 - \omega_p^2)^2 + 8\Gamma_p^2(\omega_{21}^2 + \omega_p^2)} \\ & \quad \times 2\sigma_h(\omega_{21}, p) \sigma_\psi(\omega_{21}, p) , \end{aligned} \quad (6.35)$$

where the symmetry relations for σ_h and σ_ψ from Eqs. (5.70) and (5.71), i.e.

$$\sigma_h(-p^0, p_{||}) = \sigma_\psi(p^0, p_{||}) , \quad (6.36)$$

$$\sigma_\psi(-p^0, p_{||}) = \sigma_h(p^0, p_{||}) , \quad (6.37)$$

as well as the fact that $f_F(\omega_{21}) + f_F(-\omega_{21}) \equiv 1$ have been used. If one now uses the fact that the fraction in Eq. (6.35) is strongly peaked around $\omega_{21} = \omega_p$ with a width proportional to Γ_p , one may approximate $\sigma_h(\omega_{21}, p) \simeq \sigma_h(\omega_p, p)$ as well as $\sigma_\psi(\omega_{21}, p) \simeq \sigma_\psi(\omega_p, p)$ due to the smallness of $\Gamma_p \ll \omega_p$, cf. Sec. 7.2, under the integral over ω_{21} , and therefore find

$$\lim_{t \rightarrow \infty} L_{ii}(t, t) \simeq -\frac{64\epsilon_{ii}}{\pi} \int_0^\infty dp \frac{p^2}{\omega_p} f_F(\omega_p) \frac{1}{\Gamma_p} \sigma_h(\omega_p, p) \sigma_\psi(\omega_p, p) . \quad (6.38)$$

One should note three things here. Firstly, the results in Eqs. (6.35) and (6.38) may be used to check any calculated expressions for the lepton number matrix for correct thermalization, which is a necessary condition. Secondly, the form of Eq. (6.35) means that one cannot naively use a Taylor expansion in the zeroth component of the argument

of σ_h and σ_ψ to compute corrections to Eq. (6.38). The reason for this is that any non-vanishing term of $\mathcal{O}(\omega_{21})$ would lead to a divergence of the completely thermalized lepton number matrix as long as one does not restrict the integration interval of ω_{21} . This is not surprising, since the divergence occurs as $\omega_{21} \rightarrow \infty$, where one would have $|\sigma_h|, |\sigma_\psi| \rightarrow \infty$ with any non-constant term in a finite order Taylor expansion. Since this divergence cannot be physical and also an approximation by a Taylor expansion only holds close to the expansion point, one should restrict the integration interval to a finite one located around $\omega_{21} = \omega_p$ if one wants to use terms of linear or higher order. Thirdly, $\Gamma_p > 0$ is used here. Since $\Gamma_p = 0$ can occur for the tree-level expressions, this has to be discussed. However, whenever $\Gamma_p = 0$, also $\sigma_h(\omega_p, p) = \sigma_\psi(\omega_p, p) = 0$, and therefore the complete integrand is zero, since they enter quadratically in the numerator, while they enter only linearly in the denominator via Γ_p .

6.2.2. Evaluation of the t_1 , t_2 and t_3 Integrations: Dominating Regions for the Integrations over ω_{21} and ω_{23}

Also for finite t , the integration of the time-dependent part of $L_{ii}(t, t)$, Eq. (6.33), may be performed analytically. This leads to a very lengthy term presented in the appendix, Sec. B.3.1, Eq. (B.104). In the following, the result of this calculation is used to analyze the integrand in order to find the dominating regions for the integrations over ω_{21} and ω_{23} and thus be able to approximate the lepton number matrix self-consistently in Sec. 6.2.3. The denominator of the result of Eq. (6.33) for finite t reads

$$(\omega_{21} - \omega_{23})(\Gamma_p^2 + 4(\omega_{21} - \omega_p)^2)(\Gamma_p^2 + 4(\omega_{21} + \omega_p)^2)(\Gamma_p^2 + 4(\omega_{23} - \omega_p)^2)(\Gamma_p^2 + 4(\omega_{23} + \omega_p)^2), \quad (6.39)$$

which results in peaks around $\omega_{21} = \pm\omega_{23} = \pm\omega_p$. It is directly obvious that the peaks around $\omega_{21} = -\omega_{23} = \pm\omega_p$ should dominate, which will be shown later. These are also the values of ω_{21} and ω_{23} one expects to contribute from the structure of the cylindrical diagram in Fig. 6.4. If one is sufficiently far away from these peaks, one may approximate the result by performing the limit $\Gamma_p \rightarrow 0$, $\Gamma_p t = \text{const}^5$ [cf. Ani+11, p. 35], where the first should be understood in a sense that $\Gamma_p/\omega_{21}, \Gamma_p/\omega_{23}, \Gamma_p/\omega_p \rightarrow 0$. This is due to the smallness of Γ_p , cf. Sec. 7.2. Note that here, because of the regime $T \ll M$, M is not suitable as a scale. One finds as an approximation of the result of Eq. (6.33)

$$\frac{e^{-\Gamma_p t/2}}{(\omega_{21} + \omega_{23})(\omega_p^2 - \omega_{23}^2)(\omega_p^2 - \omega_{21}^2)} \left[(\omega_{21} - \omega_{23})\omega_p \sin(t\omega_p)(\cos(t\omega_{21}) - \cos(t\omega_{23})) \right. \\ \left. + (\omega_{21}\omega_{23} - \omega_p^2)(\cos(t\omega_p)(\sin(t\omega_{21}) \right. \\ \left. + \sin(t\omega_{23})) - e^{\Gamma_p t/2} \sin(t(\omega_{21} + \omega_{23})) \right]. \quad (6.40)$$

In the next paragraphs, the dominating regions for the integrals over ω_{21} and ω_{23} will be discussed. For this, the assumption $\Gamma_p \sim \mathcal{O}(\lambda^2 T)$, where λ^2 represents a combination of Yukawa couplings, i.e. involving terms like $\lambda_{ij}\lambda_{kl}$, will be used [cf. Bes10, p. 19]⁶. Note that this implies that $\sigma_h, \sigma_\psi \sim \mathcal{O}(T)$ for on-shell $\omega = \omega_p$, since they do not include $|\lambda|^2$, i.e. the coupling at the vertices. For further discussion assume that σ_h and σ_ψ do not change their estimate of order when going away from $\omega = \omega_p$. Estimates for other quantities are $t\Gamma_p \sim \mathcal{O}(1)$, since for larger times the result from Sec. 6.2.1 may be used, and $\omega_p \sim \mathcal{O}(T)$.

⁵Note that Γ_p depends on the momentum p . Therefore, any statements on the comparison of t to Γ_p are to be understood in a sense that they are true for the dominating region for the integral over p , which can be approximated a priori to be $p \sim \mathcal{O}(T)$.

⁶Here, λ is chosen instead of g since there is an explicit factor of $|\lambda|^2$ in front of the expression for Γ_p .

For the result of Eq. (6.33) for $\omega_{21} = -\omega_{23} = \pm\omega_p$ one finds

$$\begin{aligned} \frac{e^{-\Gamma_p t}}{\Gamma_p^3(\Gamma_p^2 + 16\omega_p^2)^2} & \left[-8(\Gamma_p^4 + 16\Gamma_p^2\omega_p^2 + 128\omega_p^4) \right. \\ & + 4 e^{\Gamma_p t}(\Gamma_p^4(-2 + \Gamma_p t) + 8\Gamma_p^2(-4 + 3\Gamma_p t)\omega_p^2 + 128(-2 + \Gamma_p t)\omega_p^4) \\ & + 2 e^{\Gamma_p t/2}(-(-4 + \Gamma_p t)(\Gamma_p^2 + 16\omega_p^2)^2 \\ & \left. - \Gamma_p^3(\Gamma_p(-4 + \Gamma_p t) + 16t\omega_p^2) \cos(2t\omega_p)) \right] , \end{aligned} \quad (6.41)$$

which is $\mathcal{O}(\lambda^{-6}T^{-3})$ ⁷.

For $\omega_{21} = \omega_{23} = \pm\omega_p$ one has for Eq. (6.33)

$$\frac{2e^{-\Gamma_p t}(-1 + e^{\Gamma_p t/2})}{\Gamma_p\omega_p(\Gamma_p^2 + 16\omega_p^2)} \left[4\omega_p + e^{\Gamma_p t/2}(-4\omega_p \cos(t\omega_p) + \Gamma_p \sin(2t\omega_p)) \right] , \quad (6.42)$$

which is $\mathcal{O}(\lambda^{-2}T^{-3})$.

Going away from the peaks $\omega_{21} = \pm\omega_{23} = \pm\omega_p$ one may use Eq. (6.40) to approximate the result of Eq. (6.33). Here, there are different regions to discuss. Firstly, there is the case, where $\omega_{21}, \omega_{23} \ll \omega_p$ ⁸. In this case, Eq. 6.40 goes towards

$$\frac{t - t \cos(t\omega_p)}{\omega_p^2} , \quad (6.43)$$

which is $\mathcal{O}(\lambda^{-2}T^{-3})$ for t as discussed above.

Secondly, one has the case, where $\omega_{21} \gg \omega_{23}$. Here, one has to consider three possibilities: $\omega_{21}, \omega_{23} \gg T$, $\omega_{21} \gg T$ with $\omega_{23} \lesssim T$, and $\omega_{21} \lesssim T$. In the three cases, Eq. (6.40) is $\mathcal{O}(\omega_{21}^{-2}\omega_{23}^{-1})$, $\mathcal{O}(\omega_{21}^{-2}T^{-1})$, and $\mathcal{O}(\omega_{21}^{-1}T^{-2})$ respectively. Since the case, where $\omega_{21} \ll \omega_p$, and therefore $\omega_{21} \ll T$, has been discussed before, this summarizes to maximally having $\mathcal{O}(T^{-3})$ in all three cases.

Thirdly, one has the case, where $\omega_{23} \gg \omega_{21}$. Since Eq. (6.40) is symmetric under exchange of ω_{21} and ω_{23} , this case is identical to the second one and therefore, one maximally has $\mathcal{O}(T^{-3})$ for it.

Assuming that σ_h and σ_ψ do not change their order estimate over the total range of the integrations over ω_{21} and ω_{23} such that they get much larger than at $\omega_{21} = -\omega_{23} = \pm\omega_p$ and compensate for the suppression due to the result of the integrations over the time variables, the integrals over ω_{21} and ω_{23} are hence dominated by the regions around $\omega_{21} = -\omega_{23} = \pm\omega_p$. Only in these regions, the result of the integrations over t_1, t_2 , and t_3 , Eq. (6.33), is of leading order $\mathcal{O}(\lambda^{-6}T^{-3})$. This is also supported by the fact that one can assume that $\lambda^2 \sim |\lambda|^2$, which will be set to 10^{-8} for the numerical calculations. Hence, the value of the result of the time integrations in the dominating regions is around $(|\lambda|^2)^{-2} = 10^{16}$ larger than in any other region. Since the width of the peaks is given by Eq. (6.39) and is of the order of multiples of $\Gamma_p \sim \mathcal{O}(\lambda^2 T)$, the dominating regions of the integrals in ω_{21} and ω_{23} have a width of this order in each dimension.

6.2.3. Approximating the Lepton Number Matrix for Finite Time

As it was shown in Sec. 6.2.1 in the limit $t \rightarrow \infty$, only the region, where $\omega_{21} = -\omega_{23} \simeq \pm\omega_p$ contributes (the \pm stems from the fact that in fact Eq. (6.35) has contributions from $\omega_{21} =$

⁷ $\mathcal{O}(\lambda^{-6}) = \mathcal{O}((\lambda^2)^{-3})$.

⁸Note that this is to be understood such that it does not violate the condition that $\Gamma_p/\omega_{21}, \Gamma_p/\omega_{23} \rightarrow 0$, which is not a problem due to the smallness of Γ_p , cf. Sec. 7.2.

$\pm\omega_p$ before applying Eqs. (5.70) and (5.71)). Since the interesting regime for t to estimate the effect of gauge corrections is the time, when the lepton number matrix thermalizes, one may also assume here that the relevant contributions to the lepton number matrix stem from the regions, where $\omega_{21} \simeq -\omega_{23} \simeq \pm\omega_p$. The validity of this approximation has been discussed in Sec. 6.2.2.

To apply the approximation to $L_{ii}(t, t)$, consider the part dependent on ω_{21} and ω_{23}

$$I := \int_{-\infty}^{\infty} \frac{d\omega_{21}}{2\pi} \int_{-\infty}^{\infty} \frac{d\omega_{23}}{2\pi} f_F(\omega_{21}) \operatorname{Re} \left(e^{-i(\omega_{21}y_{21} + \omega_{23}y_{23})} \right) \times [\sigma_h(\omega_{21}, p)\sigma_h(\omega_{23}, p) + \sigma_\psi(\omega_{21}, p)\sigma_\psi(\omega_{23}, p)] . \quad (6.44)$$

Next, one can approximate that only the region, where $\omega_{23} \in [-\omega_{21} - a, -\omega_{21} + a]$ with $a \gg \Gamma_p > 0$, but $a \ll |\omega_{21}|$, cf. Secs. 6.2.2 and 7.2, contributes to the integral, and that in this region $\sigma_h(\omega_{23}, p) \simeq \sigma_\psi(\omega_{21}, p)$ and $\sigma_\psi(\omega_{23}, p) \simeq \sigma_h(\omega_{21}, p)$, where Eqs. (5.70) and (5.71) have been used. This gives

$$\begin{aligned} I &\simeq \operatorname{Re} \left(\int_{-\infty}^{\infty} \frac{d\omega_{21}}{2\pi} \int_{-\omega_{21}-a}^{-\omega_{21}+a} \frac{d\omega_{23}}{2\pi} f_F(\omega_{21}) e^{-i(\omega_{21}y_{21} + \omega_{23}y_{23})} 2\sigma_h(\omega_{21}, p)\sigma_\psi(\omega_{21}, p) \right) \\ &= \operatorname{Re} \left(\int_{-\infty}^{\infty} \frac{d\omega_{21}}{2\pi} f_F(\omega_{21}) e^{-i\omega_{21}(y_{21}-y_{23})} \frac{\sin(ay_{23})}{\pi y_{23}} 2\sigma_h(\omega_{21}, p)\sigma_\psi(\omega_{21}, p) \right) \\ &= \operatorname{Re} \left(\int_0^{\infty} \frac{d\omega_{21}}{2\pi} (f_F(\omega_{21}) e^{-i\omega_{21}(y_{21}-y_{23})} + f_F(-\omega_{21}) e^{i\omega_{21}(y_{21}-y_{23})}) \right. \\ &\quad \left. \times \frac{\sin(ay_{23})}{\pi y_{23}} 2\sigma_h(\omega_{21}, p)\sigma_\psi(\omega_{21}, p) \right) \\ &= \operatorname{Re} \left(\int_0^{\infty} \frac{d\omega_{21}}{2\pi} e^{-i\omega_{21}(y_{21}-y_{23})} \frac{\sin(ay_{23})}{\pi y_{23}} 2\sigma_h(\omega_{21}, p)\sigma_\psi(\omega_{21}, p) \right) , \end{aligned}$$

where the fact that one can change the sign in the purely imaginary argument of the exponential function when taking only the real part has been used. In the expression above, the dominating region for the integral is the region around $\omega_{21} = \omega_p$ ⁹. Hence, $\sigma_h(\omega_{21}, p) \simeq \sigma_h(\omega_p, p)$ and $\sigma_\psi(\omega_{21}, p) \simeq \sigma_\psi(\omega_p, p)$ may be used for the whole integral as an approximation, since the width of the peak in the dominating region for the integral is given by multiples of $\Gamma_p \ll \omega_p$, cf. Sec. 7.2. One finds

$$\begin{aligned} I &\approx \operatorname{Re} \left(\int_0^{\infty} \frac{d\omega_{21}}{2\pi} e^{-i\omega_{21}(y_{21}-y_{23})} \frac{\sin(ay_{23})}{\pi y_{23}} 2\sigma_h(\omega_p, p)\sigma_\psi(\omega_p, p) \right) \\ &= \frac{1}{\pi y_{23}} \delta(y_{21} - y_{23}) \sin(ay_{23}) \sigma_h(\omega_p, p)\sigma_\psi(\omega_p, p) . \end{aligned} \quad (6.45)$$

The result after the integrations over t_1 , t_2 , and t_3 with the rest of the time-dependent part of the integrand therefore becomes

$$\begin{aligned} \int_0^t dt_1 \int_0^t dt_2 \int_0^{t_2} dt_3 I e^{-\Gamma_p \frac{t_1+t_3}{2}} \cos(\omega_p y_{13}) &\simeq \frac{e^{-\Gamma_p t}}{4\pi\Gamma_p} [-i(2\operatorname{Ei}(t(-ia + \Gamma_p)) - 2\operatorname{Ei}(t(ia + \Gamma_p))) \\ &\quad - \ln \left(\frac{-a - i\Gamma_p}{a - i\Gamma_p} \right) + \ln \left(\frac{-a + i\Gamma_p}{a + i\Gamma_p} \right)] \\ &\quad + 4e^{\Gamma_p t} \operatorname{Si}(at) \sigma_h(\omega_p, p)\sigma_\psi(\omega_p, p) , \end{aligned} \quad (6.46)$$

⁹Note that there is no \pm here, since Eqs. (5.70) and (5.71) have been used already.

where $\text{Ei}(z)$ is the exponential integral and $\text{Si}(z)$ is the sine integral. In the limit, where $at \rightarrow \infty$, while $\Gamma_p t = \text{const}$, i.e. $a \gg \Gamma_p$, this gives

$$\begin{aligned} \int_0^t dt_1 \int_0^{t_1} dt_2 \int_0^{t_2} dt_3 I e^{-\Gamma_p \frac{t_1+t_3}{2}} \cos(\omega_p y_{13}) &\simeq \frac{e^{-\Gamma_p t}}{4\pi\Gamma_p} \left[-i(2(-i\pi) - 2i\pi - \ln(-1 - i0^+)) \right. \\ &\quad \left. + \ln(-1 + i0^+) + 2\pi e^{\Gamma_p t} \right] \\ &\quad \times \sigma_h(\omega_{21}, p) \sigma_\psi(\omega_{21}, p) \\ &= \frac{1 - e^{-\Gamma_p t}}{2\Gamma_p} \sigma_h(\omega_p, p) \sigma_\psi(\omega_p, p), \end{aligned} \quad (6.47)$$

where 0^+ indicates an infinitesimal shift in positive direction, since the natural logarithm of a negative real number is not defined. Note that the limit is approached very fast, so that in practice, the restriction to $a \gg \Gamma_p$, while $t \gtrsim 1/\Gamma_p$ is sufficient in order to have numerically equivalent results to the result above. In total, this gives for the lepton number matrix

$$L_{ii}(t, t) \simeq -\frac{64\epsilon_{ii}}{\pi} \int_0^\infty dp \frac{p^2}{\omega_p} f_F(\omega_p) \frac{1 - e^{-\Gamma_p t}}{\Gamma_p} \sigma_h(\omega_p, p) \sigma_\psi(\omega_p, p). \quad (6.48)$$

This expression includes all leading order gauge as well as other SM corrections when using the fully resummed σ_h and σ_ψ and only hard gauge and other SM corrections when using the tree-level σ_h^{tree} and $\sigma_\psi^{\text{tree}}$.

There are four things one should note here. Firstly, Eq. (6.48) has the correct thermalization as $\Gamma_p t > 0$ and therefore, $e^{-\Gamma_p t} \rightarrow 0$ for $t \rightarrow \infty$, which gives Eq. (6.38).

Secondly, the time-dependence exactly corresponds to the one of the solution of the Boltzmann equations. This result is very similar to the result from [Ani+11], where also this time-dependence and a result of the Kadanoff-Baym calculation without gauge corrections similar to the Boltzmann result has been found for large times $t \gtrsim 1/\Gamma_p$ after the inclusion of thermal widths for the lepton and the Higgs propagators [see Ani+11, p. 35] and also for small $\Gamma_p/M \rightarrow 0$, while $\Gamma_p t = \text{const}$ [see Ani+11, Erratum], cf. Sec. 4.3.2. A similar result in this case means that they have the same time-dependence and the Boltzmann result is approached by the Kadanoff-Baym result in the corresponding limits. Of course, Γ_p is gauge-corrected in this thesis.

Thirdly, as for the infinite time limit in Sec. 6.2.1, for $\Gamma_p = 0$, which can occur for the tree-level expressions, the whole integrand gives zero for the same reasons discussed before. Therefore, this case does not need to be considered any further.

Fourthly, the result in Eq. (6.48) only holds for $t \gtrsim 1/\Gamma_p$, which is also illustrated by the comparison to [Ani+11]. The reason for this is mainly that for earlier times, all quantum effects, i.e. memory and off-shell effects, would have to be kept [cf. Ani+11, pp. 35, 42]. This means that for earlier times, the restriction to the regions around $\omega_{21} = -\omega_{23} = \pm\omega_p$, which is essentially an on-shell restriction, would not be justified. Note that also in Sec. 6.2.2, a time with $\Gamma_p t \sim \mathcal{O}(1)$ was assumed to get an estimate of order, since for larger times it is clear that the discussion from Sec. 6.2.1 holds. In the above calculation, one finds this assumption also in the limit $at \rightarrow \infty$, since a is required to be small compared to ω_{21} , but large compared to Γ_p . However, the applicability of Eq. (6.48) for $t \gtrsim 1/\Gamma_p$ is not a massive drawback, since the purpose of this thesis is the estimation of the effect of gauge corrections to leptogenesis. For this, it is enough to discuss these times as they are needed to estimate the effect of gauge corrections to the generated lepton asymmetry.

One should also remark that one finds a very similar result to Eq. (6.48) if one restricts the integration regions in ω_{21} and ω_{23} to $(\omega_{21}, \omega_{23}) \in ([\omega_p - a, \omega_p + a] \times [-\omega_p - a, -\omega_p + a]) \cup ([-\omega_p - a, -\omega_p + a] \times [\omega_p - a, \omega_p + a])$ with $\Gamma_p \ll a \ll \omega_p$. However, it turns out to be very difficult to do the integrations over t_1 , t_2 and t_3 after the integrations over ω_{21} and ω_{23} analytically in this case. Performing all but the one over t_2 analytically, and numerically approximating the limit, where $a \gg \Gamma_p$ with $at \rightarrow \infty$, one finds a numerically equivalent result to Eq. (6.48). Since an analytic solution is always preferred, only the above has been presented in detail.

7. Numerical Results

In this chapter, the numerical results for the evaluation of the lepton number matrix and all related quantities are presented.

7.1. Setup

In order to estimate the effect of soft and hard gauge corrections on thermal leptogenesis, the fully resummed and the tree-level results are used for the Majorana neutrino self-energy. The fully resummed result includes all leading order gauge and other SM corrections, which are soft and hard gauge corrections and other hard SM corrections. The tree-level result only includes hard gauge and other hard SM corrections. With the usage of the results, the corresponding corrections are included in the thermal width and the lepton number matrix. Following [Ani+11] and [ABB11], calculations were performed for two masses of the heavy Majorana neutrino, $M = 10^{10}$ GeV as in [Ani+11], and $M = 10^7$ GeV as in [ABB11]. Apart from that, $|\lambda|^2 = 10^{-8}$ is chosen [cf. Bes10, p. 64]. This is done just for the calculation, since any other value for $|\lambda|^2$ can be obtained by rescaling t such that $|\lambda|^2 t$ stays the same and $L_{ii}(t, t)$ by a corresponding factor, since it only enters via $(1 - \exp(-\Gamma_p t))/\Gamma_p$ with $\Gamma_p \sim |\lambda|^2$ in the calculation¹. In the physical scenario described in Sec. 4.1, $\epsilon = 10^{-6}$ was used. Continuing to use this choice, one has, cf. Eq. (4.8),

$$\sum_i \epsilon_{ii} = \epsilon |\lambda|^2 = 10^{-14}, \quad (7.1)$$

which means that each $\epsilon_{ii} \ll 1$. However, all results for the lepton number matrix will be given as $L_{ii}(t, t)/\epsilon_{ii}$, i.e. no value for ϵ_{ii} is chosen.

7.1.1. Renormalization Group Equations

In analogy to [ABB11, p. 16], [Bes10, p. 63], and [Hüt13, p. 46], the renormalization group equations (RGEs) from [SW96] were used. Neglecting the tau and bottom quarks Yukawa couplings because of their smallness compared to the other couplings they are

$$\frac{dg_1^2}{d\tau} = \frac{g_1^4}{8\pi^2} \frac{41}{10} + \mathcal{O}(g^6), \quad (7.2a)$$

$$\frac{dg_2^2}{d\tau} = \frac{g_2^4}{8\pi^2} \left(-\frac{19}{6}\right) + \mathcal{O}(g^6), \quad (7.2b)$$

$$\frac{dg_3^2}{d\tau} = \frac{g_3^4}{8\pi^2} (-7) + \mathcal{O}(g^6), \quad (7.2c)$$

$$\frac{d\lambda_t^2}{d\tau} = \frac{\lambda_t^2}{8\pi^2} \left(\frac{9}{2}\lambda_t^2 - \frac{17}{20}g_1^2 - \frac{9}{4}g_2^2 - 8g_3^2\right) + \mathcal{O}(g^6), \quad (7.2d)$$

$$\begin{aligned} \frac{d\Lambda}{d\tau} = \frac{1}{16\pi^2} \left(\frac{27}{200}g_1^4 + \frac{9}{20}g_1^2g_2^2 + \frac{9}{8}g_2^4 - \frac{9}{5}g_1^2\Lambda - 9g_2^2\Lambda \right. \\ \left. - 6\lambda_t^4 + 12\lambda_t^2\Lambda + 24\Lambda^2 \right) + \mathcal{O}(g^6), \end{aligned} \quad (7.2e)$$

¹In fact, if one considers a fixed ϵ , then the value of the lepton number matrix stays the same (after rescaling of the time), since $\epsilon_{ii}/|\lambda|^2$ stays the same. This especially applies for the thermalized L_{ii} .

where $\tau := \ln(\mu/\mu_0)$ with $\mu = 2\pi T$ being the scale [cf. Giu+04, p. 1]. Here, $\mu_0 = 2\pi T_R$ is chosen with the reheating temperature as $T_R = 10^9 \text{ GeV}$ [cf. Bes10, p. 63]. g^6 denotes any combination of standard model couplings and $\Lambda \sim \mathcal{O}(g^2)$ for this counting [see Hüt13, p. 46]. In the equations for the thermal and Debye masses, g_Y is g_1 and g_W is g_2 .

In order to solve the RGEs, the following initial conditions are used with the values from [Pat+16]²

$$\mu_Z := m_Z = 91.1876(21) \text{ GeV} , \quad (7.3a)$$

$$\alpha_{em}(\tau_Z) = 1/127.950(17) , \quad (7.3b)$$

$$\alpha_s(\tau_Z) = 0.1182(16) , \quad (7.3c)$$

$$\sin^2 \theta_W(\tau_Z) = 0.23129(5) , \quad (7.3d)$$

$$m_t = 173.21(1.22) \text{ GeV} , \quad (7.3e)$$

$$m_H = 125.09(24) \text{ GeV} , \quad (7.3f)$$

$$G_F = 1.1663787(6) \cdot 10^{-5} \text{ GeV}^{-2} \Rightarrow v = \frac{1}{\sqrt{\sqrt{2}G_F}} = 246.2197(1) \text{ GeV} , \quad (7.3g)$$

where $\tau_Z = \ln(\mu_Z/\mu_0)$. For better comparability to [Bes10], also simulations with $m_H = 150 \text{ GeV}$ have been performed for $M = 10^7 \text{ GeV}$ [cf. Hüt13, p. 46]. Note that the Higgs boson mass here denotes the mass in the vacuum and is in no contradiction to the fact that the Higgs boson is assumed to be massless due to high temperatures in all other calculations for this thesis. These values are related to Eq. (7.2) via the relations [SW96], [see Bes10, p. 63], [see Hüt13, p. 47]

$$\alpha_1(\tau_Z) := \frac{g_1^2(\tau_Z)}{4\pi} = \frac{\alpha_{em}(\tau_Z)}{\cos^2(\theta_W(\tau_Z))} , \quad (7.4a)$$

$$\alpha_2(\tau_Z) := \frac{g_2^2(\tau_Z)}{4\pi} = \frac{\alpha_{em}(\tau_Z)}{\sin^2(\theta_W(\tau_Z))} , \quad (7.4b)$$

$$\alpha_3(\tau_Z) := \frac{g_3^2(\tau_Z)}{4\pi} = \alpha_s(\tau) , \quad (7.4c)$$

$$\lambda_t(\tau_Z) := g_t^2(\tau_Z) = \frac{2m_t^2}{v^2} , \quad (7.4d)$$

$$\Lambda(\tau_Z) := g_\Lambda^2(\tau_Z) = \frac{m_H}{2v^2} . \quad (7.4e)$$

The RGEs for g_1 , g_2 , and g_3 can be solved analytically giving

$$g_1^2(\tau) = \frac{c_1}{d_1 - \tau} , \quad c_1 = \frac{80\pi^2}{41} , \quad d_1 = \frac{20\pi(1 - \sin^2 \theta_W(\tau_Z))}{41\alpha_{em}(\tau_Z)} + \tau_Z , \quad (7.5a)$$

$$g_2^2(\tau) = \frac{c_2}{d_2 + \tau} , \quad c_2 = \frac{48\pi^2}{19} , \quad d_2 = \frac{12\pi \sin^2 \theta_W(\tau_Z)}{19\alpha_{em}(\tau_Z)} - \tau_Z , \quad (7.5b)$$

$$g_3^2(\tau) = \frac{c_3}{d_3 + \tau} , \quad c_3 = \frac{8\pi^2}{7} , \quad d_3 = \frac{2\pi}{7\alpha_s(\tau_Z)} - \tau_Z , \quad (7.5c)$$

whereas the RGEs for λ_t and Λ are solved numerically using an implementation of the Bulirsch-Stoer method [SB13] from the library odeint from Boost³.

Note that the running of the Majorana neutrino coupling is neglected here, since its experimental value is unknown and it therefore has to be treated as a free parameter [cf. Bes10, p. 63].

²Note that the values from the 2017 update lie within the error boundaries.

³<http://www.boost.org>

7.1.2. Numerical Methods

All numerical calculations for this thesis were done using C++ programs written in the context of the thesis.

The integral equations for \mathbf{f} and for ψ , i.e. for the resummed self-energy, are transformed into ordinary differential equations, which are then solved numerically using an implementation of the Bulirsch-Stoer method from the library `odeint` from Boost, see appendix, Sec. B.1, for details.

In order to calculate σ_h and σ_ψ , the method `qagi` from the GNU scientific library⁴ (GSL), which is an adaptive quadrature integration routine suitable for infinite integration intervals, has been used and crosschecked with the method `qag`, an adaptive quadrature integration routine for finite intervals, and an appropriate cutoff. In the case of the tree-level σ_h^{tree} and $\sigma_\psi^{\text{tree}}$, the methods `qag` and `qagp`, which can also handle singularities, has been used. The latter has not been used for the full σ_h and σ_ψ , since they are smooth and do not contain any singularities. For ill-defined points in the integration interval, a small shift has therefore been applied. All checks have shown consistency so that `qagi` has been used for the fully resummed σ_h and σ_ψ , and, depending on whether or not singularities may exist in the integration region, `qag` and `qagp` have been used for the tree-level σ_h^{tree} and $\sigma_\psi^{\text{tree}}$.

To ensure that the procedure works, a calculation of the differential production rate, cf. Eqs. (5.19) and (5.95),

$$\frac{d\tilde{\Gamma}}{d^3p} = -\frac{2}{(2\pi)^3} f_F(p) \Gamma_p(p) = \frac{2|\lambda|^2}{(2\pi)^3 p} f_F(p) \left[2p\sigma_h(\omega_p, p) + \frac{M^2}{2p} \sigma_\psi(\omega_p, p) \right] \quad (7.6)$$

with the light-like approximation for the Majorana neutrino $\omega_p + p \simeq 2p$, $\omega_p - p \simeq M/(2p)$ and $m_H = 150$ GeV has been performed and compared to the corresponding calculation in [ABB11, p. 19].

To calculate the lepton number matrix, different algorithms have been used. Firstly, for the formulation using σ_h and σ_ψ , the method `qagi`, which handles semi-infinite integration intervals similarly to `qagi` for infinite integration intervals, has been used to solve the remaining integral over p . As a crosscheck, for one set of T and M the integral has been rewritten to a three-dimensional integral using the definitions of σ_h and σ_ψ from Eqs. (5.54) and (5.55),

$$\sigma_h(\omega_p, p) = \frac{d(r)}{2} \int \frac{dk_{\parallel}}{2\pi} \frac{\mathcal{F}(p, k_{\parallel})}{k_{\parallel} - p} \frac{1}{8k_{\parallel}^2} \int \frac{d^2k_{\perp}}{(2\pi)^2} \text{Re}(\mathbf{k}_{\perp} \mathbf{f}(\mathbf{k}_{\perp})), \quad (7.7)$$

$$\sigma_\psi(\omega_p, p) = \frac{d(r)}{2} \int \frac{dk_{\parallel}}{2\pi} \frac{\mathcal{F}(p, k_{\parallel})}{k_{\parallel} - p} \int \frac{d^2k_{\perp}}{(2\pi)^2} \text{Re} \psi(\mathbf{k}_{\perp}), \quad (7.8)$$

instead of calculating σ_h and σ_ψ and then integrating over p . The three-dimensional integrals have been solved using the Vegas algorithm, a Monte Carlo algorithm with importance sampling, and the Cuhre algorithm, an adaptive multidimensional quadrature routine, of the CUBA library [Hah05]. In these cases, the compactification of infinite integration intervals has been performed using arctan and dimensionless variables by dividing with appropriate powers of the temperature.

The completely thermalized lepton number matrix from Eq. (6.38), i.e. its limit as $t \rightarrow \infty$, and its result for finite t from Eq. (6.48) have been calculated for each T and

⁴<https://www.gnu.org/software/gsl/>

M using the fully resummed and the tree-level results for the Majorana neutrino self-energy. The former has been calculated with and without explicitly entering the light-like approximation for the Majorana neutrino momentum $\omega_p + p \simeq 2p$ and $\omega_p - p \simeq M/(2p)$, whereas the latter only has been calculated without explicitly entering this approximation. The light-like approximation is only valid if the result for the lepton number matrix is dominated by the region where it holds, i.e. $p > M$ in Eq. (6.48). This can be estimated to be $p \sim T > M$. Note that nevertheless, the resummation of the Majorana neutrino self-energy uses collinearity of its momentum with the Higgs boson and lepton momenta, for which the light-like approximation is needed during the calculation for the resummation. Hence, the difference between the results with and without the light-like approximation for the Majorana neutrino momentum should not be very large in order to have self-consistent results. The validity of the approximation is discussed further in Secs. 7.3.2 and 7.4.1.

To study its thermalization, apart from the complete lepton number matrix and its limit as $t \rightarrow \infty$, also the contribution from the part of the lepton number matrix proportional to $\exp(-\Gamma_p t)/\Gamma_p$, i.e.

$$L_{ii}(t, t)^{\text{exp part}} \simeq -\frac{64\epsilon_{ii}}{\pi} \int_0^\infty dp \frac{p^2}{\omega_p} f_F(\omega_p) \frac{-e^{-\Gamma_p t}}{\Gamma_p} \sigma_h(\omega_p, p) \sigma_\psi(\omega_p, p), \quad (7.9)$$

cf. Eq. (6.48), has been calculated for each finite time considered.

Using the evaluations of the lepton number matrix for different times and temperatures as well as the limit $t \rightarrow \infty$, one can define a time t_{therm} , where

$$L_{ii}(t_{\text{therm}}, t_{\text{therm}}) = \left(1 - e^{-1}\right) \lim_{t \rightarrow \infty} L_{ii}(t, t), \quad (7.10)$$

i.e. the exponential contribution in $(1 - \exp(-\Gamma_p t))/\Gamma_p$ is $1/e$ of the absolute value of $\lim_{t \rightarrow \infty} L_{ii}(t, t)$. t_{therm} is then read off from the results for $L_{ii}(t, t)$ for different t using $\lim_{t \rightarrow \infty} L_{ii}(t, t)$. For a constant $\Gamma_p \equiv \Gamma$ that does not depend on the momentum p , this would correspond to $t_{\text{therm}} = 1/\Gamma$. As all calculations here do not deal with a constant Γ_p , but a certain region of momentum p contributes mostly to the results, t_{therm} can be viewed as an average of $1/\Gamma_p$ with some weight. It should therefore approximately scale like $1/\Gamma_p \sim \mathcal{O}(\lambda^{-2} T^{-1})$.

For more details on the settings for the different algorithms see the appendix, Sec. B.3.2.

7.1.3. Overview over the Calculations

An overview over all calculations performed in the context of this thesis can be found in table 7.1 for the differential production rate, the thermal width and the self-energies and table 7.2 for the lepton number matrix and the thermalization time. Note that the units in all plots in the following are given in powers of 10^9 GeV.

7.2. Results for the Differential Production Rate, the Thermal Width, and the Self-Energies

The differential production rate $d\tilde{\Gamma}/d^3p$ has been calculated for $M = 10^7$ GeV with $T = 2 \cdot 10^7$ GeV and $T = 10^8$ GeV, the Higgs boson mass set to $m_H = 150$ GeV, and the light-like approximation. These are the same parameters and approximations as in the corresponding calculation in [ABB11, p. 19]. The results of the calculation performed in the process of this thesis can be found in Fig. 7.1. The helicity flip term corresponds to the term involving σ_h , whereas the non-flip term corresponds to the term involving σ_ψ ,

Quantity	Eqs.	M [GeV]	T [GeV]	Var.	Fig.	Remarks
$d\tilde{\Gamma}/d^3p$	(7.6)	10^7	$2 \cdot 10^7, 10^8$	p	7.1	$m_H = 150$ GeV, light-like
Γ_p	(5.95)	10^{10}	$2 \cdot 10^{10}, 10^{11}$	p	7.2	
Γ_p	(5.95)	10^7	$2 \cdot 10^7, 10^8$	p	7.3	
$\sigma_{h/\psi}(p^0, p)$	(5.54), (5.55)	10^{10}	$2 \cdot 10^{10}, 10^{11}$	p^0	7.4	$p = T$
$\sigma_{h/\psi}^{(\text{tree})}(p^0, p)$	(5.54), (5.55), (5.90), (5.91)	10^7	10^8	p^0	7.5	$p = T$
$\sigma_{h/\psi}^{(\text{tree})}(\omega_p, p)$	(5.54), (5.55), (5.90), (5.91)	10^{10}	$2 \cdot 10^{10}, 10^{11}$	p	7.6	
$\sigma_{h/\psi}^{(\text{tree})}(\omega_p, p)$	(5.54), (5.55), (5.90), (5.91)	10^7	$2 \cdot 10^7, 10^8$	p	7.7	

Table 7.1.: Details on calculations for differential production rate, thermal width and self-energies. Light-like denotes corresponding approximation for Majorana neutrino momentum, not inserted if not indicated. $m_H = 125.09$ GeV if not indicated otherwise.

Quantity	Eq.	M [GeV]	Var.	Tree	Figs.	Remarks
$L_{ii}(t, t)$	(6.48)	10^{10}	t	no	7.8, 7.9, 7.10	$T = 10^{11}$ GeV
$\lim_{t \rightarrow \infty} L_{ii}(t, t)$	(6.38)	10^{10}	T	both	7.11	
$\lim_{t \rightarrow \infty} L_{ii}(t, t)$	(6.38)	10^{10}	T	both	7.12	(non-)light-like
$L_{ii}(t, t)$	(6.48)	10^{10}	T, t	no	7.13, 7.14	
$L_{ii}(t, t)$	(6.48)	10^{10}	T, t	yes	7.15, 7.16	
$L_{ii}(t, t)$	(6.48)	10^{10}	T, t	both	7.17	
t_{therm}	(7.10)	10^{10}	T	both	7.18	
$\lim_{t \rightarrow \infty} L_{ii}(t, t)$	(6.38)	10^7	T	both	7.19	both m_H
$\lim_{t \rightarrow \infty} L_{ii}(t, t)$	(6.38)	10^7	T	both	7.20	(non-)light-like
$\lim_{t \rightarrow \infty} L_{ii}(t, t)$	(6.38)	10^7	T	both	7.21	$m_H = 150$ GeV, (non-)light-like
$L_{ii}(t, t)$	(6.48)	10^7	T, t	no	7.22, 7.23	
$L_{ii}(t, t)$	(6.48)	10^7	T, t	yes	7.24, 7.25	
$L_{ii}(t, t)$	(6.48)	10^7	T, t	both	7.26	
t_{therm}	(7.10)	10^7	T	both	7.27	

Table 7.2.: Details on calculations for lepton number matrix. Tree denotes tree-level. Light-like denotes corresponding approximation for Majorana neutrino momentum, not inserted if not indicated, (non-)light-like denotes both are calculated. $m_H = 125.09$ GeV if not indicated otherwise.

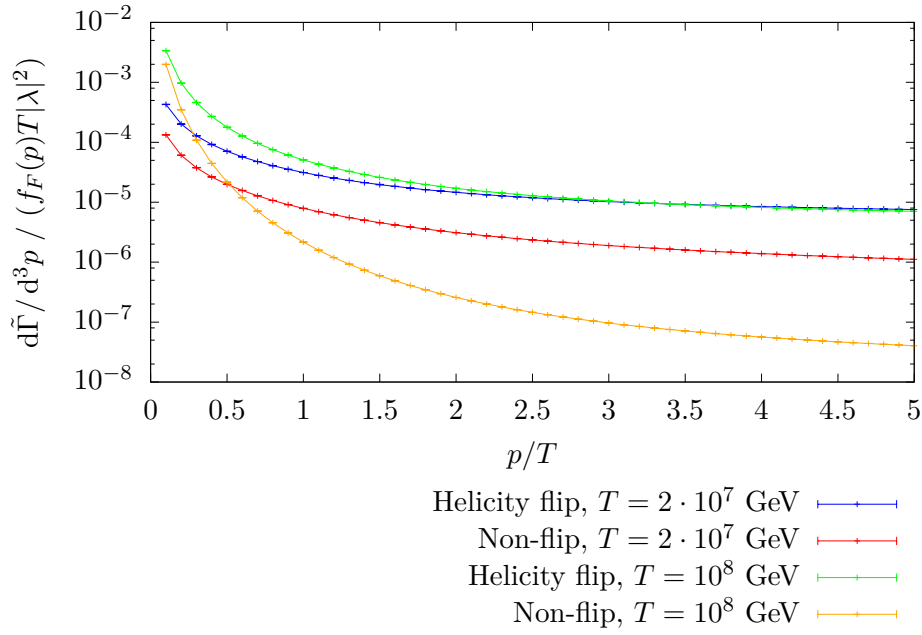


Figure 7.1.: Results for the contributions to differential production rate $d\tilde{\Gamma}/d^3p$ for different T ; $M = 10^7$ GeV, $m_H = 150$ GeV, light-like approximation.

cf. Sec. 5.6.4. The results agree with the results from [ABB11, p. 19]. Hence, it can be assumed that the procedure for calculating σ_h and σ_ψ works. Only these parameters could be checked, since no other calculations for $d\tilde{\Gamma}/d^3p$ was done in [ABB11]. A discussion of the results can be found in [ABB11] and is not performed here, since the results are of no further relevance. All further calculations in this section are done with the physical Higgs mass $m_H = 125.09$ GeV and without the light-like approximation for the Majorana neutrino.

In order to justify the approximations for the lepton number matrix in Sec. 6.2, the fully resummed as well as the tree-level thermal widths Γ_p have been calculated for $M = 10^{10}$ GeV with $T = 2 \cdot 10^{10}$ GeV and $T = 10^{11}$ GeV, and for $M = 10^7$ GeV with $T = 2 \cdot 10^7$ GeV and $T = 10^8$ GeV as sample sets. The results can be found in Figs. 7.2 and 7.3. Note that for $M = 10^{10}$ GeV with $T = 2 \cdot 10^{10}$ GeV, the tree-level thermal width is constantly zero. A drop in the tree-level rate, which goes to zero for every set of parameters except for $M = 10^7$ GeV with $T = 10^8$ GeV, can be observed for all sets of parameters. This drop is connected to the fact the tree-level Majorana neutrino self-energy is suppressed for these temperatures above a certain p , cf. Secs. 5.6.6 and 7.3.2. Furthermore, the tree-level thermal width is smaller than the fully resummed one for all calculated values. It is evident that, no matter whether the tree-level or the fully resummed result is used, $\Gamma_p \ll \omega_p$, which has been assumed before, holds.

For further justification of the approximations, $\sigma_h(p^0, p)$, $\sigma_\psi(p^0, p)$, $\sigma_h^{\text{tree}}(p^0, p)$, and $\sigma_\psi^{\text{tree}}(p^0, p)$ have been calculated for $p^0 \in [\omega_p - 10^7 \cdot \Gamma_p, \omega_p + 10^7 \cdot \Gamma_p]$ for the parameter sets $M = 10^{10}$ GeV with $p = T = 2 \cdot 10^{10}$ GeV and $p = T = 10^{11}$ GeV for the fully resummed case, and $M = 10^7$ GeV with $p = T = 10^8$ GeV for both, the fully resummed and the tree-level cases. The results normalized by the on-shell values can be found in Figs. 7.4 and 7.5. They show that the dependence on p^0 is negligible within the peaks of the integrand. Outside the peaks on the other hand, the rest of the integrand for the

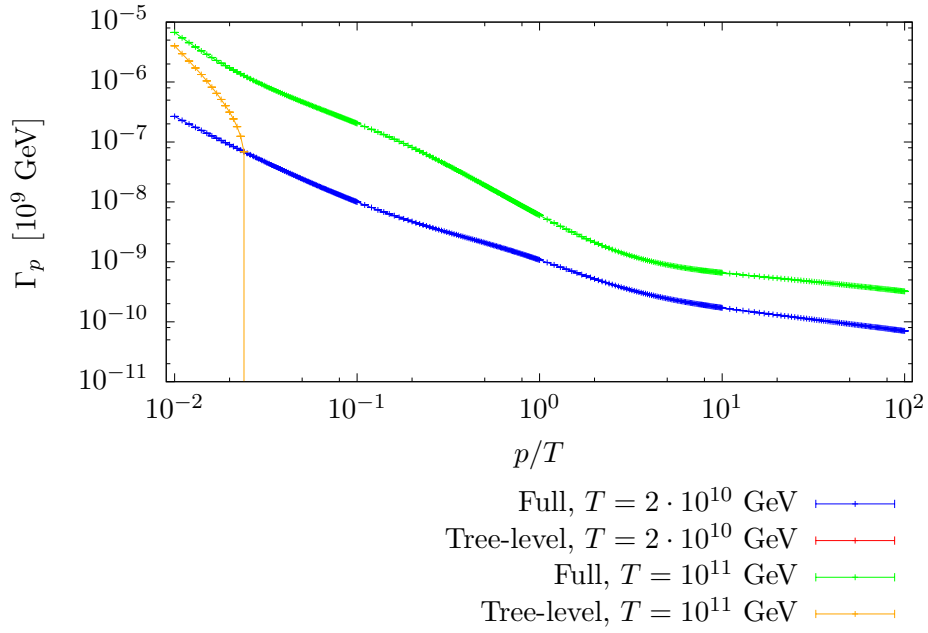


Figure 7.2.: Results for the thermal width Γ_p for different T ; $M = 10^{10}$ GeV.

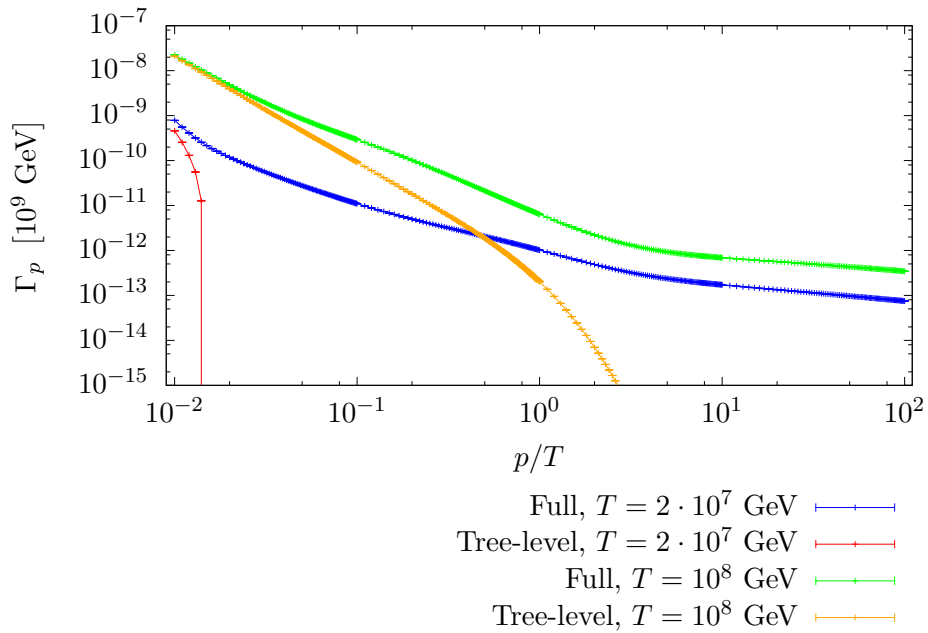


Figure 7.3.: Results for the thermal width Γ_p for different T ; $M = 10^{10}$ GeV.

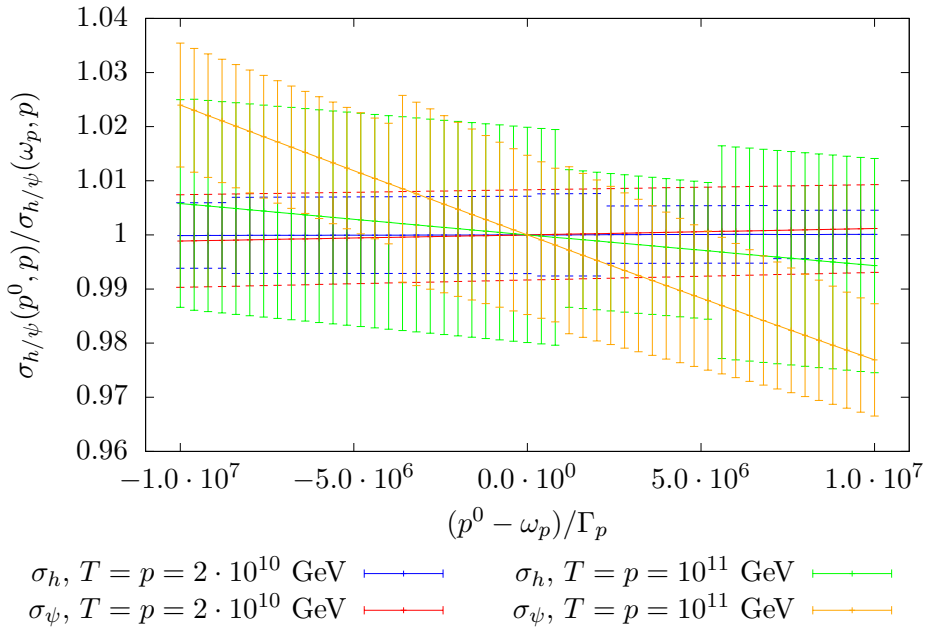


Figure 7.4.: Results for the full $\sigma_h(p^0, p)$ and $\sigma_\psi(p^0, p)$ with varying p^0 around $p^0 = \omega_p$ for different p, T ; $M = 10^{10}$ GeV.

lepton number matrix after the integrations over t_1 , t_2 , and t_3 is significantly less than at the peaks, cf. Sec. 6.2.2. It is therefore justified to assume a very small width for the peaks, since the width is given by multiples of Γ_p , and to assume that σ_h and σ_ψ are constant in these peaks. Hence, the approximations made in Sec. 6.2 are well motivated and supported by the results presented here.

Furthermore, $\sigma_h(\omega_p, p)$, $\sigma_\psi(\omega_p, p)$, $\sigma_h^{\text{tree}}(\omega_p, p)$, and $\sigma_\psi^{\text{tree}}(\omega_p, p)$ have been calculated for $M = 10^{10}$ GeV with $T = 10^{11}$ GeV and $M = 10^7$ GeV with $T = 10^8$ GeV to illustrate their dependence on p . The results can be found in Figs. 7.6 and 7.7. Also here, one observes that the tree-level σ_h^{tree} and $\sigma_\psi^{\text{tree}}$ are smaller than their fully resummed counterparts for almost all values considered. This is further discussed in Secs. 7.3.4 and 7.4.3. Only for the σ_ψ with $p < 1.1 \cdot 10^7$ GeV and $M = 10^7$ GeV, $T = 10^8$ GeV this does not hold.

7.3. Results for the Lepton Number Matrix for $M = 10^{10}$ GeV

All calculations for $M = 10^{10}$ GeV have been performed with $m_H = 125.09$ GeV.

7.3.1. Cross-Check of Different Algorithms

In order to cross-check different integration algorithms, for $T = 10^{11}$ GeV simulations have been performed using the Vegas and the Cuhre algorithms from the CUBA library as well as the algorithm qagi from the GSL library. The results can be found in Figs. 7.8, 7.9, and 7.10. For the Vegas and Cuhre calculations, a maximal relative error of 0.05 has been chosen, whereas for the qag calculation a maximal relative error of 0.01 for the p -integration has been chosen with a maximal relative error of 10^{-3} for σ_h and σ_ψ . Note that however, for the first two algorithms the completely thermalized result has been calculated during

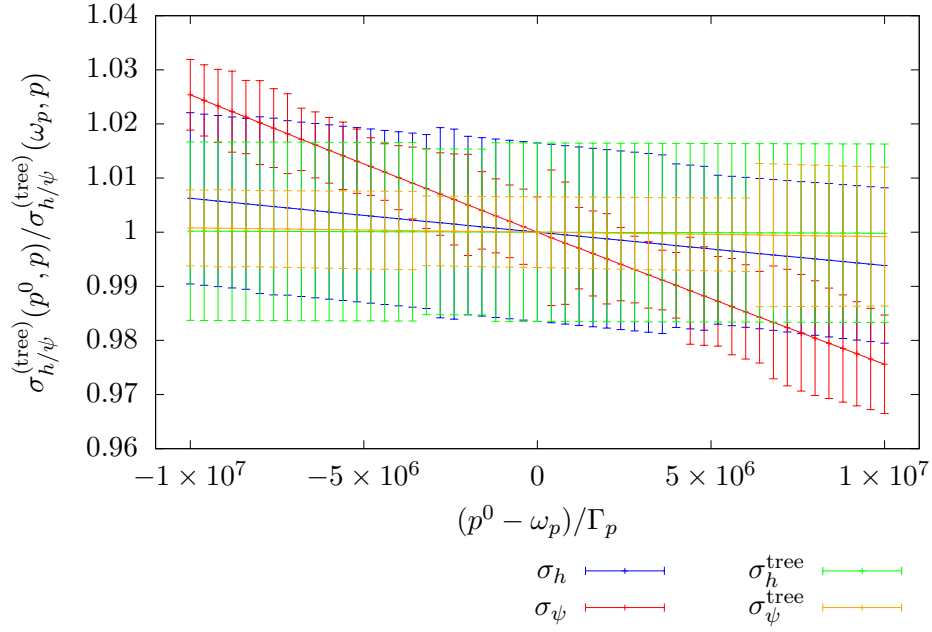


Figure 7.5.: Results for the full $\sigma_h(p^0, p)$ and $\sigma_\psi(p^0, p)$ and the tree-level $\sigma_h^{\text{tree}}(p^0, p)$ and $\sigma_\psi^{\text{tree}}(p^0, p)$ with varying p^0 around $p^0 = \omega_p$ for $M = 10^7$ GeV, $T = p = 10^8$ GeV.

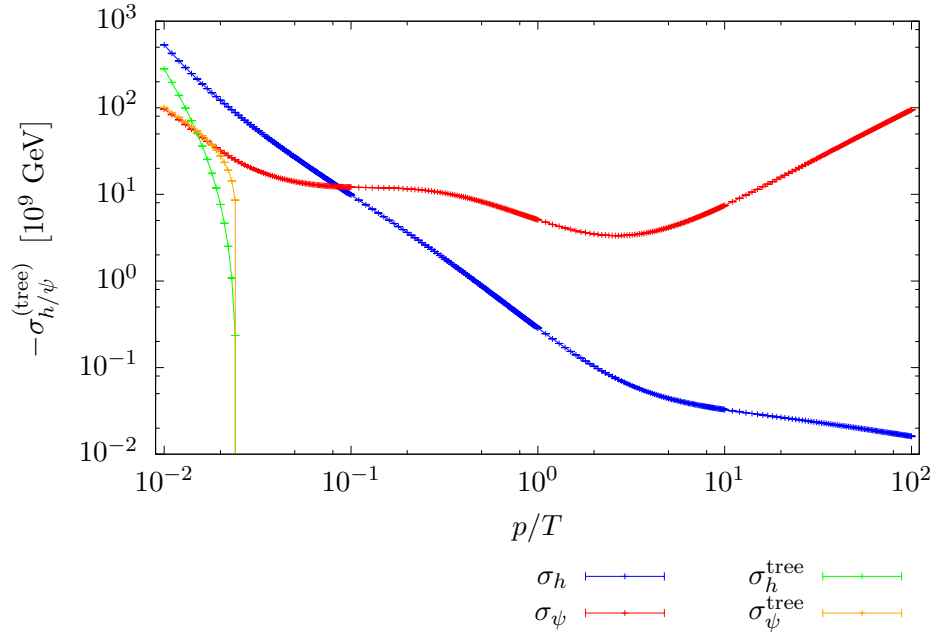


Figure 7.6.: Results for the full $\sigma_h(\omega_p, p)$ and $\sigma_\psi(\omega_p, p)$ and the tree-level $\sigma_h^{\text{tree}}(\omega_p, p)$ and $\sigma_\psi^{\text{tree}}(\omega_p, p)$; $M = 10^{10}$ GeV, $T = 10^{11}$ GeV.

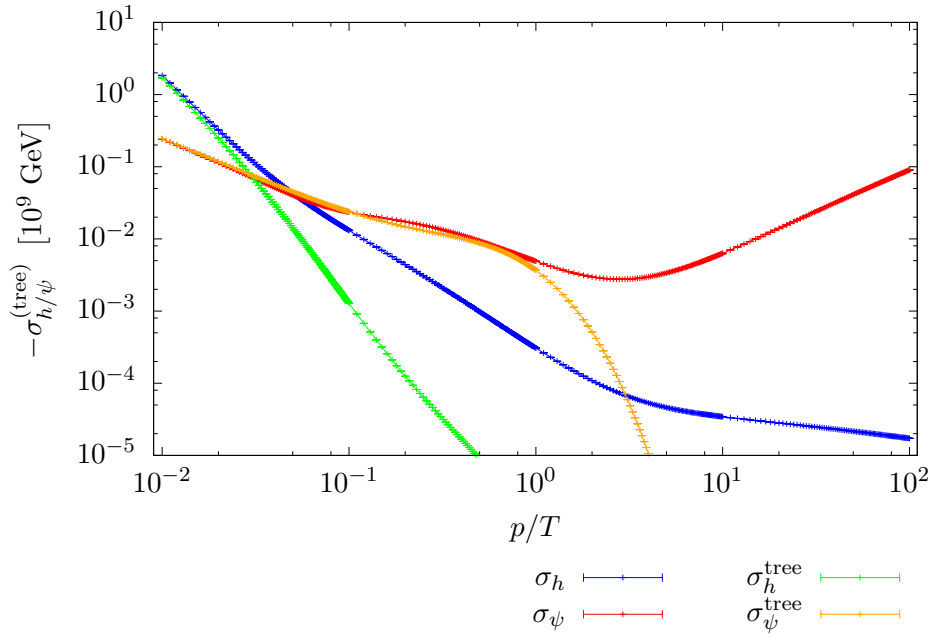


Figure 7.7.: Results for the full $\sigma_h(\omega_p, p)$ and $\sigma_\psi(\omega_p, p)$ and the tree-level $\sigma_h^{\text{tree}}(\omega_p, p)$ and $\sigma_\psi^{\text{tree}}(\omega_p, p)$; $M = 10^7$ GeV, $T = 10^8$ GeV.

every calculation, since it is obtained by omitting the part proportional to $\exp(-\Gamma_p t)$ in the integrand and the CUBA library offers the possibility of multidimensional integrands. Therefore, the value for $\lim_{t \rightarrow \infty} L_{ii}(t, t)/\epsilon_{ii}$ for the Vegas and Cuhre algorithms is obtained as an average value of all corresponding results. Hence, the error is very small. With qag, this value has only been calculated once with a maximal relative error of 0.01.

All algorithms show that the lepton number matrix thermalizes as expected, where thermalization is reached around $t \gtrsim 1/\text{GeV}$, which corresponds to $1/\Gamma_p$ for the relevant region in p . This is further discussed in Sec. 7.3.4. As for all results later on, $L_{ii}(t, t)$ is always negative, which means that there is an abundance of anti-leptons. This is expected, since the purpose of Leptogenesis is to create an abundance of baryons by creating a lepton asymmetry, which is then converted into a baryon asymmetry via sphaleron processes. Equilibrium is reached when a fraction of $a_{\text{sph}} = 28/79$ of $N_B - N_L$ is converted into a baryon asymmetry [see KS88; HT90] [as cited in BDP05, p. 4], i.e. $N_B = a_{\text{sph}}(N_B - N_L)$, see Eqs. (2.12) and (2.13). Therefore, $N_L < 0$ is needed in order to create $N_B > 0$.

The different algorithms show good agreement within the error boundaries, which one can see explicitly from the limit $t \rightarrow \infty$. For computational simplicity, in all following calculations the qagi algorithm will be used, since σ_h and σ_ψ have to be evaluated anyhow for every evaluation of the integrand because they are needed for Γ_p . For the calculations using algorithms from the CUBA library, Γ_p has been calculated on a grid with a maximal relative error of 0.001 for each value and a maximum of relative difference of 0.05 between two neighboring values in advance. Therefore, only an interpolation has been performed for each integration point in the actual computation of L_{ii} . However, simulating at different T and M would mean that for every set of these two parameters, a new grid would have to be calculated. This would be unfeasible.

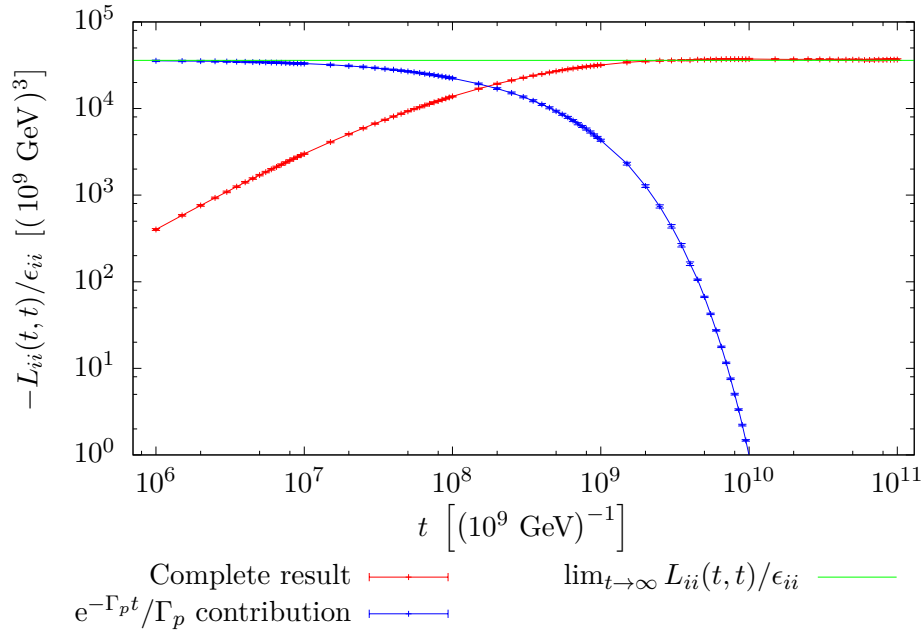


Figure 7.8.: Results for $L_{ii}(t, t)$ for $M = 10^{10}$ GeV, $T = 10^{11}$ GeV from Vegas algorithm, CUBA library. $\lim_{t \rightarrow \infty} L_{ii}(t, t)/\epsilon_{ii} = -3.605(2) \cdot 10^4 \cdot (10^9 \text{ GeV})^3$. $\exp(-\Gamma_p t)/\Gamma_p$ contribution does not include "-" from $(1 - \exp(-\Gamma_p t))/\Gamma_p$, i.e. it is the negative of the summand in the integrand.

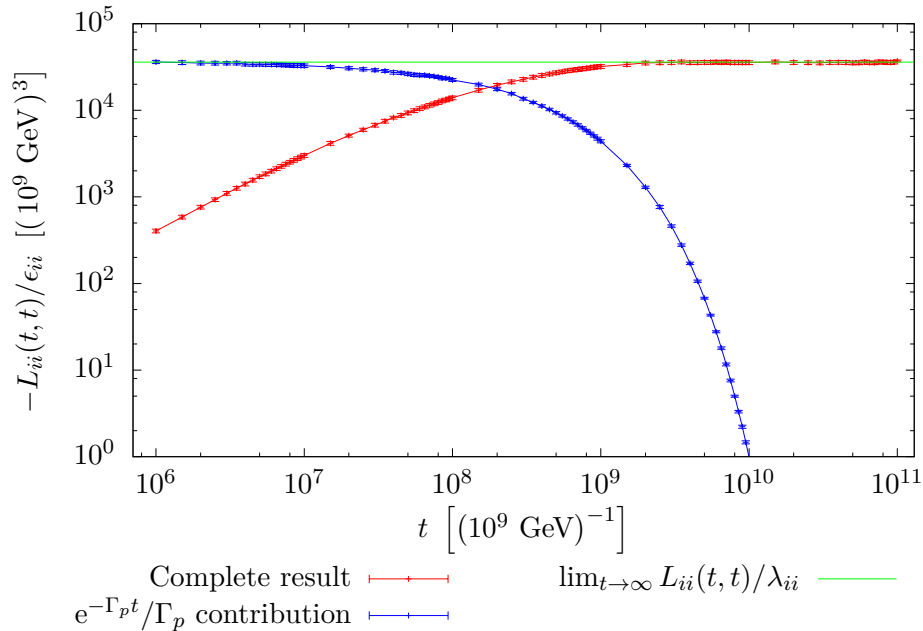


Figure 7.9.: Results for $L_{ii}(t, t)$ for $M = 10^{10}$ GeV, $T = 10^{11}$ GeV from Cuhre algorithm, CUBA library. $\lim_{t \rightarrow \infty} L_{ii}(t, t)/\epsilon_{ii} = -3.599(3) \cdot 10^4 \cdot (10^9 \text{ GeV})^3$.

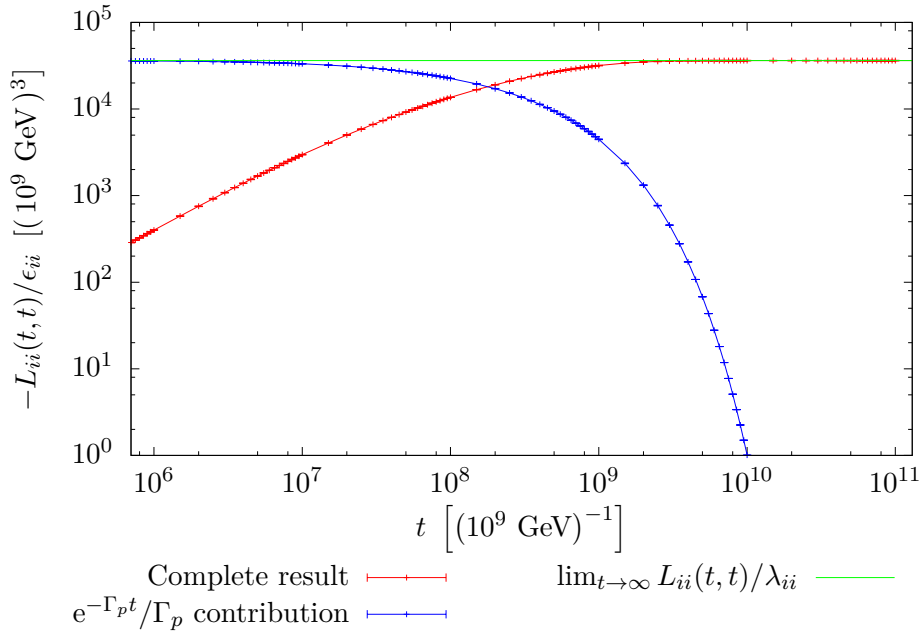


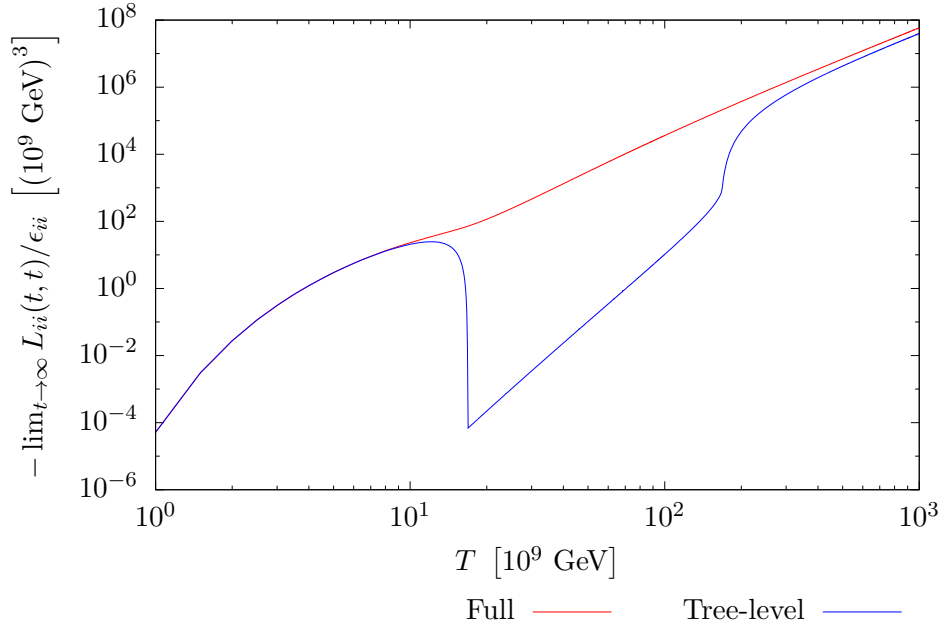
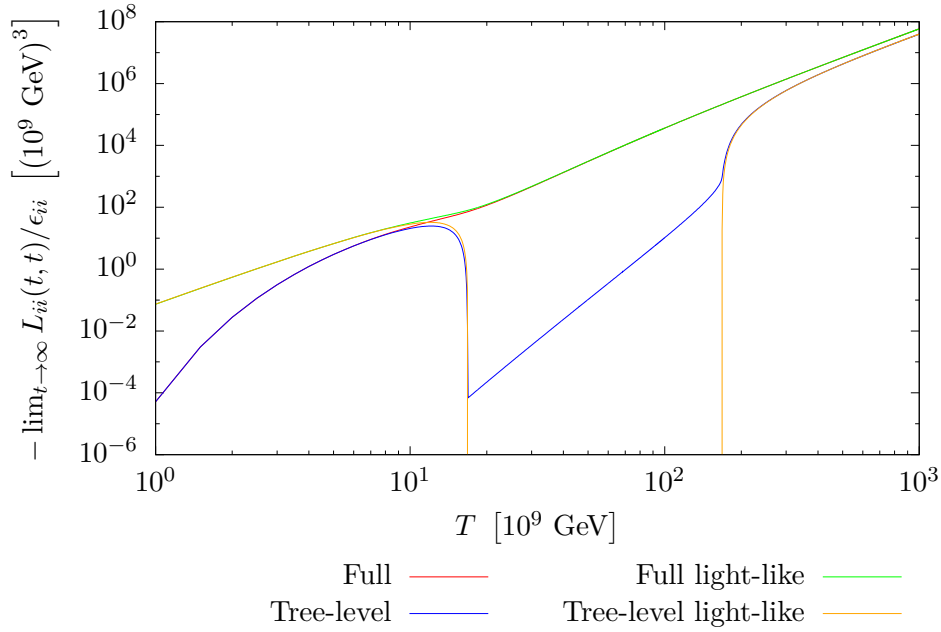
Figure 7.10.: Results for $L_{ii}(t, t)$ for $M = 10^{10}$ GeV, $T = 10^{11}$ GeV from qagi algorithm, GSL. $\lim_{t \rightarrow \infty} L_{ii}(t, t)/\epsilon_{ii} = -3.62(3) \cdot 10^4 \cdot (10^9 \text{ GeV})^3$.

7.3.2. Results for Infinite Time: Thermalized Results

In order to estimate the effect of gauge corrections on the lepton number matrix, it is useful to consider the limit as $t \rightarrow \infty$, i.e. the completely thermalized lepton number matrix from Eq. (6.38). For this purpose, calculations have been performed using the fully resummed self-energy, i.e. including all leading-order gauge and other SM corrections, and the tree-level self-energy, which only contains thermal masses for the Higgs boson and the leptons, i.e. no soft gauge corrections, but only hard gauge and other SM corrections [cf. ABB11, pp. 15-16]. The results can be found in Figs. 7.11 and 7.12, where there are also the results for the light-like calculation, i.e. explicitly entering the light-like approximation for the Majorana neutrino $p_{\parallel} + \omega_p \simeq 2p$ and $\omega_p - p \simeq M^2/(2p)$ in the calculation for its self-energy. Note that errorbars have been left out due to smallness (max. 0.01 relative error except for light-like calculation with $T < 10^{10}$ GeV, where max. 0.1 relative error) and the number of calculated points.

First, the results in Fig. 7.11 are discussed. These show that as for the production rate $\tilde{\Gamma}$ computed in [ABB11], gauge corrections (explicitly soft gauge interactions) have a large impact on the thermalized lepton number matrix for $T \gtrsim M$. For $T < M$, the effect becomes negligible. Note however that the fully resummed self-energy as well as the tree-level one are computed using the approximation that all particles are ultrarelativistic. This approximation becomes questionable for $T \lesssim M$. Another possibility is to use the result from [Ani+11] without gauge corrections, which has been done in [Hal17].

As in [ABB11] for the production rate, a region from $T \approx 1.7M_N = 1.7 \cdot 10^{10}$ GeV to $T \approx 17M = 1.7 \cdot 10^{11}$ GeV is found, where the tree-level lepton number matrix is much smaller than the fully resummed one. Note that it does not drop to zero, since the light-like approximation has not been put into the calculation for σ_h and σ_ψ . When this is used, in the corresponding region, the on-shell contributions to the self-energy and the lepton number matrix are zero as it can be seen in Fig. 7.12, since a decay or inverse decay of the

Figure 7.11.: Non-light-like results for $\lim_{t \rightarrow \infty} L_{ii}(t, t)$; $M = 10^{10}$ GeV.Figure 7.12.: Non-light-like and light-like results for $\lim_{t \rightarrow \infty} L_{ii}(t, t)$; $M = 10^{10}$ GeV.

Majorana neutrino into a Higgs boson and a lepton is kinematically forbidden [see ABB11, 15 ff.], cf. Sec. 5.6.6. If one does not explicitly plug in the light-like approximation, these processes are allowed for small $\omega_p < T$. The resummed lepton number matrix however keeps the same order of magnitude, which corresponds to the finding in [ABB11] for the production rate that gauge corrections compensate for the fact that the tree-level result is suppressed due to kinematic reasons.

Summarizing, one finds that for $T < M$, soft gauge corrections are negligible due to the fact that the tree-level and the fully resummed results are almost equal. For $T \gtrsim M$, these corrections increase the resulting lepton asymmetry and compensate for the suppression of the tree-level asymmetry because of kinematic reasons. This behavior is expected, since soft gauge interactions have been found to be important for $T \gtrsim M$ in [ABB11]. For temperatures higher than the kinematically suppressed region, the tree-level result increases again, but stays smaller than the fully resummed result by a factor of approximately 0.7. In general, one finds that the generated lepton asymmetry grows for increasing temperatures apart from the kinematically suppressed region for the tree-level result. This finding is analogous to the finding for the solution of the Boltzmann equation (4.9), where the generated asymmetry is strongly suppressed for $T < M$.

Comparing the results from the light-like calculation to the non-light-like calculation in Fig. 7.12, one notices that the differences in general decrease for increasing temperature except for the kinematically suppressed region in the tree-level calculations. This is expected, since for higher temperatures, higher momenta p contribute to the integral and in this region, the light-like approximation is satisfied better. For $T = 0.1M = 10^9$ GeV, the light-like results are larger than the non-light-like results by almost a factor of 1500. At $T \approx M$ this is reduced to a factor of around 1.3. In the kinematically suppressed region, the light-like result for the tree-level calculation is exactly zero because in this case, small momenta do not contribute as before. Apart from this region for the tree-level result, the full as well as the tree-level results become almost equal for $T > M$. Note that the lines are on top of each other at the highest temperatures considered. This discussion illustrates that due to the fact that collinearity with the inner loop momenta is assumed and these are approximated to be light-like in the calculation, all results only have controlled errors for $T \gtrsim M$. Nevertheless, it is instructive to see that the full and the tree-level results agree for $T < M$, which means that soft gauge corrections are not important for these temperatures.

7.3.3. Results for Finite Time

For finite time, simulations with different temperatures T and different times t for each T have been performed for the tree-level as well as the fully resummed results for the lepton number matrix. All calculations have been performed without the light-like approximation for the Majorana neutrino, since apart from the fact that the drop in the kinematically suppressed region is to zero, no major differences can be found for $T > M$. The fully resummed results with soft and hard gauge corrections can be found in Figs. 7.13 and 7.14, the tree-level results can be found in Figs. 7.15 and 7.16, and the complete resummed as well as tree-level results can be found again in Fig. 7.17.

As already seen for the fully resummed lepton number matrix in Sec. 7.3.1, the fully resummed and the tree-level lepton number matrix thermalize as expected within a time $t \sim 1/\Gamma_p \sim \mathcal{O}(g^{-2}T^{-1})$, i.e. the contribution of the $\exp(-\Gamma_p t)/\Gamma_p$ part, cf. Eq. (7.9), become smaller with larger t . This part is the difference from the completely thermalized $\lim_{t \rightarrow \infty} L_{ii}(t, t)$. Note that in the plots, the $-$ -sign in front $\exp(-\Gamma_p t)/\Gamma_p$ is always excluded so that it is negative. Also, the thermalization time scales as expected, i.e. it gets

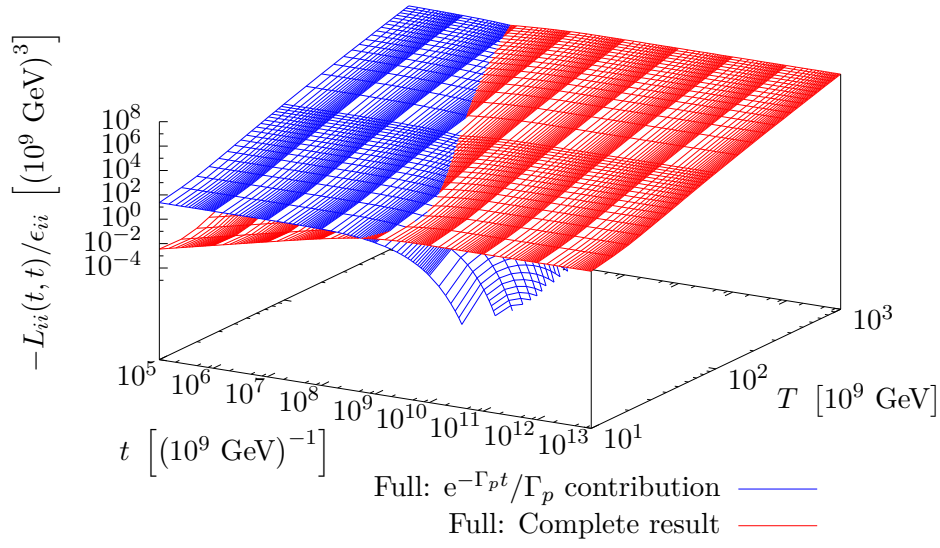


Figure 7.13.: Fully resummed $L_{ii}(t, t)$ for different t and T , complete result $L_{ii}(t, t)$ and $\exp(-\Gamma_p t)/\Gamma_p$ contribution, $M = 10^{10}$ GeV.

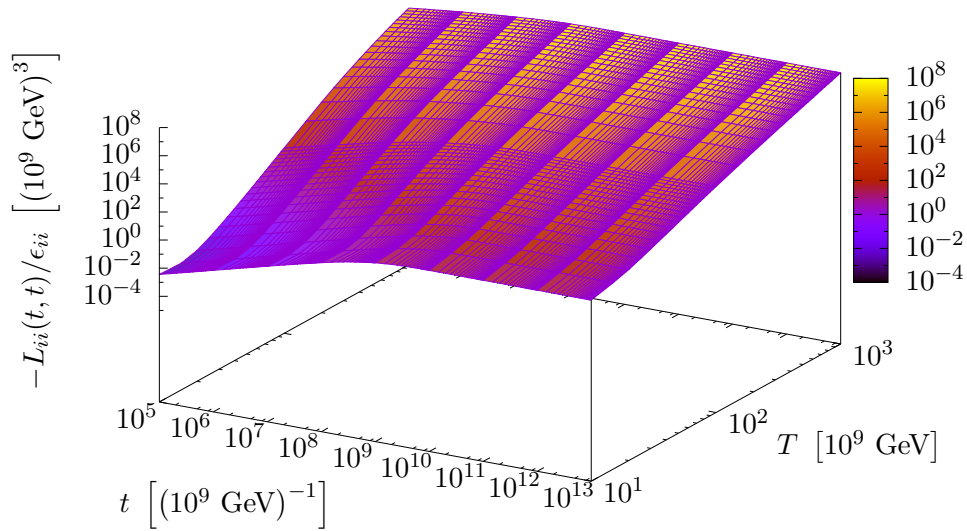


Figure 7.14.: Fully resummed $L_{ii}(t, t)$ for different t and T , complete $L_{ii}(t, t)$ in color-coded plot, $M = 10^{10}$ GeV.

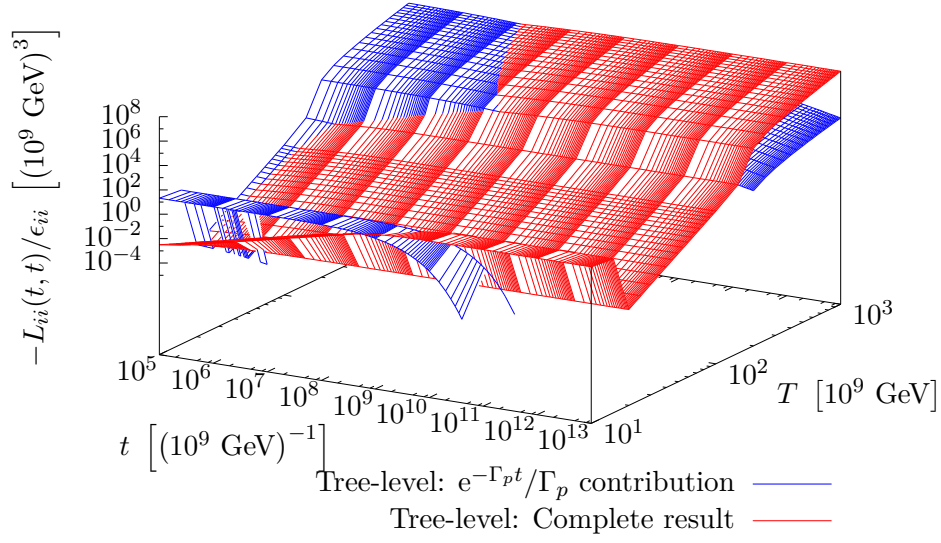


Figure 7.15.: Tree-level $L_{ii}(t, t)$ for different t and T , complete $L_{ii}(t, t)$ and $\exp(-\Gamma_p t)/\Gamma_p$ contribution, $M = 10^{10}$ GeV.

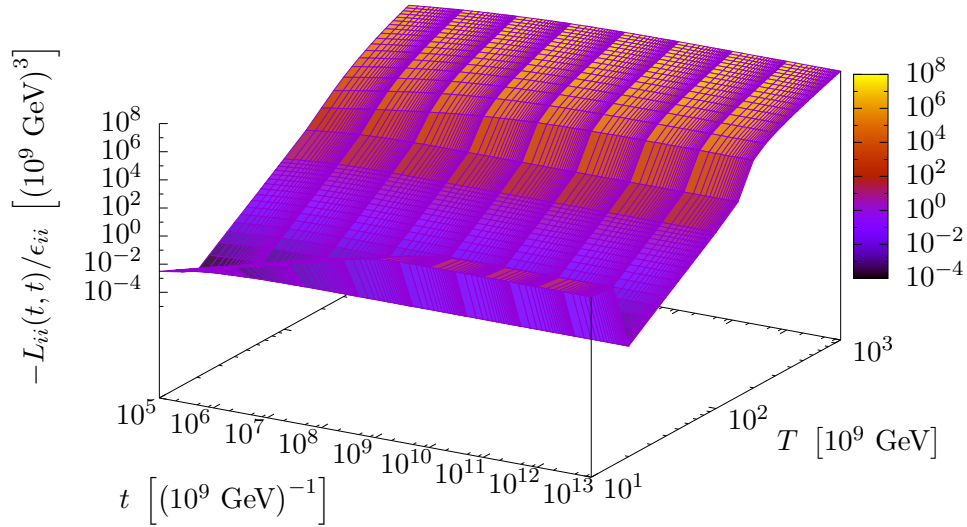


Figure 7.16.: Tree-level $L_{ii}(t, t)$ for different t and T , complete $L_{ii}(t, t)$ in color-coded plot, $M = 10^{10}$ GeV.

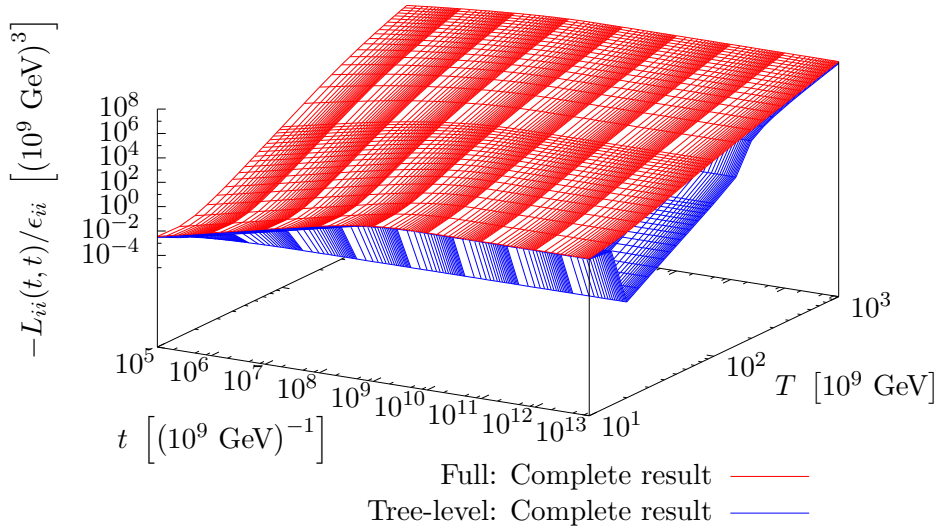


Figure 7.17.: Fully resummed and tree-level $L_{ii}(t, t)$ for different t and T , complete $L_{ii}(t, t)$, $M = 10^{10}$ GeV.

smaller when T gets larger⁵. This is visible in Figs. 7.13 and 7.15 from the intersection line of the red (complete result) and blue (exp part) surfaces. The thermalization time is discussed further in Sec. 7.3.4.

The tree-level results behave similarly to the thermalized tree-level results in Sec. 7.3.2. The complete result as well as the $\exp(-\Gamma_p t)/\Gamma_p$ contribution have a region, where they drop approximately two to six orders of magnitude. The explanation is the same as before: Only regions with small $\omega_p < T$ contribute to the integral, since the leading-order contribution is kinematically not allowed. This effect is visible for all times as the time only enters in the argument of the exponential function. Note that in this temperature region, thermalization occurs very quickly, since only small p contribute and Γ_p is large for these⁶, cf. Sec. 7.3.4.

Also, the comparison between the resummed and the tree-level results is very similar to the results from Sec. 7.3.2 and does not depend qualitatively on the time. For small temperatures $T \approx M$, both results are approximately equal. Then, the soft gauge corrections cause the fully resummed result to be larger than the tree-level result and compensate for the kinematic suppression in the corresponding temperature region.

7.3.4. Thermalization Times

The results for t_{therm} of the fully resummed and the tree-level lepton number matrix that were read off from the results in Figs. 7.13 and 7.15 using the infinite time results from Fig. 7.11 can be found in Fig. 7.18 together with fits of the thermalization times to functions a/T with $a = \text{const}$. This is the expected behavior, cf. Sec. 7.1.2. In the fits, only points with high temperatures $T \geq 3 \cdot 10^{11}$ GeV have been included, since then, the form of the fitted function and the results agree well for the fully resummed and tree-level

⁵Note that of course, the kinematically suppressed region for the tree-level result falls out of this scaling.

⁶For the p , where $\Gamma_p = 0$ one has that the integrand is zero, see Sec. 6.2.3.

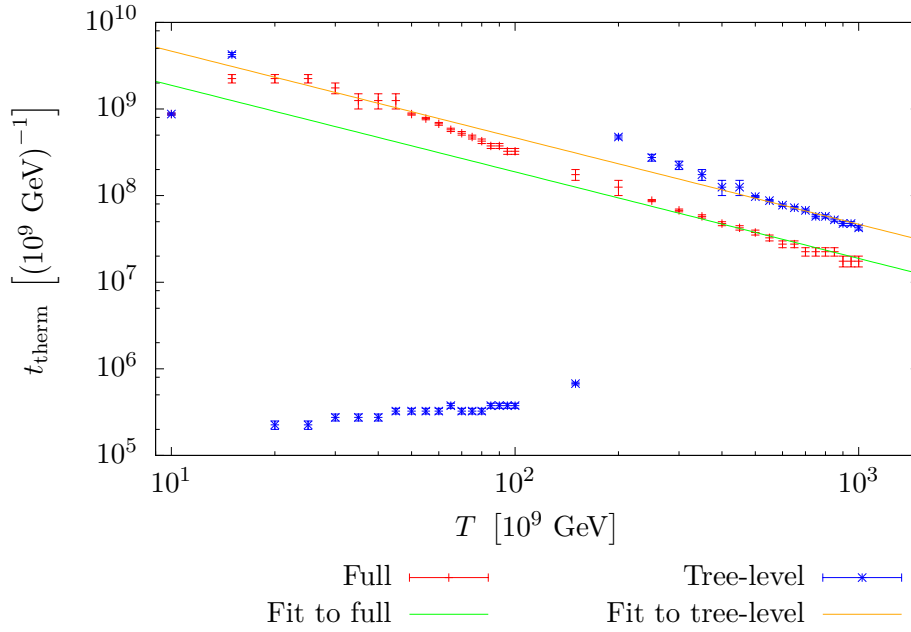


Figure 7.18.: Thermalization times and fits to functions a/T with $a = \text{const}$ for $T \geq 3 \cdot 10^{11}$ GeV, $\chi^2/N_{\text{DOF}} = 1.18$ for fully resummed and $\chi^2/N_{\text{DOF}} = 1.87$ for tree-level, $M = 10^{10}$ GeV.

calculations. Since it is a double logarithmic plot, all lines parallel to the fitted functions also have the form a/T with $a = \text{const}$. Therefore, one can also estimate the scaling of the thermalization times simply by estimating whether or not the connecting line is parallel to a fitted function.

For the fully resummed calculation, one notices that for high temperatures, the scaling is as expected. For lower temperatures $T < 10^{11}$ GeV, first, t_{therm} even increases, then drops faster than $1/T$, but slowly approaches a function $\sim 1/T$. The fit has a value of $\chi^2/N_{\text{DOF}} = 1.18$, which illustrates the good agreement with the scaling for high temperatures $T \geq 3 \cdot 10^{11}$ GeV.

In the results for the tree-level calculation, one clearly sees a drop in the kinematically suppressed region. This is due to the fact that only low momenta p contribute to the generated asymmetry and Γ_p is large for these low momenta. Apart from that, the general behavior is as for the results of the fully resummed calculation. One should also note that for $T = M = 10^{10}$ GeV, the thermalization times for both calculations are equal. For the fit, one finds a value of $\chi^2/N_{\text{DOF}} = 1.87$ again showing good agreement with the expected scaling for high temperatures $T \geq 3 \cdot 10^{11}$ GeV. Apart from the kinematically suppressed region, the thermalization times are larger in the tree-level calculation compared to the fully resummed one for $T > M$. This can be connected to the fact that the tree-level lepton number matrix is smaller than the fully resummed one, cf. Fig. 7.11, since Γ_p depends linearly on σ_h and σ_ψ , whereas, apart from the exponential function, the self-energies enter in the lepton number matrix via $\sigma_h \cdot \sigma_\psi / \Gamma_p$. More explicitly, the tree-level σ_h^{tree} and $\sigma_\psi^{\text{tree}}$ are smaller than the fully resummed ones in the region of p that mostly contributes to the integral, cf. Fig. 7.6, and hence, $t_{\text{therm}} \sim 1/\Gamma_p$ is larger. Also, in [ABB11, p. 19], a similar behavior was found for the production rate $\tilde{\Gamma}$. The tree-level result for it was found to be smaller than the fully resummed result.

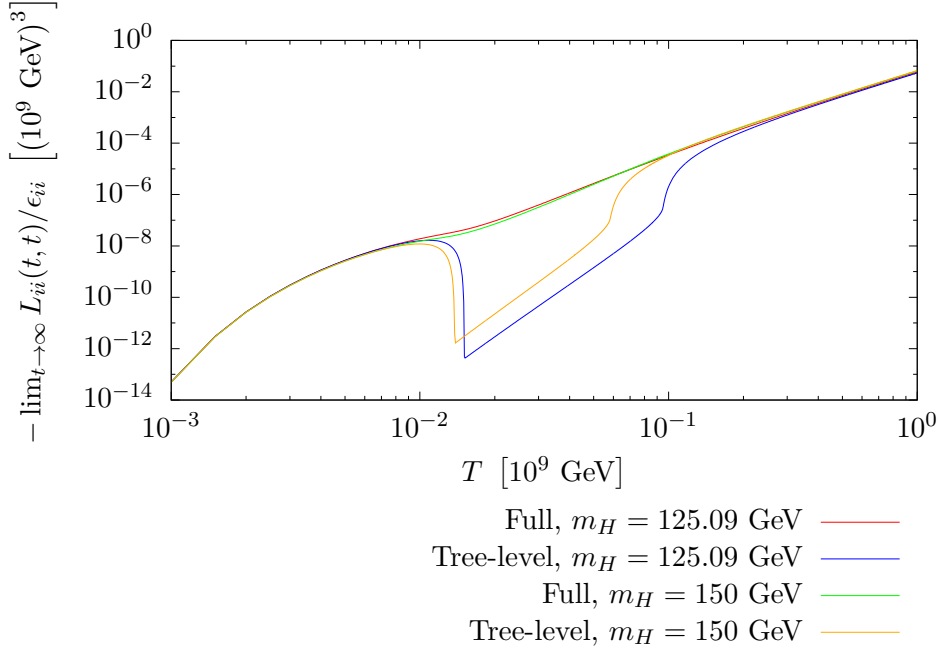


Figure 7.19.: Non-light-like results for $\lim_{t \rightarrow \infty} L_{ii}(t, t)$; $M = 10^7$ GeV.

7.4. Results for the Lepton Number Matrix for $M = 10^7$ GeV

7.4.1. Results for Infinite Time: Thermalized Results

The results for $M = 10^7$ GeV with $m_H = 125.09$ GeV and $m_H = 150$ GeV can be found in Fig. 7.19 for non-light-like calculations and Figs. 7.20 and 7.21 for non-light-like and light-like calculations. The non-light-like results are qualitatively very similar. For both Higgs boson masses, a region, where the tree-level result is suppressed due to kinematic reasons, exists as discussed in Sec. 7.3.2. The position of the suppressed region for $m_H = 150$ GeV, which is $1.4M = 1.4 \cdot 10^7$ GeV $\lesssim T \lesssim 5.8M = 5.8 \cdot 10^7$ GeV, is in very good agreement with the corresponding region for the production rate $\tilde{\Gamma}$ from [ABB11, p. 18]. This is obvious, since they exist due to the same reasons. The light-like results in Fig. 7.21 further support this statement. For the physical $m_H = 125.09$ GeV, the region, where the lepton asymmetry is suppressed is located at $1.5M = 1.5 \cdot 10^7$ GeV $\lesssim T \lesssim 9.5M = 9.5 \cdot 10^7$ GeV. For higher T , the tree-level result gets larger and is no longer kinematically suppressed, but still is smaller than the fully resummed result for $m_H = 125.09$ GeV by a factor of around 0.9. For $m_H = 150$ GeV, the tree-level result even grows larger than the fully resummed result by a factor of around 1.02 at $T = 10^2 M = 10^9$ GeV. Note that this is, however, almost within error boundaries. For $T \lesssim M$, all non-light-like results assume similar values.

To summarize the non-light-like calculations, one has similar behavior as in Sec. 7.3.2. For small $T \lesssim M$, the fully gauge corrected and the tree-level lepton number matrix are approximately equal. For larger T , soft gauge corrections enhance the generated lepton asymmetry and compensate for the kinematically suppressed region. Only for the unphysical Higgs boson mass $m_H = 150$ GeV, the tree-level result grows larger than the fully resummed result, but by a small factor. As for $M = 10^{10}$ GeV, the generated lepton asymmetry grows with T apart from the kinematically suppressed region for the tree-level

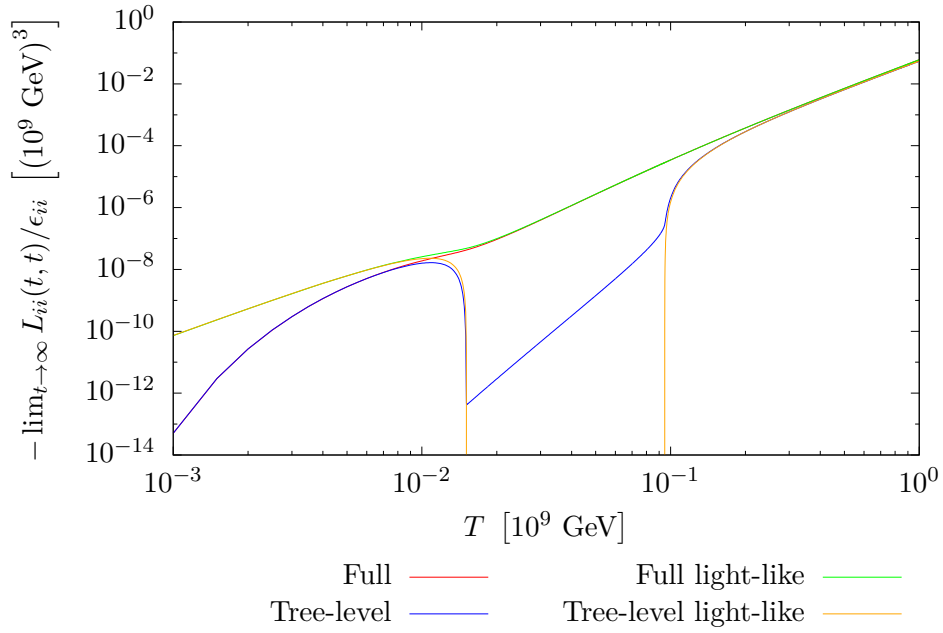


Figure 7.20.: Non-light-like and light-like results for $\lim_{t \rightarrow \infty} L_{ii}(t, t)$; $M = 10^7$ GeV, $m_H = 125.09$ GeV.

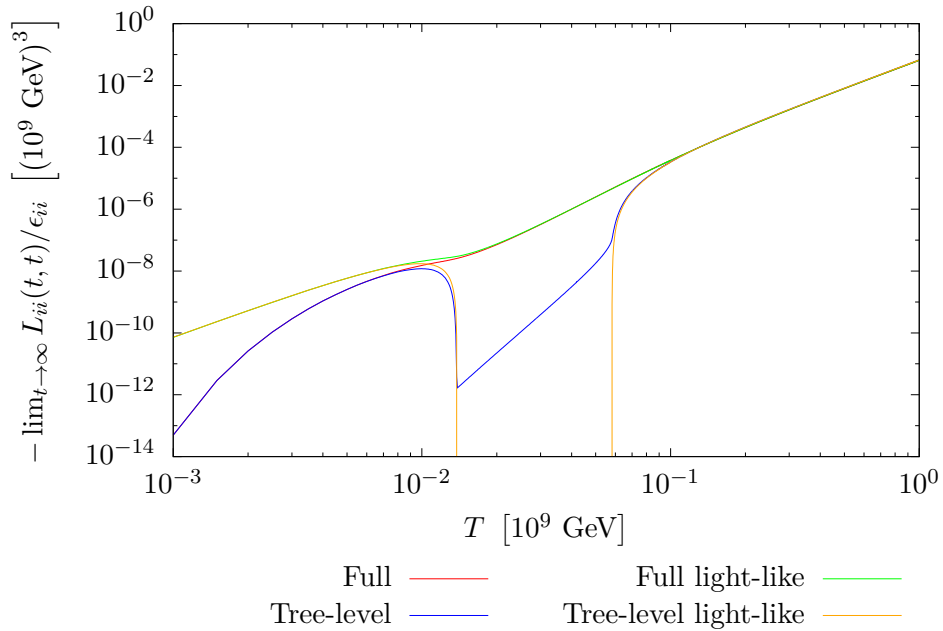


Figure 7.21.: Non-light-like and light-like results for $\lim_{t \rightarrow \infty} L_{ii}(t, t)$; $M = 10^7$ GeV, $m_H = 150$ GeV.

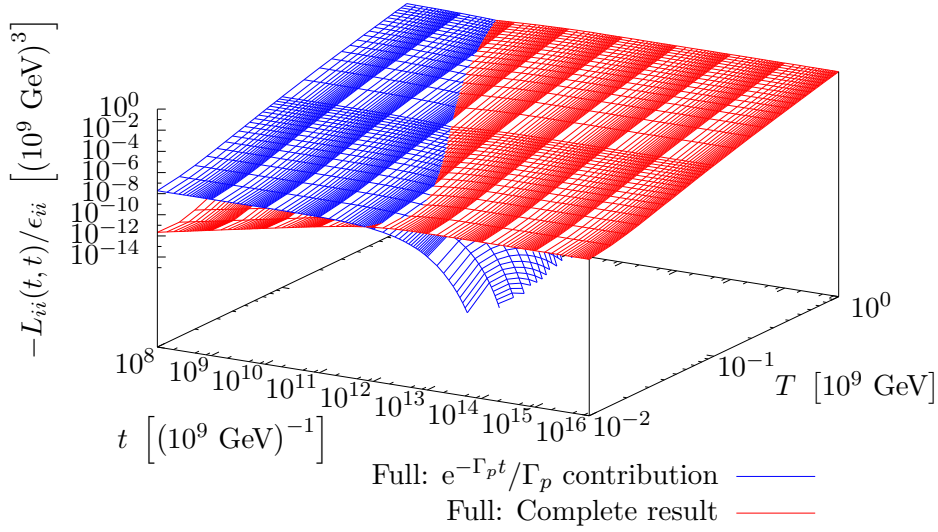


Figure 7.22.: Fully resummed $L_{ii}(t,t)$ for different t and T , complete $L_{ii}(t,t)$ and $\exp(-\Gamma_p t)/\Gamma_p$ contribution, $M = 10^7$ GeV.

result.

Since there are little or no qualitative differences, and the quantitative ones are reasonably small for the fully gauge corrected result, only calculations for $m_H = 125.09$ GeV with finite time are presented in Sec. 7.4.2. The results for $m_H = 150$ GeV show a similar behavior. The fact that the tree-level result gets a little larger than the fully resummed one for the larger Higgs mass is not important.

The comparison between non-light-like and light-like results is very similar to Sec. 7.3.2 for both Higgs boson masses. The differences between corresponding results decrease with increasing temperature apart from the kinematically suppressed region for the tree-level result. Also, the tree-level light-like results drop to zero in the kinematically suppressed region due to the reasons discussed before.

7.4.2. Results for Finite Time

As for $M = 10^{10}$ GeV, calculations with different temperatures and times have been performed for the tree-level and the fully resummed L_{ii} without entering the light-like approximation for the Majorana neutrino to study the thermalization of the lepton number matrix. Only the results for $m_H = 125.09$ GeV are presented as discussed before. The fully resummed results can be found in Figs. 7.22 and 7.23, the tree-level results can be found in Figs. 7.24 and 7.25, and the complete resummed as well as tree-level results can be found in Fig. 7.26.

One finds a similar behavior as for $M = 10^{10}$ GeV. The gauge corrected as well as the tree-level lepton number matrix thermalize within the expected times $t \sim 1/\Gamma_p \sim \mathcal{O}(\lambda^{-2} T^{-1})$, i.e. the contribution from the $\exp(-\Gamma_p t)/\Gamma_p$ parts become smaller with larger t (note the sign of this part in the plots as discussed in Sec. 7.3.3). Similarly to $M = 10^{10}$ GeV, also the scaling of the thermalization time can be seen in Figs. 7.22 and 7.24 from the intersection line of the blue and red surfaces with the exception of the kinematically

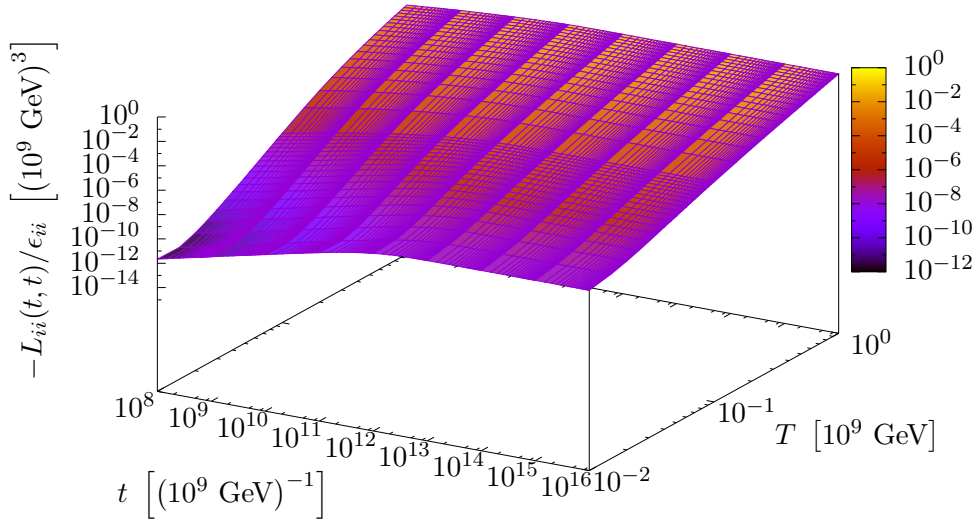


Figure 7.23.: Fully resummed $L_{ii}(t, t)$ for different t and T , complete $L_{ii}(t, t)$ in color-coded plot, $M = 10^7$ GeV.

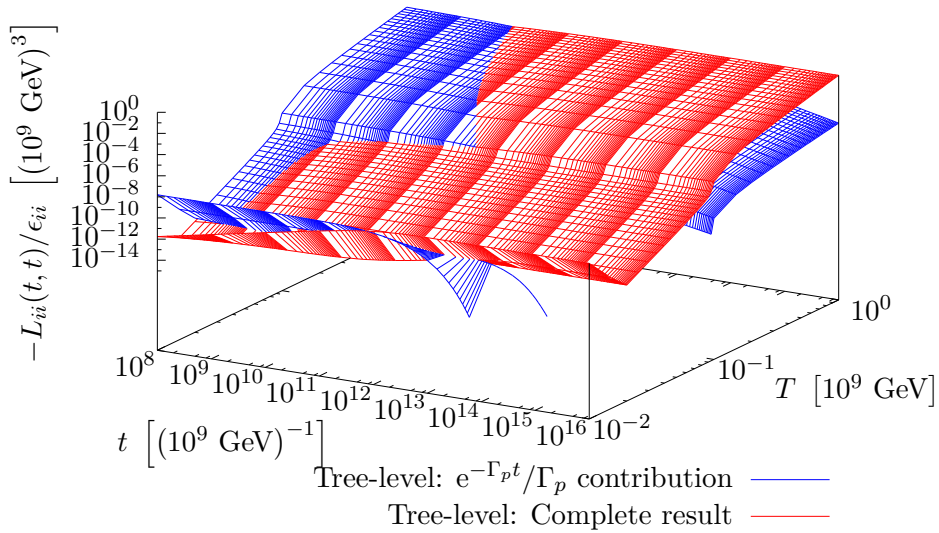


Figure 7.24.: Tree-level $L_{ii}(t, t)$ for different t and T , complete $L_{ii}(t, t)$ and $\exp(-\Gamma_p t)/\Gamma_p$ contribution, $M = 10^7$ GeV.

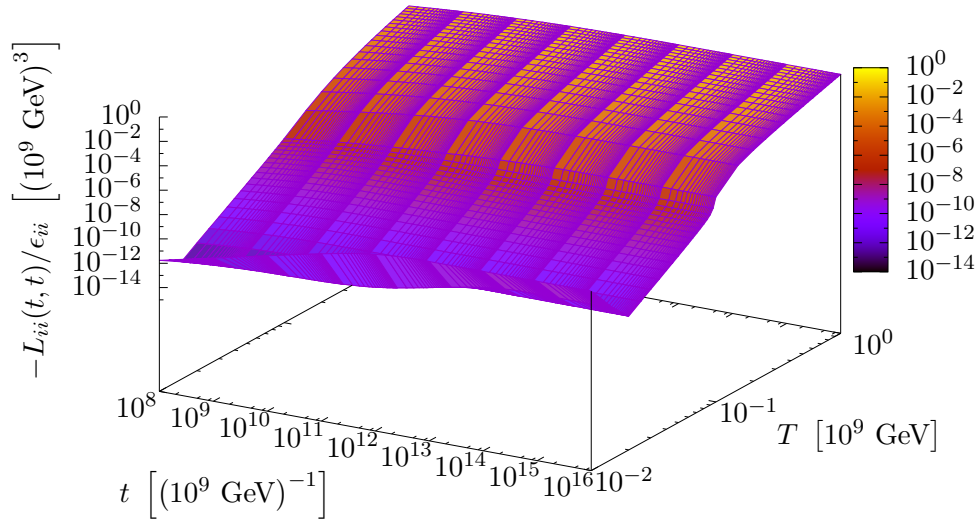


Figure 7.25.: Tree-level $L_{ii}(t, t)$ for different t and T , complete $L_{ii}(t, t)$ in color-coded plot, $M = 10^7$ GeV.

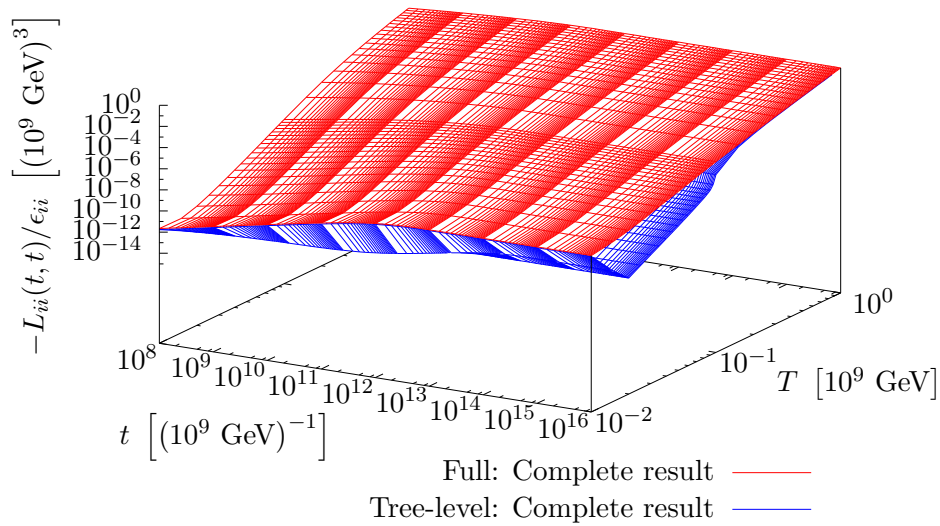


Figure 7.26.: Fully resummed and tree-level $L_{ii}(t, t)$ for different t and T , complete $L_{ii}(t, t)$, $M = 10^7$ GeV.

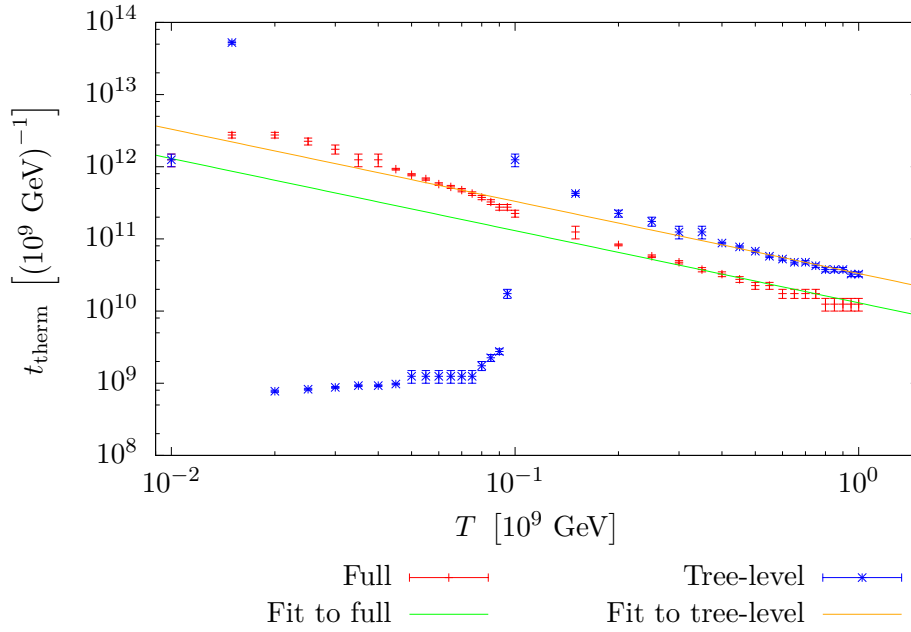


Figure 7.27.: Thermalization times and fits to functions a/T with $a = \text{const}$ for $T \geq 2.5 \cdot 10^8$ GeV, $\chi^2/N_{\text{DOF}} = 1.23$ for fully resummed and $\chi^2/N_{\text{DOF}} = 1.30$ for tree-level, $M = 10^7$ GeV.

suppressed region in the tree-level result. The scaling is discussed further in Sec. 7.4.3.

One again finds the kinematically suppressed regions in the tree-level result with fast thermalization. The reasons for this stay the same.

The comparison between the tree-level and the gauge corrected results is similar to Secs. 7.3.3 and 7.4.1. For small temperatures $T \lesssim M$, both results are approximately equal. Going to higher T , the soft gauge corrections cause the fully resummed result to be larger than the tree-level result for all times, cf. Fig. 7.26. Note the kinematically suppressed region in the tree-level result.

7.4.3. Thermalization Times

The thermalization times for $M = 10^7$ GeV can be found in Fig. 7.27 together with fits to functions a/T with $a = \text{const}$, where only points with $T \geq 2.5 \cdot 10^8$ GeV have been considered, since they agree well with the form of the fitted functions.

The results are very similar to the results for $M = 10^{10}$ GeV in Fig. 7.18. The results from the fully resummed calculation first increase, then decrease faster than $1/T$ for $T < 10^8$ GeV. For higher temperatures, the scaling approaches the expected $1/T$ and the fit has a value of $\chi^2/N_{\text{DOF}} = 1.23$ showing a good agreement with the expected scaling. In the result from the tree-level calculation, one can see the drop in the kinematically suppressed region. For $T = M$, both results, i.e. the ones from the fully resummed and tree-level calculations, are equal. The fit has a value of $\chi^2/N_{\text{DOF}} = 1.30$ again showing good agreement with the expected scaling for high temperatures $T \geq 2.5 \cdot 10^8$ GeV. Apart from the kinematically suppressed region, the tree-level results' thermalization times are larger. This can be connected to the fact that the tree-level σ_h^{tree} and $\sigma_\psi^{\text{tree}}$ are smaller than the fully resummed results, cf. Sec. 7.3.4 and Fig. 7.7.

7.5. Discussion

The results presented in this chapter show that soft and hard gauge corrections have a strong effect on thermal leptogenesis for temperatures higher than the Majorana neutrino mass. By only including hard gauge and other SM corrections, one generates asymptotic masses of the Higgs boson and lepton that give a temperature region, where the generated lepton asymmetry is strongly suppressed due to kinematic reasons. The inclusion of corrections due to interactions with soft gauge bosons compensates for this kinematic suppression. This finding is analogous to the finding for the production rate in [ABB11]. For the physical Higgs mass, it enhances the generated lepton asymmetry at all $T > M$. Only for the unphysical $m_H = 150$ GeV, the tree-level result grows larger than the fully resummed result at very high temperatures for $M = 10^7$ GeV.

With and without soft gauge corrections, the lepton number matrix thermalizes as expected, which is in very good agreement with the solution of the Boltzmann equation (4.9). The scaling of the thermalization times is also approximately as expected, since $t_{\text{therm}} \sim 1/\Gamma_p \sim \mathcal{O}(\lambda^{-2}T^{-1})$ is approached and found for high T . Furthermore, the generated lepton asymmetry grows for increasing temperatures apart from the kinematically suppressed region in the tree-level result. This is in accordance with the finding for the solution of the Boltzmann equation that the generated lepton asymmetry is strongly suppressed for $T < M$.

Comparing the two considered Majorana neutrino masses, no qualitative differences can be seen. Quantitatively, the generated lepton asymmetry is around nine orders of magnitude smaller for the smaller $M = 10^7$ GeV compared to the larger $M = 10^{10}$ GeV. Note that however, the physical scenario described in Sec. 4.1, for which the initial lepton asymmetry is calculated, only applies for the larger Majorana neutrino mass. One should always keep in mind that the calculations carried out in the context of this thesis are performed in a setting, where the temperature of the thermal bath does not change. Therefore, every temperature considered corresponds to a calculation, where one starts with zero Majorana neutrino abundance, then generates an abundance due to the interactions with the thermal bath of SM particles, and thereby generates a lepton asymmetry. All of this happens at a constant temperature.

A comparison to the result without any gauge and other SM corrections from [Ani+11] is performed in [Hal17] and therefore not considered here.

8. Conclusions and Research Perspectives

In this thesis, the effect of soft and hard gauge corrections, i.e. corrections due to interactions with gauge bosons of soft and hard momenta, on thermal leptogenesis has been studied systematically. Besides, corrections because of interactions with other standard model particles with hard momenta have been considered. This has been done assuming hierarchically ordered Majorana neutrino masses so that the two heavier ones could be integrated out giving an effective theory. Furthermore, a physical scenario, where the expansion of the universe and washout terms could be neglected, has been regarded. After a presentation of the results needed from [Ani+11] and [ABB11], an expression for the lepton number matrix systematically including all leading order gauge and other standard model corrections via a resummed Majorana neutrino self-energy has been derived following [Hüt13]. Soft gauge corrections can explicitly be excluded in this expression to study the effect of hard gauge corrections as well as other hard standard model corrections. As the lepton number matrix is derived in the framework of Kadanoff-Baym equations, it in principle contains all quantum effects, i.e. off-shell and memory effects. It has been further studied and approximated for numerical evaluation.

The approximations require that the thermal width of the Majorana neutrino is very small compared to its energy, which leads to strong peaks around the on-shell values. Furthermore, the Majorana neutrino self-energy is assumed to not depend strongly on the zeroth component of the four-momentum around the on-shell value. These assumptions have been verified numerically. Using the approximations, one essentially restricts the integral around on-shell values and hence neglects off-shell effects. Thereby, one finds the same time-dependence as the solution of the Boltzmann equations in the physical scenario considered. This is similar to the findings in [Ani+11], where for a small thermal width of the Majorana neutrino and when thermal widths for the standard model lepton and Higgs boson fields are included, this time-dependence was found.

The numerical evaluation showed the relevance of soft and hard gauge corrections for thermal leptogenesis when the temperature of the thermal bath of standard model particles is greater than or similar to the Majorana neutrino mass. When only interactions with hard gauge bosons and other standard model particles are included, a temperature region, where the generated lepton asymmetry is suppressed due to kinematic reasons, has been found. The inclusion of soft gauge corrections compensates this kinematic suppression. This is analogous to the finding in [ABB11] for the Majorana neutrino production rate. Soft gauge corrections enhance the generated lepton asymmetry for all values with the physical Higgs mass. A comparison to the result without any gauge corrections is performed in [Hal17].

Summarizing, this thesis shows the effect of soft and hard gauge corrections on thermal leptogenesis, thus expanding the temperature regime considered in [Ani+11]. It can hence be stated that also with the inclusion of all leading order gauge corrections, a lepton asymmetry can be generated successfully. This asymmetry can be converted into a baryon asymmetry using standard model sphaleron processes.

Working in the framework of Kadanoff-Baym equations, there are different effects that need to be considered in order to arrive at a "theory of leptogenesis" [see Buc01, p. 10] [as cited in Ani+11, p. 42], which include the following research perspectives [cf. Men10; Hüt13]:

- Expansion of the universe: The expansion of the universe should be included in order to arrive at a more realistic calculation, where the temperature is not kept constant. This involves solving the Kadanoff-Baym equations in the Friedmann-Lemaître-Robertson-Walker metric. These equations have been considered for a scalar particle in [HKL08].
- Inclusion of washout terms: Only the two-loop diagrams of the lepton self-energy contributing to a CP-violation at zero chemical potential, e) and f) in Fig. 4.2, have been considered in this thesis following [Ani+11]. However, the washout terms a) - d) in Fig. 4.2 violate CP when a chemical potential is introduced [see Men10, pp. 75-76]. Hence, they can become important.
- Inclusion of more than one heavy Majorana neutrino: This thesis assumes that two Majorana neutrinos are much heavier than the other one. By not doing so, a broader range of physical scenarios becomes accessible, e.g. resonant leptogenesis [see e.g. PU04], where the Majorana neutrino masses are degenerate or quasi-degenerate.

By considering these effects, more scenarios for leptogenesis would become accessible for a quantum field theoretical calculation from first principles.

A. Conventions and Feynman Rules

A.1. Conventions

All calculations in this thesis have been performed in natural units $\hbar = c = k_B = 1$.

For the Minkowski metric, the convention most common in high energy physics

$$(\eta_{\mu\nu}) = (\eta^{\mu\nu}) = \text{diag}(1, -1, -1, -1) \quad (\text{A.1})$$

has been used, which gives

$$x \cdot y = x^\mu \eta_{\mu\nu} y^\nu = x_\mu y^\mu = x^\mu y_\mu = x_0 y_0 - \mathbf{x} \cdot \mathbf{y} \quad (\text{A.2})$$

as the scalar product between two four-vectors x and y .

For the Dirac matrices, which fulfill the Clifford algebra

$$\{\gamma^\mu, \gamma^\nu\} = 2\eta^{\mu\nu} \mathbb{1}_4, \quad (\text{A.3})$$

the Weyl basis has been chosen for all calculations. In this basis one has

$$\gamma^0 = \begin{pmatrix} 0 & \mathbb{1}_2 \\ \mathbb{1}_2 & 0 \end{pmatrix}, \quad \gamma^k = \begin{pmatrix} 0 & \sigma^k \\ \sigma^k & 0 \end{pmatrix}, \quad \gamma^5 = i\gamma^0\gamma^1\gamma^2\gamma^3 = \begin{pmatrix} -\mathbb{1}_2 & 0 \\ 0 & \mathbb{1}_2 \end{pmatrix} \quad (\text{A.4})$$

with the Pauli matrices

$$\sigma^1 = \begin{pmatrix} 0 & 1 \\ 1 & 0 \end{pmatrix}, \quad \sigma^2 = \begin{pmatrix} 0 & -i \\ i & 0 \end{pmatrix}, \quad \sigma^3 = \begin{pmatrix} 1 & 0 \\ 0 & -1 \end{pmatrix}. \quad (\text{A.5})$$

The Pauli matrices fulfill the relations

$$\text{Tr}[\sigma^i \sigma^j] = 2\delta_{ij}, \quad \text{Tr}[\sigma^i] = 0. \quad (\text{A.6})$$

In the Weyl basis, one finds for the left- and right-handed projectors

$$P_L = \frac{\mathbb{1}_4 - \gamma^5}{2} = \begin{pmatrix} \mathbb{1}_2 & 0 \\ 0 & 0 \end{pmatrix}, \quad P_R = \frac{\mathbb{1}_4 + \gamma^5}{2} = \begin{pmatrix} 0 & 0 \\ 0 & \mathbb{1}_2 \end{pmatrix}. \quad (\text{A.7})$$

A.2. Feynman Rules

The Feynman rules for the effective Lagrangian in Eq. (2.7) [see Ani+11, pp. 45-46], that is used in this thesis as an effective theory for thermal leptogenesis, are given in the following, where α, β and a, b, c, d are always spinor and SU(2) indices, respectively:

- Majorana neutrino

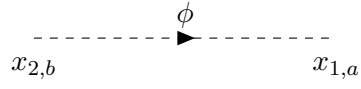
$$\begin{array}{c} \text{-----} \\ \text{-----} \\ \text{-----} \end{array} \begin{array}{c} N \\ \\ \end{array} \begin{array}{c} \\ \\ G_{\alpha\beta}(x_1, x_2) \end{array} \begin{array}{c} \\ \\ \end{array} \begin{array}{c} x_{2,\beta} \\ \\ x_{1,\alpha} \end{array}$$

- Lepton doublet



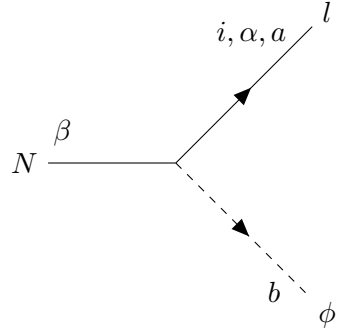
$$\delta_{ij}\delta_{ab}S_{\alpha\beta}(x_1, x_2)$$

- Higgs doublet

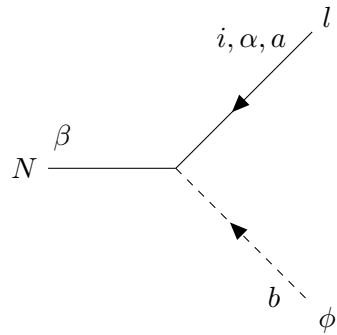


$$\delta_{ab}\Delta(x_1, x_2)$$

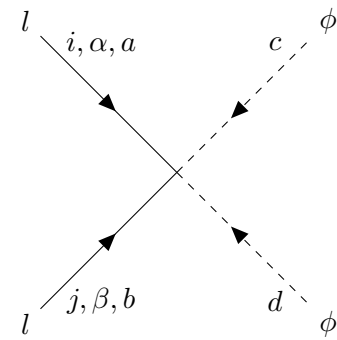
- Vertices



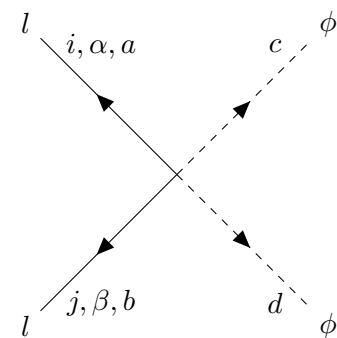
$$i\lambda_{i1}^*\epsilon_{ab}(P_R)_{\alpha\beta}$$



$$i\lambda_{i1}(CPL)_{\beta\alpha}\epsilon_{ab}$$



$$i\eta_{ij}(\epsilon_{ac}\epsilon_{bd} + \epsilon_{ad}\epsilon_{bc})(CPL)_{\alpha\beta}$$



$$i\eta_{ij}^*(\epsilon_{ac}\epsilon_{bd} + \epsilon_{ad}\epsilon_{bc})(P_R C)_{\alpha\beta}$$

B. Details on the Resummation of the Majorana Neutrino Self-Energy and on the Lepton Number Matrix

B.1. Solving the Integral Equations

In this section, the method for solving the integral equations for \mathbf{f} and for ψ , Eqs. (5.49) and (5.50), which are needed in order to calculate the resummed Majorana neutrino self-energy, is discussed. This procedure for the Majorana neutrino self-energy was first presented in [ABB11] and closely follows [AGZ02; Aur+02]. The details of this section are however also taken from [Bes10; Hüt13].

B.1.1. From Integral Equations to Ordinary Differential Equations

Recall the integral equations

$$i\epsilon(p, \mathbf{k})\mathbf{f}(\mathbf{k}_\perp) - \int \frac{d^2q_\perp}{(2\pi)^2} \mathcal{C}(\mathbf{q}_\perp) [\mathbf{f}(\mathbf{k}_\perp) - \mathbf{f}(\mathbf{k}_\perp - \mathbf{q}_\perp)] = 2\mathbf{k}_\perp, \quad (\text{B.1})$$

$$i\epsilon(p, \mathbf{k})\psi(\mathbf{k}_\perp) - \int \frac{d^2q_\perp}{(2\pi)^2} \mathcal{C}(\mathbf{q}_\perp) [\psi(\mathbf{k}_\perp) - \psi(\mathbf{k}_\perp - \mathbf{q}_\perp)] = 1, \quad (\text{B.2})$$

where

$$\begin{aligned} \epsilon(p, \mathbf{k}) &= \alpha(p^0, p_\parallel, k_\parallel) + \beta(p_\parallel, k_\parallel) \mathbf{k}_\perp^2 \\ &= \beta(p_\parallel, k_\parallel) \left(M_{\text{eff}}^2(p^0, p_\parallel, k_\parallel) + \mathbf{k}_\perp^2 \right) \end{aligned} \quad (\text{B.3})$$

with

$$\alpha(p^0, p_\parallel, k_\parallel) = p^0 - p_\parallel + \frac{m_\phi^2}{2(k_\parallel - p_\parallel)} - \frac{m_l^2}{2k_\parallel}, \quad (\text{B.4})$$

$$\beta(p_\parallel, k_\parallel) = \frac{p_\parallel}{2k_\parallel(k_\parallel - p_\parallel)}, \quad (\text{B.5})$$

$$M_{\text{eff}}^2(p^0, p_\parallel, k_\parallel) := \frac{\alpha(p^0, p_\parallel, k_\parallel)}{\beta(p_\parallel, k_\parallel)}. \quad (\text{B.6})$$

M_{eff} is called effective mass. From now on, the arguments of α , β , and M_{eff} are suppressed. Performing Fourier transformations in \mathbf{k}_\perp with the definitions

$$\mathbf{f}(\mathbf{b}) = \int \frac{d^2k_\perp}{(2\pi)^2} e^{i\mathbf{k}_\perp \cdot \mathbf{b}} \mathbf{f}(\mathbf{k}_\perp), \quad \mathbf{f}(\mathbf{k}_\perp) = \int d^2b e^{-i\mathbf{k}_\perp \cdot \mathbf{b}} \mathbf{f}(\mathbf{b}), \quad (\text{B.7})$$

$$\psi(\mathbf{b}) = \int \frac{d^2k_\perp}{(2\pi)^2} e^{i\mathbf{k}_\perp \cdot \mathbf{b}} \psi(\mathbf{k}_\perp), \quad \psi(\mathbf{k}_\perp) = \int d^2b e^{-i\mathbf{k}_\perp \cdot \mathbf{b}} \psi(\mathbf{b}), \quad (\text{B.8})$$

one finds simple expressions for the results after perpendicular momentum integration [see ABB11, p. 20]

$$\int \frac{d^2 k_\perp}{(2\pi)^2} \operatorname{Re} \mathbf{k}_\perp \mathbf{f}(\mathbf{k}_\perp) = \lim_{b \rightarrow 0} \operatorname{Im} \nabla \mathbf{f}(\mathbf{b}), \quad (\text{B.9})$$

$$\int \frac{d^2 k_\perp}{(2\pi)^2} \operatorname{Re} \psi(\mathbf{k}_\perp) = \lim_{b \rightarrow 0} \operatorname{Re} \psi(\mathbf{b}), \quad (\text{B.10})$$

which will be proven in Sec. B.2.2. Using the representation of the δ -distribution

$$\delta^2(\mathbf{b}) = \int \frac{d^2 \mathbf{k}_\perp}{(2\pi)^2} e^{i\mathbf{k}_\perp \mathbf{b}} \quad (\text{B.11})$$

and the relations

$$\int \frac{d^2 \mathbf{k}_\perp}{(2\pi)^2} e^{i\mathbf{k}_\perp \mathbf{b}} \mathbf{k}_\perp^2 \mathbf{f}(\mathbf{k}_\perp) = \delta_b \mathbf{f}(\mathbf{b}), \quad (\text{B.12})$$

$$\int \frac{d^2 \mathbf{k}_\perp}{(2\pi)^2} e^{i\mathbf{k}_\perp \mathbf{b}} i\mathbf{k}_\perp = \nabla_b \delta^2(\mathbf{b}), \quad (\text{B.13})$$

and analogously for ψ with the Laplace- and Nabla-operators Δ_b and ∇_b with respect to \mathbf{b} , one finds

$$-i\beta(\Delta_b - M_{\text{eff}}^2)\mathbf{f}(\mathbf{b}) - \mathcal{K}(\mathbf{b})\mathbf{f}(\mathbf{b}) = -2i\nabla_b \delta^2(\mathbf{b}), \quad (\text{B.14})$$

$$-i\beta(\Delta_b - M_{\text{eff}}^2)\psi(\mathbf{b}) - \mathcal{K}(\mathbf{b})\psi(\mathbf{b}) = \delta^2(\mathbf{b}), \quad (\text{B.15})$$

where

$$\mathcal{K}(\mathbf{b}) = \int \frac{d^2 q_\perp}{(2\pi)^2} (1 - e^{i\mathbf{q}_\perp \mathbf{b}}) \mathcal{C}(\mathbf{q}_\perp). \quad (\text{B.16})$$

Recall that

$$\mathcal{C}(\mathbf{q}_\perp) := T \left[C_2(r) g_W^2 \left(\frac{1}{\mathbf{q}_\perp^2} - \frac{1}{\mathbf{q}_\perp^2 + m_D^2} \right) + y_l^2 g_Y^2 \left(\frac{1}{\mathbf{q}_\perp^2} - \frac{1}{\mathbf{q}_\perp^2 + (m'_D)^2} \right) \right] \quad (\text{B.17})$$

so that integrals of the form

$$I(\mathbf{b}) := \int \frac{d^2 q}{(2\pi)^2} \left(\frac{1}{\mathbf{q}^2} - \frac{1}{\mathbf{q}^2 + m^2} \right) (1 - e^{i\mathbf{q}\mathbf{b}}) \quad (\text{B.18})$$

need to be calculated to find $\mathcal{K}(\mathbf{b})$. These to be renormalized due to divergences [see Hüt13, p. 76]. In dimensional regularization, one finds for $n = 2 - 2\varepsilon$, [Col84, cf.] [as cited in Hüt13, pp. 76-77]

$$\int \frac{d^n q}{(2\pi)^n} \frac{e^{\pm i\mathbf{q}\mathbf{b}}}{\mathbf{q}^2} = \frac{\Gamma(\frac{n}{2} - 1)}{4\pi^{n/2} \mathbf{b}^{n-2}}, \quad (\text{B.19})$$

$$\int \frac{d^n q}{(2\pi)^n} \frac{1}{\mathbf{q}^2} = 0, \quad (\text{B.20})$$

$$\int \frac{d^n q}{(2\pi)^n} \frac{1}{\mathbf{q}^2 + m^2} = \frac{\Gamma(1 - \frac{n}{2})}{(4\pi)^{n/2} m^{2-n}}, \quad (\text{B.21})$$

$$\int \frac{d^n q}{(2\pi)^n} \frac{e^{\pm i\mathbf{q}\mathbf{b}}}{\mathbf{q}^2 + m^2} = \frac{b^{1-n/2}}{(2\pi)^{n/2}} K_{\frac{n}{2}-1}(mb) \xrightarrow{n \rightarrow 2} \frac{1}{2\pi} K_0(mb), \quad (\text{B.22})$$

$$(\text{B.23})$$

where $K_0(z)$ is the modified Bessel function of second kind. For the divergent terms, one can use the expansions [see AS72, pp. 255-256]

$$\Gamma\left(1 - \frac{n}{2}\right) = \Gamma(\varepsilon) = \frac{1}{\varepsilon} - \gamma_E + \mathcal{O}(\varepsilon), \quad (\text{B.24})$$

$$\Gamma\left(\frac{n}{2} - 1\right) = \Gamma(-\varepsilon) = \frac{1}{\varepsilon} - \gamma_E + \mathcal{O}(\varepsilon), \quad (\text{B.25})$$

$$x^\varepsilon = e^{\varepsilon \ln(x)} = 1 + \varepsilon \ln(x) + \mathcal{O}(\varepsilon^2), \quad (\text{B.26})$$

where $\gamma_E = 0.57721566\dots$ is the Euler-Mascheroni constant. Subtracting the poles in ε and carrying out the limit $\varepsilon \rightarrow 0$, one finds

$$\int \frac{d^n q}{(2\pi)^n} \left(\frac{e^{\pm i\mathbf{q}\mathbf{b}}}{\mathbf{q}^2} + \frac{1}{\mathbf{q}^2 + m^2} \right) \xrightarrow[\text{Poles subtracted}]{\varepsilon \rightarrow 0} -\frac{1}{2\pi} \left(\gamma_E + \ln\left(\frac{mb}{2}\right) \right). \quad (\text{B.27})$$

In total, this gives

$$I(b) = \frac{1}{2\pi} \left(\gamma_E + \ln\left(\frac{mb}{2}\right) + K_0(mb) \right) =: D(mb) \quad (\text{B.28})$$

so that

$$\mathcal{K}(b) = T[C_2(r)g_W^2 D(m_D b) + y_l^2 g_Y^2 D(m'_D b)], \quad (\text{B.29})$$

where \mathcal{K} only depends on $b := |\mathbf{b}|$.

Therefore, using the ansatz $\mathbf{f}(\mathbf{b}) = \mathbf{b}h(b)$, one can use rotational invariance to rewrite Eqs. (B.14) and (B.15) for $b > 0$ into the ordinary differential equations (ODEs) [see Hüt13, p. 76]

$$-i\beta \left(\partial_b^2 + \frac{3}{b}\partial_b - M_{\text{eff}}^2 \right) h(b) - \mathcal{K}(b)h(b) = 0, \quad (\text{B.30})$$

$$-i\beta \left(\partial_b^2 + \frac{1}{b}\partial_b - M_{\text{eff}}^2 \right) \psi(b) - \mathcal{K}(b)\psi(b) = 0, \quad (\text{B.31})$$

where $\Delta_{\mathbf{b}}\psi(b) = (\partial_b^2 + \frac{1}{b}\partial_b)\psi(b)$ and $\Delta_{\mathbf{b}}\mathbf{f}(\mathbf{b}) = \mathbf{b}(\partial_b^2 + \frac{3}{b}\partial_b)h(b)$ have been used. Note that due to the fact that only the limits for $b \rightarrow 0$ need to be considered numerically, it is sufficient to regard $b > 0$, i.e. $\delta^2(\mathbf{b}) \equiv 0$, as well as the boundary conditions presented in the next section [see ABB11, p. 22].

B.1.2. Boundary Conditions

Due to the fact that the Fourier integrals have to converge, one has the conditions [see ABB11, p. 21]

$$\lim_{b \rightarrow \infty} \mathbf{f}(\mathbf{b}) = \mathbf{0}, \quad (\text{B.32})$$

$$\lim_{b \rightarrow \infty} \psi(b) = 0, \quad (\text{B.33})$$

where the first condition implies that $h(b)$ has to fall off faster than $1/b$ for $b \rightarrow 0$.

For $b \rightarrow 0$, all terms without derivatives, which do not contain a δ -distribution, in Eqs. (B.14) and (B.15) can be neglected due to the fact that $\mathcal{K}(b) \sim b^2 \ln(b)$ [see ABB11, p. 21], i.e.

$$-i\beta \Delta_{\mathbf{b}}\mathbf{f}(\mathbf{b}) = -2i\nabla_{\mathbf{b}}\delta^2(\mathbf{b}), \quad (\text{B.34})$$

$$-i\beta \Delta_{\mathbf{b}}\psi(\mathbf{b}) = \delta^2(\mathbf{b}). \quad (\text{B.35})$$

The solutions of these equations can be derived from the fundamental solution $\phi(\mathbf{b}) = \ln(|\mathbf{b}|)/(2\pi)$ of the Poisson equation $\Delta_{\mathbf{b}}\phi(\mathbf{b}) = v(\mathbf{b})$ [see Hüt13, pp. 77-78], which can be obtained via the method of Green's functions. The solutions are then given by [see Hüt13, p. 77]

$$\mathbf{f}(\mathbf{b}) = \left(\phi * \left(-\frac{2}{\beta} \nabla_{\mathbf{b}} \delta^2 \right) \right) (\mathbf{b}) = \frac{1}{\pi\beta} \int d^2t \ln(|\mathbf{t}|) \nabla_{\mathbf{b}-\mathbf{t}} \delta^2(\mathbf{b}-\mathbf{t}), \quad (\text{B.36})$$

$$\psi(\mathbf{b}) = \left(\phi * \left(\frac{i}{\beta} \delta^2 \right) \right) (\mathbf{b}) = \frac{i}{2\pi\beta} \int d^2t \ln(|\mathbf{t}|) \delta^2(\mathbf{b}-\mathbf{t}). \quad (\text{B.37})$$

Therefore, one finds the limiting behaviors [cf. ABB11, p. 11] [as cited in Hüt13, p. 78]

$$\mathbf{f}(\mathbf{b}) = c_f \frac{\mathbf{b}}{b^2} + \mathcal{O}(b) \Rightarrow h(b) = c_f \frac{1}{b^2} + \mathcal{O}(b^0), \quad (\text{B.38})$$

$$\psi(b) = c_\psi \ln b + \mathcal{O}(b^0), \quad (\text{B.39})$$

where

$$c_f := \frac{1}{\pi\beta}, \quad (\text{B.40})$$

$$c_\psi := \frac{i}{2\pi\beta}. \quad (\text{B.41})$$

Note that here, only the dependence on b is considered. It becomes clear in Sec. B.1.4, how a dimensionless argument in the logarithm is achieved. The limiting behaviors show that divergences only occur in $\text{Re } h(b)$ and $\text{Im } \psi(b)$, while $\text{Im } h(b)$ and $\text{Re } \psi(b)$ stay regular for $b \rightarrow 0$ and therefore everywhere, since they can only occur for this value due to the ODEs (B.30) and (B.31). Hence, the results for Eqs. (B.9) and (B.10) needed for the resummed Majorana neutrino self-energies stays finite.

Also, the first corrections, that are given by the order estimates in Eqs. (B.38) and (B.39), have to fulfill $(\Delta_{\mathbf{b}} - M_{\text{eff}}^2) \tilde{\mathbf{f}} = (\tilde{h}'' + 3\tilde{h}'/b - M_{\text{eff}}^2 \tilde{h}) \mathbf{b} = 0$ and $(\Delta_{\mathbf{b}} - M_{\text{eff}}^2) \tilde{\psi} = \tilde{\psi}'' + \tilde{\psi}'/b - M_{\text{eff}}^2 \tilde{\psi} = 0$, respectively, since $\mathcal{K}(b) = b^2 \ln(b) \rightarrow 0$ for $b \rightarrow 0$. The solutions give the order estimates in Eqs. (B.38) and (B.39) as well as $\tilde{h}'(b) \rightarrow 0$ and $\tilde{\psi}'(b) \rightarrow 0$ for $b \rightarrow 0$, i.e. the corrections in Eqs. (B.38) and (B.39) have a vanishing first derivative for $b \rightarrow 0$.

B.1.3. Numerical Procedure

In order to provide an overview, the procedure needed for the numerical evaluation of the ODEs (B.30) and (B.31) is presented shortly in this section following [ABB11, pp. 22-23] [as cited in Hüt13, pp. 78-79] with the modification that the numerical value for the limit $b \rightarrow \infty$ is chosen dynamically for better stability. Here, only the steps for $\psi(b)$ and the necessary modifications for $h(b)$ are presented.

1. Split $\psi(b)$ into a tree-level and a higher order part following $\psi(b) = \psi_0(b) + \psi_1(b)$, where $\psi_0(b)$ solves (B.30) with $\mathcal{K}(b)$ set to 0. Solve for $\psi_0(b)$ implementing the boundary conditions from Eqs. (B.33) and (B.39).
2. Make an ansatz for the general solution of $\psi_1(b) = c_{1,\psi} \psi_1^{(1)}(b) + c_{2,\psi} \psi_1^{(2)}(b) + \psi_1^{(p)}(b)$ with a particular solution $\psi_1^{(p)}(b)$ of the emerging inhomogeneous equation and the linearly independent solutions $\psi_1^{(1,2)}(b)$ of the corresponding homogeneous equation.

3. Use the BCs from Eqs. (B.33) and (B.39) and appropriate initial conditions (ICs), see next step, such that $c_{1,\psi} = 0$ and

$$\int \frac{d^2 k_{\perp}}{(2\pi)^2} \operatorname{Re} \psi(\mathbf{k}_{\perp}) = \lim_{b \rightarrow 0} \operatorname{Re} \psi(b) = \operatorname{Re} c_{2,\psi} = - \lim_{b \rightarrow \infty} \operatorname{Re} \left(\frac{\psi_1^{(p)}(b)}{\psi_1^{(2)}(b)} \right). \quad (\text{B.42})$$

4. Use the following algorithm to compute $\operatorname{Re} c_{2,\psi}$, where b_0 and b_{∞} are the numerical values for the limits $b \rightarrow 0$ and $b \rightarrow \infty$, whereas $b_{\infty,\max}$ is the maximum value for b_{∞} , and $\varepsilon_{\max} > 0$ is the maximum relative error:

- 1: Choose b_0 , b_{∞} , $b_{\infty,\max}$, and ε_{\max} .
- 2: $b_i \leftarrow b_0$.
- 3: Solve homogeneous equation for $\psi_1^{(2)}(b)$ with ICs $\psi_1^{(2)}(b_0) = 1$, $\psi_1^{(2)'}(b_0) = 0$ from b_i to b_{∞} .
- 4: Solve inhomogeneous equation for $\psi_1^{(p)}(b)$ with ICs $\psi_1^{(p)}(b_0) = i[\psi]$, $\psi_1^{(p)'}(b_0) = 0$ from b_i to b_{∞} .
- 5: Calculate $\operatorname{Re} c_{2,\psi}$ according to Eq. (B.42) with $\psi_1^{(2)}(b_{\infty})$ and $\psi_1^{(p)}(b_{\infty})$.
- 6: $b_i \leftarrow b_{\infty}$.
- 7: Increase b_{∞} .
- 8: **repeat**
- 9: Solve homogeneous equation for $\psi_1^{(2)}(b)$ from b_i to b_{∞} with previous solution at current b_i as ICs.
- 10: Solve inhomogeneous equation for $\psi_1^{(p)}(b)$ from b_i to b_{∞} with previous solution at current b_i as ICs.
- 11: $\operatorname{Re} c_{2,\psi,\text{old}} \leftarrow \operatorname{Re} c_{2,\psi}$.
- 12: Calculate $\operatorname{Re} c_{2,\psi}$ according to Eq. (B.42) with $\psi_1^{(2)}(b_{\infty})$ and $\psi_1^{(p)}(b_{\infty})$.
- 13: $b_i \leftarrow b_{\infty}$.
- 14: Increase b_{∞} .
- 15: **until** $|\operatorname{Re} c_{2,\psi,\text{old}} - \operatorname{Re} c_{2,\psi}| / \operatorname{Re} c_{2,\psi} < \varepsilon_{\max}$ or $b_{\infty} > b_{\infty,\max}$.

The same procedure can be used for $h(b)$. Only the ICs for the particular solution have to be changed to $h_1^{(p)}(b_0) = 1[h]$ and $h_1^{(p)'} = 0$ such that

$$\lim_{b \rightarrow 0} \operatorname{Im} h(b) = \operatorname{Im} c_{2,h} = \lim_{b \rightarrow \infty} \operatorname{Im} \left(\frac{h_1^{(p)}(b)}{h_1^{(2)}(b)} \right). \quad (\text{B.43})$$

$[\psi] = \text{energy}$ and $[h] = (\text{energy})^3$ denote the units of $\psi(b)$ and $h(b)$, respectively.

B.1.4. Modifying the ODEs for Numerical Evaluation

In this section, the steps needed to bring the ODEs (B.30) and (B.31) into a form that can then be solved numerically, i.e. the steps 1. to 3. from the previous Sec. B.1.3, are presented following [Hüt13, pp. 79-81]. Following this reference, the calculation for ψ is presented first.

Recall the ODE (B.31) that needs to be solved for $b > 0$

$$-i\beta \left(\partial_b^2 + \frac{1}{b} \partial_b - M_{\text{eff}}^2 \right) \psi(b) - \mathcal{K}(b) \psi(b) = 0. \quad (\text{B.44})$$

The first step is to split the function into $\psi(b) = \psi_0(b) + \psi_1(b)$, where $\psi_0(b)$ fulfills the equation

$$-i\beta \left(\partial_b^2 + \frac{1}{b} \partial_b - M_{\text{eff}}^2 \right) \psi_0(b) = 0, \quad (\text{B.45})$$

i.e. is the tree-level solution and $\psi_1(b)$. Eq. (B.45) is a Bessel differential equation with the general solution [see AS72, p. 358], [see Hüt13, p. 79]

$$\psi_0(b) = a_1 J_0 \left(\pm i b \sqrt{M_{\text{eff}}^2} \right) + a_2 Y_0 \left(\pm i b \sqrt{M_{\text{eff}}^2} \right), \quad (\text{B.46})$$

where $J_n(z)$ and $Y_n(z)$ are the Bessel functions of first and second kind, respectively, and $a_1, a_2 \in \mathbb{C}$. The signs in the arguments are discussed later. Keeping in mind that

$$M_{\text{eff}}^2 = \frac{2k_{\parallel}(k_{\parallel} - p_{\parallel})(p^0 - p_{\parallel}) + k_{\parallel}m_{\phi}^2 - (k_{\parallel} - p_{\parallel})m_l^2}{p_{\parallel}} \quad (\text{B.47})$$

can become negative, one has to differentiate between the cases $M_{\text{eff}}^2 \geq 0$ and $M_{\text{eff}}^2 \leq 0$. Starting with $M_{\text{eff}}^2 \geq 0$ one uses the +sign in both arguments in Eq. (B.46). Using properties of the Bessel functions

$$J_0(ix) = I_0(x), \quad (\text{B.48})$$

$$Y_0(ix) = iI_0(x) - \frac{2}{\pi}K_0(x) \quad (\text{B.49})$$

with $x \in \mathbb{R}$ given in [AS72, p. 375], one can rewrite the solutions in terms of the modified Bessel functions of first and second kind $I_0(x)$ and $K_0(x)$ of real arguments x . These have the limiting forms [see AS72, p. 375]

$$I_0(x) \sim 1, \quad (\text{B.50})$$

$$K_0(x) \sim -\ln(x) \quad (\text{B.51})$$

for $x \rightarrow 0$. Comparison to Eq. (B.39) gives¹

$$\psi_0(b) = \left(a_1^{(1)} - \frac{1}{4\beta} \right) I_0 \left(b \sqrt{M_{\text{eff}}^2} \right) - \frac{i}{2\pi\beta} K_0 \left(b \sqrt{M_{\text{eff}}^2} \right) \quad (\text{B.52})$$

with $a_1^{(1)} \in \mathbb{C}$. Since $\lim_{x \rightarrow \infty} I_0(x) = \infty$ [cf. AS72, p. 377], any non-zero prefactor before I_0 would violate the boundary conditions for $b \rightarrow \infty$. Therefore, one has $a_1^{(1)} = 1/(4\beta)$ and finds [cf. Hüt13, p. 80]

$$\psi_0(b) = -\frac{i}{2\pi\beta} K_0 \left(b \sqrt{M_{\text{eff}}^2} \right) \text{ for } M_{\text{eff}}^2 \geq 0. \quad (\text{B.53})$$

For $M_{\text{eff}}^2 \leq 0$ one uses --sign in both arguments in Eq. (B.46). In this case, the arguments of J_0 and Y_0 are real. These have limiting forms for $x \rightarrow 0$ [see AS72, p. 360]

$$J_0(x) \sim 1, \quad (\text{B.54})$$

$$Y_0(x) \sim \frac{2}{\pi} \ln(x). \quad (\text{B.55})$$

Comparison to Eq. (B.39) gives

$$\psi_0(b) = a_1^{(2)} J_0 \left(b \sqrt{|M_{\text{eff}}^2|} \right) + \frac{i}{4\pi} Y_0 \left(b \sqrt{|M_{\text{eff}}^2|} \right). \quad (\text{B.56})$$

¹The difference in the prefactor of I_0 compared to [Hüt13, p. 79] is due to different signs in the arguments of Eq. (B.46).

To ensure a continuous transition from $M_{\text{eff}}^2 \leq 0$ to $M_{\text{eff}}^2 \geq 0$ [cf. Hüt13, p. 80], i.e. the well-definedness at $M_{\text{eff}}^2 = 0$, the limiting forms have to be matched. This forces one to choose $a_1^{(2)} = 0$ and therefore find [cf. Hüt13, p. 80]

$$\psi_0(b) = \frac{i}{4\pi} Y_0 \left(b \sqrt{|M_{\text{eff}}^2|} \right) \text{ for } M_{\text{eff}}^2 < 0. \quad (\text{B.57})$$

The next step is to realize that the complete differential equation for $\psi(b)$ is an inhomogeneous ordinary differential equation of second order. Therefore, $\psi_1(b)$ is given by the sum of the superposition of the two linearly independent solutions $\psi_1^{(1)}(b)$ and $\psi_1^{(2)}(b)$ of the homogeneous equation and a particular solution $\psi_1^{(p)}(b)$ of the inhomogeneous equation, where the term occuring from the fact that $\psi_0(b)$ only is a tree-level solution with $\mathcal{K}(b)$ set to zero is considered as an inhomogeneity, i.e.

$$c_{1,\psi} \psi_1^{(1)}(b) + c_{2,\psi} \psi_1^{(2)}(b) + \psi_1^{(p)}(b) = \psi_1(b), \quad (\text{B.58})$$

$$-i\beta \left(\partial_b^2 + \frac{1}{b} \partial_b - M_{\text{eff}}^2 \right) \psi_1(b) - \mathcal{K}(b) (\psi_0(b) + \psi_1(b)) = 0. \quad (\text{B.59})$$

Since the limiting behavior from Eq. (B.39) for $b \rightarrow 0$ is already implemented in $\psi_0(b)$, $\psi_1(b)$ is regular and $\psi_1(b) \rightarrow 0$ for $b \rightarrow 0$. By choosing the initial conditions appropriately, one can achieve [see Hüt13, p. 80]

$$\psi_1^{(1)} \sim c_\psi \ln b (\sim K_0(b)) \Rightarrow c_{1,\psi} = 0, \quad (\text{B.60})$$

$$\psi_1^{(2)} \sim \text{regular} (\sim I_0(b)) \Rightarrow c_{2,\psi} = - \lim_{b \rightarrow \infty} \frac{\psi_1^{(p)}(b)}{\psi_1^{(2)}(b)}, \quad (\text{B.61})$$

where $\lim_{b \rightarrow \infty} \psi_1(b) = 0$ has been used.

Since the ODEs have to be solved numerically from $b \rightarrow 0$ to $b \rightarrow \infty$, one has to choose a small b_0 and find a b_∞ to achieve the limits numerically, where the latter can be found during the calculation such that a certain accuracy is met. Details on how they are chosen are given below. Solving the homogeneous ODE with ICs $\psi_1(b_0) = 1[\psi]$ and $\psi_1'(b_0) = 0$ then gives $\psi_1^{(2)}(b)$ due to its regularity for $b \rightarrow 0$, and $c_{1,\psi} = 0$. Similarly, the inhomogeneous ODE is solved with ICs $\psi_1(b_0) = i[\psi]$ and $\psi_1'(b_0) = 0$ to obtain $\psi_1^{(p)}(b)$ such that $\lim_{b \rightarrow 0} \text{Re } \psi(b) = \text{Re } c_{2,\psi}$. Splitting $\psi_1^{(2)}(b)$, $\psi_1^{(p)}(b)$, and $\psi_0(b)$ into a real and an imaginary part according to $\psi_1^{(2)}(b) =: \psi_{1,r}^{(2)}(b) + i\psi_{1,i}^{(2)}(b)$, and analogously for $\psi_1^{(p)}$ and $\psi_0(b)$, one now has to solve the real-valued coupled ODEs

$$\left(\partial_b^2 + \frac{1}{b} \partial_b - M_{\text{eff}}^2 \right) \psi_{1,r}^{(2)}(b) + \frac{\mathcal{K}(b)}{\beta} \psi_{1,i}^{(2)}(b) = 0, \quad (\text{B.62a})$$

$$\left(\partial_b^2 + \frac{1}{b} \partial_b - M_{\text{eff}}^2 \right) \psi_{1,i}^{(2)}(b) - \frac{\mathcal{K}(b)}{\beta} \psi_{1,r}^{(2)}(b) = 0, \quad (\text{B.62b})$$

and

$$\left(\partial_b^2 + \frac{1}{b} \partial_b - M_{\text{eff}}^2 \right) \psi_{1,r}^{(p)}(b) + \frac{\mathcal{K}(b)}{\beta} (\psi_{0,i}(b) + \psi_{1,i}^{(p)}(b)) = 0, \quad (\text{B.63a})$$

$$\left(\partial_b^2 + \frac{1}{b} \partial_b - M_{\text{eff}}^2 \right) \psi_{1,i}^{(p)}(b) - \frac{\mathcal{K}(b)}{\beta} \psi_{1,r}^{(p)}(b) = 0, \quad (\text{B.63b})$$

numerically with the ICs

$$\psi_{1,r}^{(2)}(b_0) = 1, \quad \psi_{1,r}^{(2)'}(b_0) = 0, \quad (\text{B.64a})$$

$$\psi_{1,i}^{(2)}(b_0) = 0, \quad \psi_{1,i}^{(2)'}(b_0) = 0, \quad (\text{B.64b})$$

and

$$\psi_{1,r}^{(p)}(b_0) = 0, \quad \psi_{1,r}^{(p)'}(b_0) = 0, \quad (\text{B.65a})$$

$$\psi_{1,i}^{(p)}(b_0) = 1[\psi], \quad \psi_{1,i}^{(p)'}(b_0) = 0, \quad (\text{B.65b})$$

$$(\text{B.65c})$$

where $\psi_{0,r}(b) \equiv 0$ and $\mathcal{K}(b), \beta \in \mathbb{R}$ have been used. Note that for $\psi_1^{(2)}(b)$, no unit is necessary as it is contained in $c_{2,\psi}$.

Applying the same procedure to the ODE (B.30) with the analogous splitting into $h(b) = h_0(b) + h_1(b)$, where $h_0(b)$ is the tree-level part with $\mathcal{K}(b)$ set to 0, one finds [cf. Hüt13, p. 81]

$$h_0 = -\frac{a_1}{b} J_1(\pm ib\sqrt{M_{\text{eff}}^2}) + \frac{a_2}{b} Y_1(\pm ib\sqrt{M_{\text{eff}}^2}), \quad a_1, a_2 \in \mathbb{C} \quad (\text{B.66})$$

for the general solution [cf. Hüt13, p. 81] with the same signs as before. Using again properties of the Bessel functions [see AS72, pp. 360, 375-378], the limiting behavior from Eqs. (B.32) and (B.38), and the argument of continuity, one finds [see Hüt13, p. 81]

$$h_0(b) = \frac{\sqrt{M_{\text{eff}}^2}}{\pi\beta b} K_1(b\sqrt{M_{\text{eff}}^2}) \text{ for } M_{\text{eff}}^2 \geq 0, \quad (\text{B.67})$$

$$h_0(b) = -\frac{\sqrt{|M_{\text{eff}}^2|}}{2\beta b} Y_1(b\sqrt{|M_{\text{eff}}^2|}) \text{ for } M_{\text{eff}}^2 \leq 0. \quad (\text{B.68})$$

Continuing with the separation $h_1(b) = c_{1,h}h_1^{(1)}(b) + c_{2,h}h_1^{(2)}(b) + h_1^{(p)}(b)$, where $h_1(b)$ is regular and $h_1(b) \rightarrow 0$ for $b \rightarrow 0$ as before, one finds with an appropriate choice of ICs

$$c_{1,h} = 0, \quad c_{2,h} = -\lim_{b \rightarrow \infty} \frac{h_1^{(p)}(b)}{h_1^{(2)}(b)}. \quad (\text{B.69})$$

With the same conventions for the real and imaginary parts, one now has to solve the real-valued coupled ODEs [cf. Hüt13, p. 81]

$$\left(\partial_b^2 + \frac{3}{b}\partial_b - M_{\text{eff}}^2\right) h_{1,r}^{(2)}(b) + \frac{\mathcal{K}(b)}{\beta} h_{1,i}^{(2)}(b) = 0, \quad (\text{B.70a})$$

$$\left(\partial_b^2 + \frac{3}{b}\partial_b - M_{\text{eff}}^2\right) h_{1,i}^{(2)}(b) - \frac{\mathcal{K}(b)}{\beta} h_{1,r}^{(2)}(b) = 0, \quad (\text{B.70b})$$

and

$$\left(\partial_b^2 + \frac{3}{b}\partial_b - M_{\text{eff}}^2\right) h_{1,r}^{(p)}(b) + \frac{\mathcal{K}(b)}{\beta} (\psi_{0,i}(b) + h_{1,i}^{(p)}(b)) = 0, \quad (\text{B.71a})$$

$$\left(\partial_b^2 + \frac{3}{b}\partial_b - M_{\text{eff}}^2\right) h_{1,i}^{(p)}(b) - \frac{\mathcal{K}(b)}{\beta} h_{1,r}^{(p)}(b) = 0, \quad (\text{B.71b})$$

numerically with the ICs

$$h_{1,r}^{(2)}(b_0) = 1, \quad h_{1,r}^{(2)'}(b_0) = 0, \quad (\text{B.72a})$$

$$h_{1,i}^{(2)}(b_0) = 0, \quad h_{1,i}^{(2)'}(b_0) = 0, \quad (\text{B.72b})$$

and

$$h_{1,r}^{(p)}(b_0) = 1[h], \quad h_{1,r}^{(p)'}(b_0) = 0, \quad (\text{B.73a})$$

$$h_{1,i}^{(p)}(b_0) = 0, \quad h_{1,i}^{(p)'}(b_0) = 0, \quad (\text{B.73b})$$

$$(\text{B.73c})$$

where $h_{0,i}(b) \equiv 0$ and $\mathcal{K}(b), \beta \in \mathbb{R}$ have been used. Note that for $h_1^{(2)}(b)$, no unit is necessary as it is contained in $c_{2,h}$. The ICs are chosen such that

$$\lim_{b \rightarrow 0} \text{Im } h(b) = \text{Im } c_{2,h} \quad (\text{B.74})$$

as $\text{Im } h_0(b \rightarrow 0) = 0$, $\text{Im } h_1^{(p)}(b \rightarrow 0) = 0$, and $h_1^{(2)}(b \rightarrow 0) \in \mathbb{R}$.

B.1.5. Numerical Details for Solving the ODEs

As mentioned in the last Sec. B.1.4, the coupled ODEs (B.62), (B.63), (B.70), and (B.71) with the ICs (B.64), (B.65), (B.72), and (B.73) have to be solved numerically. In order to do so, they get rewritten into ODEs of first order using

$$y_\psi^{(2)}(b) := \begin{pmatrix} y_{\psi,1}^{(2)}(b) \\ y_{\psi,2}^{(2)}(b) \\ y_{\psi,3}^{(2)}(b) \\ y_{\psi,4}^{(2)}(b) \end{pmatrix} := \begin{pmatrix} \psi_{1,r}^{(2)}(b) \\ \psi_{1,i}^{(2)}(b) \\ \psi_{1,r}^{(2)'}(b) \\ \psi_{1,i}^{(2)'}(b) \end{pmatrix}, \quad y_\psi^{(p)}(b) := \begin{pmatrix} y_{\psi,1}^{(p)}(b) \\ y_{\psi,2}^{(p)}(b) \\ y_{\psi,3}^{(p)}(b) \\ y_{\psi,4}^{(p)}(b) \end{pmatrix} := \begin{pmatrix} \psi_{1,r}^{(p)}(b) \\ \psi_{1,i}^{(p)}(b) \\ \psi_{1,r}^{(p)'}(b) \\ \psi_{1,i}^{(p)'}(b) \end{pmatrix} \quad (\text{B.75})$$

so that the ODEs

$$\partial_b y_\psi^{(2)}(b) = \begin{pmatrix} y_{\psi,3}^{(2)}(b) \\ y_{\psi,4}^{(2)}(b) \\ M_{\text{eff}}^2 y_{\psi,1}^{(2)}(b) - \frac{\mathcal{K}(b)}{b} y_{\psi,2}^{(2)}(b) - \frac{1}{b} y_{\psi,3}^{(2)}(b) \\ M_{\text{eff}}^2 y_{\psi,2}^{(2)}(b) + \frac{\mathcal{K}(b)}{b} y_{\psi,1}^{(2)}(b) - \frac{1}{b} y_{\psi,4}^{(2)}(b) \end{pmatrix} \quad (\text{B.76})$$

and

$$\partial_b y_\psi^{(p)}(b) = \begin{pmatrix} y_{\psi,3}^{(p)}(b) \\ y_{\psi,4}^{(p)}(b) \\ M_{\text{eff}}^2 y_{\psi,1}^{(p)}(b) - \frac{\mathcal{K}(b)}{b} (\psi_{0,i}(b) + y_{\psi,2}^{(p)}(b)) - \frac{1}{b} y_{\psi,3}^{(p)}(b) \\ M_{\text{eff}}^2 y_{\psi,2}^{(p)}(b) + \frac{\mathcal{K}(b)}{b} y_{\psi,1}^{(p)}(b) - \frac{1}{b} y_{\psi,4}^{(p)}(b) \end{pmatrix} \quad (\text{B.77})$$

with ICs

$$y_\psi^{(2)}(b_0) := \begin{pmatrix} 1 \\ 0 \\ 0 \\ 0 \end{pmatrix}, \quad y_\psi^{(p)}(b_0) := \begin{pmatrix} 0 \\ 1[\psi] \\ 0 \\ 0 \end{pmatrix}, \quad (\text{B.78})$$

and analogously for $h_1^{(2)}(b)$ and $h_1^{(p)}(b)$ have to be solved numerically. In total, one now has two systems of four coupled ODEs of first order for each, $\text{Re } c_{2,\psi}$ and $\text{Im } c_{2,h}$. A Bulirsch-Stoer algorithm is well suited for this problem as it provides high accuracy solutions with minimal computational effort by applying a modified midpoint method with the number

of substeps varied in a special sequence [SB13] [as cited in Hüt13, p. 82]. In the context of this thesis, the implementation of the Bulirsch-Stoer algorithm of the odeint library from Boost is chosen. The program itself is written in C++.

As described in Sec. B.1.3 the ODEs have to be solved starting from b_0 . A good choice for this is $b_0 = 10^{-5}/T$ [see ABB11, p. 22]. In contrast to this reference, however, it was observed that in order to have a stable program over a broad range of p^0 , p_{\parallel} , and k_{\parallel} , one has to choose the value for b_{∞} dynamically. This is done using the algorithm described in Sec. B.1.3. Explicitly, the values $b_{\infty} - b_0 = 0.2/T, 0.4/T, 0.6/T, 2.6/T, 4.6/T, \dots$ have proven to give very stable results in the context of this thesis. $b_{\infty, \max} = 10^4 T$ has shown to be sufficient for all sets of parameters giving a relevant contribution to the thermal width and the lepton number matrix. For each b_{∞} , the solutions of the homogeneous and inhomogeneous ODEs for $\psi(b)$ or $h(b)$, respectively, are computed with the solutions of the previous b_{∞} or the given values at b_0 as ICs. Using these, one computes

$$\operatorname{Re} c_{2,\psi} \simeq -\operatorname{Re} \left(\frac{\psi_1^{(p)}(b_{\infty})}{\psi_1^{(2)}(b_{\infty})} \right) = -\frac{\psi_{1,r}^{(p)}(b_{\infty})\psi_{1,r}^{(2)}(b_{\infty}) + \psi_{1,i}^{(p)}(b_{\infty})\psi_{1,i}^{(2)}(b_{\infty})}{(\psi_{1,r}^{(2)}(b_{\infty}))^2 + (\psi_{1,i}^{(2)}(b_{\infty}))^2} \quad (\text{B.79})$$

and

$$\operatorname{Im} c_{2,h} \simeq -\operatorname{Im} \left(\frac{h_1^{(p)}(b_{\infty})}{h_1^{(2)}(b_{\infty})} \right) = -\frac{-h_{1,r}^{(p)}(b_{\infty})h_{1,i}^{(2)}(b_{\infty}) + h_{1,i}^{(p)}(b_{\infty})h_{1,r}^{(2)}(b_{\infty})}{(h_{1,r}^{(2)}(b_{\infty}))^2 + (h_{1,i}^{(2)}(b_{\infty}))^2}, \quad (\text{B.80})$$

respectively, for each b_{∞} until the relative error between the previous value and the current one is less than ε_{\max} , i.e. $|(\operatorname{Re} c_{2,\psi, \text{old}} - \operatorname{Re} c_{2,\psi}) / \operatorname{Re} c_{2,\psi}| < \varepsilon_{\max}$ and $|(\operatorname{Im} c_{2,h, \text{old}} - \operatorname{Im} c_{2,h}) / \operatorname{Im} c_{2,h}| < \varepsilon_{\max}$, respectively, or the next b_{∞} would be greater than $b_{\infty, \max}$. In the context of this thesis, $\varepsilon_{\max} = 10^{-3}$ with absolute and relative accuracy of 10^{-9} and 10^{-6} , respectively, as settings for the Bulirsch-Stoer algorithm gave good results with acceptable numerical effort. The result of this procedure is

$$\int \frac{d^2 k_{\perp}}{(2\pi)^2} \operatorname{Re} \psi(\mathbf{k}_{\perp}) = \lim_{b \rightarrow 0} \operatorname{Re} \psi(\mathbf{b}) = \operatorname{Re} c_{2,\psi} \simeq -\frac{\psi_{1,r}^{(p)}(b_{\infty})\psi_{1,r}^{(2)}(b_{\infty}) + \psi_{1,i}^{(p)}(b_{\infty})\psi_{1,i}^{(2)}(b_{\infty})}{(\psi_{1,r}^{(2)}(b_{\infty}))^2 + (\psi_{1,i}^{(2)}(b_{\infty}))^2}, \quad (\text{B.81})$$

$$\int \frac{d^2 k_{\perp}}{(2\pi)^2} \operatorname{Re} \mathbf{k}_{\perp} \mathbf{f}(\mathbf{k}_{\perp}) = \lim_{b \rightarrow 0} \nabla \mathbf{f}(\mathbf{b}) = 2 \operatorname{Im} c_{2,h} \simeq -2 \frac{-h_{1,r}^{(p)}(b_{\infty})h_{1,i}^{(2)}(b_{\infty}) + h_{1,i}^{(p)}(b_{\infty})h_{1,r}^{(2)}(b_{\infty})}{(h_{1,r}^{(2)}(b_{\infty}))^2 + (h_{1,i}^{(2)}(b_{\infty}))^2} \quad (\text{B.82})$$

with b_{∞} as discussed above.

B.2. Proofs

B.2.1. Lepton Propagator

Here, the relation

$$\sigma \cdot \tilde{k} = 2k_{\parallel} \eta(\tilde{k}) \eta^{\dagger}(\tilde{k}), \quad (\text{B.83})$$

where

$$\eta(\tilde{k}) = \begin{pmatrix} 0 \\ 1 \end{pmatrix} - \frac{\sigma \tilde{\mathbf{k}}_{\perp}}{2\tilde{k}_{\parallel}} \begin{pmatrix} 0 \\ 1 \end{pmatrix} + \begin{pmatrix} \mathcal{O}(g^2) \\ 0 \end{pmatrix} = \begin{pmatrix} -\frac{\tilde{k}^1 - i\tilde{k}^2}{2\tilde{k}_{\parallel}} + \mathcal{O}(g^2) \\ 1 \end{pmatrix}, \quad (\text{B.84})$$

is shown. Recall that \tilde{k} is assumed to be light-like, i.e. $\tilde{k}^2 = 0$, and $\tilde{k}^3 = \tilde{k}_{\parallel}$. Then, one finds using $\tilde{k}^1, \tilde{k}^2 \sim gT$ and $\tilde{k}_0 = \tilde{k}_{\parallel} + \mathcal{O}(g^2T) \sim T$

$$2\tilde{k}_{\parallel}\eta(\tilde{k})\eta^{\dagger}(\tilde{k}) = \begin{pmatrix} (\tilde{k}^1)^2 + (\tilde{k}^2)^2 + \mathcal{O}(g^3T) & -\tilde{k}^1 + i\tilde{k}^2 + \mathcal{O}(g^2T) \\ -\tilde{k}^1 - i\tilde{k}^2 + \mathcal{O}(g^2T) & 2\tilde{k}_{\parallel} \end{pmatrix}. \quad (\text{B.85})$$

The relation

$$\tilde{k}^2 = (\tilde{k}^0)^2 - (\tilde{k}^1)^2 - (\tilde{k}^2)^2 - \tilde{k}_{\parallel}^2 = 0 \quad (\text{B.86})$$

gives

$$(\tilde{k}^1)^2 + (\tilde{k}^2)^2 = (\tilde{k}^0)^2 - \tilde{k}_{\parallel}^2 = \tilde{k}_+ \tilde{k}_- = 2\tilde{k}_{\parallel}(\tilde{k}_0 - \tilde{k}_{\parallel}) + \mathcal{O}(g^4T^2) \quad (\text{B.87})$$

so that together with $2\tilde{k}_{\parallel} = \tilde{k}_0 + \tilde{k}_{\parallel} + \mathcal{O}(g^2T)$, one arrives at

$$2\tilde{k}_{\parallel}\eta(\tilde{k})\eta^{\dagger}(\tilde{k}) = \begin{pmatrix} \tilde{k}_0 - \tilde{k}_{\parallel} + \mathcal{O}(g^3T) & -\tilde{k}^1 + i\tilde{k}^2 + \mathcal{O}(g^2T) \\ -\tilde{k}^1 - i\tilde{k}^2 + \mathcal{O}(g^2T) & \tilde{k}_0 + \tilde{k}_{\parallel} + \mathcal{O}(g^2T) \end{pmatrix}, \quad (\text{B.88})$$

which proves Eq. (B.83) to leading order in each component.

B.2.2. Perpendicular Momentum Integrations

In this section, the relations from Eqs. (B.9) and (B.10) with the continuations from Sec. B.1.3

$$\int \frac{d^2k_{\perp}}{(2\pi)^2} \text{Re } \mathbf{k}_{\perp} \mathbf{f}(\mathbf{k}_{\perp}) = \lim_{b \rightarrow 0} \nabla \mathbf{f}(\mathbf{b}) = \lim_{b \rightarrow 0} 2 \text{Im } h(b) = 2 \text{Im } c_{2,h}, \quad (\text{B.89})$$

$$\int \frac{d^2k_{\perp}}{(2\pi)^2} \text{Re } \psi(\mathbf{k}_{\perp}) = \lim_{b \rightarrow 0} \text{Re } \psi(\mathbf{b}) = \text{Re } c_{2,\psi} \quad (\text{B.90})$$

are proven following [Bes10, pp. 95-96] and using the representation of the δ -distribution from Eq. (B.11) with the fact that $\delta^2(-\mathbf{b}) = \delta^2(\mathbf{b})$.

Starting with the second equation, one finds

$$\begin{aligned} \int \frac{d^2k_{\perp}}{(2\pi)^2} \text{Re } \psi(\mathbf{k}_{\perp}) &= \text{Re} \left(\int \frac{d^2k_{\perp}}{(2\pi)^2} \int d^2b e^{-i\mathbf{k}\mathbf{b}} \psi(b) \right) \\ &= \text{Re} \left(\int d^2b \delta^2(\mathbf{b}) \psi(b) \right) \\ &= \lim_{b \rightarrow 0} \text{Re } \psi(b) \\ &= \lim_{b \rightarrow 0} \text{Re} \left(\psi_0(b) + c_{2,\psi} \psi_1^{(2)}(b) + \psi_1^{(p)}(b) \right) \end{aligned} \quad (\text{B.91})$$

$$= \text{Re } c_{2,\psi}, \quad (\text{B.92})$$

where the fact that $\text{Re } \psi(b)$ stays regular and continuous for $b \rightarrow 0$, cf. Eq. (B.39), as well as the choice of ICs from Sec. B.1.4 have been used.

For the first equation, a similar calculation gives

$$\begin{aligned}
\int \frac{d^2 k_\perp}{(2\pi)^2} \operatorname{Re} \mathbf{k}_\perp \mathbf{f}(\mathbf{k}_\perp) &= \operatorname{Re} \left(\int \frac{d^2 k_\perp}{(2\pi)^2} \int d^2 b [f_1(\mathbf{b})k^1 + f_2(\mathbf{b})k^2] e^{-i\mathbf{k}\mathbf{b}} \right) \\
&= \operatorname{Re} \left(\int \frac{d^2 k_\perp}{(2\pi)^2} \int d^2 b i \left[f_1(\mathbf{b}) \frac{\partial}{\partial b_1} + f_2(\mathbf{b}) \frac{\partial}{\partial b_2} \right] e^{-i\mathbf{k}\mathbf{b}} \right) \\
&= -\operatorname{Re} \left(\int d^2 b i \delta^2(\mathbf{b}) \left[\frac{\partial f_1(\mathbf{b})}{\partial b_1} + \frac{\partial f_2(\mathbf{b})}{\partial b_2} \right] \right) \\
&= \lim_{b \rightarrow 0} \operatorname{Im} \nabla \mathbf{f}(\mathbf{b}) , \tag{B.93}
\end{aligned}$$

where partial integration, $\partial_{b_i} \mathbf{f}(\mathbf{b}) \rightarrow 0$, $i = 1, 2$, for $b \rightarrow \infty$ due to the existence of the Fourier transform, cf. Eq. (B.32), and the fact that $\operatorname{Im} \nabla \mathbf{f}(b)$ stays regular for $b \rightarrow 0$, cf. Eq. (B.38), have been used. With $\mathbf{f}(\mathbf{b}) = h(b)\mathbf{b}$ one has

$$\frac{\partial f_i(\mathbf{b})}{\partial b_j} = \delta_{ij} h(b) + \frac{b_i b_j}{b} h'(b) , \quad i, j = 1, 2 . \tag{B.94}$$

Therefore, one finds

$$\begin{aligned}
\int \frac{d^2 k_\perp}{(2\pi)^2} \operatorname{Re} \mathbf{k}_\perp \mathbf{f}(\mathbf{k}_\perp) &= \lim_{b \rightarrow 0} \operatorname{Im}(2h(b) + bh'(b)) \\
&= \lim_{b \rightarrow 0} 2 \operatorname{Im} h(b) \\
&= \lim_{b \rightarrow 0} 2 \operatorname{Im}(h_0(b) + c_{2,\psi} h_1^{(2)}(b) + h_1^{(p)}(b)) \\
&= 2 \operatorname{Im} c_{2,h} \tag{B.95}
\end{aligned}$$

with $\operatorname{Im} h'(b) \rightarrow 0$ for $b \rightarrow 0$, cf. Eq. (B.38), and the choice of ICs from Sec. B.1.4.

B.2.3. Imaginary Part of the Retarded Self-Energy

In this section, Eq. (5.53)

$$\operatorname{Im} \Sigma_{p_\parallel}^{\operatorname{R}, \operatorname{ret}}(p^0) = -|\lambda|^2 \frac{d(r)}{2} \int \frac{d^3 k}{(2\pi)^3} \frac{\mathcal{F}(p_\parallel, k_\parallel)}{k_\parallel - p_\parallel} \begin{pmatrix} \frac{\operatorname{Re} \mathbf{k}_\perp \mathbf{f}}{8k_\parallel} & 0 \\ 0 & \operatorname{Re} \psi \end{pmatrix} \tag{B.96}$$

is proven. Starting with Eq. (5.52)

$$\Sigma_{p_\parallel}^{\operatorname{R}, \operatorname{ret}}(p^0) = -|\lambda|^2 \frac{id(r)}{2} \int \frac{d^3 k}{(2\pi)^3} \frac{\mathcal{F}(p_\parallel, k_\parallel)}{k_\parallel - p_\parallel} \begin{pmatrix} \frac{(k^1 - ik^2)(f_1 + if_2)}{8k_\parallel^2} & -\frac{k^1 - ik^2}{2k_\parallel} \psi \\ -\frac{f_1 + if_2}{4k_\parallel} & \psi \end{pmatrix} \tag{B.97}$$

one has with the definition of the imaginary part of a matrix Eq. (3.69)

$$\operatorname{Im} \Sigma_{p_\parallel}^{\operatorname{R}, \operatorname{ret}}(p^0) = -|\lambda|^2 \frac{d(r)}{2} \int \frac{d^3 k}{(2\pi)^3} \frac{\mathcal{F}(p_\parallel, k_\parallel)}{k_\parallel - p_\parallel} \begin{pmatrix} \frac{\operatorname{Re} \mathbf{k}_\perp \mathbf{f} - k^1 \operatorname{Im} f_2 + k^2 \operatorname{Im} f_1}{8k_\parallel^2} & -\frac{k^1 - ik^2}{2k_\parallel} \psi - \frac{f_1^* - if_2^*}{4k_\parallel} \\ -\frac{f_1 + if_2}{4k_\parallel} - \frac{k^1 + ik^2}{2k_\parallel} \psi^* & \operatorname{Re} \psi \end{pmatrix} . \tag{B.98}$$

Using the rotational invariance of $h(b)$ and

$$\begin{aligned}
\mathbf{f}(\mathbf{k}_\perp) &= \int d^2b h(b) \mathbf{b} e^{-i\mathbf{k}_\perp \mathbf{b}} \\
&= \int d^2b i h(b) \left(\mathbf{e}_1 \frac{\partial}{\partial k^1} + \mathbf{e}_2 \frac{\partial}{\partial k^2} \right) e^{-i\mathbf{k}_\perp \mathbf{b}} \\
&= i \left(\mathbf{e}_1 \frac{\partial}{\partial k^1} + \mathbf{e}_2 \frac{\partial}{\partial k^2} \right) h(|\mathbf{k}_\perp|) \\
&= i \left(\mathbf{e}_1 \frac{k^1}{|\mathbf{k}_\perp|} + \mathbf{e}_2 \frac{k^2}{|\mathbf{k}_\perp|} \right) h'(|\mathbf{k}_\perp|), \tag{B.99}
\end{aligned}$$

where \mathbf{e}_i is the unit vector in i -direction, one can rewrite $\mathbf{f}(\mathbf{k}_\perp) = \bar{h}(|\mathbf{k}_\perp|) \mathbf{k}_\perp$. Hence, $-k^1 \text{Im } f_2 + k^2 \text{Im } f_1 \equiv 0$.

Analogously to the calculations in Sec. B.2.2, one finds ($i = 1, 2$)

$$\int \frac{d^2k_\perp}{(2\pi)^2} \text{Im } f_i = \lim_{b \rightarrow 0} b_i \text{Im } h(b) = 0, \tag{B.100}$$

$$\int \frac{d^2k_\perp}{(2\pi)^2} k_i \text{Im } \psi = \lim_{b \rightarrow 0} \frac{b_i}{b} \text{Re } \psi'(b) = 0, \tag{B.101}$$

where the limiting behavior, cf. Eqs. (B.38) and (B.39), has been used as well as $\text{Re } \psi'(b) \rightarrow 0$, which is clear from the discussion of the error estimates and the fact that $\text{Re } c_\psi = 0$.

The remaining off-diagonal terms contain $\int \frac{d^2k_\perp}{(2\pi)^2} \text{Re } f_i$ and $\int \frac{d^2k_\perp}{(2\pi)^2} k_i \text{Re } \psi$, $i = 1, 2$. When trying to apply the same procedure as in Sec. B.2.2 to these expressions, one notices that the occurring $h(b) \sim 1/(\pi\beta b^2)$ and $\psi(b) \sim i \ln(b)/(2\pi\beta)$ diverge for $b \rightarrow 0$. Therefore, these integrals diverge. However, as mentioned in [Hüt13, pp. 56-57], the divergences occur in the temperature independent part of the self-energy, since the only part directly dependent on the temperature is $\mathcal{F}(p_\parallel, k_\parallel)$, which does not depend on \mathbf{k}_\perp . Furthermore, the limiting behavior giving the divergence is not dependent on the temperature at all. Therefore, the divergences get removed by the renormalization at $T = 0$ and one can omit the divergent part, since only the temperature dependent parts are of interest for leptogenesis [cf. Hüt13, pp. 56-57]. It is also clear that the off-diagonal terms should at least be suppressed by a factor of g compared to the diagonal ones due to the Dirac structure of the Majorana self-energy, which is, cf. Eq. (5.21),

$$\text{Im } \Sigma_{\mathbf{p}}^{\text{R, ret}}(p^0) = \frac{1}{2} (a_{\mathbf{p}}(p^0) \mathbb{1}_2 + b_{\mathbf{p}}(p^0) \mathbf{p} \boldsymbol{\sigma}), \tag{B.102}$$

giving the suppression due to the fact that they involve p^1 and p^2 . The choice $\mathbf{p}_\perp = \mathbf{0}$ and $p^3 = p_\parallel$ then even causes them to vanish.

In total, this gives

$$\text{Im } \Sigma_{p_\parallel}^{\text{R, ret}}(p^0) = -|\lambda|^2 \frac{d(r)}{2} \int \frac{d^3k}{(2\pi)^3} \frac{\mathcal{F}(p_\parallel, k_\parallel)}{k_\parallel - p_\parallel} \begin{pmatrix} \frac{\text{Re } \mathbf{k}_\perp \mathbf{f}}{8k_\parallel} & 0 \\ 0 & \text{Re } \psi \end{pmatrix}, \tag{B.103}$$

what needed to be shown.

B.3. Details for the Lepton Number Matrix

B.3.1. Evaluation of the t_1 , t_2 and t_3 Integrations

The integrals over t_1 , t_2 , and t_3 in Eq. (6.29) can be carried out analytically. One finds for the parts depending on the time variables, cf. Eq. (6.33):

$$\begin{aligned}
& \int_0^t dt_1 \int_0^{t_1} dt_2 \int_0^{t_2} dt_3 e^{-\Gamma_p \frac{t_1+t_3}{2}} \cos(\omega_p y_{13}) \operatorname{Re} \left(e^{-i(\omega_{21} y_{21} + \omega_{23} y_{23})} \right) = \\
& \frac{1}{(\omega_{21} - \omega_{23})(\Gamma_p^2 + 4(\omega_{21} - \omega_p)^2)(\Gamma_p^2 + 4(\omega_{21} + \omega_p)^2)(\Gamma_p^2 + 4(\omega_{23} - \omega_p)^2)(\Gamma_p^2 + 4(\omega_{23} + \omega_p)^2)} \\
& \times \left(4e^{-\Gamma_p t} \left(2\Gamma_p(\omega_{21} - \omega_{23}) \left(-8\omega_p^2 \left(\Gamma_p^2 + 2 \left(\omega_{21}^2 + 4\omega_{21}\omega_{23} + \omega_{23}^2 \right) \right) \right) \right. \right. \\
& + \left. \left. \left(-\Gamma_p^2 - 4\omega_{21}^2 \right) \left(\Gamma_p^2 + 4\omega_{23}^2 \right) - 16\omega_p^4 \right) - 2\Gamma_p e^{\Gamma_p t} (\omega_{21} - \omega_{23}) \right. \\
& \times \left. \left(8\omega_p^2 \left(\Gamma_p^2 + 2 \left(\omega_{21}^2 + 4\omega_{21}\omega_{23} + \omega_{23}^2 \right) \right) + \left(\Gamma_p^2 + 4\omega_{21}^2 \right) \left(\Gamma_p^2 + 4\omega_{23}^2 \right) + 16\omega_p^4 \right) \right. \\
& \times \left. \cos(t(\omega_{21} - \omega_{23})) + 2\Gamma_p e^{\frac{\Gamma_p t}{2}} (\omega_{21} - \omega_{23}) \cos(t\omega_{21}) \cos(t\omega_p) \right. \\
& \times \left. \left(8\omega_p^2 \left(\Gamma_p^2 + 2 \left(\omega_{21}^2 + 4\omega_{21}\omega_{23} + \omega_{23}^2 \right) \right) + \left(\Gamma_p^2 + 4\omega_{21}^2 \right) \left(\Gamma_p^2 + 4\omega_{23}^2 \right) + 16\omega_p^4 \right) \right. \\
& + \left. e^{\frac{\Gamma_p t}{2}} \left(2\Gamma_p(\omega_{21} - \omega_{23}) \cos(t\omega_{23}) \cos(t\omega_p) \left(8\omega_p^2 \left(\Gamma_p^2 + 2 \left(\omega_{21}^2 + 4\omega_{21}\omega_{23} + \omega_{23}^2 \right) \right) \right) \right. \right. \\
& + \left. \left. \left(\Gamma_p^2 + 4\omega_{21}^2 \right) \left(\Gamma_p^2 + 4\omega_{23}^2 \right) + 16\omega_p^4 \right) + \frac{1}{2} \left(\Gamma_p^2 + 4 \left(\omega_{21}\omega_{23} + \omega_p^2 \right) \right) \right. \\
& \times \left. \left(\Gamma_p^4 + 4\Gamma_p^2 \left(\omega_{21}^2 + \omega_{23}^2 + 2\omega_p^2 \right) + 16(\omega_{21} - \omega_p)(\omega_{21} + \omega_p)(\omega_{23} - \omega_p)(\omega_{23} + \omega_p) \right) \right. \\
& \times \left. \left(2e^{\frac{\Gamma_p t}{2}} \sin(t(\omega_{21} - \omega_{23})) + 2 \cos(t\omega_p) (\sin(t\omega_{23}) - \sin(t\omega_{21})) \right) - 8\omega_p(\omega_{21} + \omega_{23}) \sin(t\omega_p) \right. \\
& \times \left. \sin \left(\frac{1}{2} t(\omega_{21} + \omega_{23}) \right) \left(\left(\Gamma_p^4 - 4\Gamma_p^2 \left(\omega_{21}^2 - 4\omega_{21}\omega_{23} + \omega_{23}^2 - 2\omega_p^2 \right) + 16(\omega_{21} - \omega_p)(\omega_{21} + \omega_p) \right. \right. \right. \\
& \times \left. \left. (\omega_{23} - \omega_p)(\omega_{23} + \omega_p) \right) \sin \left(\frac{1}{2} t(\omega_{21} - \omega_{23}) \right) - 4\Gamma_p(\omega_{21} - \omega_{23}) \left(\Gamma_p^2 + 4 \left(\omega_{21}\omega_{23} + \omega_p^2 \right) \right) \right. \\
& \times \left. \left. \left. \left. \cos \left(\frac{1}{2} t(\omega_{21} - \omega_{23}) \right) \right) \right) \right) \right) \right) \tag{B.104}
\end{aligned}$$

B.3.2. Details for the Numerical Evaluation

All programs have been written in C++. Depending on the problem, the libraries GSL (for numerical integration, algorithms qag (41-point Gauss-Kronrod rule as setting), qagi (15-point quadrature rule for infinite integration intervals), qagiu (21-point Gauss-Kronrod rule for semi-infinite integration intervals), and qagp (21-point Gauss-Kronrod rule for integrals over regions containing singularities)), Boost (odeint for solving ODEs, Bulirsch-Stoer algorithm), and CUBA (for multidimensional numerical integration, algorithms Vegas (importance sampling) and Cuhre (degree-11 rule for three-dimensional quadrature as setting)) have been used. For error settings refer to table B.1. Note that the maximal relative error of 10^{-1} for L_{ii} with the qagiu algorithm is only used for the light-like calculations with $T < M$. In all other cases, 10^{-2} is used as maximal relative error. All calculations have been performed on personal computers of the Institute for Theoretical Physics of the Goethe-University Frankfurt and on LOEWE-CSC.

Quantity	Algorithm	Settings
Re $c_{2,\psi}$ and Im $c_{2,h}$	Bulirsch-Stoer	see Sec. B.1.5
σ_ψ and σ_h	qagi and qag	max. rel. error 10^{-3}
$\sigma_\psi^{\text{tree}}$ and σ_h^{tree}	qag and qagp	max. rel. error 10^{-3}
L_{ii}	qagiu	max. rel. error 10^{-2} and 10^{-1}
L_{ii}	Vegas	max. rel. error $5 \cdot 10^{-2}$
L_{ii}	Cuhre	max. rel. error $5 \cdot 10^{-2}$

Table B.1.: Numerical details.

Bibliography

- [AS72] Abramowitz, M. and Stegun, I. A. (1972). *Handbook of Mathematical Functions With Formulas, Graphs, and Mathematical Tables*. 10th Printing. Washington D.C.: National Bureau of Standards.
- [Ade+16] Ade, P. A. R. et al. (2016). “Planck 2015 results. XIII. Cosmological parameters”. In: *Astron. Astrophys.* 594, A13. DOI: 10.1051/0004-6361/201525830. arXiv: 1502.01589.
- [Adl69] Adler, S. L. (1969). “Axial vector vertex in spinor electrodynamics”. In: *Phys. Rev.* 177, pp. 2426–2438. DOI: 10.1103/PhysRev.177.2426.
- [ABB11] Anisimov, A., Besak, D., and Bödeker, D. (2011). “Thermal production of relativistic Majorana neutrinos: Strong enhancement by multiple soft scattering”. In: *JCAP* 1103, p. 042. DOI: 10.1088/1475-7516/2011/03/042. arXiv: 1012.3784.
- [Ani+09] Anisimov, A., Buchmüller, W., Drewes, M., and Mendizabal, S. (2009). “Nonequilibrium Dynamics of Scalar Fields in a Thermal Bath”. In: *Annals Phys.* 324, pp. 1234–1260. DOI: 10.1016/j.aop.2009.01.001. arXiv: 0812.1934.
- [Ani+11] Anisimov, A., Buchmüller, W., Drewes, M., and Mendizabal, S. (2011). “Quantum Leptogenesis I”. In: *Annals Phys.* 326. [Erratum: *Annals Phys.* 338, p. 376 (2011)], pp. 1998–2038. DOI: 10.1016/j.aop.2011.02.002, 10.1016/j.aop.2013.05.00. arXiv: 1012.5821.
- [Aur+02] Aurenche, P., Gelis, F., Moore, G. D., and Zaraket, H. (2002). “Landau-Pomeranchuk-Migdal resummation for dilepton production”. In: *JHEP* 12, p. 006. DOI: 10.1088/1126-6708/2002/12/006. arXiv: hep-ph/0211036.
- [AGZ02] Aurenche, P., Gelis, F., and Zaraket, H. (2002). “A Simple sum rule for the thermal gluon spectral function and applications”. In: *JHEP* 05, p. 043. DOI: 10.1088/1126-6708/2002/05/043. arXiv: hep-ph/0204146.
- [BJ69] Bell, J. S. and Jackiw, R. (1969). “A PCAC puzzle: $\pi^0 \rightarrow \gamma\gamma$ in the sigma model”. In: *Nuovo Cim.* A60, pp. 47–61. DOI: 10.1007/BF02823296.
- [Bes10] Besak, D. (2010). “Thermal particle production in the early universe”. PhD thesis. Bielefeld U.
- [BB10] Besak, D. and Bödeker, D. (2010). “Hard Thermal Loops for Soft or Collinear External Momenta”. In: *JHEP* 05, p. 007. DOI: 10.1007/JHEP05(2010)007. arXiv: 1002.0022.
- [BD12] Blanchet, S. and Di Bari, P. (2012). “The minimal scenario of leptogenesis”. In: *New J. Phys.* 14, p. 125012. DOI: 10.1088/1367-2630/14/12/125012. arXiv: 1211.0512.
- [BP90] Braaten, E. and Pisarski, R. D. (1990). “Soft Amplitudes in Hot Gauge Theories: A General Analysis”. In: *Nucl. Phys.* B337, pp. 569–634. DOI: 10.1016/0550-3213(90)90508-B.

- [Buc01] Buchmüller, W. (2001). “Recent progress in leptogenesis”. In: *8th International Symposium on Particles Strings and Cosmology (PASCOS 2001) Chapel Hill, North Carolina, April 10-15, 2001*. arXiv: hep-ph/0107153.
- [BDP02] Buchmüller, W., Di Bari, P., and Plümacher, M. (2002). “Cosmic microwave background, matter - antimatter asymmetry and neutrino masses”. In: *Nucl. Phys.* B643. [Erratum: *Nucl. Phys.* B793, p. 362 (2008)], pp. 367–390. DOI: 10.1016/S0550-3213(02)00737-X, 10.1016/j.nuclphysb.2007.11.030. arXiv: hep-ph/0205349.
- [BDP05] Buchmüller, W., Di Bari, P., and Plümacher, M. (2005). “Leptogenesis for pedestrians”. In: *Annals Phys.* 315, pp. 305–351. DOI: 10.1016/j.aop.2004.02.003. arXiv: hep-ph/0401240.
- [BF00] Buchmüller, W. and Fredenhagen, S. (2000). “Quantum mechanics of baryogenesis”. In: *Phys. Lett.* B483, pp. 217–224. DOI: 10.1016/S0370-2693(00)00573-6. arXiv: hep-ph/0004145.
- [BP95] Buchmüller, W. and Philipsen, O. (1995). “Phase structure and phase transition of the SU(2) Higgs model in three-dimensions”. In: *Nucl. Phys.* B443, pp. 47–69. DOI: 10.1016/0550-3213(95)00124-B. arXiv: hep-ph/9411334.
- [CDS12] Canetti, L., Drewes, M., and Shaposhnikov, M. (2012). “Matter and Antimatter in the Universe”. In: *New J. Phys.* 14, p. 095012. DOI: 10.1088/1367-2630/14/9/095012. arXiv: 1204.4186.
- [Car92] Carrington, M. E. (1992). “The Effective potential at finite temperature in the Standard Model”. In: *Phys. Rev.* D45, pp. 2933–2944. DOI: 10.1103/PhysRevD.45.2933.
- [Col84] Collins, John C. (1984). *Renormalization: An Introduction to Renormalization, the Renormalization Group and the Operator-Product Expansion*. Cambridge Monographs on Mathematical Physics. Cambridge: Cambridge University Press. DOI: 10.1017/CB09780511622656.
- [CFH99] Csikor, F., Fodor, Z., and Heitger, J. (1999). “Endpoint of the hot electroweak phase transition”. In: *Phys. Rev. Lett.* 82, pp. 21–24. DOI: 10.1103/PhysRevLett.82.21. arXiv: hep-ph/9809291.
- [Di 12] Di Bari, P. (2012). “An introduction to leptogenesis and neutrino properties”. In: *Contemp. Phys.* 53.4, pp. 315–338. DOI: 10.1080/00107514.2012.701096. arXiv: 1206.3168.
- [FNR12] Fong, C. S., Nardi, E., and Riotto, A. (2012). “Leptogenesis in the Universe”. In: *Adv. High Energy Phys.* 2012, p. 158303. DOI: 10.1155/2012/158303. arXiv: 1301.3062.
- [FY86] Fukugita, M. and Yanagida, T. (1986). “Baryogenesis Without Grand Unification”. In: *Phys. Lett.* B174, pp. 45–47. DOI: 10.1016/0370-2693(86)91126-3.
- [Giu+04] Giudice, G. F. et al. (2004). “Towards a complete theory of thermal leptogenesis in the SM and MSSM”. In: *Nucl. Phys.* B685, pp. 89–149. DOI: 10.1016/j.nuclphysb.2004.02.019. arXiv: hep-ph/0310123.
- [Hah05] Hahn, T. (2005). “CUBA: A Library for multidimensional numerical integration”. In: *Comput. Phys. Commun.* 168, pp. 78–95. DOI: 10.1016/j.cpc.2005.01.010. arXiv: hep-ph/0404043.

- [HPW09] Hahn-Woernle, F., Plümacher, M., and Wong, Y. Y. Y. (2009). “Full Boltzmann equations for leptogenesis including scattering”. In: *JCAP* 0908, p. 028. DOI: 10.1088/1475-7516/2009/08/028. arXiv: 0907.0205.
- [Hal17] Halsch, A. (2017). “Evaluating Gauge Corrections to Thermal Leptogenesis”. MA thesis. Frankfurt U.
- [HT90] Harvey, J. A. and Turner, M. S. (1990). “Cosmological baryon and lepton number in the presence of electroweak fermion-number violation”. In: *Phys. Rev. D* 42 (10), pp. 3344–3349. DOI: 10.1103/PhysRevD.42.3344.
- [HKL08] Hohenegger, A., Kartavtsev, A., and Lindner, M. (2008). “Deriving Boltzmann Equations from Kadanoff-Baym Equations in Curved Space-Time”. In: *Phys. Rev. D* 78, p. 085027. DOI: 10.1103/PhysRevD.78.085027. arXiv: 0807.4551.
- [HS95] Huet, P. and Sather, E. (1995). “Electroweak baryogenesis and standard model CP violation”. In: *Phys. Rev. D* 51, pp. 379–394. DOI: 10.1103/PhysRevD.51.379. arXiv: hep-ph/9404302.
- [Hüt13] Hütig, J. (2013). “Including gauge corrections to thermal leptogenesis”. PhD thesis. Frankfurt U.
- [KB62] Kadanoff, L. P. and Baym, G. (1962). *Quantum Statistical Mechanics*. New York: W.A. Benjamin Inc.
- [Kaj+97] Kajantie, K., Laine, M., Rummukainen, K., and Shaposhnikov, M. E. (1997). “A Nonperturbative analysis of the finite T phase transition in $SU(2) \times U(1)$ electroweak theory”. In: *Nucl. Phys. B* 493, pp. 413–438. DOI: 10.1016/S0550-3213(97)00164-8. arXiv: hep-lat/9612006.
- [Kel64] Keldysh, L. V. (1964). “Diagram technique for nonequilibrium processes”. In: *Zh. Eksp. Teor. Fiz.* 47. [Sov. Phys. JETP20,1018(1965)], pp. 1515–1527.
- [KS88] Khlebnikov, S. Y. and Shaposhnikov, M. E. (1988). “The Statistical Theory of Anomalous Fermion Number Nonconservation”. In: *Nucl. Phys. B* 308, pp. 885–912. DOI: 10.1016/0550-3213(88)90133-2.
- [KPT10] Kiessig, C. P., Plümacher, M., and Thoma, M. H. (2010). “Decay of a Yukawa fermion at finite temperature and applications to leptogenesis”. In: *Phys. Rev. D* 82, p. 036007. DOI: 10.1103/PhysRevD.82.036007. arXiv: 1003.3016.
- [Kle99] Klein, S. (1999). “Suppression of Bremsstrahlung and pair production due to environmental factors”. In: *Rev. Mod. Phys.* 71, pp. 1501–1538. DOI: 10.1103/RevModPhys.71.1501. arXiv: hep-ph/9802442.
- [KM84] Klinkhamer, F. R. and Manton, N. S. (1984). “A Saddle Point Solution in the Weinberg-Salam Theory”. In: *Phys. Rev. D* 30, p. 2212. DOI: 10.1103/PhysRevD.30.2212.
- [Kom+11] Komatsu, E. et al. (2011). “Seven-Year Wilkinson Microwave Anisotropy Probe (WMAP) Observations: Cosmological Interpretation”. In: *Astrophys. J. Suppl.* 192, p. 18. DOI: 10.1088/0067-0049/192/2/18. arXiv: 1001.4538.
- [KRS85] Kuzmin, V. A., Rubakov, V. A., and Shaposhnikov, M. E. (1985). “On the Anomalous Electroweak Baryon Number Nonconservation in the Early Universe”. In: *Phys. Lett.* 155B, p. 36. DOI: 10.1016/0370-2693(85)91028-7.
- [LP53] Landau, L. D. and Pomeranchuk, I. (1953). “Limits of applicability of the theory of bremsstrahlung electrons and pair production at high-energies”. In: *Dokl. Akad. Nauk Ser. Fiz.* 92, pp. 535–536.

- [Le 96] Le Bellac, M. (1996). *Thermal Field Theory*. Cambridge Monographs on Mathematical Physics. Cambridge: Cambridge University Press. DOI: 10.1017/CB09780511721700.
- [Men10] Mendizabal Cofre, S. (2010). “Quantum mechanics of leptogenesis”. PhD thesis. Hamburg U.
- [Mig56] Migdal, A. B. (1956). “Bremsstrahlung and Pair Production in Condensed Media at High Energies”. In: *Phys. Rev.* 103 (6), pp. 1811–1820. DOI: 10.1103/PhysRev.103.1811.
- [MQF99] Morales, J., Quimbay, C., and Fonseca, F. (1999). “Fermionic dispersion relations at finite temperature and nonvanishing chemical potentials in the minimal standard model”. In: *Nucl. Phys.* B560, pp. 601–616. DOI: 10.1016/S0550-3213(99)00459-9. arXiv: hep-ph/9906207.
- [NAS12] NASA / WMAP Science Team (2012). *Timeline of the Universe*. URL: <https://map.gsfc.nasa.gov/media/060915/index.html> (visited on 13/09/2017).
- [Pat+16] Patrignani, C. et al. (2016). “Review of Particle Physics”. In: *Chin. Phys.* C40.10, p. 100001. DOI: 10.1088/1674-1137/40/10/100001.
- [PU04] Pilaftsis, A. and Underwood, T. E. J. (2004). “Resonant leptogenesis”. In: *Nucl. Phys.* B692, pp. 303–345. DOI: 10.1016/j.nuclphysb.2004.05.029. arXiv: hep-ph/0309342.
- [Pis89] Pisarski, R. D. (1989). “Scattering amplitudes in hot gauge theories”. In: *Phys. Rev. Lett.* 63 (11), pp. 1129–1132. DOI: 10.1103/PhysRevLett.63.1129.
- [Rin88] Ringwald, A. (1988). “Sphaleron and Level Crossing”. In: *Phys. Lett.* B213, pp. 61–63. DOI: 10.1016/0370-2693(88)91047-7.
- [Sak67] Sakharov, A. D. (1967). “Violation of CP Invariance, C Asymmetry, and Baryon Asymmetry of the Universe”. In: *Pisma Zh. Eksp. Teor. Fiz.* 5. [Usp. Fiz. Nauk161,61(1991)], pp. 32–35. DOI: 10.1070/PU1991v034n05ABEH002497.
- [SW96] Schrempf, B. and Wimmer, M. (1996). “Top quark and Higgs boson masses: Interplay between infrared and ultraviolet physics”. In: *Prog. Part. Nucl. Phys.* 37, pp. 1–90. DOI: 10.1016/0146-6410(96)00059-2. arXiv: hep-ph/9606386.
- [Sch61] Schwinger, J. S. (1961). “Brownian motion of a quantum oscillator”. In: *J. Math. Phys.* 2, pp. 407–432. DOI: 10.1063/1.1703727.
- [Ste10] Steigman, G. (2010). “Primordial Nucleosynthesis: The Predicted and Observed Abundances and Their Consequences”. In: *PoS NICXI*, p. 1. arXiv: 1008.4765.
- [SB13] Stoer, J. and Bulirsch, R. (2013). *Introduction to numerical analysis*. Vol. 12. Berlin, Heidelberg: Springer Science & Business Media.
- [t H76a] ’t Hooft, G. (1976a). “Computation of the Quantum Effects Due to a Four-Dimensional Pseudoparticle”. In: *Phys. Rev.* D14. [Erratum: *Phys. Rev.* D18, p. 2199 (1978)], pp. 3432–3450. DOI: 10.1103/PhysRevD.14.3432.
- [t H76b] ’t Hooft, G. (1976b). “Symmetry Breaking Through Bell-Jackiw Anomalies”. In: *Phys. Rev. Lett.* 37, pp. 8–11. DOI: 10.1103/PhysRevLett.37.8.
- [Wel82] Weldon, H. A. (1982). “Effective fermion masses of order gT in high-temperature gauge theories with exact chiral invariance”. In: *Phys. Rev. D* 26 (10), pp. 2789–2796. DOI: 10.1103/PhysRevD.26.2789.
- [Wel83] Weldon, H. A. (1983). “Simple Rules for Discontinuities in Finite Temperature Field Theory”. In: *Phys. Rev.* D28, p. 2007. DOI: 10.1103/PhysRevD.28.2007.

Danksagung

An dieser Stelle danke ich Prof. Owe Philipsen für die Ermöglichung und Betreuung dieser Masterarbeit. Besonders dankbar bin ich für die vielen beratenden Gespräche, Hilfestellungen und das entgegengebrachte Vertrauen. Ohne diese Unterstützung wäre diese Arbeit nicht möglich gewesen.

Selbstständigkeitserklärung

Erklärung nach § 30 (12) Ordnung für den Bachelor- und den Masterstudiengang

Hiermit erkläre ich, dass ich die Arbeit selbstständig und ohne Benutzung anderer als der angegebenen Quellen und Hilfsmittel verfasst habe. Alle Stellen der Arbeit, die wörtlich oder sinngemäß aus Veröffentlichungen oder aus anderen fremden Texten entnommen wurden, sind von mir als solche kenntlich gemacht worden. Ferner erkläre ich, dass die Arbeit nicht - auch nicht auszugsweise - für eine andere Prüfung verwendet wurde.

Frankfurt am Main, den 24. Oktober 2017

Paul Frederik Depta